

The molecular mechanisms underlying the development and progression of pediatric astrocytoma

Adam M. Fontebasso

Division of Experimental Medicine

Faculty of Medicine

McGill University, Montreal

August, 2014

A thesis submitted to McGill University in partial fulfillment of the requirements
of the degree of Doctor of Philosophy

© Copyright Adam M. Fontebasso, 2014

TABLE OF CONTENTS

LIST OF FIGURES, TABLES & SUPPLEMENTARY MATERIAL	4
ACKNOWLEDGEMENTS	9
ABSTRACT.....	14
RESUMÉ	16
FORMAT OF THE THESIS	18
PREFACE AND CONTRIBUTIONS OF THE AUTHORS	19
ABBREVIATIONS.....	24
CHAPTER 1: INTRODUCTION.....	29
<i>1.1. Pediatric brain tumor epidemiology, pathology and treatment.....</i>	<i>29</i>
<i>1.2 Genomic studies of high-grade gliomas</i>	<i>33</i>
<i>1.3 Epigenetic driver mutations in pediatric and young adult high-grade gliomas.....</i>	<i>36</i>
<i>1.4 Telomerase-dependent and independent telomere dysregulation in adult and pediatric gliomas</i>	<i>47</i>
<i>1.5 Mitogen-activated Protein Kinase (MAPK) Pathway Activation in Gliomas</i>	<i>50</i>
<i>1.6 Aneuploidy and chromothripsis phenotypes in adult and pediatric brain tumors..</i>	<i>57</i>
<i>1.7 Rationale and hypotheses of the study.....</i>	<i>61</i>
<i>1.8 Objectives of the thesis.....</i>	<i>63</i>
<i>1.9 Figures</i>	<i>65</i>
CHAPTER 2: Mutations in <i>SETD2</i> and genes affecting histone H3K36 methylation target hemispheric high-grade gliomas.....	77
<i>2.1 Abstract.....</i>	<i>78</i>
<i>2.2 Introduction.....</i>	<i>79</i>
<i>2.3 Materials and Methods</i>	<i>80</i>
<i>2.4 Results and discussion</i>	<i>84</i>

2.5 Acknowledgments.....	90
2.6 Conflict of interest.....	91
2.7 Figures	92
2.8 Tables.....	95
2.9 Supplementary Material.....	96
2.10 Connecting text Chapter 2 and Chapter 3.....	101

CHAPTER 3: Recurrent mutations in *ACVR1* in pediatric midline high-grade

astrocytoma	103
3.1 Abstract.....	104
3.2 Introduction.....	105
3.3 Materials and Methods	105
3.4 Results.....	113
3.5 Discussion.....	117
3.6 Acknowledgments.....	119
3.7 Competing financial interests	120
3.8 Figures	121
3.9 Supplementary Material.....	125
3.10 Connecting text from Chapter 3 to Chapter 4	143

CHAPTER 4: Characterization of age-associated aneuploidy in pilocytic

astrocytoma	145
4.2 Introduction.....	148
4.3 Materials and Methods	149
4.4 Results.....	154
4.5 Discussion.....	158
4.6 Acknowledgements.....	167
4.7 Conflicts of Interest.....	167
4.8 Accession Numbers	168
4.9 Figures	169
4.10 Supplementary Material.....	176

CHAPTER 5: Discussion.....	184
<i>5.1 General summary and significance of findings</i>	<i>184</i>
<i>5.2 Histone mutations and epigenetic driver mutations as central regulators of tumorigenesis in pediatric brain tumors: possible “epigenetic addiction”?</i>	<i>185</i>
<i>5.3 ACVR1 mutations: New targets and further evidence for pediatric brain tumors as neurodevelopmental diseases.....</i>	<i>188</i>
<i>5.4 Aneuploidy, aging and pilocytic astrocytoma: Inner workings of a tumor beyond the MAPK pathway</i>	<i>193</i>
<i>5.5 Future prospects and experimentation</i>	<i>196</i>
<i>5.6 Conclusion</i>	<i>198</i>
BIBLIOGRAPHY	199

LIST OF FIGURES, TABLES & SUPPLEMENTARY MATERIAL

CHAPTER 1: INTRODUCTION

Figure 1.1: Central nervous system cellular development and tumorigenesis.

Figure 1.2: Gliomas, including astrocytomas, are the largest subgroup of brain tumor across the lifespan.

Figure 1.3: Astrocytoma subtype distribution across the age spectrum.

Figure 1.4: Survival of patients with different histological grades of astrocytoma.

Figure 1.5: Molecular pathways altered in adult glioblastoma.

Figure 1.6: Mutations in histone H3.3 and chromatin remodeling genes identified in pediatric glioblastoma.

Figure 1.7: Six epigenetic subgroups of glioblastoma.

Figure 1.8: Neuroanatomical specificity of epigenetic subgroups of glioblastoma.

Figure 1.9: Functional impact of major genetic and epigenetic driver alterations identified in pediatric and adult glioblastoma.

Figure 1.10: Frequency and brain region specificity of MAPK pathway alterations in pilocytic astrocytoma.

Figure 1.11: Major MAPK genetic alterations identified in pilocytic astrocytoma.

Figure 1.12: Mechanisms leading to the generation of aneuploid cells.

CHAPTER 2: MUTATIONS IN *SETD2* AND GENES AFFECTING HISTONE H3K36 METHYLATION TARGET HEMISPHERIC HIGH-GRADE GLIOMAS.

Figure 2.1: Missense/truncating mutations of the H3K36 trimethyltransferase *SETD2* identified in pediatric and adult high-grade gliomas.

Figure 2.2: Missense/truncating mutations in *SETD2* impair H3K36 trimethyltransferase activity of the enzyme.

Figure 2.3: Mutations affecting H3K36 methylation confer distinct global DNA methylation signatures

Table 1: Frequencies of *SETD2* mutations in 183 pediatric and adult gliomas.

Supplementary Figure 2.1: Age distribution of driver mutations identified in pediatric and adult high-grade gliomas.

Supplementary Figure 2.2: *SETD2* mutations do not show similar patterns of promoter methylation at *OLIG1* and *OLIG2* loci as H3.3K36 affected G34R/V tumors.

Supplementary Table 2.1: Clinical and molecular characteristics of 183 pediatric and adult gliomas included in the study.

Supplementary Table 2.2: Genes significantly mutated in 60 pediatric high-grade glioma samples

CHAPTER 3: RECURRENT SOMATIC MUTATIONS IN *ACVR1* IN PEDIATRIC MIDLINE HIGH-GRADE ASTROCYTOMA

Figure 3.1: Genomic landscape of pediatric midline HGAs.

Figure 3.2: Increased levels of phosphorylated SMAD1/5/8 in *ACVR1*-mutant mHGAs.

Figure 3.3: Clustering analysis of global DNA methylation profiles for 98 high-grade astrocytomas.

Figure 3.4: Mutations identified in *ACVR1* are associated with activation of downstream SMAD signaling pathways.

Supplementary Figure 3.1: Patterns of K27M-associated mutations among midline pediatric high-grade astrocytomas.

Supplementary Figure 3.2: *PDGFRA* amplification is present in a minority of cells in DIPG.

Supplementary Figure 3.3: Copy number variant analysis using biopsy material from five different anatomical loci in a single tumor.

Supplementary Figure 3.4: H3.1 and H3.3 K27M variants demonstrate similar patterns of global DNA methylation.

Supplementary Figure 3.5: Multiscale bootstrapping of the high-grade astrocytoma methylation cluster.

Supplementary Figure 3.6: Mutation subgroup-specific overall survival of midline high-grade astrocytomas (mHGAs) and diffuse intrinsic pontine gliomas (DIPGs).

Supplementary Table 3.1: Clinical characteristics of midline and cortical high-grade astrocytomas included in the study

Supplementary Table 3.2 Functional assessment of *ACVR1* growth factor receptor mutations reported herein

Supplementary Table 3.3 Deep sequencing statistics for *H3F3A*, *HIST1H3B*, *HIST1H3C* of midline high-grade astrocytomas included in the study

Supplementary Table 3.4 Significant copy number gains seen in candidate genes of interest across 98 high-grade astrocytomas.

Supplementary Table 3.5 Significant copy number losses seen in candidate genes of interest across 98 high-grade astrocytomas.

Supplementary Table 3.6 SNVs and insertion/deletion variants in candidate genes of interest

Supplementary Table 3.7 Gross structural alterations in high-grade astrocytomas according to *H3F3A* or *IDH1* mutation show increased genomic instability in *H3F3A* G34R/V mutants

Supplementary Table 3.8 Primer sequences utilized for targeted sequencing and quantitative PCR analyses in the study.

CHAPTER 4: CHARACTERIZATION OF AGE-ASSOCIATED ANEUPLOIDY IN PILOCYTIC ASTROCYTOMA

Figure 4.1: Characterization of aneuploidy observed in pilocytic astrocytoma.

Figure 4.2: Aneuploid PA tumors do not show differential immunohistochemical markers of proliferation or senescence.

Figure 4.3: Comparative gene expression analysis identifies specific pathways aberrantly regulated in aneuploid tumors.

Figure 4.4: Elevated *MDM2* expression is associated with aneuploidy, age and SNP 309 genotypes in pilocytic astrocytoma.

Figure 4.5: Robust *MDM2* correlated signatures exist in pilocytic astrocytoma tumors.

Supplementary Figure 4.1: Aneuploidy is associated with increased age and *BRAF* mutations in PA tumors.

Supplementary Figure 4.2: *MDM2*-correlated pathways are not observed in non-PA gliomas.

Supplementary Table 4.1: Clinico-pathologic and molecular characteristics of 280 pilocytic astrocytomas included in the study

Supplementary Table 4.2: Gene Ontology (GO) analysis of MDM2 correlated genes at FDR < 1e-15

ACKNOWLEDGEMENTS

“If I have seen further it is by standing on the shoulders of giants.”

–Isaac Newton

Having the privilege to pursue higher education as part of the MD-PhD program at McGill University is not solely the product of my hard work and efforts, but of the central people around me from whom I derive absolutely critical personal and professional support. The past four years have allowed me to mature as both a scientist and a person, constantly testing, challenging and exceeding my limits in every way. As in everything, there were trying times, especially in science, and I take pride in admitting that oftentimes, it was not easy, but knowing that now I have developed the patience and wherewithal to see projects through until the end. I am confident that these qualities are a necessary realization for all PhD students wanting to pursue their own research endeavors in the future as the clarity that comes with patience and focus from doctoral training truly is unique. I am so very fortunate to have had this opportunity to grow and contribute to the research being done on deadly pediatric brain tumors that would not have been possible without the influence of very key individuals in my life.

I would first like to thank my supervisors Dr. Nada Jabado and Dr. Michel Tremblay at the Montreal Children’s Hospital Research Institute and the Rosalind and Morris Goodman Cancer Research Centre at McGill University. Dr. Jabado my primary supervisor, without question, has challenged me more than anyone I have ever met in my academic career. As a mentor she saw to it that I was constantly moving forward in my studies, even while working on multiple projects amongst obligations to the MD-PhD program. Her talent, enthusiasm, passion and intensity for her work are unparalleled and

to have witnessed this firsthand, I can say that I had the pleasure of working on a PhD under a scientist with both world-class vision (she thinks about ten steps ahead of most individuals I have met!) and absolutely incredible work ethic. Although the workload was high, knowing that my supervisor was working ten times as hard made it easier. I say with confidence that Dr. Jabado has shown me what it takes to succeed in science on a global level and I thank her from the bottom of my heart.

I have known Dr. Tremblay since my undergraduate degree in Biochemistry where I worked as a summer and honours student in his lab trying to hone my skills in a variety of molecular biological areas. I credit Dr. Tremblay with giving me a love and appreciation for science, as his excitement, enthusiasm and motivation for it in general is truly infectious. Following my decision to apply for the MD-PhD program, he was nothing but supportive, giving me the confidence I needed to succeed. With my acceptance, he guided me and offered his honest opinion based on my personal interests in neuroscience and cancer to work with Dr. Jabado for my PhD. Although we still have many projects unfinished together, Dr. Tremblay has continuously expressed his faith in me and has been a great advisor. I have the capacity of submitting this thesis because of the incredible guidance of my co-supervisors, Dr. Jabado and Dr. Tremblay, as they each played very different, yet unifying roles in my scientific development.

A lab is very much like a family, and I have had the pleasure of working with some amazing siblings. Without Damien Faury, I would still be buried under a pile of work without expertise or organization. Damien taught me the skills, walked me through every protocol and worked with me side-by-side for my projects. We handled hundreds

of samples together, did many experiments and all the while enjoyed some great times.
Damien: un collègue aussi dévoué et vaillant je ne trouverai jamais, merci beaucoup.

Noha Gerges has been a fellow PhD student, friend and therapist to me. When stress got high, I knew I could pick up the phone, walk over to her desk or message her for some support. Thank you for being there Noha!

Once Cathy Russo joined our lab she immediately had an impact and I do not know what us students would do without her. She was a driving force for our mouse studies and all the while helping with virtually every aspect of the lab. Caterina: grazie mille!

To all of the students/fellows who have been a part of the lab during my four years, I would like express my sincere gratitude. Dong-Anh Khuong-Quang, Karine Jacob, Margret Shirinian and Xiaoyang Liu were in the lab on my first day of PhD and for everyday they were there afterwards, helped me with techniques, protocols, data analysis, you name it. They have since moved onto the next steps in their lives in Montreal and around the world and I wish them all the best. Denise Bechet, Tenzin Gayden, Nisreen Ibrahim, Michael Neirinck, Nicolas De Jay, Pierre-Olivier Fiset, Leonie Mikael and Eef Harmsen joined the lab during my four years and added their immense talents to our hard-working team. They helped me, supported me and contributed to so many aspects of my PhD experience; I am very grateful.

To our collaborating students/fellows and scientists I must extend my immense thanks. Jeremy Schwartzentruber and Dr. Jacek Majewski are without a doubt, two of the most talented individuals I have ever encountered. Our collaborative efforts have led to the first two chapters of my thesis and I am so fortunate to have worked with and learned

from them. Simon Papillion-Cavanagh was both a driving force and a buddy through chapter 3 of this thesis and I cannot thank him enough for his excellent DNA methylation analysis. To Dr. Steffen Albrecht and the amazing staff at the Montreal Children's Hospital Departments of Neurosurgery, Pathology and Hematology and Oncology, I am very grateful and in awe of the care you give to your patients and contributing to research. To Dr. David Jones and Dr. Stefan Pfister from the DKFZ in Heidelberg and Dr. Keith Ligon and Dr. Mark Kieran from Harvard in Boston and their teams, I extend my sincere thanks for all of your contributions and expertise towards our collaborative projects. To James Fraser and Dr. Josée Dostie I wish to extend my sincere thanks for the incredible partnership studying the three-dimensional structure of DNA in brain tumors. To Dr. Mitra Cowan, a great collaborator, I wish to say thank you for not only your hard work for our mouse models, but also sincere appreciation for your support and enthusiasm.

I would also like to greatly thank my thesis committee members composed of my supervisors Nada and Michel, Dr. Cindy Goodyer my chair, Dr. Josée Dostie, Dr. Anne McKinney and Dr. Janusz Rak. I would not only like to thank them for excellent feedback and scientific support at my committee meetings but also for being excellent advocates for my education.

I would also like to acknowledge the MD-PhD program and the Director, Dr. Alyson Fournier for providing great few years in the program (and counting) and my funding sources, the Canadian Institutes of Health Research (CIHR) for an MD-PhD studentship and the CIHR-McGill Systems Biology Training Program for an award.

More than anyone however, I would like to thank my family, my mother Helen, my father Peter and my brother David and the love of my life, Caitlin, for the faith, the support, the confidence you instill and the better person that you inspire me to try to be everyday. The lessons my parents taught my brother and I have allowed us to never abandon our work ethic, believe in ourselves and strive to attain our dreams. Never once did my family let me down, and so lucky I wish everyone in this world could be to have such wonderful people in their lives. To have a mother, a father and a brother who would drop it all to help me no matter what is truly what family is all about. I am so lucky to have them and to have met Caitlin, whose love and support over the past four years has been the stuff of legend. You have been the epitome of a true partner, day in and day out, with me through the tough times and celebrating with me during the great ones. You guys make me feel like I can do anything; I love you so much.

I dedicate this thesis to the unbelievably courageous patients and their families who have been affected by pediatric brain tumors. Your bravery and your contributions to the improvement of the care of future patients across the world are inspiring. You are the true giants.

Sincerely,

Adam M. Fontebasso

ABSTRACT

Brain tumors are the leading cause of cancer-related mortality and morbidity in the pediatric years. Pediatric brain tumor treatment has been driven largely by findings in adult tumors, and in the case of high-grade gliomas (HGGs) including glioblastoma (GBM), universal failure of therapy across patients of all ages is continuously observed. Recent years have seen a plethora of studies emerge exploring the cancer genome of HGGs to better understand and target the molecular mechanisms that make these cancers some of the deadliest and most aggressive encountered in oncology. Recent studies have uncovered the epigenome as a critical component altered in HGGs. Mutations resulting in vital amino acid substitutions at lysine 27 (p.Lys27Met, K27M) and glycine 34 (p.Gly34Arg/Val, G34R/V) in histone variant H3.3 were shown by our lab and others to characterize about one-third of pediatric GBM tumors, a discovery that marked the first recurrent mutations identified in histone genes in human disease, which are highly conserved across species. Herein, we will discuss the major aspects of my doctoral work that was centered on better characterizing H3.3 and related mutations and alterations in pediatric HGGs as well as characterizing the genomic landscape of the low-grade astrocytoma, pilocytic astrocytoma (PA). Strikingly, we identify genetic alterations leading to changes in histone 3 lysine 36 (H3K36) methylation specifically in HGGs of the cerebral hemispheres, including mutations in the only H3K36 trimethyltransferase encoded in humans, *SETD2*. Conversely, when analyzing pediatric high-grade tumors of the neuroanatomical midline, we uncover a large majority with H3 K27M mutations and associated with specific growth factor receptor mutations in defined brain regions, such as recurrent *ACVR1* mutations in tumors of the pontine area. In PA, we explore molecular

mechanisms leading to and maintaining aneuploidy seen with increasing age in this tumor. Taken together, we describe the molecular profile of pediatric astrocytomas and lay a foundation for targeted therapeutic development in future studies.

RESUMÉ

Les tumeurs cérébrales sont la première cause de mortalité et morbidité reliées au cancer chez l'enfant. Les traitements des tumeurs cérébrales pédiatriques sont dérivés des études élaborées chez les adultes, et dans le cas spécifique des gliomes de haut grade ou *high-grade gliomas* (HGGs), incluant le glioblastome (*glioblastoma*, GBM), un échec universel des thérapies chez les patients de tout âge est observé. Au cours de ces dernières années de nombreuses études sur l'aspect génomique des HGGs ont permis de mettre en exergue une meilleure compréhension des mécanismes moléculaires qui sont impliqués dans ces cancers connus pour être parmi les plus agressifs en oncologie. De récentes études ont démontré que l'altération de l'épigénome joue un rôle crucial dans les gliomes de haut grade. Des mutations, au niveau de l'histone 3 notamment au niveau du variant H3.3, ont été découverte par notre laboratoire et d'autres équipes. Celles-ci résultent de la substitution d'un acide aminé, de la lysine 27 en méthionine (p.Lys27Met, K27M), de la glycine 34 en arginine ou en valine (p.Gly34Arg/Val, G34R/V). Cette découverte a été la première à identifier des mutations récurrentes au niveau des gènes des histones impliqués dans des maladies humaines et normalement hautement conservés entre les espèces. Dans cette thèse, je vais discuter des aspects majeurs de mon travail de doctorat qui ont été essentiellement centrés sur la caractérisation de l'histone H3 et des mutations qui lui sont reliées, et sur la meilleure compréhension des altérations de l'épigénome retrouvées dans les tumeurs cérébrales de haut grade. L'investigation a également été menée sur les aspects génomiques des astrocytomes pilocytaires (*pilocytic astrocytoma*, PA), un astrocytome de bas grade. De plus, nous avons identifiés des altérations génétiques qui peuvent affecter la méthylation de la lysine 36 de l'histone 3

(H3K36) dans plus de la moitié des tumeurs cérébrales pédiatriques de haut grade. Ces mutations ont été retrouvées dans le seul gène humain codant pour la méthyl- transférase de l'H3K36 nommée *SETD2*. Lors de l'analyse des tumeurs pédiatriques de haut grade au niveau de la ligne médiane (en neuro-anatomie), nous avons découvert qu'une grande majorité des mutations H3 K27M, et l'association à des mutations de récepteurs spécifiques au facteur de croissance, de prolifération et développement des différentes régions du cerveau, tel que des mutations récurrentes de *ACVRI* (*activin A receptor, type I*) étaient localisées au niveau de la région du pons du tronc cérébral. Chez les tumeurs PA, nous avons approfondi notre étude en explorant les mécanismes moléculaires qui conduisent et entretiennent l'aneuploïdie en corrélation avec un augmentation de l'âge de diagnostique du patient portant un PA. Dans l'ensemble, nous avons décrit le profil moléculaire des astrocytomes pédiatriques et poser les bases pour développer des traitements plus efficaces chez les patients dans le futur.

FORMAT OF THE THESIS

This thesis is organized as a manuscript-based document according to the guidelines and specifications outlined by the Faculty of Graduate and Postdoctoral Studies of McGill University. Herein, the reader will first encounter Chapter 1, which provides an introduction to the clinical picture of pediatric brain tumors, major genomic alterations as well as recent findings implicating the epigenome as a central aspect in their pathogenesis. Background information on the basic biology of critical signaling and histone regulation pathways will be provided to enable the reader to best critically appraise the following 3 chapters. Chapters 2 through 4 are presented in manuscript format, with Chapter 2 and Chapter 3 published in *Acta Neuropathol.* 2013 May;125(5):659-69. doi: 10.1007/s00401-013-1095-8 [72] and *Nat Genet.* 2014 May;46(5):462-6. doi: 10.1038/ng.2950 [71] respectively. To best allow the reader to relate each section, connecting text sections are provided to demonstrate the inter-relationship between each chapter. Chapter 5, the final section, is a discussion and global summary of the main results of this dissertation. Included as well are future directions and further experimentation of note in the near future to continue progress in this rapidly evolving field.

PREFACE AND CONTRIBUTIONS OF THE AUTHORS

The work presented in this thesis encompasses our investigation into the genomic landscapes of pediatric astrocytoma and constitutes novel contributions to the field of pediatric brain tumor biology. Throughout the course of my doctoral work, our lab and others have been central to implicating the epigenome as a vital component required for tumorigenesis within pediatric and young adult tumors specifically and have published to that effect. Within Chapter 2, we identify for the first time in high-grade gliomas, loss-of-function mutations in the histone H3 lysine 36 trimethyltransferase *SETD2* with a predilection for tumors occurring in the cerebral hemispheres, work that was published in [72]. Within Chapter 3, we studied 40 high-grade tumors of the neuroanatomical midline, namely the thalamus, brainstem, cerebellum and spinal cord and uncover a predominance of H3 K27M mutations defining 93% of tumors. For the first time in human cancer and published in [71], we identify somatic gain-of-function mutations in the activin A, receptor type I encoded by *ACVRI* in high-grade tumors of the pons, termed diffuse intrinsic pontine gliomas (DIPGs). In Chapter 4, we studied the whole chromosomal copy number profiles of 222 adult and pediatric pilocytic astrocytoma (PA) tumors and determined the prevalence and characteristics of aneuploidy, in the form of chromosomal gains, in PAs. We show its differential association with common hits along the mitogen-activated protein kinase (MAPK) pathway and notably with the expression of genes promoting and tolerating aneuploidy. *MDM2* a gene seen upregulated in aneuploid tumors, was shown to correlate strongly with specific expression programs, including the unfolded protein response, which may underlie these aneuploid phenotypes and present an ideal target for further investigation.

CHAPTER 2: Mutations in *SETD2* and genes affecting histone H3K36 methylation target hemispheric high-grade gliomas

Adam M. Fontebasso participated in the study design, extracted and prepared DNA and histone lysates from patient samples for sequencing, methylation profiling, participated in the analysis of sequencing data and DNA methylation clustering, performed Western blotting, performed statistics and drafted and revised the manuscript and figures. **Jeremy Schwartzentruber** contributed equally to the manuscript, implemented the bioinformatics pipeline for whole-exome sequencing analysis, alignment and variant calling, performed statistical comparisons of variants between the dataset and the set of non-cancer control exomes and participated in drafting the manuscript and figures. **Dong-Anh Khuong-Quang, Dominik Sturm, David T.W. Jones, Hendrik Witt, Marcel Kool, Jihad Hadjadj, Stephan Busche, Noha Gerges** participated in DNA methylation analysis. **Xiao-Yang Liu, Damien Faury** aided in extracting and preparing patient samples. **Pierre Lepage, Alexandre Montpetit, Alfredo Staffa** coordinated whole-exome sequencing library preparation and designed the approach for targeted next-generation sequencing of *SETD2*. **Andrey Korshunov, Steffen Albrecht, Adam Fleming, Magdalena Zakrzewska, Krzysztof Zakrzewski, Pawel P. Liberski, Peter Hauser, Miklos Garami, Almos Klekner, Laszlo Bognar, Gelareh Zadeh, Stefan M. Pfister, Nada Jabado** provided patient materials, resources and clinical information. **Stefan M. Pfister, Nada Jabado and Jacek Majewski** conceived the study, supervised the project, experimentation and analysis, drafted and revised the manuscript and figures. All authors approved of the final manuscript.

CHAPTER 3: Recurrent somatic mutations in *ACVRI* in pediatric midline high-grade astrocytoma

Adam M. Fontebasso participated in the study design, organized, extracted and prepared DNA and RNA from patient samples, analyzed and summarized whole-exome and deep sequencing data, performed cell culture experiments, Western blotting, analyzed and participated in quantitative PCR for target genes, performed survival analysis on patient samples, performed statistical comparisons of mutations, drafted and revised the manuscript and figures. **Simon Papillon-Cavanagh** contributed equally to the study and performed DNA methylation analysis for clustering and co-developed (with **Nicolas De Jay**) an algorithm to extract copy number variant (CNV) information from methylation data. **Jeremy Schwartzentruber** contributed equally to the study and implemented the bioinformatics pipeline for whole-exome sequencing data analysis, alignment and variant calling and identification. **Hamid Nikbakht** implemented a data analysis pipeline for MiSeq targeted deep sequencing data alignment and variant calling and analysis. **Noha Gerges, Damien Faury** extracted and prepared patient samples and performed quantitative PCR experiments. **Pierre-Olivier Fiset, Denise Bechet, Zhifeng Dong, Peter M. Siegel** optimized and performed blinded immunohistochemistry analysis on patient samples. **Nicolas De Jay** co-developed a methylation CNV analysis algorithm, implemented the gene fusion discovery pipeline and analyzed RNA sequencing data. **Lori A. Ramkissoon, Aoife Corcoran** aided in Western blotting experimentation and manuscript revisions. **David T. W. Jones, Dominik Sturm, Pascal Johann** participated in DNA methylation analysis. **Tadanori Tomita, Stewart Goldman, Mahmoud Nagib, Anne Bendel, Liliana Goumnerova, Daniel C. Bowers, Jeffrey R. Leonard, Joshua**

B. Rubin, Tord Alden, Samuel Browd, J. Russell Geyer, Sarah Leay, George Jallo, Kenneth Cohen, Nalin Gupta, Michael D. Prados were members of the BATS DIPG study and performed patient biopsies and provided materials. **Anne-Sophie Carret, Benjamin Ellezam, Louis Crevier, Almos Klekner, Laszlo Bognar, Peter Hauser, Miklos Garami, John Myseros, Hayley Malkin, Steffen Albrecht, Stefan M. Pfister, Keith L. Ligon, Nada Jabado Mark W. Kieran** provided patient materials and resources. **Azra H. Ligon** performed FISH experiments. **Keith L. Ligon, Jacek Majewski, Nada Jabado, Mark W. Kieran** conceived the study, participated in study design, coordinated and supervised experimentation and analysis, drafted and revised the manuscript. All authors approved of the final manuscript.

CHAPTER 4: Characterization of age-associated aneuploidy

Adam M. Fontebasso participated in study design, organized, extracted and prepared DNA and RNA from patient samples, performed *KIAA1549-BRAF* fusion PCR, analyzed SNP array data and recruited meta-analysis data, performed gene expression analysis, correlations and clustering, performed contingency statistics, drafted the manuscript and figures. **Margret Shirinian** contributed equally to the study, extracted and prepared DNA and RNA from patient samples, performed *KIAA1549-BRAF* fusion PCR, analyzed SNP array data and contributed to the manuscript. **Dong-Anh Khuong-Quang, Tenzin Gayden, Karine Jacob, Noha Gerges, Damien Faury** prepared DNA from patient samples. **Karine Jacob, Marcel Kool, Huriye Cin, Hendrik Witt, Sally Lambert, David T. W. Jones** provided meta-analysis data. **Tenzin Gayden, Marcel Kool, Nicolas De Jay, Tony Kwan** aided in performing gene expression analysis. **Alexandre**

Montpetit, Sébastien Brunet, Pierre Lepage, Geneviève Bourret performed sequencing of *BRAF* V600E mutation and *MDM2* SNP 309. **Almos Klekner, Lászlo Bognár, Peter Hauser, Miklós Garami, Jean-Pierre Farmer, Jose-Luis Montes, Jeffrey Atkinson, Adam J. Fleming, Sally Lambert, Andrey Korshunov, Uri Tabori, V Peter Collins, Steffen Albrecht, Stefan M. Pfister, Werner Paulus, Martin Hasselblatt, Nada Jabado** provided patient materials, resources and clinical information. **Steffen Albrecht** analyzed immunohistochemistry slides. **David T. W. Jones** and **Nada Jabado** conceived the study, supervised experimentation, analysis and drafted the manuscript.

ABBREVIATIONS

The following includes an alphabetical list of all the abbreviations used throughout this thesis, defined at mention within text and summarized here for reference. Italics within text signify an individual gene or transcript, whereas normal text refers to the protein product of a gene according to standard nomenclature:

2-HG: 2-hydroxyglutarate

5hmC: 5-hydroxymethylcytosine

5mC: 5-methylcytosine

ACVR1: activin A receptor, type I

aCGH: array-based comparative genomic hybridization

ALK2: alternate name for ACVR1; activin A receptor, type I

AML: acute myeloid leukemia

ALL: acute lymphoblastic leukemia

ALT: alternative lengthening of telomeres

ATRX: alpha-thalassemia/mental retardation X-linked

BMP: bone morphogenetic protein

BRAF: v-raf murine sarcoma viral oncogene homolog B1

CDK: cyclin-dependent kinase

ChIP-seq: chromatin immunoprecipitation sequencing

CIN: chromosomal instability

CNS: central nervous system

CRAF: v-raf-leukemia viral oncogene 1

CRISPR: clustered regularly interspaced short palindromic repeats

DAXX: death-domain associated protein

DMEM: Dulbecco's modified Eagle's medium

EGFR: epidermal growth factor receptor

EP: ependymoma

ERK: extracellular regulated kinase

EZH2: enhancer of zeste 2

FBS: fetal bovine serum

FDR: False discovery rate

FFPE: formalin-fixed, paraffin embedded

FGFR1/3: fibroblast growth factor receptor 1/3

GBM: glioblastoma

GCT: giant cell tumor of bone

G-CIMP: glioma-CpG island methylator phenotype

GFR: growth factor receptor

GO: Gene Ontology

G34R/V: glycine 34 to arginine or valine substitution in histone 3 variants

GTR: Gross-total resection

GWAS: Genome-wide association studies

H2A: histone 2A

H2B: histone 2B

H3: histone 3

H4: histone 4

H3.1: histone 3 variant 1

H3.3: histone 3 variant 3

H3F3A: H3 histone, family 3A

H3F3B: H3 histone, family 3B

HIST1H3B: histone cluster 1, H3b

HIST1H3C: histone cluster 1, H3c

H3K4: histone 3 lysine 4

H3K9: histone 3 lysine 9

H3K27: histone 3 lysine 27

H3K27me1/2/3: mono-, di- or tri-methylated histone 3 lysine 27

H3K27ac: acetylated histone 3 lysine 27

H3K36: histone 3 lysine 36

H3K36me1/2/3: mono-, di- or tri-methylated histone 3 lysine 27

HGA: high-grade astrocytoma

HGG: high-grade glioma

ICGC: International Cancer Genome Consortium

ID1/2/3: genes encoding inhibitor of DNA binding 1/2/3, dominant negative helix-loop-helix protein

IDH1: isocitrate dehydrogenase 1

KDM: histone lysine demethylase

KIAA1549: KIAA1549 gene of the UPF0606 family

K27M: lysine 27 to methionine amino acid substitution in histone 3 variants

K36M: lysine 36 to methionine amino acid substitution in histone 3 variants

LFS: Li-Fraumeni syndrome

LGA: low-grade astrocytoma

MB: medulloblastoma

MDM2: proto-oncogene, E3 ubiquitin protein ligase

MET: MET proto-oncogene, receptor tyrosine kinase

MGMT: O⁶-methylguanine-DNA methyltransferase

mHGA: midline high-grade astrocytoma

NF1: neurofibromatosis type 1 (referring to syndrome), neurofibromin 1 (referring to gene or gene product)

NGS: next-generation sequencing

NHA: normal human astrocytes

NHLBI: National Heart, Lung and Blood Institute

PA: pilocytic astrocytoma

PCR: polymerase chain reaction

PDGFRA: platelet-derived growth factor receptor alpha

PI3K: phosphoinositide-3-kinase

PIK3CA: phosphatidylinositol-4,5-bisphosphate 3-kinase, catalytic subunit alpha

PIK3R1: phosphoinositide-3-kinase, regulatory subunit 1 (alpha)

PRC2: Polycomb Repressor Complex 2

PTEN: phosphatase and tensin homolog

PTPN11: protein tyrosine phosphatase, non-receptor type 11 (encodes SHP-2)

RAF1: gene encoding CRAF, v-raf-leukemia viral oncogene 1

RB1: retinoblastoma 1

RCAS/Tv-a: replication-competent avian leukosis virus with splice acceptor retroviral gene delivery system

RT-PCR: reverse transcriptase-polymerase chain reaction

RTK: receptor tyrosine kinase

SHH: sonic hedgehog

SNP: single nucleotide polymorphism

SMAD: SMAD family member, homologs of the *Drosophila* 'Mothers against decapentaplegic' (Mad)

SNAI1: snail family zinc finger 1

TACC1/3: transforming, acidic, coiled-coil containing protein 1/3

TALEN: transcription activator-like effector nuclease

TCGA: The Cancer Genome Atlas

TERC/TR: telomerase RNA

TERT: telomerase reverse transcriptase

TMA: tissue microarray

TP53: gene encoding tumor protein p53

UPR: unfolded protein response

WES: whole-exome sequencing

WGS: whole-genome sequencing

WHO: World Health Organization

WT: wild-type

ZFN: zinc-finger nuclease

CHAPTER 1: INTRODUCTION

1.1. Pediatric brain tumor epidemiology, pathology and treatment

According to recent statistics, one in every 285 children will be diagnosed with cancer before the age of 20 years [273]. This translates into an approximate 15,780 new cases and 1960 new deaths from pediatric cancer in 2014 in the United States alone [273]. This same report by the American Cancer Society estimates that 1 in 530 young adults aged 20-39 years is a childhood cancer survivor, implicating an essential need for proper follow-up amongst clinicians who see and care for these patients longitudinally [273]. As such, cancer is an extremely significant contributor to pediatric and young adult morbidity and mortality. Although leukemias are the most frequently occurring malignancy in the childhood years, brain tumors are a leading cause of cancer-related death in children [206,90], and between the years of 2007-2010 accounted for the largest proportion of cancer-related mortality (31%) in children less than 15 years old [242]. The largest subgroup of brain tumor occurring across the lifespan are gliomas, which are tumors arising from cells of the glial lineage and include astrocytomas, oligodendrogliomas, mixed oligoastrocytomas and ependymomas (Figure 1.1) [138,167]. Astrocytomas are the most common subtype of glioma in adults and children and account for over half of all primary brain tumors (Figure 1.2) [293,138]. Astrocytomas are subdivided by the World Health Organization (WHO) into four histopathological grades based on specific features including cellularity, proliferative index, nuclear atypia and importantly necrosis and microvascular proliferation amongst other characteristics [167]. Grades I and II astrocytomas are termed low-grade astrocytomas (LGAs), and grades III-IV are termed high-grade astrocytomas (HGAs) [167].

The spectrum of tumor grade and brain location of astrocytoma subtypes differs greatly between children and adults (Figure 1.3). Brain tumors in children often arise below a structure called the tentorium cerebelli, which divides the forebrain from the posterior fossa and hindbrain structures such as the brainstem, cerebellum and spinal cord [206]. These tumors are most commonly low-grade tumors, notably the grade I astrocytoma, pilocytic astrocytoma (PA), which represents the most common primary brain tumor in children (Figure 1.3) [196,61,82]. Malignant tumors of neuronal origin can also arise in the posterior fossa compartment in children, including embryonal tumors such as medulloblastoma (MB) (Figure 1.3) [138]. In adults, the spectrum is quite different, with high-grade gliomas (HGGs) including high-grade astrocytomas (HGAs) being the most common tumors in older patients [138]. Glioblastoma (GBM), a highly aggressive and lethal WHO grade IV astrocytoma, is the most common primary brain tumor, and has the largest incidence in older patients (Figure 1.3) [138]. HGAs including GBMs can also arise in pediatric patients, throughout the brain, but also distinctly in the ventral brainstem, where they are invariably fatal and termed diffuse intrinsic pontine gliomas (DIPGs) [177,76,15,136].

PAs are well-circumscribed and often considered “benign” tumors if amenable to gross-total surgical resection. They harbor features of low cellularity, are slow-growing and indolent in nature, and often have a loose appearance on histology with the presence of long hair-like cellular projections termed Rosenthal fibers, hence the name “pilocytic” [167]. Patients with PA have an excellent prognosis, with 10-year survival rates estimated at 96% (Figure 1.4) [194]. Although they most commonly occur within the cerebellum, where gross-total resection (GTR) and excellent patient outcome is often possible, they

can occur throughout the brain and in surgically inaccessible locations such as the optic pathway, thalamus, brainstem and spinal cord [117]. GBM tumors conversely are highly infiltrative, most often occur within the cerebral cortex and harbor distinct features of pseudopallisading necrosis and microvascular proliferation (angiogenesis) which are diagnostic on histopathology [167]. Patients with GBM have very poor survival, even in response to multimodal treatment strategies involving surgery, radiotherapy and chemotherapy [194]. GBM 5-year survival rates have been reported at less than 3% (Figure 1.4) [193], a feature which has not ameliorated much over the past few decades. HGAs arising in the brainstem, termed DIPG, demonstrate the poorest survival amongst brain tumors and arise exclusively in children [15]. This diagnosis is fatal with children demonstrating a median survival time less than one year [76], and 90% of children dying of their disease within 2 years [15]. As DIPGs arise in such sensitive neuroanatomical locations near cardiovascular and respiratory centers within the brainstem, most research on the molecular basis of these tumors has been conducted in autopsied tissues to date [198,289].

Patients who are childhood cancer survivors necessitate follow-up to screen for potential recurrences or secondary malignancies, as well as a variety of sequelae associated with disease and treatment [201,77,217]. Brain cancer survivors can be diagnosed with secondary CNS tumors, notably in cases that were previously treated with both chemotherapy and radiation exceeding 25 Gy [44]. High-risk pediatric MB, which can disseminate throughout the nervous system and seed, necessitates cranial-spinal irradiation [111]. Studies of the impact of cranial-spinal irradiation in young children have revealed a profound impact on physical growth impairment, problems at school and

finding and maintaining work later in life [141]. Neurological deficits, psychosocial dysfunction and endocrine complications were reported frequently overall in 45 medulloblastoma patients followed-up after cranial-spinal irradiation at a single institution between 1980-2000 [74]. As brain tumors can occur throughout functionally sensitive forebrain and hindbrain areas, subsequent sequelae may also be incurred due to mass effect, tumor infiltration or surgical damage within these locations. Childhood CNS tumor survivors can as a result of their primary tumor and treatment, demonstrate a variety of morbidities including secondary neoplasms, physical, psychosocial and mental disabilities, impaired endocrine function and an increased risk of cardiac and cerebrovascular death [201].

Recent years have seen modest advances in the treatment of patients with GBM. The most significant of which involved the concomitant and adjuvant use of the alkylating agent temozolomide (TMZ) along with radiotherapy following surgical resection and was shown to improve GBM median survival from 12.1 to 14.6 months in a landmark randomized controlled trial [248]. Moreover this benefit was seen most strikingly in patients demonstrating methylation of the promoter of *MGMT*, which encodes the O⁶-methylguanine methyltransferase and enzymatically removes an alkyl group from the O⁶ position of guanine [104]. Patients with methylated *MGMT* promoters and thus lacking MGMT expression, demonstrated significant improvement in survival of 21.7 months when receiving concomitant and adjuvant TMZ and radiotherapy compared to 15.3 months for radiotherapy alone [104]. As pediatric and adult tumors appear identical under the microscope, pediatric treatment strategies have largely been passed down from adult studies. In summary, current treatment protocols, which are not tailored

to the pediatric setting in the context of high-grade astrocytomas, offer a substantial degree of risk for serious morbidity and mortality. As such there is a desperate need for targeted approaches, safe to utilize in the developing child that will effectively treat tumorigenesis in this age group. Within the next sections of this Chapter, I intend to outline the major genomic and epigenomic studies and resultant identified alterations in astrocytomas. As a result, I hope to demonstrate the important molecular distinctions between tumors occurring across the lifespan and outline the need for a molecular re-classification of approaches to the diagnosis and treatment of gliomas.

1.2 Genomic studies of high-grade gliomas

Recent years have seen an explosion of genomic data across many types of human cancer, through the efforts of independent laboratories, as well as large consortia such as The Cancer Genome Atlas (TCGA) and the International Cancer Genome Consortium (ICGC) [48,107]. Initial studies employing the use of high-density arrays for gene expression profiling and copy number analysis revealed the existence of multiple subgroups of high-grade gliomas (HGGs) including glioblastoma (GBM) [204,68,98,199,262]. Profiling studies showed that molecular subgroups of HGGs recapitulate stages of neurogenesis, with recurrent tumors clustering according to more mesenchymal signatures [204]. Further to this, important work by our lab revealed that pediatric and adult GBM tumors were molecularly distinct through gene expression profiling [68], suggesting that although these tumors looked identical under the pathologists' microscope, they were vitally different in their genetic make-up. Candidate genes and pathways such as the shuttling protein Y-box-protein-1 (YB-1) and Ras/Akt

growth pathways were shown to be uniquely upregulated in pediatric GBM tumors, identifying putative targets for therapeutic development in the context of pediatric disease [68]. These findings could be reproduced on archival formalin-fixed paraffin-embedded (FFPE) sections of pediatric GBM, demonstrating the critical utility of profiling on more readily available pathological material [98]. These initial data pointed to critical molecular differences between adult and pediatric tumors.

Studies conducted by large consortia have fueled progress towards understanding the molecular basis of adult GBM. The TCGA chose to study GBM as its pilot integrative profiling project and identified recurrent mutations, copy number aberrations and methylation defects in critical genes and pathways in 206 adult GBM tumors studied [48]. In addition, they selected 601 candidate oncogenes and tumor suppressor genes to sequence in 91 GBM tumors as a targeted approach [48]. In their initial comprehensive report, the TCGA described a variety of hits along three important pathways encompassing receptor tyrosine kinase (RTK)/RAS/phosphoinositide-3-kinase (PI3K) signaling, p53 signaling and retinoblastoma protein (RB) signaling in 86%, 87% and 78% of adult GBM tumors studied respectively (Figure 1.5) [48]. *TP53* itself was altered via hotspot mutations, or copy number loss in 35% of GBM tumors [48]. RTK genes epidermal growth factor receptor (*EGFR*, 45%), platelet-derived growth factor receptor alpha (*PDGFRA*, 13%), v-erb-b2 avian erythroblastic leukemia viral oncogene homolog 2 (*ERBB2*, also abbreviated as *HER2*, 8%) and MET proto-oncogene, receptor tyrosine kinase (*MET*, 4%) were among the most frequently altered receptor genes by mutation or focal copy number amplification [48]. Frequent somatic loss or missense/truncating mutations were also identified in the neurofibromin 1 (*NFI*) gene in 23% of GBM tumors

[48]. Germline defects in *NF1* are responsible for the autosomal dominant glioma predisposition syndrome neurofibromatosis type I (NF1), and prior data from mouse models suggested a strong role for *NF1* defects and gliomagenesis [215,292]. Tumor suppressor genes other than *TP53* or *NF1* were also affected at high frequency, including homozygous deletions or inactivating mutations in *CDKN2A*, which encodes ARF or p16/INK4A in 49%-52% of GBM tumors studied [48]. This gene is a critical inhibitor of cyclin-dependent kinases (CDKs) and MDM2, an E3-ubiquitin ligase, amplified in 14% of GBM tumors studied, and a central regulator of p53 protein levels and p53 pathway activity [48]. In addition novel mutations involving the regulatory subunit of the PI3K complex p85 α , encoded by *PIK3RI*, were identified in 10% (9/91) sequenced GBMs [48]. Gain-of-function mutations in the catalytic p110 α subunit of PI3K (*PIK3CA*) have been previously shown to be involved in a variety of cancers including GBM and other gliomas, and in 7% (6/91) of GBM tumors in the TCGA cohort [223,26,186,189,100]. Phosphatase and tensin homolog (PTEN), a well-characterized tumor suppressor gene and inhibitor of PI3K activity, was altered at a very high frequency of 36% through homozygous deletion or loss-of-function mutations, demonstrating multiple hits converging on PI3K regulated activity in GBM tumors [48].

Further investigations conducted by TCGA utilizing integrative gene expression profiling and copy number analysis continued earlier work by Phillips and colleagues in the subgrouping of HGGs including GBM [262,204]. Seminal work by Verhaak and colleagues within the context of the TCGA identified four molecular subgroups of adult GBM through molecular profiling that were delineated by alterations described above in *PDGFRA*, *NF1*, *EGFR* and hotspot mutations in the metabolic gene isocitrate

dehydrogenase 1 (*IDH1*) (discussed in section 1.3) [262]. These molecular subgroups were described as ‘neural,’ ‘proneural,’ ‘mesenchymal,’ and ‘classical’ based on active molecular programs and correlated with differential survival of patients with these expression signatures [262]. Pediatric cohorts of HGG tumors studied by integrative profiling have revealed critical differences with adult disease [199], illustrating that while TCGA consortium projects have shaped the biology of adult disease, further genome-wide investigations of pediatric and young adult tumors is warranted.

1.3 Epigenetic driver mutations in pediatric and young adult high-grade gliomas

In addition to TCGA, other independent projects have contributed to the understanding of HGG and GBM occurring across the lifespan. The advent of next-generation sequencing (NGS) technology, including whole-exome sequencing (WES), has fueled an incredible expansion in our knowledge database of genomic alterations in cancer, complex and Mendelian disease (reviewed in [172]). Initial applications of NGS to the study of GBM greatly expanded the repertoire of protein-coding gene mutations in this disease. In their landmark study, Parsons and colleagues utilized NGS to sequence 20,661 protein-coding genes and identified recurrent hotspot mutations in *IDH1* at arginine 132 resulting most often in histidine substitutions (R132H) in 12% of GBM tumors [197]. *IDH1* is one of 5 encoded isocitrate dehydrogenase proteins in humans [197], and demonstrates localization to the cytosol and peroxisomal subcellular compartments [81]. *IDH1* normally catalyzes the oxidative decarboxylation of its substrate, isocitrate, to α -keto-glutarate, producing nicotinamide adenine dinucleotide phosphate (NADPH), with R132 amino acid substitutions initially suspected to abrogate

its enzymatic activity due to their presence within its substrate binding site [197]. *IDH1* mutations were harbored by 83% of secondary GBM tumors whose clinical presentation involves progression from evidence of a lower-grade lesion, and in younger patients with a mean age of 33 years old, substantially lower than *IDH1* wild-type GBM tumors (53 years old) [197]. Patients with GBM harboring *IDH1* mutations demonstrated a significantly improved overall survival of 3.8 years compared to 1.1 years for *IDH1* wild-type GBM patients [197]. Expanded sequencing analyses involving 939 CNS and non-CNS tumors revealed an incredible prevalence of *IDH1* and more rarely *IDH2* (R172G/M/K substitutions) with a striking specificity to grades II-IV gliomas including oligodendrogliomas, astrocytomas, mixed oligoastrocytomas and secondary GBM occurring in younger adult patients ranging in mean age 20-45 years [287]. Enzymatic assays of oligodendroglial cell line lysates transfected with *IDH1* and *IDH2* mutant genes indicated a dramatic reduction of NADPH production associated with the mutant enzymes [287]. Studies in acute myeloid leukemia (AML) also revealed recurrent mutations in *IDH1/IDH2* demonstrating them as oncogenes in a variety of brain and hematological cancers [176]. These seminal data point to *IDH* mutations as highly frequent alterations in gliomas and other cancers and outline their use as a diagnostic and prognostic marker in these groups of diseases.

Initial studies described above pointed to abrogated NADPH production associated with *IDH* mutant enzymes. Strikingly, *IDH1* mutation was shown soon after to yield neomorphic enzyme activity, enabling the NADPH-dependent conversion of the product α -keto-glutarate to the R-enantiomer of 2-hydroxyglutarate (2-HG) [56,274]. 2-HG production is also elevated in the genetic syndrome D-2-hydroxyglutaric aciduria due

to a mutation in the enzyme D-2-hydroxyglutarate dehydrogenase which catalyzes α -keto-glutarate to 2-HG conversion [247]. Strikingly, patients with D-2-hydroxyglutaric aciduria have been associated with increased glioma risk and other neuropathologies such as leukoencephalopathy [149,3]. 2-HG can be detected in brain tissue and cerebrospinal fluid in D-2-hydroxyglutaric aciduria patients [149], and is elevated in human malignant glioma samples harboring *IDH1* mutations [56]. This data strongly supports the theory that oncogenesis associated with *IDH1* mutation may be mediated through production and accumulation of the oncometabolite 2-HG.

A variety of hypotheses were initially proposed with regard to the mechanism of action of 2-HG and its impact on various enzymatic functions. Seminal work elucidated that 2-HG blocks the activity of α -keto-glutarate-dependent dioxygenases including histone lysine demethylases and TET family 5-methylcytosine (5mC) hydroxylases through its action as a competitive inhibitor of these enzymes [286,45]. In glioma tumors, *IDH1* mutation was associated with increased levels of histone methylation and reduced 5-hydroxymethylcytosine (5hmC) levels, illustrating the global impact of *IDH1* R132-mutation on the epigenome [286].

Numerous studies have since emerged focusing on the genome-wide epigenomic effects of *IDH1* mutations. As discussed above, TCGA molecular profiling studies conducted in GBM demonstrated that *IDH1* mutant tumors formed a distinct clinical and biological subgroup of GBM, with largely proneural expression signatures [262]. Further work conducted by TCGA utilizing DNA methylation arrays demonstrated distinct clustering of *IDH1* mutant HGGs, which exhibited global DNA hypermethylation, associating the glioma-CpG island methylator phenotype (G-CIMP) with these tumors

[192]. *IDH1* mutation was shown to be sufficient to create G-CIMP in cells demonstrating the immense impact of this mutation on global DNA methylation [255]. Concurrent studies demonstrated increases in methylation at numerous histone 3 (H3) lysines (K) such as H3K27, H3K36, H3K4 and H3K9 and inhibition of cellular differentiation by ectopic expression of *IDH1* mutation [168]. Increased levels of histone methylation were also seen in human tissue samples harboring *IDH1* mutations [168]. Increased histone methylation at these critical lysines was shown in recent knock-in mouse models of *IDH1* mutation, accurately recapitulating the epigenomic impact of the disease [226]. Recent reports studying a targeted inhibitor highly selective for mutant IDH1 R132H (AGI-5198) have emerged showing that it is capable of reversing histone methylation and blocking glioma cell growth, without changes in global levels of DNA methylation [219]. Taken together, although the effects of IDH1 mutant expression on the epigenome are profound, other epigenome-independent mechanisms of oncogenesis remain a mystery.

Histones are assembled as octamers involving two copies each of H3, H4, H2A and H2B, and are critical components of the nucleosome. They function to properly package our DNA into chromatin and regulate the expression of our genes (reviewed in [59,58]). As discussed above, histone marks, notably methylation at critical lysines, can be altered in cancer. Young adult tumors with a secondary GBM clinical presentation were shown to harbor *IDH1* mutations leading to increased histone methylation and establishing widespread epigenomic defects as a novel mechanism of tumorigenesis in GBM [197,168]. In pediatric and adolescent GBM patients, the mutational picture also points to epigenomic dysregulation, however in a manner at the time, unseen in any other

human disease to date. Our group, and simultaneously reported by another independent group, identified recurrent somatic mutations in the histone variant H3.3 encoded by *H3F3A* at two perfectly conserved residues across species in 31% of pediatric GBM (Figure 1.6) [231,281]. Recurrent mutations in histone genes had never before been identified in association with any other human disease. These mutations resulted in lysine 27 to methionine (p.Lys27Met, K27M) and glycine 34 to arginine or valine (p.Gly34Arg/Val, G34R/V) amino acid substitutions at these positions and were only present in tumor genomes and not matched constitutional DNA from patients [231,281]. A large expanded cohort of 784 gliomas of all ages and histopathological grades (WHO I-IV) confirmed the specificity of *H3F3A* mutations to pediatric GBM and not adult GBM or low-grade gliomas [231]. K27M mutations in H3.3 and histone variant H3.1 (encoded by *HIST1H3B*) were also shown to be present in 71-78% of diffuse intrinsic pontine gliomas (DIPGs) [281,136]. *H3F3A* K27M mutations characterized pediatric tumors arising in the thalamus, a deep diencephalic structure difficult to access for complete surgical resection [231]. K27M mutant thalamic high-grade tumors arising in young adult patients with an age range of 17-46 years have also been reported [4], demonstrating a strong association of thalamic and other midline structures such as the brainstem, and a propensity for K27M mutations. The frequency and specificity of these mutations in histones strongly supports their use in diagnosis and as biomarkers for these HGG tumors in children and younger patients.

Although initial data convincingly established the prevalence and specificity of *H3F3A* mutations to HGG tumors arising in the pediatric years, additional sequencing studies have emerged across a variety of human cancers. *H3F3A* G34R mutations have

also been identified in 11% of another subtype of CNS tumor, termed primitive neuroectodermal tumor (PNET) [84]. In non-CNS cancers, *H3F3A* mutations have remained absent or extremely scarce other than a few exceptions. In a large dataset of 1004 human leukemia and lymphoma samples, only a single *H3F3A* mutation was identified in a case of childhood B-cell acute lymphoblastic leukemia (B-cell ALL) [112]. This mutation was not present at hotspot residues identified in GBM, but rather in an intron and as yet has unknown significance [112]. Although very rare, a recent study identified K27-mutations in T-cell ALL in 3 out of 102 cases (3%) [9]. In a study of solid tumors comprising osteosarcoma (13 cases), myxoid liposarcoma (8 cases) and synovial sarcoma (7 cases), *H3F3A* mutation was identified in a single osteosarcoma tumor, encoding a novel glycine to tryptophan amino acid substitution at position 34 (G34W) [123]. A large study of solid tumors encompassing gastric, colorectal, breast, prostate, ovarian carcinomas and many other cancer types totaling 1351 cases identified only a single isolated case of *H3F3A* mutation, yielding another novel substitution of glycine to glutamate (G34E) at position 34 in a colorectal carcinoma sample [113]. However, a seminal study of chondroblastoma and giant cell tumors of bone (GCT) revealed a striking frequency of H3.3 mutations in these tumors of 95% and 92% respectively [16]. H3.3 mutations in chondroblastoma tumors were largely present in *H3F3B*, the other one of two genes which encodes H3.3, in 68/77 cases, but also in *H3F3A* in 5/77 cases, both encoding amino acid substitutions of lysine to methionine at position 36 (K36M) [16]. GCT cases involved coding mutations in *H3F3A* at position 34 with the vast majority encoding the G34W substitution, and an isolated case of glycine to leucine (G34L) substitution [16]. This group sequenced additional bone and cartilagenous tumors and

identified two G34R mutant osteosarcomas in each *H3F3A* or *H3F3B* (2%, 2/100 cases), a single mutant clear-cell chondrosarcoma with K36M mutation in *H3F3B* and a conventional chondrosarcoma with K36M mutation in *H3F3A* (1%, 1/75 cases) with no mutations identified in chondromyxoid fibroma (0/43), chordoma (0/25) or chondroma (0/7) [16]. Most strikingly, mutant allele fraction in chondroblastoma and GCTs analyzed by cell sorting revealed presence of the H3.3 mutation exclusively in cells of the stromal compartment, and not osteoclasts, implicating the stroma as the source of neoplastic cells in these tumors [16]. Taken together, these data point to the exquisite cell type specificity of H3.3 mutations and amino acid substitutions at hotspot residues.

H3F3A mutations were found to occur in association with mutations in cell cycle regulatory genes and chromatin remodelers in pediatric GBM. *H3F3A* G34R/V mutations co-occurred with *TP53* and *ATRX* mutations in 100% of cases initially identified, and a large subset of *H3F3A* K27M mutant tumors also harbored these defects (Figure 1.6) [231]. *ATRX* or its co-factor *DAXX*, are H3.3 chaperones operating at pericentromeric or telomeric chromatin and were found to be mutated in 31% of tumors, yielding 44% of pediatric GBM tumors with at least one defect in the H3.3-*ATRX*-*DAXX* pathway (Figure 1.6) [231]. Tumors that had mutations in *H3F3A/ATRX/TP53* genes demonstrated significantly increased copy number alterations (CNAs), demonstrating that these mutations were associated with genome instability and structural variation [231]. In addition, K27M and G34R/V mutant tumors demonstrated distinct gene expression profiles demonstrating that they correlated with different molecular programs [231]. Tumors harboring *ATRX/DAXX* mutations correlated with alternative lengthening of telomeres (ALT) in a large cohort analyzed by fluorescence *in situ* hybridization (FISH)

on tissue microarray (TMA) [231]. Taken together, initial data identifying and characterizing *H3F3A* mutations pointed to newly defined subgroups of pediatric GBM with distinct features.

Mutations in H3.3 in early reports appeared to delineate novel subgroups of pediatric GBM with distinct features. The TCGA had utilized DNA methylation profiling to subgroup *IDH1* tumors and assigned them the designation G-CIMP due to their levels of global hypermethylation as one of three initial epigenetic subgroups of HGG [192]. Encompassing 210 GBM tumors across the lifespan including a substantial pediatric GBM cohort, Sturm and colleagues in collaboration with our laboratory were able to define six clinical and epigenetic subgroups of GBM (Figure 1.7) [250]. Three of these subgroups were importantly delineated by epigenetic driver mutations identified above, namely H3.3 K27M, G34R/V or *IDH1* hotspot mutations, and characterized GBM tumors arising in the childhood, adolescent and young adult years [250]. In addition, incorporation of clinical data from GBM tumors revealed distinct associations of K27M mutations with midline regions encompassing the thalamus, brainstem including pons, spinal cord and cerebellum and G34R/V mutations to areas of cerebral cortex (Figure 1.8) [250]. Gene expression profiling of K27M and G34R/V mutant tumors demonstrated similarity to mid- to late-stages or early- to mid- fetal stages of fetal development of striatum and thalamus or striatum and neocortex development respectively [250]. This comparison, with a large published dataset of 1340 transcriptomes involving a comprehensive array of developing and adult brain regions [129], demonstrates a potential unique cell of origin or developmental window of tumorigenesis of H3.3 K27M or G34R/V tumor development. Consistent with this, Sturm and colleagues utilized

expression profiling in conjunction with immunohistochemical staining to identify differential lack of FOXG1 or OLIG2 expression as diagnostic surrogate markers for K27M and G34R/V tumors respectively [250]. Distinct survival profiles were seen for H3.3 and *IDH1* mutant tumors, with better overall survival seen for *IDH1* mutant and G34R/V mutant GBM, and poor survival seen for K27M mutant tumors (Figure 1.8) [250]. This association is also seen in DIPG tumors, with poor overall survival seen for K27M mutant DIPG patients [136]. These data illustrate the importance of tumor subgrouping in GBM as tumors occurring in different brain regions with distinct mutations can undergo unique disease course.

H3.3 K27M and G34R/V mutations were shown above to correlate with distinct global epigenomic profiles, distinct clinical variables and gene expression signatures. The mechanism of action of the effects of K27M and G34R/V mutant histones are still largely unknown, however a number of notable results have allowed us to gain insight into their oncogenic functions. Work by Lewis and colleagues and other independent groups, has elucidated novel avenues of epigenomic dysregulation associated with H3.3 mutations (Figure 1.9) [161,39,261]. Human GBM and DIPG harboring H3.3 and H3.1 mutations were shown to have reduced overall levels of trimethylated H3K27 (H3K27me3) [161], without any corresponding decrease in the H3K27 trimethyltransferase *EZH2* expression [261]. Murine DIPGs elicited in a PDGF brainstem glioma model which expressed H3.3 K27M transgenes recapitulated reduced H3K27me3 levels [161]. In addition, human and murine tumors, and cells ectopically expressing H3K27M transgenes showed elevated levels of acetylated H3K27 (H3K27ac) [161]. Additional reports of decreased dimethylated H3K27 (H3K27me2) have been shown in H3.3 K27M mutant primary

tumor cells [39]. Moreover, this effect was dependent on precise amino acid identity of substitutions with only long hydrophobic side-chain containing methionine (M) and isoleucine (I) at lysine 27 (K27M and K27I) capable of decreasing H3K27me₃ when expressed ectopically [161]. Utilizing *in vitro* assays, Lewis and colleagues were able to demonstrate that this effect could be mediated in *cis* and *trans* through inhibition of the EZH2-containing Polycomb Repressor Complex 2 (PRC2) and was dependent specifically on interactions with EZH2 (Figure 1.9) [161]. Further to this, exploration of the inhibition of EZH2 and SET-domain containing enzymatic activity demonstrated K-to-M amino acid substitutions at H3K9 and H3K36 to inhibit H3K9me_{2/3} and H3K36me_{2/3}, establishing these mutations as novel mechanisms to block enzymes which methylate these residues [161]. Although global levels of H3K27me₃ are diminished in H3.3 K27M mutant cells, residual H3K27me₃ genomic binding is observed at H3K4me₃-containing loci, termed bivalent genes [39]. Through Gene Ontology (GO) pathway analysis of chromatin immunoprecipitation-sequencing (ChIP-seq) data identifying genes targeted by bivalent marks, cancer pathways, embryonic morphogenesis and pattern specification pathways amongst others emerged [39]. Further work studying large cohorts of pediatric HGGs demonstrated that inhibited PRC2 H3K27 methyltransferase activity and overall levels of DNA hypomethylation contribute to gene expression associated with K27M mutation [17]. However, although H3.3 K27M lentivirally-transduced cell lines recapitulated reduced H3K27me₃ binding similar to human tumors, no consistent changes in DNA methylation or gene expression accompanied this [17]. This finding is similar to lack of DNA methylation changes seen in *IDH1*-mutant glioma cells treated with an IDH1 R132H inhibitor discussed above

[219]. Although DNA methylation patterns have been shown to be strongly associated with H3K27me3 marks [25,244], these data argue for caution in isogenic cell models of epigenetic driver mutations discussed herein. In summary, H3.3 K27M mutations exert robust genome-wide influences on the levels and distribution of H3K27me3 histone marks. They are also associated with dramatic changes in DNA methylation and future modeling of this mutation will require involvement of both of these characteristics.

To date, most efforts have focused on K27M mutations, with much less known about the impact of G34R/V mutations. Sturm and colleagues identified a global CpG hypomethylator phenotype (CHOP) in G34-mutant tumors and proposed the striking hypomethylation notably at subtelomeric regions near chromosome ends to potentially underlie ALT seen in these tumors [250]. Initial reports of H3.3 G34R/V mutations proposed potential effects of this mutation on adjacent residue H3K36 histone marks and demonstrated very preliminary data to this effect [231]. Further more comprehensive histone profiling studies revealed no changes in global levels of H3K27me2/3 or H3K36me3 in association with H3.3 G34R/V mutations (Figure 1.9) [39,161]. However, purified epitope-tagged H3.2/H3.3 G34R/V mono- and oligo-nucleosomes (more than 95% involving 4-5 nucleosomes) revealed decreases in K36me2 and K36me3 of approximately 2.7 and 18.5 fold respectively compared to wild-type [161]. In addition, *in vitro* assays revealed an impaired ability of the human recombinant H3K36 methyltransferase SETD2 (also known as SET2) to methylate K36 in the presence of H3.3 G34R/V heterotypic mononucleosomes [161]. ChIP-seq data studying H3K36me3 marks demonstrated differential binding in a cell line, KNS42 harboring G34V mutation and demonstrated that this may drive expression of programs of forebrain development

and self-renewal, including genes such as *MYCN* [20]. In summary, these data demonstrate a potent *cis*-regulated effect of G34R/V mutations on K36 methylation within mono- and oligo-nucleosomes that may drive novel programs linked specifically to forebrain/cortical tumorigenesis.

1.4 Telomerase-dependent and independent telomere dysregulation in adult and pediatric gliomas

Telomeres cap the ends of our DNA and are critical mediators of cellular longevity as well as maintaining the integrity of our genomes [99,6]. Human telomeres are structured stretches of the repetitive 6-nucleotide sequence 5'-TTAGGG-3' located at the ends of chromosomes and function to safeguard elements in our genome by absorbing the inevitable shortening which comes with lagging strand synthesis in DNA replication as dividing cells age [159,188,99,6]. Telomeric DNA is maintained in cells by the ribonucleoprotein complex telomerase, comprised of telomerase reverse transcriptase, TERT, and an RNA molecule termed TERC or TR (telomerase RNA) utilized as a template for telomere repeat synthesis ([89] and reviewed in [7]). Telomerase activity has been found to be elevated in cancer and germ cells [142], and taken together with studies demonstrating telomere shortening with cellular ageing [99,6], is thought to mediate the immortal nature of proliferating cancer cells.

Elevated *TERT* mRNA levels and activity has been identified in gliomas [21]. Furthermore, Genome-Wide Association Studies (GWAS) have identified a subset of polymorphisms associated with increased risk of glioma susceptibility, two of which map to telomere regulatory genes: *TERT* (5p15.33, rs2736100) which discussed above, codes for the enzymatic component of telomerase, and *RTEL1* (20q13.33, rs6010620)

[236,210,280], or *regulator of telomerase elongation helicase 1*, a gene involved in maintaining genome stability through suppression of homologous recombination [13]. A recent meta-analysis of GWAS data identified another SNP associated with glioma risk near the key telomere component *TERC* (or TR, rs1920116), strongly demonstrating that polymorphic variants affecting telomere length at a subset of loci can influence glioma susceptibility [269]. Coding mutations affecting telomere regulation have recently been identified recurrently in gliomas through telomerase-dependent and independent pathways [102,231,166,131,114,19,140,264,139]. Core promoter mutations occurring at -124bp and -146bp (positions hg19: 1,295,228 G>A and hg19:1,295,250 G>A respectively) upstream of the *TERT* ATG start site have recently been uncovered in a large proportion of sporadic melanomas and have been shown to correlate with increased *TERT* expression levels due to formation of a consensus binding site for Ets/TCF transcription factors [105,106]. Studies examining large cohorts of tumors of the central nervous system (CNS) including gliomas, have uncovered *TERT* promoter mutations most frequently in adult primary GBM, with a prevalence reported as high as 83% [140,264,148]. In addition, these studies have demonstrated an association of the occurrence of *TERT* promoter mutations with higher mean patient age at diagnosis, more often characterizing adult over pediatric disease [140,264,148], a phenomenon also recapitulated in medulloblastoma, with adult sonic hedgehog (SHH) subtype tumors demonstrating the highest incidence amongst subgroups [216].

Pediatric GBM tumors do not demonstrate as high a rate of *TERT* promoter mutations (11% of 19 tumors analyzed in [140]), although they do demonstrate a telomere dysregulation phenotype known as alternative lengthening of telomeres (ALT)

in 44% of cases [102]. ALT was first described in tumors and cell lines that had long telomeres, without evidence for increased telomerase activity [30,29,28]. The ALT mechanism was later shown to occur through homologous recombination and copy switching in immortalized human cell lines [62]. Overall in GBM, ALT was shown to be present in 25% of cases and correlated strongly with better median overall survival of 542 days compared to 247 days for GBM patients with normal telomeres, a substantial difference that was independent of age [94]. More recently, ALT was shown in strong association with *ATRX* or *DAXX* mutations in gliomas including pediatric GBM [102]. *ATRX*, termed *α-thalassemia/mental retardation syndrome X-linked*, is an ATPase/helicase of the SWI/SNF family that has functions as a chromatin remodeler and histone H3.3 chaperone at telomeres [160]. *ATRX* along with its co-factor, *DAXX*, *death domain associated protein*, functions importantly to suppress transcription of telomeric RNA through incorporation of H3.3 at telomeres [85]. These mechanisms operate independently of H3.3 deposition at active and repressed genes, mediated by another histone chaperone HIRA [85]. Pediatric GBM and DIPG tumors are characterized by recurrent mutations in histone H3.3 at critical residues, K27M and G34R/V that occur in conjunction with mutations in *ATRX/DAXX* [231,136]. *ATRX* mutation or loss of expression correlates strongly with ALT in pediatric GBM [231], but not in an *ATRX*-mutant adult grade II-IV gliomas [166]. Killela and colleagues showed strikingly that *ATRX* and *TERT* mutations are mutually exclusive and govern independent mechanisms for telomere dysregulation in gliomas [140]. These and other cohorts [231,148] demonstrate that *ATRX* mutations (associated strongly with ALT) occur more frequently in pediatric GBM, whereas *TERT* promoter mutations mediating increased telomerase

expression dominate adult primary GBM tumors. Mechanisms leading to ALT in adult grade II and III appear to be unclear due to lack of correlations seen with *ATRX* mutations, suggesting other putative mechanisms for ALT observed in these tumors [166]. Within pediatric DIPG and GBM cohorts, *ATRX* mutations tended to occur in older children in the adolescent years [136,231,250]. These results primarily point to critical defects in telomere maintenance pathways, both telomerase-dependent and independent, in pediatric and adult gliomas. GBM or DIPG tumors arising in adolescents harbor mutations in *ATRX* that correlate strongly with ALT (telomerase-independent) in these tumors. GBM tumors occurring in adults frequently harbor mutations in the core promoter of *TERT* leading to elevated telomerase activity and longer telomeres. Monogenic telomere disorders in various genes have been shown to manifest at differing ages and with a variety of phenotypes ranging from idiopathic pulmonary fibrosis to hematologic cancer (reviewed in [7]), with genetic anticipation worsening with generations observed [8,266]. Taken together, somatic mutations affecting the telomere machinery that are found in GBM tumors can arise via telomerase-dependent and independent pathways and may hijack the normal regulation of telomeres with cellular aging.

1.5 Mitogen-activated Protein Kinase (MAPK) Pathway Activation in Gliomas

Pilocytic astrocytomas (PAs) comprise the most common primary brain tumor subtype in children (Figure 1.3) [138]. Unlike the dramatic inter-patient heterogeneity seen above for adult and pediatric HGGs, work over the past few years has implicated MAPK cascade hyper-activity through *BRAF* activation as being critical in the

pathogenesis of virtually all PA tumors (Figure 1.10) [202,121,122,73,12,109,240,46,118,291]. *BRAF* gene duplication at chromosomal region 7q34 was first shown using array-based comparative genomic hybridization (aCGH) methods to be a dominant mechanism of MAPK activation through increased copy number and subsequent expression of *BRAF* [202,12]. Landmark studies soon after demonstrated that tandem duplication of 7q34 created a novel *BRAF* in-frame fusion with the uncharacterized gene, *KIAA1549*, eliminating the N-terminal auto-regulatory region of BRAF, allowing for constitutive activity of the kinase domain in the fusion protein [121]. *In vitro* kinase assays comparing *KIAA1549-BRAF* transfected cells demonstrated similar levels of increased kinase activity as other well-characterized *BRAF* V600E constitutive mutants [121]. In addition, *KIAA1549-BRAF*-infected NIH 3T3 cells demonstrated increases in anchorage-independent growth in soft agar assays, further supporting the role of this fusion in oncogenesis and transformation of cells [121]. *KIAA1549-BRAF* fusion was shown to define the majority of PA tumors analyzed amounting to 66% of 44 tumors, with a striking specificity of 98.5% to PA in an expanded tumor set including 406 gliomas encompassing diffuse (grade II) and anaplastic (grade III) astrocytomas, GBM, oligodendroglial and mixed oligoastrocytic tumors [121]. These fusion genes had a variety of genomic breakpoints: the majority were represented by *KIAA1549* exons 1-16 fused to *BRAF* exons 9-18 (69%, 20/29 fused cases), with the remainder of initial cases being *KIAA1549* exons 1-16 fused to *BRAF* exons 11-18 (24%, 7/29) and *KIAA1549* exons 1-15 to *BRAF* exons 9-18 (7%, 2/29), all of which could be detected by RT-PCR [121]. Taken together, *KIAA1549-BRAF* fusion identification

suggests an important new avenue for diagnostic and potentially therapeutic development in PA tumors.

Many additional reports confirm the role of *BRAF* and notably the MAPK pathway as a central mediator of gliomagenesis in PA tumors. Novel fusions, gain-of-function point mutations, loss-of-function mutations and copy number aberrations all leading to MAPK cascade hyper-activation have been reported in many genes (Figure 1.10 and Figure 1.11). Increasingly rare *KIAA1549-BRAF* fusion variants have been reported in isolated cases, encompassing fusion between exons 1-18 and exons 10-18 or exons 1-19 and exons 9-18 of *KIAA1549* and *BRAF* genes respectively [73,157], with an additional single case report of the most recent variant of *KIAA1549* exons 1-16 fused to *BRAF* exons 10-18 [54]. *In silico* reconstructions and functional assays in a subset of cases confirm constitutive activity of fused *BRAF* kinase domains and MAPK activation in these rare fusion-positive PA samples [73,54].

A diversity of *BRAF* and *RAF*-family fusion genes exclusive to *KIAA1549-BRAF* fusions have been identified in PA tumors. Jones and colleagues followed up additional work in identifying *KIAA1549-BRAF* fusion and pinpointed an additional fusion gene, albeit a much more rare event occurring in 1 out of their initial 44 sample cohort [122]. This fusion was present in a copy number gain at chromosomal region 3p25 first seen by aCGH array [119], and involved tandem duplication of the MAPK *RAF1* fused in-frame to *SRGAP3* (*SLIT-ROBO Rho GTPase activating protein 3*) [122]. Reminiscent of *KIAA1549-BRAF* fusion, *SRGAP3-RAF1* fusion was found to retain the kinase domain of *RAF1*, demonstrated increased kinase activity in *in vitro* assays and promoted anchorage-independent growth of NIH 3T3 fibroblasts, confirming it as a novel form of MAPK

activation in PA tumors [122]. Alternative fusion partners have been identified for *BRAF* as well, suggesting in much the same way as for other kinase fusion genes in human cancer, dysregulation of the target kinase domain is the driving force for these rearrangements. These mechanisms are not limited to areas of copy number gain, but can also arise in areas of genomic deletion [46]. Fusion of the *BRAF* kinase domain with another uncharacterized gene at 7q34, *FAM131B*, through an interstitial deletion of approximately 2.5 Mb, was identified in 2.4% of PA, 3 of 125 cases screened [46]. This mechanism similarly eliminated the BRAF N-terminal auto-regulatory sequence, and achieved constitutive MAPK activation and loss of contact inhibition in NIH 3T3 cells [46]. Recent large-scale whole-genome sequencing (WGS) and RNA sequencing efforts have identified a plethora of additional *BRAF* and *RAF1* fusion genes in supratentorial diffuse low-grade astrocytomas including *FXR1-BRAF*, *BRAF-MACF1*, *QKI-RAF1* [291], as well as *RNF130-BRAF*, *CLCN6-BRAF*, *MKRNI-BRAF* and *GNAII-BRAF* fusions in rare cases of PA tumors [118]. Taken together, promiscuous fusion of *RAF*-family kinase domains through a striking diversity of mechanisms constitutes a dominant means of acquiring transforming ability in pediatric PA tumors.

BRAF has emerged as an important oncogene in human cancer. Initial discovery of activating mutations in *BRAF* in 8% (71 of 923 cases screened) of human cancer encompassing primary tumors or cell lines of glioma, melanoma, colorectal cancer and many other types [57], has fueled further investigation into its use as a therapeutic target in oncology. In their seminal study, Davies and colleagues reported *BRAF* V600E (previously V599E in the initial study) in 11% of glioma cell lines studied, with mutation at the hotspot valine 600 residue to a glutamate (V600E) in exon 15 accounting for 80%

of all cases across cancer types [57]. Importantly, cancer cell lines harboring *BRAF* V600E continued to proliferate when treated with a RAS-neutralizing monoclonal antibody, demonstrating that this mutation permitted RAS-independent growth of these cells [57]. Within gliomas, *BRAF* V600E mutation is unevenly harbored amongst histological subtypes, with large-scale sequencing studies demonstrating higher frequencies in WHO grade I gangliogliomas (18%), WHO grade II pleomorphic xanthoastrocytomas (66%) and PA tumors (9%), most commonly in tumors arising outside of the cerebellum [228]. Rare 3bp insertions at codon 598 of *BRAF* have also been reported and have been shown to act similarly to V600E-mutated *BRAF* [122,65,228].

PA tumors can also arise in a variety of genetic syndromes, the most well-characterized of which is known as neurofibromatosis type I (NF1) (reviewed in [42]). NF1 is one of the most frequently encountered autosomal dominant disorders in humans and the locus for NF1, formerly known as von Recklinghausen neurofibromatosis, was first localized to chromosome 17 through several linkage analysis efforts [14,232,233,245,200,256,278,279,86]. Physical mapping studies and eventual positional cloning led to the identification of the entire *NF1* sequence [268,265,36,175]. Homology and functional biochemical assays demonstrated that the gene product of the *NF1* locus was a protein harboring GTPase-activating protein (GAP) activity capable of RAS-GTP hydrolysis and inactivation [285,284,11,179,93]. NF1-associated PA develops uniquely in the optic pathway or brainstem, in contrast to *KIAA1549-BRAF* fused sporadic PA, which occurs overwhelmingly in the cerebellum, demonstrating a neuroanatomical specificity of these alterations along the MAPK pathway (Figure 1.10) (reviewed in

[117,42]). Children developing PA tumors in the context of NF1 tumor predisposition syndrome account for approximately 15-20% of cases (reviewed in [42]). Similarly to *BRAF* fusions and mutations discussed above, *NF1* defects lead to hyper-activation along the Ras/MAPK pathway, although in a loss-of-function manner. Recent reports demonstrate that in the context of NF1 syndrome, somatic inactivating alterations including frameshift mutations, loss of heterozygosity and DNA methylation of the remaining *NF1* allele are sufficient for PA tumorigenesis in NF1 patients [92]. Other inherited genetic syndromes, termed ‘RASopathies,’ arising from mutations along the MAPK axis have also been associated with PA and low-grade glioma tumor development in rare cases [78,224,230,152]. A large analysis of 1941 cases of RASopathies reported in the literature between 1937 and 2010 encompassing Noonan syndrome, Costello syndrome, cardiofaciocutaneous syndrome and LEOPARD syndrome (also termed Noonan syndrome with multiple lentigines, NSML), identified 88 cases of cancer, including 6 cases (0.31% of RASopathy patients) of low-grade glioma [152]. In summary, this demonstrates that inherited genetic syndromes such as NF1 and other RASopathies arising from mutations along the MAPK pathway are associated with low-grade gliomas including PA.

Inherited low-grade glioma predisposition syndromes such as NF1 and Noonan syndrome discussed above provide candidate genes that may be affected by somatic alterations in sporadic cases of PA. Whole-genome sequencing of a large cohort of 96 PA tumors revealed missense mutations in the gene *PTPN11*, which encodes the phosphatase SHP-2, resulting in amino acid substitutions p.E69K and p.E76A located in one of two *Src homology 2* (SH2) domains of the protein [118]. These mutations were present in

2.1% (2/96) tumors screened [118]. Gene expression profiling analysis revealed increased *PTPN11* mRNA levels in 118 PA tumors compared to other low- and high-grade gliomas, and normal fetal and adult brain and non-brain tissues [118]. Germline SHP-2 mutations in Noonan syndrome and somatic mutations in sporadic PA form another MAPK cascade defect contributing to PA tumorigenesis.

SHP-2 mutations did not occur independently in PA tumors, unlike other mutually exclusive alterations in MAPK genes such as *KIAA1549-BRAF* fusion, *BRAF* mutations or *NF1* alterations. Hotspot mutations in the receptor tyrosine kinase gene *FGFR1*, encoding *fibroblast growth factor receptor 1*, were identified in 6% (6/96) cases of PA (Figure 1.11) [118]. These mutations encoded amino acid substitutions p.N546K and p.K656E/D/N/M within tyrosine kinase 1 and 2 (TK1 and TK2) domains respectively of *FGFR1*, and resulted in autophosphorylation of the receptor and activation of downstream MAPK genes [118,291]. A small subset of cases occurred in association with *PTPN11* mutation, however *FGFR1* mutations occurred independently of other MAPK defects, suggesting that they form an additional sufficient hit along the MAPK axis for tumor development [118]. Indeed, additional rare mechanisms of *FGFR1* activation were identified in PA and other diffuse low-grade gliomas, including internal tandem duplication (ITD) of the tyrosine kinase domains (TKD), termed *FGFR1* ITD or Dual-TKD *FGFR1*, also leading to constitutive activation of the receptor and MAPK and phosphoinositide-3-kinase (PI3K) signaling [118,291]. Originally identified in adult GBM tumors [241], *FGFR1-TAC1* fusions were also identified in rare cases of low-grade gliomas [291]. These comprehensive large-scale sequencing projects have

importantly shown that pediatric PA tumors are affected by MAPK alterations in all cases, and have classified it as a ‘single-pathway’ disease.

1.6 Aneuploidy and chromothripsis phenotypes in adult and pediatric brain tumors

As Hanahan and Weinberg have proposed in their seminal reviews, cancer is a disease encompassing many dysregulated hallmarks including genomic instability [95,96]. Thus far we have described major mutations, gene fusions and epigenomic alterations at play in adult and pediatric high- and low-grade gliomas. A largely mysterious phenotype present in virtually all cancers including brain tumors is one involving numerical chromosomal abnormalities termed aneuploidy [40,88]. The role that individual aneuploid chromosomes play in diverse cell types is largely unknown, however the undeniable presence of non-random aneuploidy and its frequency in many hematological and solid tumors is striking (reviewed in [88]). Chromosomal instability (CIN), which reflects the rate of genomic change, has been associated with aberrant function of proteins involved in proper chromosomal segregation including those involved in microtubule dynamics, centrosome number and the spindle assembly checkpoint (Figure 1.12) [88]. Improper chromosomal segregation can result in cell death, or in certain cases cell survival in a limited number of cases including germline genetic syndromes and cancer [88]. Defects in proteins such as p53 and p21 may then permit the growth of aneuploid cells [253]. Genetic syndromes involving aneuploidy such as Down’s syndrome (constitutional trisomy 21) and rare mosaic variegated aneuploidy (MVA) demonstrate an increased incidence of and are associated with various forms of cancer [88]. MVA in humans is caused by loss-of-function mutations in the spindle

checkpoint gene *BUB1B* (which encodes BUBR1) and is associated with chromosomal gains and losses (aneuploidy) and a variety of other phenotypes including childhood cancer [97]. MVA has been associated with embryonal rhabdomyosarcoma, leukemia, Wilms tumor, medulloblastoma, an uncategorized intraorbital tumor in an isolated case as well as adult-onset gastrointestinal neoplasia [97,5,143,124,225], demonstrating a strong association between aberrant spindle checkpoint gene function, aneuploidy and adult and pediatric cancer. Patients with MVA show defects in cerebellar vermis development and have an enlarged posterior fossa; with knockdown studies in the medaka fish strongly implicating BUBR1 in cerebellar development and left-right asymmetry [184]. Taken together, genetic syndromes such as MVA involving aneuploidy are associated with abnormal development, CNS abnormalities and a variety of cancers.

Changes in ploidy including aneuploidy have been reported in brain tumors including gliomas. In the childhood cancer medulloblastoma, Group 3 and 4 classified tumors have been reported with tetraploidy (4n) as a frequent early initiating event in tumorigenesis [120]. In GBM tumors, mutations and copy number losses leading to loss-of-function of a critical member of the cohesin complex, encoded by *STAG2*, are associated with aneuploidy [243]. In addition in hypertriploid and hypertetraploid GBM cell lines, somatic cell gene targeting approaches to correct mutant *STAG2* resulted in amelioration of chromosome numbers [243]. Converse experiments introducing mutant *STAG2* in wild-type HCT-116 cells resulted in chromosomal defects [243]. Other alterations present in rare cases of GBM tumors have been associated with aneuploidy. Recurrent fusions involving *FGFR* and *TACC* genes have been reported in GBM, low-grade gliomas and a variety of human cancers [241,291,283]. *FGFR-TACC* fusion genes

demonstrated constitutive FGFR1/3 kinase activity and transforming ability when expressed ectopically [241]. Of note, FGFR1-TACC1 or FGFR3-TACC3 demonstrated subcellular localization to mitotic spindle poles and a capacity to induce chromosomal segregation defects and aneuploidy, with inhibition of FGFR capable of correcting aneuploid defects [241]. Strikingly, numerical defects were seen in a non-random fashion in cells analyzed by spectral karyotyping (SKY) favoring gains in chromosomes 7, 18, 19, 20 amongst others [241]. Specific non-random whole chromosomal aneuploidies have been detected with unknown significance in PA tumors utilizing aCGH technology [119]. Notable chromosomal gains reported included chromosomes 5, 7, 11, 15 and 20, with the most common affecting chromosomes 5 and 7 [119]. In addition, older patients with PA demonstrated an increased frequency of aneuploid genomes, illustrating a relationship with age [119]. Mechanisms leading to the formation or maintenance of aneuploidy in PA are largely unknown, notably given the paucity of reported mutations or losses of *TP53* in this tumor [118], which would otherwise permit the growth of aneuploid cells [253]. Other p53 pathway regulators have also been reported in association with age-related aneuploidy in tumor cells. MDM2, a central regulator of p53 protein levels, has been shown to induce chromosomal instability in B-lymphocytes [271], and in addition, this effect has proven to be p53-independent [23]. Mdm2 transgenic mice strikingly demonstrated increased chromosomal instability associated with aging [171]. Interestingly, Mdm2 expression correlated with an increase in the rate of whole chromosomal gains, but not losses in aging mice [171], illustrating a specific mechanism that can lead to an aneuploid state harboring greater than diploid number of chromosomes. Taken together, these data demonstrate that human cancers including

high- and low-grade gliomas demonstrate aneuploidy that can be promoted in a subset of cases by specific genetic alterations affecting the mitotic spindle apparatus or the cell cycle.

Thus far we have discussed mechanisms leading to the development of numerical chromosomal abnormalities in cancer. The impact of aneuploid chromosomes themselves and their direct role in tumorigenesis is controversial and largely unknown [88]. Recent landmark studies have shed light on a novel mechanism with which cancer cells acquire genomic alterations, termed chromothripsis [246,150]. Stephens and colleagues describe chromothripsis in their initial report as the massive localized shattering and subsequent repair of a chromosomal region in a single event, rather than the traditional step-wise evolution of genomic alterations in cancer [246]. This mechanism was initially reported in 2-3% of 746 cancer cell lines and 2792 cancer samples studied and was especially frequent amongst bone tumors (25%) [246]. Further studies revealed chromothripsis in association with *TP53* mutation in medulloblastoma [212]. Analysis of medulloblastoma tumors from patients with Li-Fraumeni syndrome (LFS), a genetic syndrome caused by germline mutations in *TP53*, revealed a striking number of complex rearrangements consistent with chromothripsis [212]. An association of somatic *TP53* mutation and chromothripsis was also seen specifically in sonic hedgehog (SHH) subtype medulloblastoma tumors, as well as *Ptch* +/-; *Trp53* -/- mutant mice allograft medulloblastoma tumors, strongly implicating chromothripsis in this tumor subtype [212]. Oncogenes previously identified in medulloblastoma are often amplified and altered due to chromothriptic events, illustrating an important link between this mechanism and tumorigenesis [212,191]. To investigate associations of germline *TP53*

mutation and LFS-associated tumors and chromothripsis, Rausch and colleagues analyzed additional LFS tumors including GBM and identified evidence for chromothripsis [212]. A mechanism linking whole chromosomal gain and chromothripsis has also been proposed. Massive DNA breakage resembling chromothripsis is seen in small structures termed micronuclei, which contain lagging chromosomes from mitotic errors [50]. Crasta and colleagues identify defective DNA replication in micronuclei and subsequent “pulverization” of chromosomes within these structures [50]. As errors in mitosis occur, micronuclei containing chromosomes can undergo massive DNA damage, establishing a potential mechanism for the localized shattering of chromosomes observed in chromothripsis [50]. In summary, although the roles of aneuploidy and chromothripsis in tumorigenesis are largely unknown, they represent mechanisms that can lead to the accumulation of genomic defects, a hallmark of cancer.

1.7 Rationale and hypotheses of the study

Throughout the introductory chapter of this dissertation we have discussed pediatric brain tumor epidemiology, treatment and patient outcome. We have accentuated the significant morbidities associated with tumors requiring intensive multimodal treatment strategies during the developmental pediatric years. Based on the significant mortality observed in patients with HGGs, specifically GBM, and the sequelae associated with current treatments, novel approaches are required to improve outcome.

Our lab and others have elucidated important molecular differences of pediatric and adult HGG and GBM tumors (reviewed in [249]). Of note, next-generation sequencing studies have led to the identification of mutations in histone variant H3.3 (*H3F3A*) at K27M or G34R/V in a large proportion of pediatric GBM and DIPG

[231,281]. Moreover, studies involving GBM tumors across the lifespan revealed distinct epigenetic subgrouping of tumors into six groups, three of which were delineated by H3.3 K27M, G34R/V or *IDH1* mutations and younger patients [250]. Clinical correlates of these epigenetic subgroups revealed a striking specificity for G34R/V and *IDH1* mutant tumors to occur in cortical areas, whereas midline tumors tended to harbor K27M mutations [250]. Furthermore, distinct H3.3 alterations were associated with additional defects in chromatin remodeling genes, such as *ATRX/DAXX* and critical cell regulatory genes such as *TP53*, illustrating that further genome-wide dissection may reveal mutational subgroups and needed partner hits [231]. Further investigation of pediatric brain tumors in specific areas may allow us to gain better insight into the roles of epigenome dysregulation and associated alterations in their formation.

In the context of PA tumors, these generally tend to occur in the cerebellum with recent studies showing that approximately 80% of cerebellar PA harbor *KIAA1549-BRAF* fusion (reviewed in [117]). Non-cerebellar PA can occur with a diverse set of MAPK-related alterations and in surgically challenging areas, leading to significant patient morbidity [117]. We have seen that comprehensive sequencing studies of PA have revealed that virtually 100% of tumors harbor defects along the MAPK axis, classifying it as a ‘single-pathway’ disease [118,291]. We have also discussed reports of decreased frequencies of *KIAA1549-BRAF* fusion and increased prevalence of an ominous phenotype of aneuploidy in rare adult PA tumors [101,119]. Indeed, individual MAPK alterations may harbor alternate functions independent of MAPK pathway activation. This is supported by data describing *BRAF* fusion and mutation specificity to different pediatric brain tumor types [228]. In addition, as we have seen for HGGs, adult tumors

may harbor distinct genetic alterations, which may promote aneuploid phenotypes.

Further investigation of PA tumors across the lifespan will enable better characterization of the intersection between and role of MAPK alterations and numerical chromosomal anomalies.

With the literature base outlined throughout this chapter, and the aforementioned rationale above, the primary working hypotheses of this thesis are:

1. Pediatric high-grade gliomas harbor epigenetic alterations that are brain region specific and independent of described H3.3 mutations.
2. Pediatric high-grade gliomas harbor alterations in association with epigenetic driver mutations that may be required for tumorigenesis.
3. Age-related phenotypes such as aneuploidy may be promoted or maintained by distinct mechanisms in pilocytic astrocytoma.

1.8 Objectives of the thesis

Given the emergence of reports detailing a highly distinct genomic landscape of pediatric brain tumors, the objectives of this thesis were to further characterize molecular alterations and mechanisms and associate them to specific clinical variables. As such, our general aim was to paint a better molecular picture and describe the need for molecular subgrouping and eventual diagnosis in this heterogeneous and multifaceted group of diseases. The specific objectives of this thesis were as follows:

1. To best investigate additional driver mechanisms at play within a cohort of pediatric HGGs, we aimed to utilize a case-control approach analyzing whole-exome sequencing data to compare these tumors with non-cancer controls. In

- doing so, we enabled an unbiased assessment of the enrichment of particular mutations within the pediatric HGG dataset. Given recent data pointing to dysregulation of the epigenome, we focused our attention on candidates with a chromatin-associated and regulatory role.
2. To further characterize the partner mutations associated with those in the epigenetic machinery, we aimed to utilize an expanded whole-exome sequencing dataset and focused our attention on tumors of the neuroanatomical midline encompassing regions of the thalamus, brainstem, spinal cord and cerebellum where H3 K27M mutations predominate. In addition, to best investigate the actionability of identified targets, we selected a dataset comprised of treatment-naïve tumors including small-needle biopsies.
 3. To elucidate putative mechanisms leading to aneuploidy in PA tumors, we recruited a total of 222 tumors with available whole-chromosomal copy number data and characterized associations with major MAPK alterations and clinical variables in these patients. We additionally performed gene expression profiling, integrating aneuploid data, to investigate mechanisms enriched within aneuploid tumors.

1.9 Figures

Figure 1.1

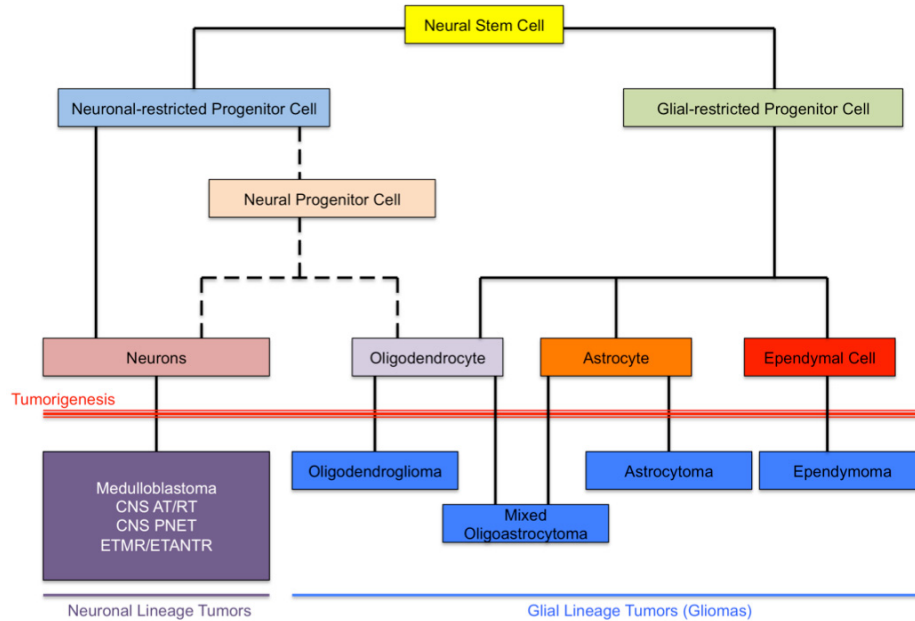


Figure 1.1: Central nervous system cellular development and tumorigenesis.

Cellular development of the central nervous system (CNS) illustrating neural stem cell (NSC), neuronal and glial differentiation pathways and restricted progenitor populations as putative cellular origins for neuronal and glial tumors. AT/RT = atypical teratoid/rhabdoid tumor, PNET = primitive neuroectodermal tumor, ETMR = embryonal tumor with multilayered rosettes, ETANTR = embryonal tumor with abundant neuropil and true rosettes. Adapted with permission from [70].

Figure 1.2

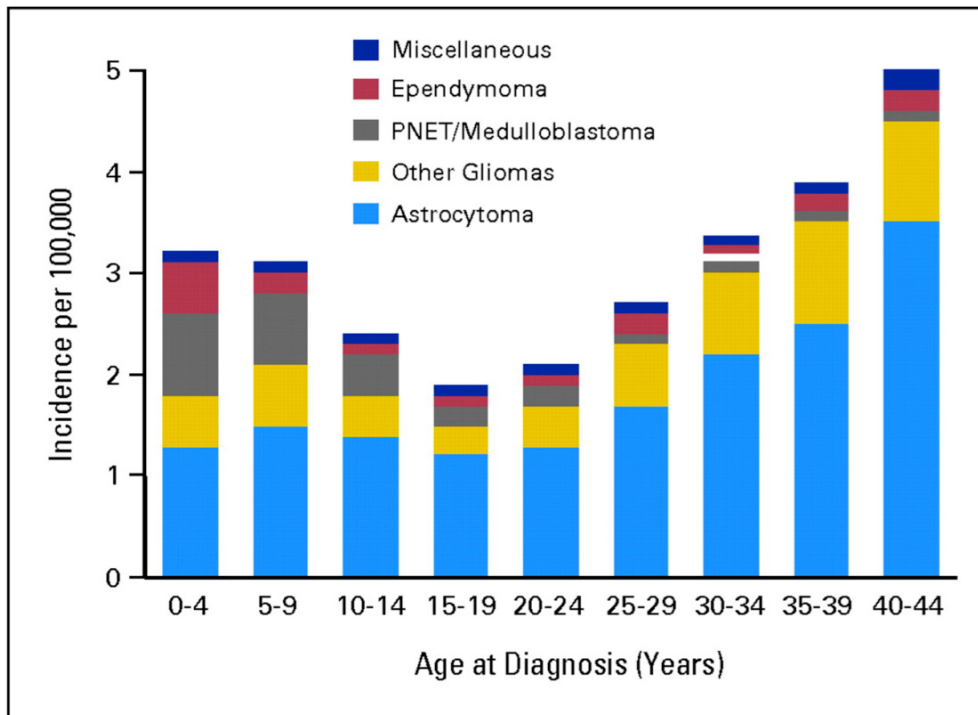


Figure 1.2: Gliomas, including astrocytomas, are the largest subgroup of brain tumor across the lifespan.

Bar representation of incidence per 100,000 distributed based on age demonstrating that in all age groups considered, gliomas and notably astrocytoma subtypes are the most common subgroup of brain tumor. Adapted with permission from [138].

Figure 1.3

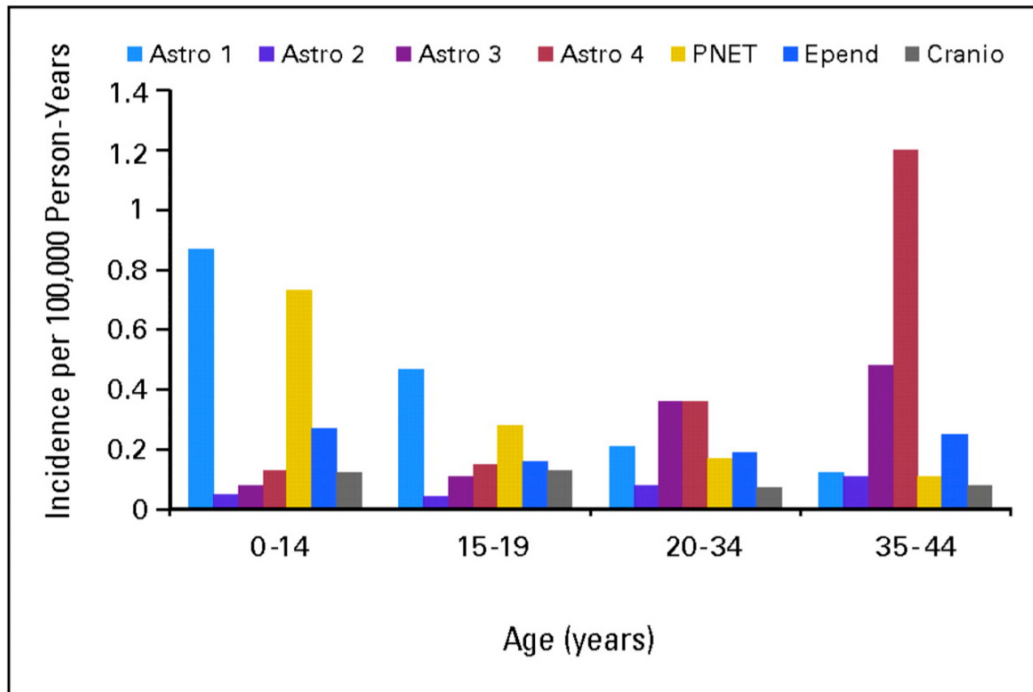


Figure 1.3: Astrocytoma subtype distribution across the age spectrum.

Graphical representation of histopathological grades of astrocytoma, designated ‘Astro 1’ (pilocytic astrocytoma, PA) through ‘Astro 4’ (glioblastoma, GBM) and other brain tumors demonstrating that PA tumors are the most common subtype within the pediatric years and GBM tumors are more frequent in adults. Adapted with permission from [138].

Figure 1.4

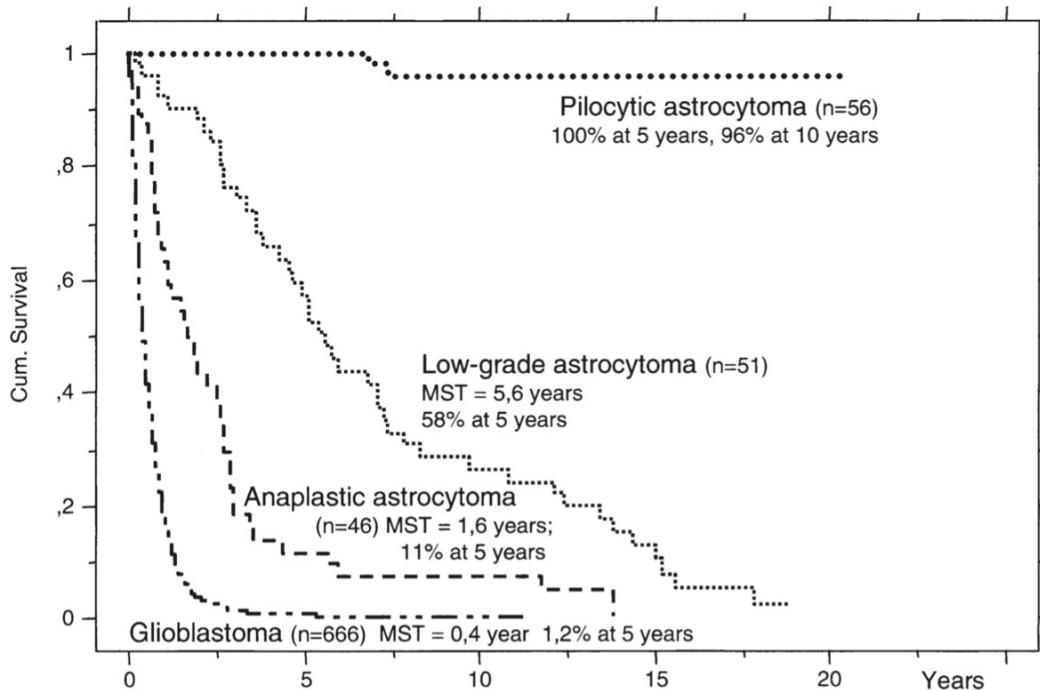


Figure 1.4: Survival of patients with different histological grades of astrocytoma.

Kaplan-Meier analysis of survival data from histological grades of astrocytoma

demonstrating significantly different cumulative survival for individual tumor grades.

Pilocytic astrocytoma (PA) patients demonstrate the best survival profile, with 96%

survival rate at 10-years post-diagnosis. Glioblastoma (GBM) patients demonstrate the

worst cumulative survival with only 1.2% surviving at 5-years post-diagnosis and a

median survival time (MST) 0.4 years. Adapted with permission from [194].

Figure 1.5

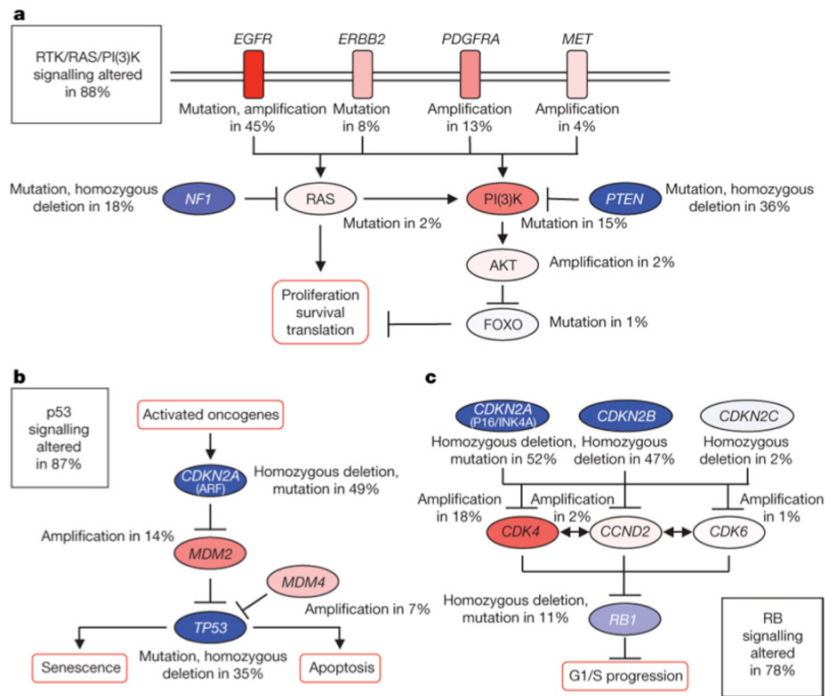


Figure 1.5: Molecular pathways altered in adult glioblastoma.

Integrative genomic analysis from The Cancer Genome Atlas (TCGA) project performed on GBM tumors and illustrating frequencies of mutations/genetic alterations in receptor tyrosine kinase (RTK)/RAS/Phosphoinositide-3-kinase (PI3K) signaling pathways in 88% of tumors and p53 signaling in 87% of tumors. Adapted with permission from [48].

Figure 1.6

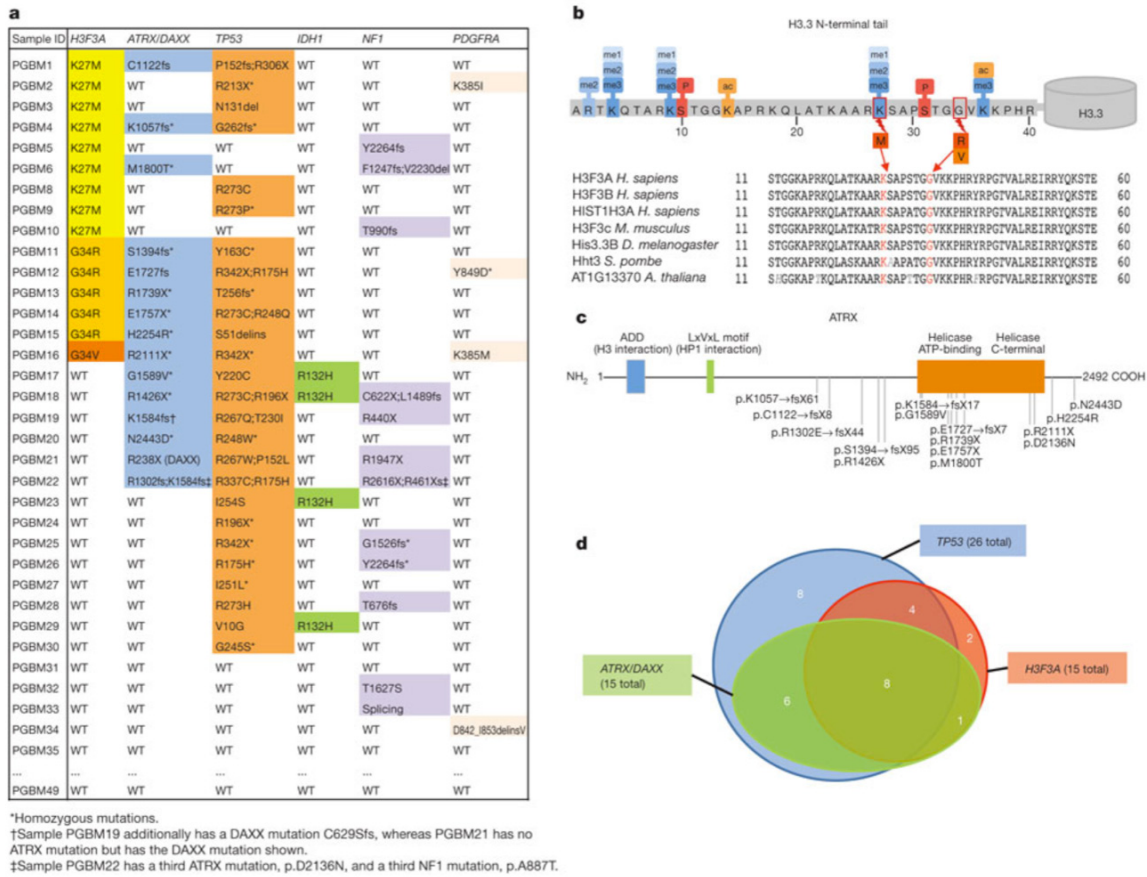


Figure 1.6: Mutations in histone H3.3 and chromatin remodeling genes identified in pediatric glioblastoma.

a, Mutations in histone variant H3.3, encoded by *H3F3A*, and chromatin remodeling genes *ATRX/DAXX* and other driver mutations identified by whole-exome sequencing (WES) in a group of 48 pediatric glioblastoma (PGBM) tumors. **b**, Histone H3.3 N-terminal tail demonstrating residues targeted by post-translational modifications (PTMs) and locations of mutations encoding amino acid substitutions lysine 27 to methionine (K27M) or glycine 34 to arginine or valine (G34R/V). **c**, Mapping of missense/truncating mutations identified in *ATRX*. **d**, Venn diagram illustrating strong overlap of *H3F3A*, *TP53* and *ATRX* mutations in PGBM tumors. Adapted with permission from [231].

Figure 1.7

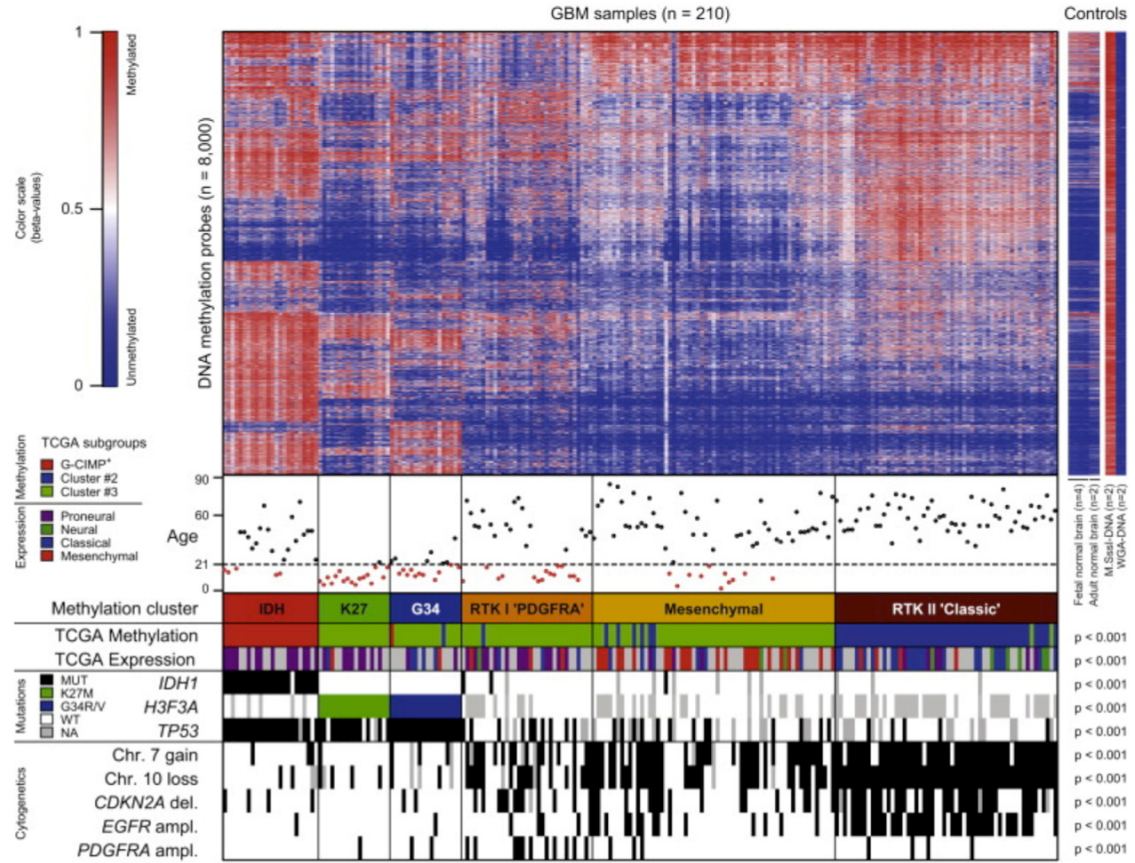


Figure 1.7: Six epigenetic subgroups of glioblastoma.

DNA methylation profiling heatmap illustrating the top 8,000 most variable CpG probe Beta-values amongst 210 adult and pediatric GBM samples, patient age and integrated genetic alterations including *H3F3A* and *IDH1* mutation status. Adapted with permission from [250].

Figure 1.8

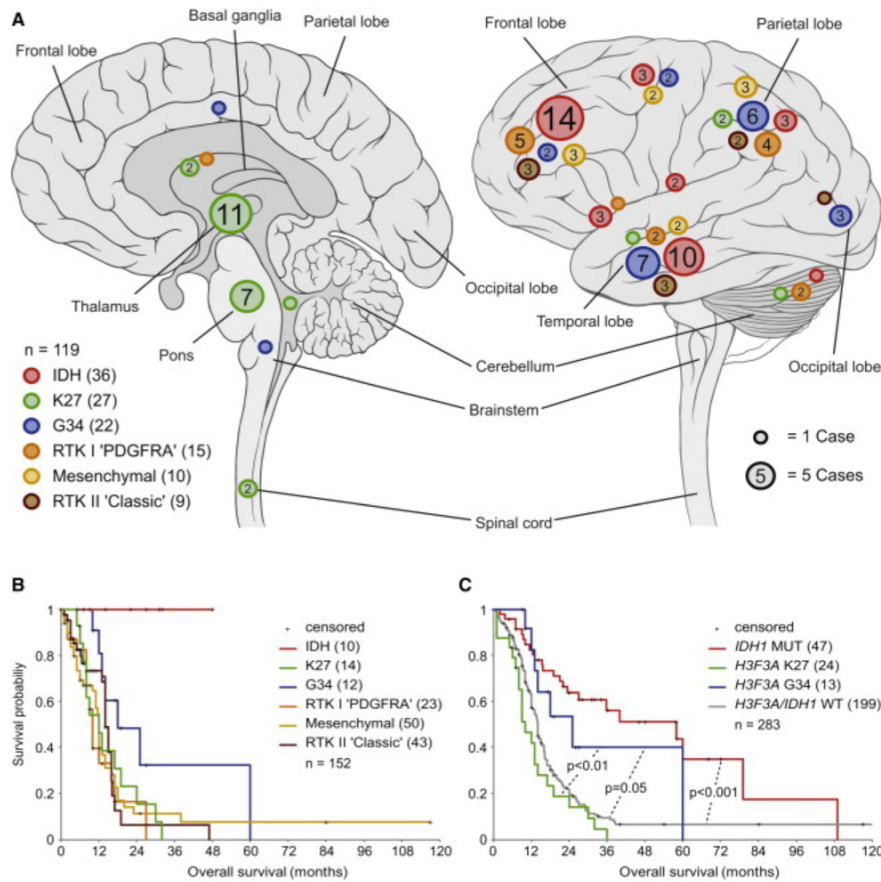


Figure 1.8: Clinical correlates of epigenetic subgroups of glioblastoma.

a, Illustration of the human brain and mapping of GBM tumors from the six epigenetic subgroups identified via DNA methylation profiling. Tumors harboring mutations of H3.3 K27M were prominent in midline brain locations including the thalamus/diencephalon, pontine area of the brainstem, cerebellum and spinal cord (left panel **a**). Tumors harboring *IDH1* or H3.3 G34R/V mutations were more prominent in fronto-temporal or parieto-temporal cortical areas respectively (right panel **a**). **b**, **c**, Kaplan-Meier analyses of patient survival data utilizing groupings from DNA methylation profiling (**b**) or *H3F3A* and *IDH1* sequencing data (**c**). Adapted with permission from [250].

Figure 1.9

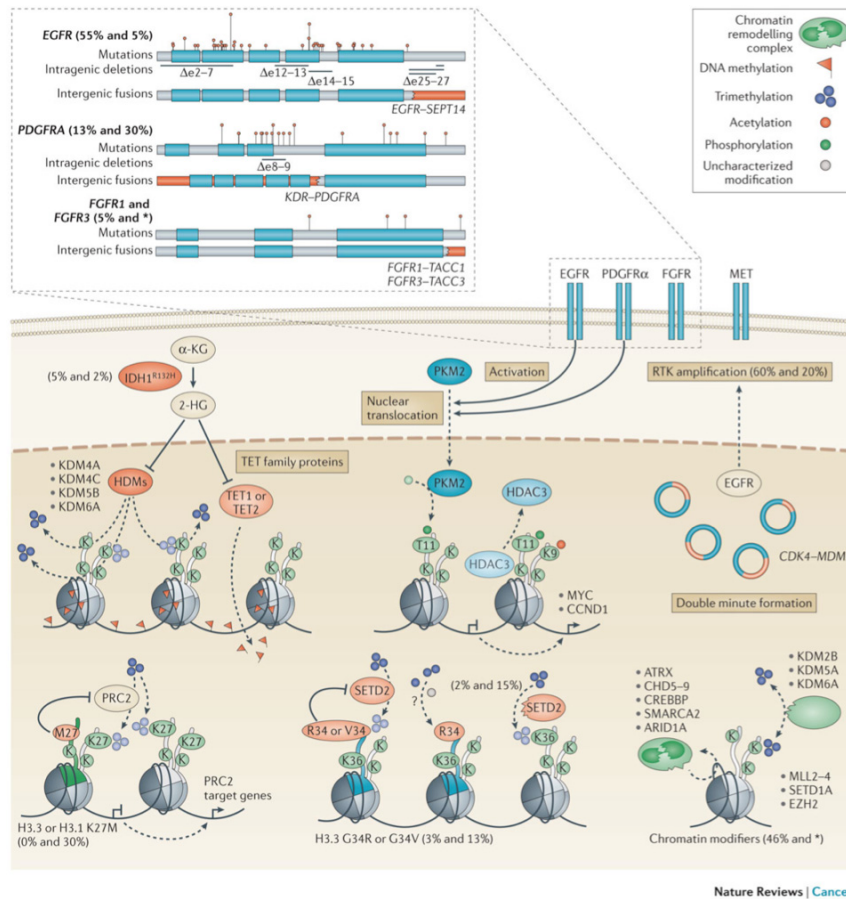


Figure 1.9: Functional impact of major genetic and epigenetic driver alterations identified in pediatric and adult glioblastoma.

Illustration of functional implications of receptor gene mutations, alterations and fusions occurring in pediatric and adult GBM, including growth factor receptors encoded by *EGFR*, *PDGFRA*, *FGFR1/3* (top panel). Bottom (intracellular) panel illustrating alterations leading to epigenomic dysregulation observed in GBM including *IDH1* mutations, H3.3/H3.1 K27M mutation and inhibition of Polycomb Repressor Complex 2 (PRC2) activity, H3.3 G34R/V related loss of mononucleosomal/oligonucleosomal H3K36me2/3, *SETD2* missense/truncating mutations leading to diminished H3K36me3 levels and defects in other chromatin modifiers. Adapted with permission from [249].

Figure 1.10

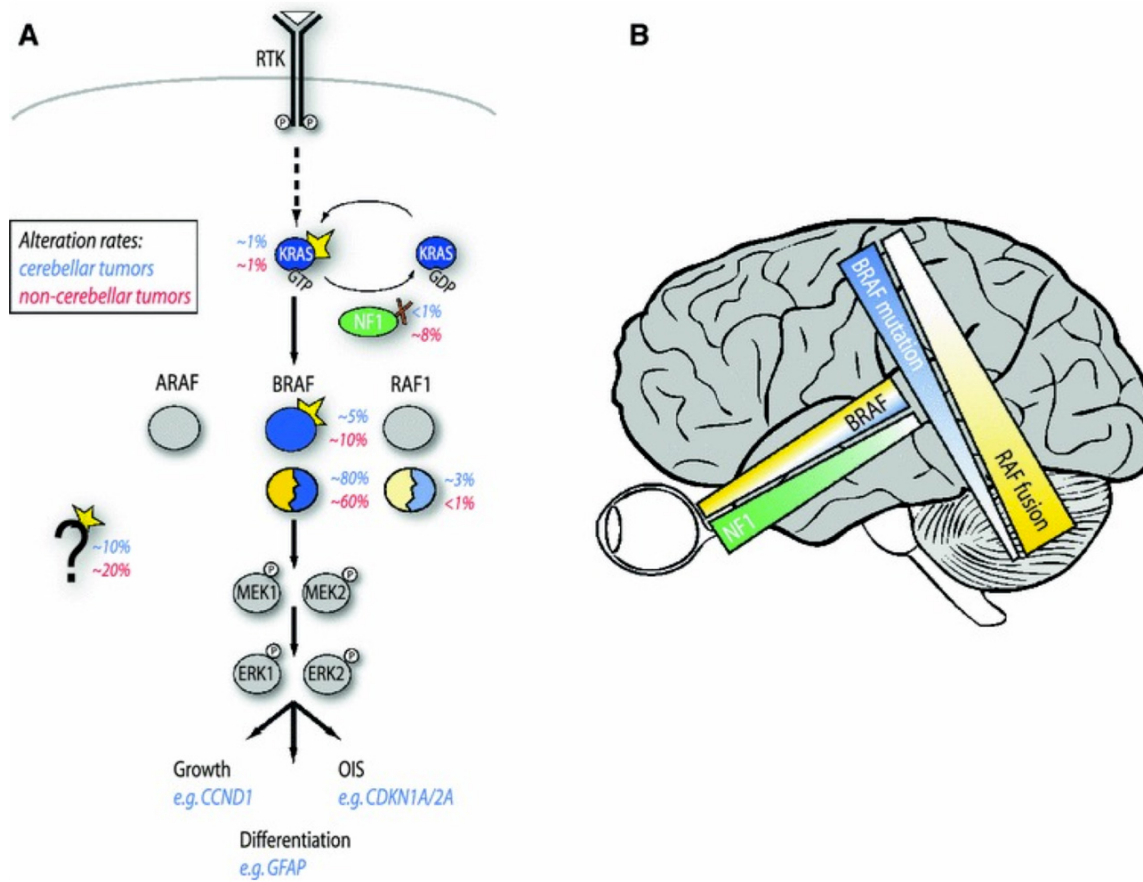


Figure 1.10: Frequency and brain region specificity of MAPK pathway alterations in pilocytic astrocytoma.

a, Mitogen-activated protein kinase (MAPK) pathway signaling demonstrating frequency of alterations in cerebellar and non-cerebellar tumors. A distinct specificity for *KIAA1549-BRAF* fusion and the cerebellum is noted. b, Schematic of the human brain demonstrating the relative frequency of MAPK alterations in different brain regions.

Adapted with permission from [117].

Figure 1.11

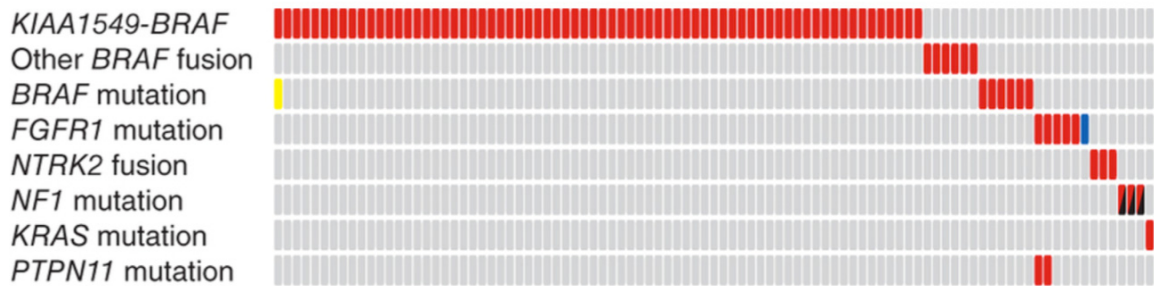


Figure 1.11: Major MAPK genetic alterations identified in pilocytic astrocytoma.

Comprehensive sequencing studies and identified MAPK alterations in 100% of 96 pilocytic astrocytoma tumors sequenced including newly identified *FGFR1* hotspot mutations, *PTPN11* mutations, novel *BRAF* fusions and other MAPK hits. Adapted with permission from [118].

Figure 1.12

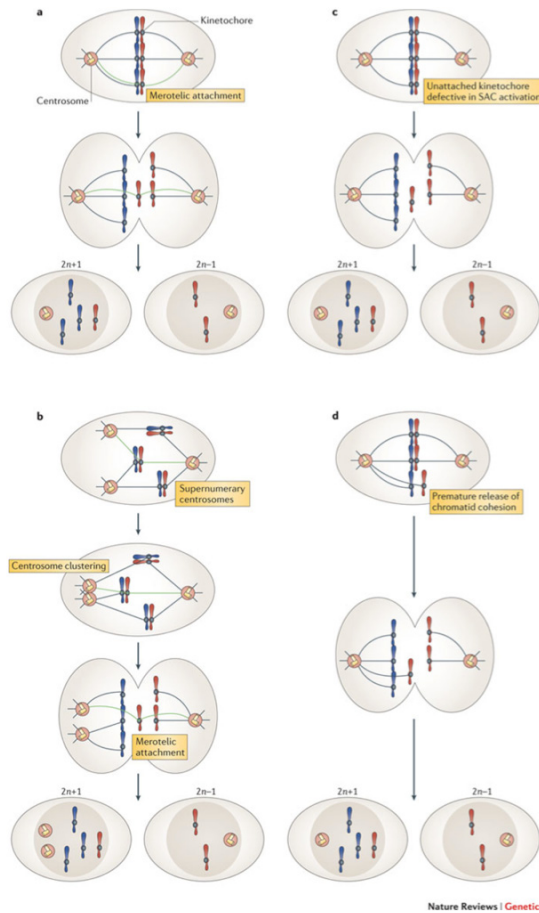


Figure 1.12: Mechanisms leading to the generation of aneuploid cells.

a, Defects in merotelic attachments can lead to daughter nuclei with gains or losses from the diploid number of chromosomes. **b**, More than two centrosomes can lead to aberrant spatial organization of the division process and clustering of centrosomes, leading to defects in merotelic attachments and aneuploidy. **c**, Lack of kinetochore attachment and spindle assembly checkpoint (SAC) mechanisms can lead to chromosomal missegregation and aneuploidy. **d**, Early release from cohesion of chromatids can lead to numerical chromosome abnormalities and aneuploid daughter cells. Adapted with permission from [88].

CHAPTER 2: Mutations in *SETD2* and genes affecting histone H3K36 methylation target hemispheric high-grade gliomas

Adam M. Fontebasso*, Jeremy Schwartzentruber*, Dong-Anh Khuong-Quang, Xiao-Yang Liu, Dominik Sturm, Andrey Korshunov, David T.W. Jones, Hendrik Witt, Marcel Kool, Steffen Albrecht, Adam Fleming, Djihad Hadjadj, Stephan Busche, Pierre Lepage, Alexandre Montpetit, Alfredo Staffa, Noha Gerges, Magdalena Zakrzewska, Krzysztof Zakrzewski, Pawel P. Liberski, Peter Hauser, Miklos Garami, Almos Klekner, Laszlo Bogнар, Gelareh Zadeh, Damien Faury, Stefan M. Pfister#, Nada Jabado#, Jacek Majewski#

*These authors contributed equally to the manuscript.

#These authors are co-senior and co-corresponding authors.

Published in [72]:

Fontebasso *et al.* Mutations in *SETD2* and genes affecting histone H3K36 methylation target hemispheric high-grade gliomas. *Acta Neuropathol.* 2013 May;125(5):659-69. doi:

10.1007/s00401-013-1095-8

The article is **Open Access** and is distributed according to the Creative Commons Attribution License permitting any use, distribution, and reproduction in any medium, provided the original author(s) and the source are credited.

2.1 Abstract

Recurrent mutations affecting the histone H3.3 residues Lys27 or indirectly Lys36 are frequent drivers of pediatric high-grade gliomas (over 30 % of HGGs). To identify additional driver mutations in HGGs, we investigated a cohort of 60 pediatric HGGs using whole-exome sequencing (WES) and compared them to 543 exomes from non-cancer control samples. We identified mutations in *SETD2*, a H3K36 trimethyltransferase, in 15 % of pediatric HGGs, a result that was genome-wide significant (FDR = 0.029). Most *SETD2* alterations were truncating mutations. Sequencing the gene in this cohort and another validation cohort (123 gliomas from all ages and grades) showed *SETD2* mutations to be specific to high-grade tumors affecting 15 % of pediatric HGGs (11/73) and 8 % of adult HGGs (5/65) while no *SETD2* mutations were identified in low-grade diffuse gliomas (0/45). Furthermore, *SETD2* mutations were mutually exclusive with *H3F3A* mutations in HGGs ($P = 0.0492$) while they partly overlapped with *IDH1* mutations (4/14), and *SETD2*-mutant tumors were found exclusively in the cerebral hemispheres ($P = 0.0055$). *SETD2* is the only H3K36 trimethyltransferase in humans, and *SETD2*-mutant tumors showed a substantial decrease in H3K36me3 levels ($P < 0.001$), indicating that the mutations are loss-of-function. These data suggest that loss-of-function *SETD2* mutations occur in older children and young adults and are specific to HGG of the cerebral cortex, similar to the H3.3 G34R/V and IDH mutations. Taken together, our results suggest that mutations disrupting the histone code at H3K36, including H3.3 G34R/V, IDH1 and/or *SETD2* mutations, are central to the genesis of hemispheric HGGs in older children and young adults.

2.2 Introduction

Malignant primary brain and central nervous system (CNS) tumors occur at an age-adjusted incidence rate of 7.3 out of 100,000 people across all ages and are the leading cause of cancer-related death in children [61]. High-grade gliomas [HGG; grade III and grade IV astrocytomas/glioblastoma (GBM)] are highly aggressive and deadly brain tumors [61,231] and are more commonly diagnosed in adults [47]. GBM remains essentially incurable despite decades of concerted therapeutic efforts. One impediment to treatment is that GBM is diagnosed as a single pathological entity, which cannot discriminate potential genetic drivers and molecular subtypes. This impacts the design and outcome of clinical trials and likely contributes to the apparent inherent resistance of GBM to adjuvant therapies. Because of the similar histology, current treatments for GBM in children are driven by adult studies and show, as in adults, little therapeutic success.

We and others recently identified two recurrent mutations in *H3F3A*, which encodes the replication-independent histone 3 variant H3.3, in over 30 % of pediatric and young adult GBM [231,281]. The mutations, K27M and G34R/G34V, occur at positions in the histone tail that are critical for post-translational modifications involved in the histone code, which determines chromatin structure and gene expression. H3.3 K27M mutations were also identified in over 70 % of pediatric diffuse intrinsic pontine glioma (DIPG), a fatal HGG of the brainstem [136,281] as well as K27M mutations in the canonical H3.1 in 18 % of samples [281]. H3.3 mutations significantly overlapped with mutations in *TP53* and in *ATRX* (α -thalassemia/mental-retardation syndrome-X-linked) [108,263] and less frequently with the *ATRX* hetero-dimer *DAXX*, which encode subunits of a chromatin remodeling complex required for H3.3 incorporation at

pericentric heterochromatin and telomeres [60,108]. H3.3 mutations represent the pediatric counterpart of the recurrent hotspot mutations in isocitrate dehydrogenase 1 or 2 (*IDH1/2*) [197,287]. *IDH1* R132 mutations are gain-of-function, causing the enzyme to produce 2-hydroxyglutarate (2-HG) [56,197] and *IDH1*-mutant tumors display distinct DNA methylation profiles with global hypermethylation, termed a glioma-CpG island methylator phenotype (G-CIMP) [192,250,255]. Interestingly, similar to pediatric GBM, *IDH1* mutations were shown to occur in association with *TP53* [197] and *ATRX* mutations in adult diffuse astrocytic tumors [114,131,166], illustrating an important constellation of mutations in the development of pediatric and secondary GBM. In the present study, we sought to identify drivers of HGG in pediatric samples that did not carry H3.3 or IDH mutations. We investigated a cohort of 60 pediatric HGGs utilizing statistical analysis of whole-exome sequencing (WES) on a genome-wide ranking scale and validated results in an independent validation cohort of 123 gliomas from all ages and grades. Herein, we present data showing the importance and functional impact of mutations in the H3K36 trimethyltransferase *SETD2* in HGGs of the cerebral hemispheres.

2.3 Materials and Methods

Sample characteristics and pathological review

Samples were obtained with informed consent following approval of the Institutional Review Board of individual hospitals. Samples were reviewed by senior neuropathologists (S.A., A.K.) according to WHO guidelines. Fifty-one pediatric grade IV astrocytomas (glioblastoma, GBM) patients and nine pediatric grade III astrocytomas

from patients aged 1–20 years were analyzed by whole-exome sequencing (44 previously published in [231]). An additional 123 adult and pediatric gliomas of diverse histology and grade were also included for targeted sequencing of *SETD2*, *IDH1* and *H3F3A*. Available clinical and relevant mutational characteristics are detailed in Supplementary Table 2.1. Tissues were obtained from the London/Ontario Tumor Bank, the Pediatric Cooperative Health Tissue Network, the Children’s Oncology Group, The Montreal Children’s Hospital and from collaborators in Poland, Hungary and Germany.

DNA extraction

Genomic DNA was extracted from frozen tumor tissue utilizing the Qiagen DNeasy Blood and Tissue kit according to instructions from the manufacturer (Qiagen).

Alignment and variant calling for whole-exome sequencing

Standard instructions from the manufacturer were used for target capture with the Illumina TruSeq exome enrichment kit and 100 bp paired-end sequencing reads on the Illumina HiSeq platform with bioinformatic processing and variant annotation as previously described [231]. For the selected genes of interest shown in Supplementary Table 2.1, variants in these genes that were private to tumor samples are shown, i.e. those variants not seen within the 1000 genomes (<http://www.1000genomes.org/>) or NHLBI exome (<http://evs.gs.washington.edu/EVS/>) databases, or in any of our 543 control exomes. Missense mutations were highlighted if they occurred within highly conserved residues in vertebrates, assessed utilizing the UCSC Genome Browser (<http://genome.ucsc.edu/>) conservation track tool [135]. To assess significance of

mutations in our tumor dataset, we used a case–control approach to compare the frequency of private mutations in each gene in the 60 tumor exomes to 543 control exomes, which were from constitutional DNA of patients with Mendelian diseases also sequenced at the McGill University and Genome Quebec Innovation Centre (Supplementary Table 2.2). We controlled for false discovery rate using the Benjamini–Hochberg procedure. All variants in these genes are detailed in Supplementary Table 2.2, whereas only private variants, likely to be somatic, and in highly conserved residues (likely to impact function), are highlighted in Supplementary Table 2.1 and discussed in this study.

Targeted next-generation sequencing of SETD2

Coding regions of SETD2 were amplified using the Fluidigm. Access Array system (<http://www.fluidigm.com/access-array-system.html>) and sequenced on a half run of the GS FLX Titanium system from Roche 454. Forty pairs of primers were designed to cover all coding regions of the 21 exons of SETD2. Primers were designed using Primer3 (<http://frodo.wi.mit.edu/primer3/>) [221]. The parameters were set to achieve melting temperatures ranging from 57 to 59°C. Lengths of PCR products are between 197 and 394 bp. The UCSC Genome Browser (<http://genome.ucsc.edu/>) was used to download target genomic regions prior to design and identify variants (based on dbSNP135: <http://www.ncbi.nlm.nih.gov/projects/SNP/>) [135]. PCRs were performed on 48 x 48 IFC (Integrated Fluidic Circuit) chips. On each chip, 40 regions were amplified in 48 samples. Amplification of target regions and addition of 454 sequencing adapters and individual bar codes occur in the same PCR performed on the Fluidigm FC1 cycler. All samples

were individually bar coded and sequenced in one half-region of a GS FLX Titanium run. Validation of variants was done with Sanger sequencing. Following this, statistical analyses of Fisher's exact test for contingency comparisons were performed utilizing GraphPad Prism 5 software.

Immunoblotting analysis of H3K36me3 levels in patient tumors

Fresh-frozen tumor tissues with adequate material and known *SETD2*, *H3F3A* and *IDH1* mutational status were lysed using the EpiQuik Total Histone Extraction Kit (Epigentek, USA). Lysates were quantified utilizing standard BioRad protein assay (BioRad) and loaded onto 15 % acrylamide gels and run for 2 h at 100 V. Proteins were transferred to polyvinylidene difluoride (PVDF) membranes at room temperature for 5 min, using the Trans-Blot Turbo transfer system (BioRad) at LOW MW setting, blocked and immunoblotted with the following conditions overnight at 4°C: rabbit polyclonal anti-H3K36me3 (Abcam #9050) at 1:1,000 in 5 % skim milk and rabbit polyclonal anti-H3 (Abcam #1791) at 1:1,000 in 5 % skim milk. Membranes were subsequently washed thrice with tris-buffered saline-Tween 20 (TBS-T) and incubated with horseradish peroxidase (HRP)-conjugated donkey anti-rabbit IgG secondary antibody (GE Healthcare #NA934V) at 1:5,000 with Precision Protein StrepTactin-HRP conjugate at 1:10,000 (BioRad #161-0380) in 5 % skim milk for 1 h at room temperature and revealed utilizing Amersham ECL detection (Amersham Biosciences). H3K36me3 bands from four independent blots were quantified utilizing ImageQuant TL v2003.02 (Amersham Biosciences), normalized to total H3, and normalized ratios were compared statistically using two-tailed *T* test for significance.

Methylation array profiling

DNA extracted from a subset of pediatric HGGs demonstrating defects in *SETD2*, *IDH1*, or *H3F3A* at G34 and wild-type tumors (n = 36) was analyzed for genome-wide DNA methylation patterns utilizing the HumanMethylation450 BeadChip according to the manufacturer's instructions (Illumina, San Diego, USA) at the McGill University and Genome Quebec Innovation Centre. Of the >480,000 probes on the methylation chip, we discarded probes with ≥ 90 % sequence similarity to multiple genomic locations, with sequence variants in the probe binding region (1000 Genomes Project, SNPs with a minor allele frequency $\geq 2/120$), and probes located on sex chromosomes, leaving 392,904 autosomal probes for further analysis. Subset-quantile within array normalization was performed on beta values using the SWAN method [173]. For unsupervised hierarchical clustering, the top 8,000 most variable probes (by standard deviation) were utilized with average linkage and Pearson correlation algorithms across the dataset. Consensus clustering was performed utilizing the *k*-means algorithm with 1,000 iterations on the top 8,000 most variable probes in the dataset. Methylation analysis was performed utilizing R (R version 2.14.2, <http://cran.r-project.org/>) with Minfi and ConsensusClusterPlus loaded packages.

2.4 Results and discussion

SETD2 mutations affect a significant proportion of pediatric HGGs

To identify genetic drivers in samples not carrying mutations in *IDH1* and *H3F3A*, we analyzed 60 pediatric HGG tumors [grades III (n = 9) and IV (n = 51)] using WES (44

previously reported; Supplementary Table 2.1) [231]. As matched normal DNA was unavailable for the majority of tumors, we identified private mutations that were present in tumors but were absent from public databases (1000 genomes project [1], NHLBI exomes) and from our set of 543 control exomes, and considered these as candidate somatic mutations. We compared the frequency of private mutations in each gene between the 60 tumors and 543 controls using Fisher's exact test and used a false discovery rate threshold (FDR) of 0.05 to correct for multiple tests. Our case-control approach effectively corrects for the background rate of mutations in each gene (which implicitly includes the length of the gene and the mutability). We filtered out variants that were predicted to be tolerated/benign/unknown by both SIFT and PolyPhen-2 [2], and identified private mutations that we considered as candidate somatic mutations. The top genes by mutation frequency are shown in Supplementary Table 2.2. As expected, four genes previously associated with pediatric HGG showed a highly significantly number of mutations (*TP53*, *H3F3A*, *ATRX*, *NF1*) [231] (Supplementary Table 2.2). In addition, two genes not previously reported in HGG, *SETD2* and *CSMD3*, achieved genome-wide significance (FDR = 0.029 and 0.031, respectively). For *SETD2*, this significance was more striking when only truncating mutations were considered (FDR = 0.0017), as no truncating mutations were seen in 543 controls, but tumor samples had frameshift (3), nonsense (1), and splicing (1) variants. In addition, the three missense variants in tumor samples occurred at highly conserved residues and were computationally predicted as damaging by both SIFT and Polyphen scores (Figure. 2.1a, b). In contrast, of the seven private variants in the control samples (all missense), only one is predicted damaging by both SIFT and Polyphen. H3.3 mutations occur at two positions within the histone tail

involved in key regulatory post-translational modifications, K27 (directly) and K36 (indirectly). Driver loss-of-function *SETD2* mutations have recently been identified in two high-grade cancers, renal cell carcinoma [55,83] and early T-cell precursor acute lymphoblastic leukemia [290]. The other candidate gene, *CSMD3* is expressed in adult and fetal brains; however, its functions are yet unclear [237]. Hence, we focused our next efforts on *SETD2* as the top candidate gene.

SETD2 mutations affect pediatric and adult HGGs of the cerebral hemispheres

We expanded our sequencing analysis and next sequenced *SETD2* in 123 additional gliomas of various ages and grades (Table 2.1; Supplementary Table 2.1). Combining the discovery and the validation datasets, *SETD2* mutations were identified in a total of 15 % of pediatric HGG (11/73) and 8 % of adult HGG (5/65), and were not seen in low-grade diffuse gliomas (0/45) ($P = 0.0133$; Table 2.1; Supplementary Table 2.1). Except for one sample, all mutations occurred in children above the age of 12, in adolescents and in younger adults, mirroring the age range of H3.3 G34R/V and *IDH1* mutations in HGG (Figure 2.1a; Supplementary Figure 2.1) [136,137,155,166,231,250]. Notably, all tumors carrying *SETD2* mutations were localized in the cerebral hemispheres ($P = 0.0055$).

SETD2 mutations were mutually exclusive with *H3F3A* mutations ($P = 0.049$) in HGGs (0/70), but showed partial overlap with *IDH1* R132 mutations (4/14), *TP53* (4/8) and *ATRX* (3/9) mutations (Supplementary Table 2.1).

Missense/truncating mutations in SETD2 impair trimethyltransferase activity of the enzyme and confer distinct global DNA methylation signatures

SETD2 encodes the only H3K36 trimethyltransferase in humans [64,267]. To support computational predictions of the damaging nature of *SETD2* mutations, we assessed H3K36 trimethyltransferase activity in histone acidic extractions of patient tissue samples through Western blotting for H3K36me3 levels, an indicator of SETD2 activity [64]. Immunoblot analysis revealed a significant decrease in total H3K36me3 levels in *SETD2*-mutant gliomas (Figure 2.2a), as well as a significantly decreased normalized ratio of H3K36me3 to total H3 levels in *SETD2*-mutant tumors ($P < 0.001$; Figure 2.2b) showing loss-of-function as a result of *SETD2* missense/truncating mutations.

GBMs with epigenetic driver mutations such as H3.3 K27M or G34R/V, as well as those with IDH1 mutations, display distinct DNA methylation profiles and clinical characteristics. They also arise in distinct anatomic compartments, with *IDH1*- and H3.3 G34R/V-mutant tumors being restricted to areas of the cerebral hemispheres. We and others have previously described the distinct heterogeneity of epigenetic profiles underlying HGGs including GBM [192,250]. We thus sought to characterize the DNA methylation profiles of 36 pediatric HGG tumors with mutations likely to affect K36 methylation status, using the Illumina 450K array platform as previously described [250]. *SETD2* mutations yielded global DNA methylation patterns distinct from tumors with H3.3 G34R/V mutations, but which partly overlapped with *IDH1*-mutant methylation patterns (Figure 2.3a–f). Notably, promoters at *OLIG1/2* loci, characteristically hypermethylated in G34R/V-mutated samples, were not hypermethylated in *SETD2* mutants (Supplementary Figure 2.2) [250].

Mutations identified in candidate oncogenic drivers and other genes involved in histone post-translational modifications in HGGs

We further investigated our dataset for mutations in other genes affecting PTM of H3K27 or H3K36 but which did not reach the statistically significant mutation levels. Eight distinct mammalian enzymes methylate H3K36 and share the catalytic SET domain, but have varying preferences for K36 residues in different methylation states (reviewed in [267]). SETD2 is the only enzyme in humans to catalyze H3K36 tri-methylation [64], while its mono- and/or di-methylation is catalyzed by NSD1, NSD2, NSD3, SETMAR, ASH1L, SMYD2 or SETD3 (reviewed in [267]). We identified one missense and one nonsense mutation in *ASH1L* (concurrently with *SETD2* mutation) and *SETD3* (1 missense mutation concurrently with *SETD2* mutation). One PGBM mutant for *SETD2* also had a missense mutation in *UTX/KDM6A* (H3K27 demethylase). This same PGBM had a missense mutation in *PBRM1*, a gene frequently mutated in renal cell carcinoma in association with *SETD2* [258]. We also identified two mutations in *KDM5C* (H3K4 demethylase) (Supplementary Table 2.1). Interestingly, no mutations in the cancer-implicated histone methyltransferase *EZH2* were identified. Mutations in these genes were not prevalent enough to be statistically associated with HGGs in our sample set; however, it remains possible that they contribute to pathogenesis in a small fraction of HGG cases.

Further investigation of the exome dataset revealed previously described mutations in BRAF (V600E [227,228] 5/60 pediatric HGG), which did not overlap with the epigenetic driver mutations we identify (Supplementary Table 2.1; Figure 2.2c). Other alterations also previously described in GBM, which may provide pathways

alternative or complementary to epigenomic dysregulation, included *PTEN* mutations (two samples) which overlapped with H3.3 K27M while *EGFR* mutation or amplification (three samples) and *CDKN2A* mutation/loss (five samples) partially overlapped with *SETD2* mutations (Supplementary Table 2.1). Truncating mutations in the mismatch repair genes [63] *MSH6* (three samples) and *MSH2* (one sample) were identified and were concurrent with *IDH1* (two samples) and *SETD2* (three samples) mutations. Of note, *SETD2* mutations were absent in a large cohort of 125 cases of medulloblastoma [120] another major group of pediatric brain tumors.

Alteration of H3K36 post-translational modifications characterize hemispheric adolescent and younger adult HGG

Post-translational modification of resident histones modulates the properties of chromatin, impacting cell state and differentiation and determining the outcome of virtually all DNA processes in eukaryotes. Methylation of H3K36 is a key histone mark and has been widely associated with active chromatin but also with transcriptional repression, alternative splicing, DNA replication and repair, DNA methylation and the transmission of memory of gene expression from parents to offspring during development (reviewed in [267]). We identify loss-of-function mutations in *SETD2*, in 15 % of pediatric and 8 % of adult high-grade gliomas in a cohort of 183 samples from all ages and grades II–IV of glioma (Figure 2.1 a; Supplementary Table 2.1). We further show *SETD2* mutations to be specific to high-grade tumors ($P = 0.013$), to HGGs located within the cerebral hemispheres ($P = 0.005$), and to be mutually exclusive with H3.3 mutations we [136,231] and others [281] previously identified in pediatric high-grade

astrocytomas ($P = 0.049$). *SETD2* alterations overlapped with *IDH1* mutations in 4 of 14 tumors (Supplementary Table 2.1). Strikingly, the oncometabolite produced by *IDH1* mutations inhibits a plethora of histone demethylases (KDMs) causing aberrant histone methylation at defined residues including K27 and K36 and a block to cell differentiation [45,168,226,286]. We [166] and others [114] have previously shown the association of *ATRX* and *TP53* mutations in *IDH1*-mutant diffuse astrocytic gliomas, and others have pointed to mutations in *CIC* and 1p19q loss in *IDH1*-mutant oligodendroglial tumors. Thus, *IDH1* mutations may require other key genetic events in a specific context for full-blown tumorigenesis, which may include *SETD2* mutations as suggested by our cohort. H3K36 methylation can be thus disrupted by H3.3 G34R/V mutation, *IDH* mutations and the *SETD2* mutations we report herein (Figure 2.2 a, b). Furthermore, our current analysis suggests that this histone mark is specifically altered in hemispheric adolescent and younger adult HGG (Figure 2.2 c, d) [136,137,231,250] and that the functional effect differs between *SETD2* and H3.3 mutations (Figure 2.3; Supplementary Figure 2.2). Future studies directed towards elucidating the importance of H3K36 methylation in cortical astrocytes and neural progenitor cells, and its dysregulation in tumorigenesis may lend insight into the regional specificity of these defects, while improved understanding of the consequences of altered chromatin remodeling induced by these mutations will help guide alternative therapeutic avenues for these deadly cancers.

2.5 Acknowledgments

The authors would like to acknowledge the excellent staff of the McGill University and Genome Quebec Innovation Centre High-Throughput sequencing platform for

performing the exome capture and sequencing. This work was supported by the Cole Foundation, and was funded by Genome Canada and the Canadian Institute for Health Research (CIHR) with co-funding from Genome BC, Genome Quebec, CIHR-ICR (Institute for Cancer Research) and C17, through the Genome Canada/CIHR joint ATID Competition [project title: The Canadian Paediatric Cancer Genome Consortium: Translating next-generation sequencing technologies into improved therapies for high-risk childhood cancer (NJ)], the Hungarian Scientific Research Fund (OTKA) Contract No. T-04639, TAMOP-4.2.2.A-11/1/KONV-2012-0025, the National Research and Development Fund (NKFP) Contract No. 1A/002/2004 (PH, MG, LB), the PedBrain project contributing to the International Cancer Genome Consortium funded by the German Cancer Aid (109252) and the CNS tumor tissue bank within the priority program on tumor tissue banking of the German Cancer Aid (108456), the BMBF, the Samantha Dickson Brain Tumor Trust, and a grant from the National Cancer Center Heidelberg (“Paediatric Brain Tumor Preclinical Testing”). A. Fontebasso and X-Y. Liu are the recipients of studentship awards from CIHR. DA Khuong-Quang is the recipient of a studentship from the Fonds de la recherche en santé du Québec (FRSQ). S. Pfister is the recipient of the Sybille Assmus Award for Neurooncology in 2009 and N. Jabado is the recipient of a Chercheur Clinicien Award from Fonds de Recherche en Santé du Québec and an award from the Canadian Gene Cure Foundation.

2.6 Conflict of interest

The authors declare no competing financial interests.

2.7 Figures

Figure 2.1

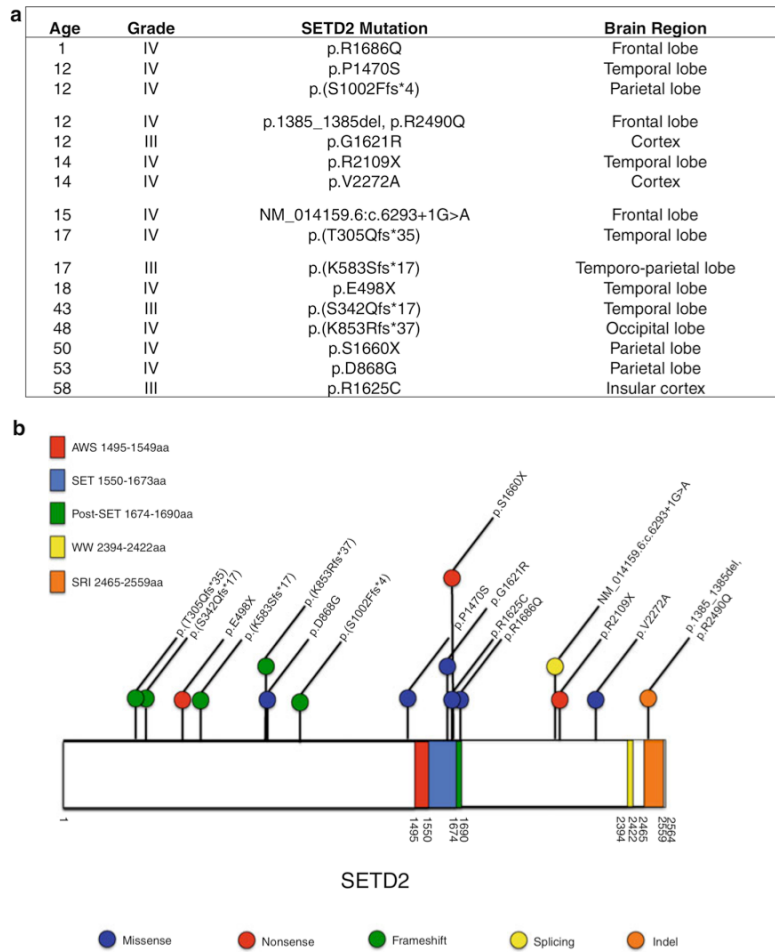


Figure 2.1: Missense/truncating mutations of the H3K36 trimethyltransferase *SETD2* identified in pediatric and adult high-grade gliomas. a Patient age, tumor grade, and affected brain region of tumors with *SETD2* mutation. **b** Schematic mapping type and distribution of missense/truncating mutations in *SETD2* in 183 gliomas included in the study.

Figure 2.2

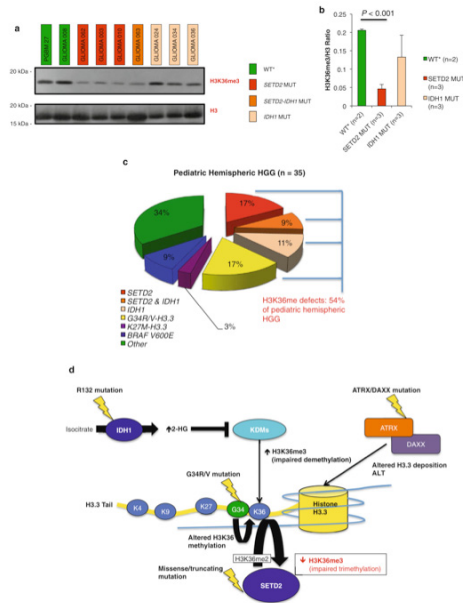


Figure 2.2: Missense/truncating mutations in *SETD2* impair H3K36

trimethyltransferase activity of the enzyme. a Western blot analysis of histone acidic

extracts of *SETD2*-mutant tumor samples demonstrating a significant decrease in H3K36me3 levels, indicating impaired H3K36 trimethyltransferase activity of the

enzyme. **b** Densitometric quantification of H3K36me3 levels assessed in four independent blots demonstrating a significant decrease in H3K36me3/Total H3 normalized ratios in *SETD2*-mutant tumors. WT* = WT for

SETD2, *IDH1* and *H3F3A*. **c** Pie representation of mutations directly or indirectly affecting H3K36 methylation (H3K36me) in pediatric HGGs of the cerebral hemispheres

($n = 35$) indicating that approximately half of these tumors display defects, pointing to H3K36 dysregulation as a critical mechanism of hemispheric high-grade

gliomagenesis. **d** Schematic representation of major genetic and epigenetic defects leading to altered H3K36 methylation in hemispheric HGGs.

Figure 2.3

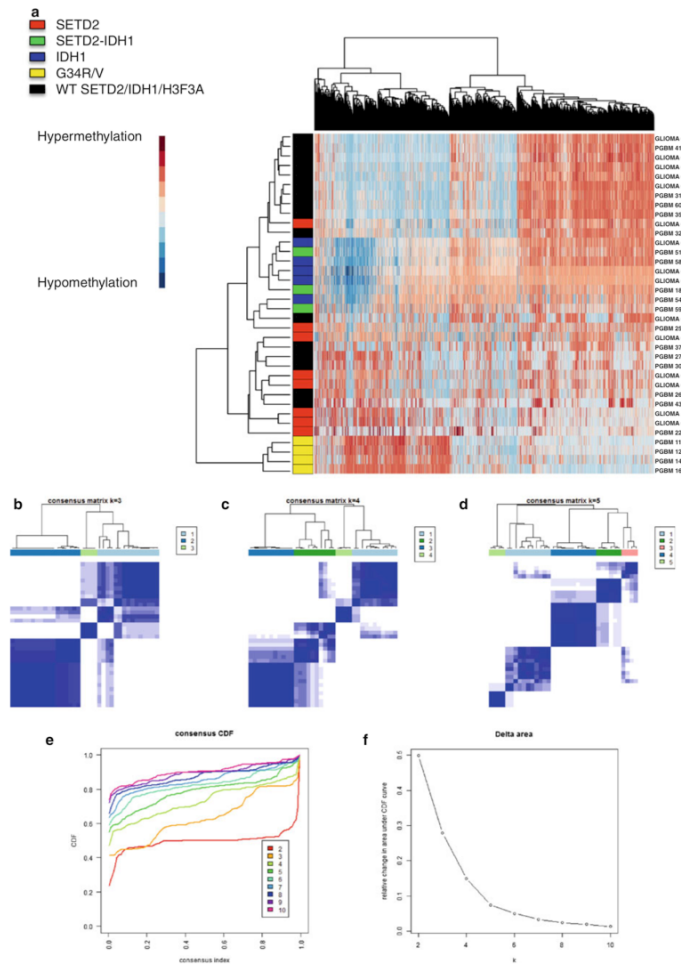


Figure 2.3: Mutations affecting H3K36 methylation confer distinct global DNA methylation signatures. **a** Unsupervised hierarchical clustering of methylation Beta-values representing the top 8,000 most variable probes between samples mutated for *SETD2*, *IDH1* or H3.3 G34R/V and high-grade gliomas wild-type (WT) for these genes ($n = 36$). **b** k -means consensus matrices for $k = 3$ (**b**), $k = 4$ (**c**) or $k = 5$ (**d**) for the top 8,000 most variable probes. **e** Empirical cumulative distribution function (CDF) plot and delta area differences (**f**) for indicated numbers of clusters ($k = 2$ to $k = 10$).

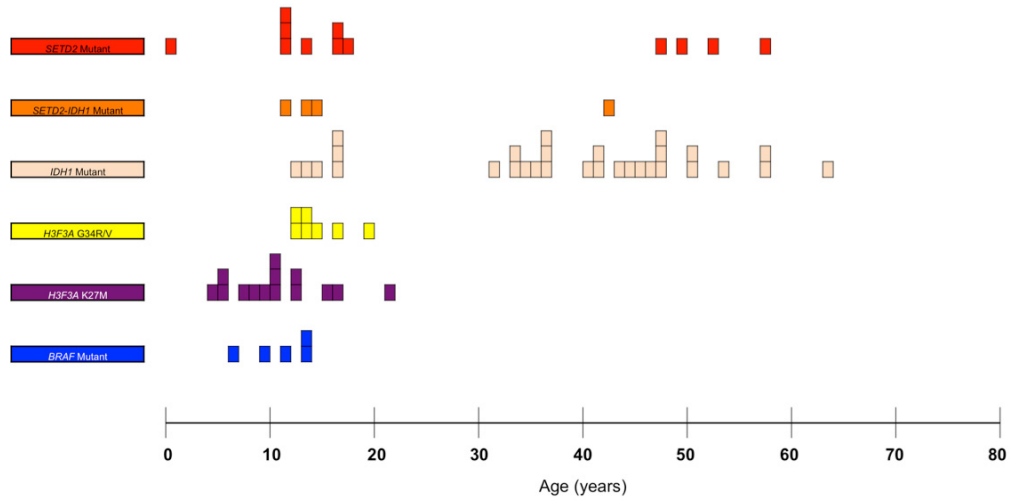
2.8 Tables

Table 2.1: Frequencies of *SETD2* mutations in 183 pediatric and adult gliomas

Glioma	Mutated	Wild type	Total	Frequency (%)
Grade IV	12	85	97	12.37
Pediatric	9	51	60	15
Adult	3	34	37	8.11
Grade III	4	37	41	9.76
Pediatric	2	11	13	15.38
Adult	2	26	28	7.14
Grade II	0	45	45	0
Pediatric	0	23	23	0
Adult	0	22	22	0
Overall gliomas	16	167	183	8.7

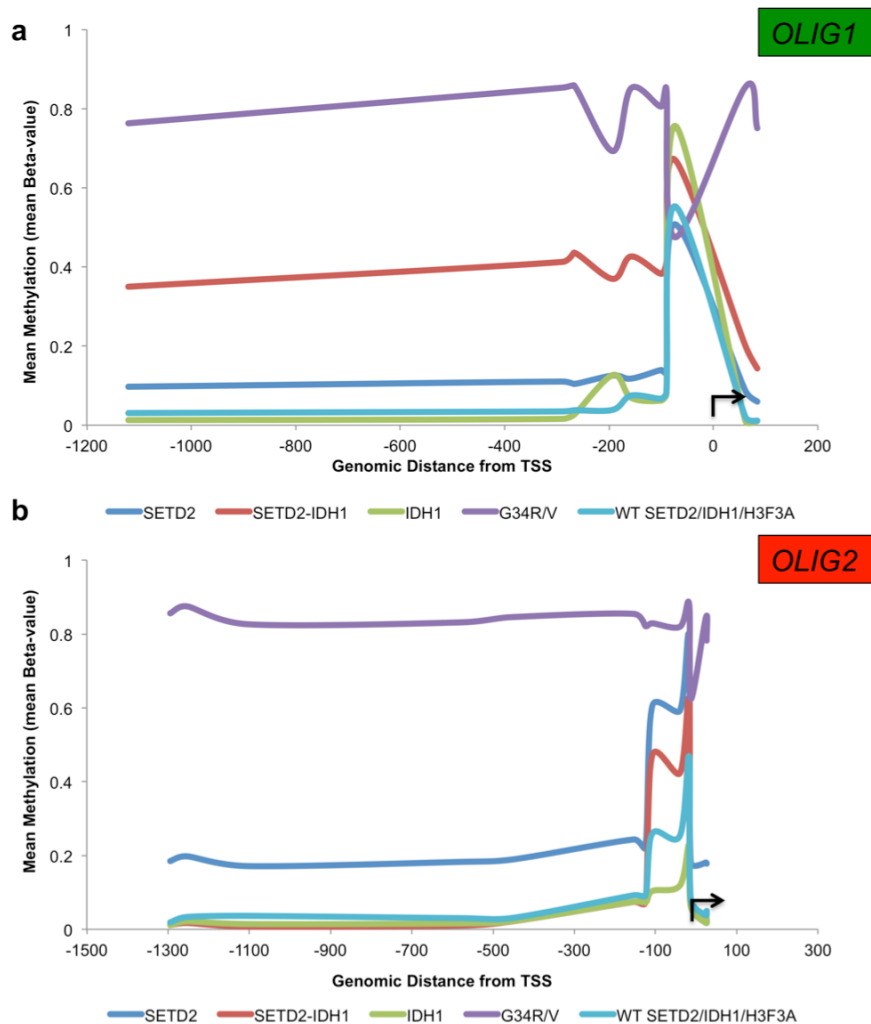
2.9 Supplementary Material

Supplementary Figure 2.1



Supplementary Figure 2.1: Age distribution of driver mutations identified in pediatric and adult high-grade gliomas. Graphical representation of mutations identified in *SETD2*, *IDH1*, *H3F3A* (K27M, G34R/V) and BRAF in all pediatric and adult high-grade gliomas included in the study.

Supplementary Figure 2.2



Supplementary Figure 2.2: *SETD2* mutations do not show similar patterns of promoter methylation at *OLIG1* and *OLIG2* loci as H3.3K36 affected G34R/V tumors. **a**, Graphical representation of mean promoter methylation probe Beta-values within promoter region of *OLIG1* (**a**) and *OLIG2* (**b**). To best represent this region, probes were chosen that were within -1500bp upstream and +200bp downstream of the transcription start site (TSS).

Code	Year	Month	Day	Time	Location	Category	Priority	Status	Comments	Responsible	Start Date	End Date	Actual End Date
GL-000001	2020	01	01	00:00

1. This report is not intended to be distributed to the general public.
 2. This report is not intended to be distributed to the general public.
 3. This report is not intended to be distributed to the general public.
 4. This report is not intended to be distributed to the general public.
 5. This report is not intended to be distributed to the general public.

Supplementary Table 2.2: Genes significantly mutated in 60 pediatric high-grade glioma samples

Table S2: Genes significantly mutated in 60 pediatric high-grade glioma samples
 Q values calculated as: $q = p * \text{numGenes} / \text{rank}$
 Number of genes with ≥ 1 mutation: 6365
 Number of genes of interest: 6365

Gene	Raw p value	All mutations	#Mutations	#Affecteds	#Mutations	#Controls
		Rank				
TP53	3.7014E-26	1	2,358E-22	27	60	4
H3F3A	2.43011E-15	2	1.235E-12	15	60	1
ATRX	5.67151E-12	3	1.203E-08	15	60	6
NF1	4.70528E-08	4	7.487E-05	12	60	9
SETD2	2.23749E-05	5	0.0297378	8	60	7
ARL1	0.00043596	6	0.00043596	1	60	1
ARL2	0.00043596	7	0.00043596	1	60	1
ARL3	0.00043596	8	0.00043596	1	60	1
ARL4	0.00043596	9	0.00043596	1	60	1
ARL5	0.00043596	10	0.00043596	1	60	1
ARL6	0.00043596	11	0.00043596	1	60	1
ARL7	0.00043596	12	0.00043596	1	60	1
ARL8	0.00043596	13	0.00043596	1	60	1
ARL9	0.00043596	14	0.00043596	1	60	1
ARL10	0.00043596	15	0.00043596	1	60	1
ARL11	0.00043596	16	0.00043596	1	60	1
ARL12	0.00043596	17	0.00043596	1	60	1
ARL13	0.00043596	18	0.00043596	1	60	1
ARL14	0.00043596	19	0.00043596	1	60	1
ARL15	0.00043596	20	0.00043596	1	60	1
ARL16	0.00043596	21	0.00043596	1	60	1
ARL17	0.00043596	22	0.00043596	1	60	1
ARL18	0.00043596	23	0.00043596	1	60	1
ARL19	0.00043596	24	0.00043596	1	60	1
ARL20	0.00043596	25	0.00043596	1	60	1
ARL21	0.00043596	26	0.00043596	1	60	1
ARL22	0.00043596	27	0.00043596	1	60	1
ARL23	0.00043596	28	0.00043596	1	60	1
ARL24	0.00043596	29	0.00043596	1	60	1
ARL25	0.00043596	30	0.00043596	1	60	1
ARL26	0.00043596	31	0.00043596	1	60	1
ARL27	0.00043596	32	0.00043596	1	60	1
ARL28	0.00043596	33	0.00043596	1	60	1
ARL29	0.00043596	34	0.00043596	1	60	1
ARL30	0.00043596	35	0.00043596	1	60	1
ARL31	0.00043596	36	0.00043596	1	60	1
ARL32	0.00043596	37	0.00043596	1	60	1
ARL33	0.00043596	38	0.00043596	1	60	1
ARL34	0.00043596	39	0.00043596	1	60	1
ARL35	0.00043596	40	0.00043596	1	60	1
ARL36	0.00043596	41	0.00043596	1	60	1
ARL37	0.00043596	42	0.00043596	1	60	1
ARL38	0.00043596	43	0.00043596	1	60	1
ARL39	0.00043596	44	0.00043596	1	60	1
ARL40	0.00043596	45	0.00043596	1	60	1
ARL41	0.00043596	46	0.00043596	1	60	1
ARL42	0.00043596	47	0.00043596	1	60	1
ARL43	0.00043596	48	0.00043596	1	60	1
ARL44	0.00043596	49	0.00043596	1	60	1
ARL45	0.00043596	50	0.00043596	1	60	1
ARL46	0.00043596	51	0.00043596	1	60	1
ARL47	0.00043596	52	0.00043596	1	60	1
ARL48	0.00043596	53	0.00043596	1	60	1
ARL49	0.00043596	54	0.00043596	1	60	1
ARL50	0.00043596	55	0.00043596	1	60	1
ARL51	0.00043596	56	0.00043596	1	60	1
ARL52	0.00043596	57	0.00043596	1	60	1
ARL53	0.00043596	58	0.00043596	1	60	1
ARL54	0.00043596	59	0.00043596	1	60	1
ARL55	0.00043596	60	0.00043596	1	60	1

The number of genes of interest is used in calculating the FDR Q values.
 Q values calculated as: $q = p * \text{numGenes} / \text{rank}$
 Number of genes with ≥ 1 TRUNC mutation: 835
 Number of genes of interest: 835

Gene	Raw p value	Truncating mutations	#Mutations	#Affecteds	#Mutations	#Controls
		Rank				
NF1	2.6959E-10	1	1,217,87E-07	11	60	1
TP53	4.71267E-10	2	1.96754E-07	10	60	2
ATRX	2.36897E-07	3	6.55808E-05	8	60	2
SETD2	8.38449E-06	4	0.001744835	5	60	0
ARL1	0.00043596	5	0.000703925	4	60	1
ARL2	0.00043596	6	0.000703925	4	60	1
ARL3	0.00043596	7	0.000703925	4	60	1
ARL4	0.00043596	8	0.000703925	4	60	1
ARL5	0.00043596	9	0.000703925	4	60	1
ARL6	0.00043596	10	0.000703925	4	60	1
ARL7	0.00043596	11	0.000703925	4	60	1
ARL8	0.00043596	12	0.000703925	4	60	1
ARL9	0.00043596	13	0.000703925	4	60	1
ARL10	0.00043596	14	0.000703925	4	60	1
ARL11	0.00043596	15	0.000703925	4	60	1
ARL12	0.00043596	16	0.000703925	4	60	1
ARL13	0.00043596	17	0.000703925	4	60	1
ARL14	0.00043596	18	0.000703925	4	60	1
ARL15	0.00043596	19	0.000703925	4	60	1
ARL16	0.00043596	20	0.000703925	4	60	1
ARL17	0.00043596	21	0.000703925	4	60	1
ARL18	0.00043596	22	0.000703925	4	60	1
ARL19	0.00043596	23	0.000703925	4	60	1
ARL20	0.00043596	24	0.000703925	4	60	1
ARL21	0.00043596	25	0.000703925	4	60	1
ARL22	0.00043596	26	0.000703925	4	60	1
ARL23	0.00043596	27	0.000703925	4	60	1
ARL24	0.00043596	28	0.000703925	4	60	1
ARL25	0.00043596	29	0.000703925	4	60	1
ARL26	0.00043596	30	0.000703925	4	60	1
ARL27	0.00043596	31	0.000703925	4	60	1
ARL28	0.00043596	32	0.000703925	4	60	1
ARL29	0.00043596	33	0.000703925	4	60	1
ARL30	0.00043596	34	0.000703925	4	60	1
ARL31	0.00043596	35	0.000703925	4	60	1
ARL32	0.00043596	36	0.000703925	4	60	1
ARL33	0.00043596	37	0.000703925	4	60	1
ARL34	0.00043596	38	0.000703925	4	60	1
ARL35	0.00043596	39	0.000703925	4	60	1
ARL36	0.00043596	40	0.000703925	4	60	1
ARL37	0.00043596	41	0.000703925	4	60	1
ARL38	0.00043596	42	0.000703925	4	60	1
ARL39	0.00043596	43	0.000703925	4	60	1
ARL40	0.00043596	44	0.000703925	4	60	1
ARL41	0.00043596	45	0.000703925	4	60	1
ARL42	0.00043596	46	0.000703925	4	60	1
ARL43	0.00043596	47	0.000703925	4	60	1
ARL44	0.00043596	48	0.000703925	4	60	1
ARL45	0.00043596	49	0.000703925	4	60	1
ARL46	0.00043596	50	0.000703925	4	60	1
ARL47	0.00043596	51	0.000703925	4	60	1
ARL48	0.00043596	52	0.000703925	4	60	1
ARL49	0.00043596	53	0.000703925	4	60	1
ARL50	0.00043596	54	0.000703925	4	60	1
ARL51	0.00043596	55	0.000703925	4	60	1
ARL52	0.00043596	56	0.000703925	4	60	1
ARL53	0.00043596	57	0.000703925	4	60	1
ARL54	0.00043596	58	0.000703925	4	60	1
ARL55	0.00043596	59	0.000703925	4	60	1
ARL56	0.00043596	60	0.000703925	4	60	1

CHAPTER 2: Mutations in *SETD2* and genes affecting histone H3K36 methylation target hemispheric high-grade gliomas

To

CHAPTER 3: Recurrent mutations in *ACVR1* in pediatric midline high-grade astrocytomas

Embryogenesis requires the careful orchestration of the expression of genes, and in tissues, correct positioning of this expression across cells. In Chapter 2, with the discovery of *SETD2* mutations in 15% of pHGGs, which, taken together with *IDH1* and H3.3 G34R/V mutations, contribute to defects in histone 3 lysine 36 (H3K36) methylation in about half of pediatric hemispheric HGGs [72], we can hypothesize that H3K36 methylation may be a critical process in cerebral cortex development. Along these same lines, previous work by our lab and others has given a glimpse into the prevalence for H3.3 and H3.1 K27M mutations in midline structures of the brain such as the thalamus, spinal cord, cerebellum and notably the pontine area of the brainstem, where high-grade tumors are referred to as diffuse intrinsic pontine gliomas (DIPGs) [231,281,136]. In Chapter 3 of this thesis and published in [71], we focused on the mutational alterations in 40 midline high-grade astrocytomas (mHGAs) including DIPGs. We report in Chapter 3 a mutational analysis of 40 mHGAs, 39 with whole-exome sequencing data, and demonstrate that while H3K36 defects predominate in cortical tumors, K27M mutations, shown to affect H3K27me3 levels in several independent studies, define the vast majority of midline tumors. These K27M mutations, across three genes coding for H3.3 and H3.1 did not occur in isolation but in association with distinct

brain region-specific partner mutations that may underlie distinct cellular origins or step-wise tumorigenesis in these regions.

CHAPTER 3: Recurrent mutations in *ACVR1* in pediatric midline high-grade astrocytoma

Adam M. Fontebasso*, Simon Papillon-Cavanagh*, Jeremy Schwartzentruber*, Hamid Nikbakht, Noha Gerges, Pierre-Olivier Fiset, Denise Bechet, Damien Faury, Nicolas De Jay, Lori A. Ramkissoon, Aoife Corcoran, David T. W. Jones, Dominik Sturm, Pascal Johann, Tadanori Tomita, Stewart Goldman, Mahmoud Nagib, Anne Bendel, Liliana Goumnerova, Daniel C. Bowers, Jeffrey R. Leonard, Joshua B. Rubin, Tord Alden, Samuel Browd, J. Russell Geyer, Sarah Leary, George Jallo, Kenneth Cohen, Nalin Gupta, Michael D. Prados, Anne-Sophie Carret, Benjamin Ellezam, Louis Crevier, Almos Klekner, Laszlo Bogнар, Peter Hauser, Miklos Garami, John Myseros, Zhifeng Dong, Peter M. Siegel, Hayley Malkin, Azra H. Ligon, Steffen Albrecht, Stefan M. Pfister, Keith L. Ligon#, Jacek Majewski#, Nada Jabado#, Mark W. Kieran#

*These authors contributed equally to the manuscript.

#These authors are co-senior and co-corresponding authors.

Published in and adapted from [71]:

Fontebasso *et al.* Recurrent somatic mutations in *ACVR1* in pediatric midline high-grade astrocytoma. *Nat Genet.* 2014 May;46(5):462-6. doi: 10.1038/ng.2950

3.1 Abstract

Pediatric midline high-grade astrocytomas (mHGAs) are incurable with few treatment targets identified. Most tumors harbor mutations encoding p.Lys27Met in histone H3 variants. In 40 treatment-naive mHGAs, 39 analyzed by whole-exome sequencing, we find additional somatic mutations specific to tumor location. Gain-of-function mutations in *ACVR1* occur in tumors of the pons in conjunction with histone H3.1 p.Lys27Met substitution, whereas *FGFR1* mutations or fusions occur in thalamic tumors associated with histone H3.3 p.Lys27Met substitution. Hyperactivation of the bone morphogenetic protein (BMP)-*ACVR1* developmental pathway in mHGAs harboring *ACVR1* mutations led to increased levels of phosphorylated SMAD1, SMAD5 and SMAD8 and upregulation of BMP downstream early-response genes in tumor cells. Global DNA methylation profiles were significantly associated with the p.Lys27Met alteration, regardless of the mutant histone H3 variant and irrespective of tumor location, supporting the role of this substitution in driving the epigenetic phenotype. This work considerably expands the number of potential treatment targets and further justifies pretreatment biopsy in pediatric mHGA as a means to orient therapeutic efforts in this disease.

3.2 Introduction

We and others recently identified recurrent mutations in *H3F3A*, encoding histone 3 variant 3 (H3.3), in 38% of pediatric supratentorial HGAs and mutations affecting histone H3.3 or H3.1 in ~80% of brainstem HGAs (diffuse intrinsic pontine gliomas, DIPGs) [136,231,281]. Mutations affecting the histone H3 tail that change the glycine at position 34 to either arginine or valine (p.Gly34Arg or p.Gly34Val), as well as mutations in genes affecting histone H3 post-translational modifications at lysine 36, predominate in cortical tumors, whereas lysine-to-methionine substitutions at residue 27 (p.Lys27Met) occur in midline tumors [136,231,250,72].

Herein we focus on the genomic (mutational spectrum and copy number alterations) and epigenetic (DNA methylation) landscape of treatment-naive pediatric midline (thalamus, cerebellum, spine and pons; non-cortical regions) high-grade astrocytomas (Figs. 1-3). These tumors are often surgically challenging or inoperable, and published studies have mainly used material collected after therapy and have provided limited genomic data other than structural alterations and mutational analysis of histone H3 variant genes and *TP53* [136,281,198,289].

3.3 Materials and Methods

Patient samples and consent

All samples were obtained with informed consent after approval of the institutional review boards (IRBs) of the respective hospitals they were treated in and were independently reviewed by senior pediatric neuropathologists (S.A. and K.L.L.) according to World Health Organization (WHO) guidelines. Samples were obtained from

the Montreal Children's Hospital (Montreal, McGill University Health Centre), Boston Children's Hospital (Boston, Harvard University), the Brain Tumor Toronto Bank (BTTB; Toronto, University Health Network) and from collaborators in Hungary, in addition to previously published mHGA samples [231,72] with sequencing data (n = 11) and with previously published DNA methylation data (n = 89) for a total of 98 tumors included herein for DNA methylation and copy number variant (CNV) analysis [250,72]. DIPG biopsy samples obtained before therapy were from Dana-Farber Cancer Institute protocol 10-321 (n = 12), a prospective phase II biopsy study of newly diagnosed DIPG. The protocol is IRB approved through the Dana-Farber Harvard Cancer Center IRB, FDA IND 111,882, <http://ClinicalTrials.gov/> identifier NCT01182350, and has local institutional approval at all participating sites; informed consent was obtained from all parents. Additional pediatric midline HGA samples were from needle biopsies or partial resections before treatment (n = 28). Sequencing and clinical data for this cohort are presented in Supplementary Table 3.1, and methylation-derived CNVs in genes of interest are presented in Supplementary Tables 3.4 and 3.5.

Whole-exome DNA sequencing

Standard genomic DNA extraction methods were performed according to described company protocols (Qiagen). Paired-end library preparations were carried out using the Nextera Rapid Capture Exome kit according to instructions from the manufacturer (Illumina) from 50 ng of total starting genomic DNA. Sequencing was performed in rapid-run mode with 100-bp paired-end reads on an Illumina HiSeq 2000. We removed adaptor sequences, quality trimmed reads using the FASTX-Toolkit and

then used a custom script to ensure that only read pairs with both mates present were subsequently used. Reads were aligned to hg19 with Burrows-Wheeler Aligner (BWA) 0.5.9 [163], and indel realignment was performed using the Genome Analysis Toolkit (GATK) [180]. Duplicate reads were then marked using Picard and excluded from downstream analyses. We assessed coverage of consensus coding sequence (CCDS) bases using GATK, which showed that the majority of samples had >92% of CCDS bases covered by at least 10 reads and >88% of CCDS bases covered by at least 20 reads.

For each sample, SNVs and short indels were called using SAMtools mpileup [164] with the extended base alignment quality (BAQ) adjustment (-E) and were then quality filtered to require at least 20% of reads supporting each variant call. Variants were annotated using both ANNOVAR [270] and custom scripts to identify whether they affected protein-coding sequence and whether they had previously been seen in the 1000 Genomes Project data set (November 2011), the National Heart, Lung, and Blood Institute (NHLBI) Grand Opportunity (GO) exomes or in approximately 1,000 exomes previously sequenced at our center. Variants in candidate genes of interest described herein in the midline HGA cohort (n = 39) are detailed in Supplementary Table 3.6.

MiSeq targeted high-depth DNA sequencing of H3F3A, HIST1H3B and HIST1H3C

Genomic DNA from midline HGA samples was used for high-depth sequencing of the *H3F3A*, *HIST1H3B* and *HIST1H3C* genes to investigate the frequency of reads encoding p.Lys27Met in samples, notably those wild type by whole-exome sequencing and high-resolution melting assays. Midline HGAs (n = 24) were sequenced using the MiSeq sequencing platform (Illumina) with an average coverage of >20,000× of the

analogous p.Lys27Met base change across the three histone variants (more specifically, for the *H3F3A* gene, the average coverage was >12,000×, for the *HIST1H3B* gene, the coverage was >12,000×, and, for the *HIST1H3C* gene, the coverage was >35,000×). Reads were mapped to the reference genome (human hg19) using the BWA genome aligner [163]. Alignment files were fed to the mpileup tool from the SAMtools package [164] to find all the variations without any filter applied by the conventional variant callers. An in-house parser program was developed to extract different variations at the desired positions (in this case, affecting Lys27) in the mapped paired reads covering the histone genes *H3F3A*, *HIST1H3B* and *HIST1H3C*. The results are provided in Supplementary Table 3.3.

RNA sequencing

RNA was extracted from case tumor mHGA37 using the Qiagen RNeasy Lipid Tissue Mini kit according to instructions from the manufacturer. Library preparation was performed with rRNA depletion methods according to instruction from the manufacturer (Epicentre) to achieve greater coverage of mRNA and other long noncoding transcripts. Paired-end sequencing was performed on the Illumina HiSeq 2000 platform.

RNA sequencing fusion analysis

RNA sequencing FASTQ files were used for fusion analysis with the deFuse software algorithm [181] according to indicated settings. Algorithmic output was then analyzed for high-confidence fusion transcripts, which were then reconstructed *in silico* using online bioinformatics tools and databases, including BLAST, Ensembl, UniProt

and the UCSC Genome Browser, to assess impact on putative fusion proteins and compare them with existing, previously described fusions [118,241].

TERT promoter mutation sequencing

Characterized mutations in the *TERT* promoter, C228T, and C250T variants with G>A nucleotide substitutions at genomic positions 1,295,228 and 1,295,250 (hg19), respectively [105], were sequenced using the Sanger method in midline samples (n = 14) and cortical samples (n = 10) using the following cycling conditions: 96 °C for 1 min, 96 °C for 10 s, 60 °C for 5 s, 72 °C for 1 s and 72 °C for 30 s, repeated for 33 cycles. Primer sequences are detailed in Supplementary Table 3.8.

DNA methylation analysis

Extracted tumor DNA was analyzed for genome-wide DNA methylation patterns using the HumanMethylation450 BeadChip platform according to instructions from the manufacturer (Illumina) and analyzed as described in [250,72]. From the selection of probes on the array, we removed probes from sex chromosomes (chromosomes X and Y) as well as those located at sites with documented SNPs (according to dbSNP).

Methylation values were normalized using the Subset-quantile Within Array Normalization (SWAN) procedure provided in the R package minfi [173]. We performed hierarchical clustering using the 10,000 most variable sites. Distance was assessed using $d = 1 - r$, where r is the Pearson product-moment coefficient. Clustering was performed using average linkage (UPGMA) and was validated for the robustness of the procedure

via multiscale resampling (1,000 iterations) using the R package pvclust [251] (Supplementary Figure 3.5).

Copy number variant detection

To assay CNVs in our samples, we used a methylation-based method and controls implemented in the R/Bioconductor packages CopyNumber450k and CopyNumber450kData, respectively. CNV analysis for copy number gains and losses in previously described genes of interest is presented in Supplementary Tables 3.4 and 3.5, respectively. Gross genomic aberrations were assessed using UCSC Genome Browser banding and our in-house algorithm described above. Bands covered with >90% significantly amplified or deleted segments were counted as 'abnormal' and summed for each sample. Samples were grouped together by mutation type, and a *t* test was performed to assess statistically significant differences in aberration count between mutation subgroups. CNV analysis for broad areas of genomic instability is included in Supplementary Table 3.7.

Cell lines and protein blotting

hTert-immortalized NHAs were obtained from A. Guha (Labatt Brain Tumour Centre) and were grown in DMEM supplemented with 10% FBS as previously described. The DIPGIV primary cell line (a kind gift from M. Monje, Stanford University) and KNS42 cells (purchased from the Japanese Collection of Research Bioresources (JCRB) Cell Bank) were grown as previously described [187]. Mycoplasma-tested cell lines were starved of serum and growth factors for 1 h before protein extraction. Proteins were

extracted in Tris-NaCl-EDTA lysis buffer as previously described [239], and blotting was performed for phosphorylated SMAD1/5/8 (Cell Signaling Technology, 9511; 1:500 dilution in 5% BSA solution) on total lysates from NHA cells and from DIPGIV cells as previously described [79]. β -actin (13E5, Cell Signaling Technology, 4970; 1:1,000 dilution in 5% BSA solution) was used as a loading control.

Quantitative PCR for BMP target genes

qPCR was performed to assess the levels of activity downstream of the ACVR1 (ALK2) receptor in total RNA extracted from DIPGIV (H3.1 Lys27Met, ACVR1 Gly328Val), KNS42 (H3.3 Gly34Val, ACVR1 wild type) and NHA cells grown in DMEM supplemented with 10% FBS using *ID1*, *ID2*, *ID3* and *SNAIL* with the primer sequences detailed in Supplementary Table 3.8. Briefly, total RNA was extracted using the miRNeasy mini kit (Qiagen) according to the manufacturer's instructions, with purity and integrity assessed using Nanodrop (Thermo Fisher) and Experion (Bio-Rad) methodologies. RNA (100 ng) was used for reverse transcription with iScript RT Supermix (Bio-Rad) following the manufacturer's instructions. RT-PCR was run on a LightCycler 96 (Roche) with the SsoFast Evagreen SuperMix kit (Bio-Rad). Cycling conditions were 95 °C for 30 s followed by 40 cycles of 95 °C for 5 s and 60 °C for 20 s. Fold change values were calculated using the $2^{-\Delta\Delta C_t}$ method with *ACTB* expression and NHA cells used as the calibrator.

Immunohistochemistry

Immunohistochemistry was performed on formalin-fixed, paraffin-embedded slides from case with (n = 4) or without (n = 3) *ACVR1* mutation and control normal brain (n = 1) to assess phosphorylation of SMAD1/5/8 downstream of the ACVR1 (ALK2) receptor (reviewed in [229]). Immunohistochemistry was carried out as previously described [147] using antibodies to phosphorylated SMAD1/5/8 (Cell Signaling Technology, 9511; 1:50 dilution) and SMAD1 (Invitrogen, 38-5400; 1:100 dilution). Immunohistochemistry processing and imaging were performed blinded to *ACVR1* mutation status with representative images presented in Figure 3.2.

FISH for PDGFRA amplification

FISH was performed as previously described in [211,69]. Briefly, FISH was performed using 4- μ m tissue sections from a subset of midline HGAs, with a BAC probe directed against the *PDGFRA* genomic locus in chromosomal region 4q12 (RP11-231c18; green) and a probe directed against 4p11.2-4q11.1 (CEN4; red) as a control to visualize chromosome 4. Scoring is included in Supplementary Table 3.1, and representative images are shown in Supplementary Figure 3.2.

URLs

FASTX-Toolkit, http://hannonlab.cshl.edu/fastx_toolkit/; Genome Analysis Toolkit (GATK), <http://www.broadinstitute.org/gsa/wiki/>; Picard, <http://picard.sourceforge.net/>; SAMtools, <http://samtools.sourceforge.net/>; BLAST, <http://blast.ncbi.nlm.nih.gov/Blast.cgi>; Ensembl, <http://useast.ensembl.org/index.html>;

UniProt, <http://www.uniprot.org/>; UCSC Genome Browser, <http://genome.ucsc.edu/>; dbSNP, <http://www.ncbi.nlm.nih.gov/SNP/>.

Accession codes

Whole-exome sequencing data can be accessed through the European Genome-phenome Archive (EGA) under accession EGAS00001000720. DNA methylation data can be accessed through the Gene Expression Omnibus (GEO) under accession GSE55712.

3.4 Results

We analyzed 40 mHGAs, with whole-exome sequencing data for 39 tumors, including 25 biopsies from DIPG cases (11 previously reported [231,118], Materials and Methods and Supplementary Table 3.1). The recurrent histone H3 gene mutation encoding p.Lys27Met was found in 37 of 40 cases (93%) and was distributed among three histone variant genes, including *H3F3A* (32/40 samples), *HIST1H3B* (4/39 samples) and *HIST1H3C* (1/39 samples). *HIST1H3C* also encodes the canonical histone H3.1 (as does *HIST1H3B*) and has not previously been reported to be mutated (Figure 3.1). All five histone H3.1 alterations occurred in the pons of younger cases (Supplementary Figure 3.1). Histone H3.3 p.Lys27Met alterations occurred in multiple midline locations, including the brainstem (19/25), thalamus (9/11) and rare locations for HGAs—the cerebellum, fourth ventricle and spinal cord (4/4). In contrast, only 1 histone H3.3 p.Lys27Met mutant was identified in 42 pediatric high-grade tumors located in cerebral hemispheres in a previously reported data set [231,72] (Figure 3.1 and Supplementary Table 3.1).

The pattern of somatic mutations in specific genes or gene pathways showed striking features (Figure 3.1 and Supplementary Figure 3.1). Recurrent somatic mutations in the activin A receptor, type I gene (*ACVR1*) occurred in 5 of 39 mHGAs and overlapped with p.Lys27Met alterations (5/5), mainly in histone H3.1 (4/5) rather than histone H3.3 or wild-type histone H3 ($P = 0.0003$, Fisher's exact test; Supplementary Figure 3.1). These specific amino acid residues in *ACVR1* have previously been reported to be affected by germline mutations causing fibrodysplasia ossificans progressiva (FOP), an inherited musculoskeletal disease [238,80,37,79,183,144]. The p.Arg206His, p.Gly328Glu and p.Gly356Asp substitutions result in ligand-independent activation of the kinase, leading to an increase in BMP signaling and increased phosphorylation of SMAD1, SMAD5 and SMAD8 (SMAD1/5/8) in tissues [80], whereas the newly identified p.Gly328Val and p.Arg258Gly substitutions are predicted to exert gain-of-function effects similar to those for the previously described p.Arg258Ser, p.Gly328Glu, p.Gly328Trp and p.Gly328Arg alterations, on the basis of the physicochemical properties of the mutant residues and predicted protein structure (Figure 3.4 and Supplementary Table 3.2)[37,79]. *ACVR1*, also known as *ALK2*, is a type I receptor of the mammalian transforming growth factor (TGF)- β signaling family with critical developmental roles in the mouse embryo [183] and in early left-right patterning [144]. Investigation of *ACVR1* pathway activation using immunohistochemical staining for phosphorylated SMAD1/5/8 in DIPG samples showed positive staining only in tumors with mutant *ACVR1* (4/4), including in DIPGs with the newly identified p.Gly328Val and p.Arg258Gly alterations (Figure 3.2). In addition, in the primary cell line DIPGIV, which carries histone H3.1 p.Lys27Met and the new *ACVR1* substitution p.Gly328Val, we demonstrated increased

levels of phosphorylated SMAD1/5/8 compared to normal human astrocytes (NHA cells) and significantly increased expression of genes containing BMP response elements—*ID1*, *ID2* and *ID3*—and *SNAI1* compared to KNS42, a cell line with the histone H3.3 p.Gly34Val alteration and wild-type *ACVR1* (Figure 3.4). These genes are early-response genes induced following active BMP2 signaling and represent SMAD1/5/8 downstream effectors [185,151].

We identified mutations in *FGFR1* in association with histone H3.3 p.Lys27Met alteration in 4 of 39 cases: 3 thalamic HGAs also having *NF1* mutations (previously reported in [118]) and 1 DIPG (Figure 3.1). These *FGFR1* mutations affected hotspot residues in the tyrosine kinase domain of the FGFR1 receptor. They have been shown to lead to its constitutive activation in a subset of thalamic pilocytic astrocytomas, a grade I tumor that rarely progresses to higher-grade astrocytoma, and in NIH 3T3 cells [118]. Comparison with our data set of non-midline cortical HGA-HGG indicated that tumors carrying *ACVR1* or *FGFR1* mutations were exclusive to midline HGAs ($P = 0.0040$, Fisher's exact test; Figure 3.1 and Supplementary Figure 3.1b).

TP53 mutations occurred in 28 of 40 samples, largely in combination with histone H3.3 p.Lys27Met alteration (25/28) as reported previously [136,231] and, to a much lesser extent, with histone H3.1 p.Lys27Met alteration (1/5) (Figure 3.1 and Supplementary Figure 3.1b). One DIPG sample (mHGA1) had histone H3.3 p.Lys27Met alteration as well as a splicing mutation in *CHEK2*, a gene associated with Li-Fraumeni syndrome similar to *TP53* (Figure 3.1 and Supplementary Tables 3.1 and 3.6). Three midline samples displayed no detectable mutation across *H3F3A*, *HIST1H3B* and *HIST1H3C*, even when sequenced at extremely high depth (average read depth across all

tumors and genes of >20,000×; Supplementary Table 3.3). These samples carried alterations described in adult HGA in the form of combined *TP53* mutation, *PDGFRA* amplification and *CDKN2A* loss (mHGA35), *PDGFRA* and *EGFR* amplification and *NFI* loss (mHGA36), or the previously identified *FGFR1-TACCI* fusion [241,291] (mHGA37) (Figure 3.1 and Supplementary Tables 3.1, 3.3 and 3.4).

We identified somatic *PDGFRA* mutations in a small subset of pediatric mHGAs (5/39; Supplementary Table 3.1). Notably, *PDGFRA* amplification occurred in 3 of 12 treatment-naive DIPGs (Supplementary Figure 3.2 and Supplementary Table 3.1). Interestingly, a cerebellar HGA sample with multiple biopsies taken from different anatomical loci showed *PDGFRA* amplification in only one tumor site, whereas similar somatic mutation and DNA methylation profiles were observed across all tumor sites (Supplementary Figure 3.3). This finding supports the view that *PDGFRA* amplifications precede therapy but can be further promoted by it, as described in radiation-induced supratentorial HGA [199]. Mutations in other growth factor receptor and component genes described to have focal gains or losses in DIPG [198,289] or HGA (*MET*, *RBI* and *PARP1*) showed low incidence in our data set (Figure 3.1 and Supplementary Tables 3.1 and 3.4–3.6), whereas recurrent mutations in components of the phosphoinositide 3-kinase (PI3K) pathway, predicted to activate AKT signaling, were present in 10 of 39 mHGAs. With respect to alterations affecting telomere length, *ATRX* mutations were identified in nine midline tumors, exclusively in samples with histone H3.3 p.Lys27Met alteration and *TP53* mutation, and affected older children [136], whereas no *TERT* promoter mutations, assessed using targeted sequencing, were identified in mHGAs (Supplementary Table 3.1).

Lysine-to-methionine substitutions in histone variants at residue Lys27 have recently been shown to inhibit SET domain–containing histone methyltransferases [161], possibly accounting for the specific DNA methylation pattern we observed in non-brainstem tumors with the histone H3.3 p.Lys27Met alteration [250]. When clustering our samples by global DNA methylation, all samples with a given histone H3 alteration (absent or affecting Lys27 or Gly34) clustered together but did not group on the basis of tumor location within the brain, the particular histone H3 gene mutated, and additional partner mutations or structural alterations identified (Figure 3.3 and Supplementary Figures 3.4 and 3.5). The global epigenetic profile is thus strongly associated with alteration of the histone H3 variant mark. Interestingly, *TP53* alteration was associated with increased broad copy number changes as we previously showed [231] (average of 32 events per sample), indicating a level of genomic instability. The number of copy number changes was significantly higher in samples with the histone H3.3 p.Gly34Arg or p.Gly34Val alteration than in other groups ($P = 0.02997$; Supplementary Table 3.7), in keeping with global hypomethylation identified in these tumors [250].

3.5 Discussion

The gain-of-function alterations in three growth factor receptor genes—*ACVR1*, *FGFR1* and *PDGFRA*—associate with histone H3 p.Lys27Met variants in midline HGA. These mutations are not seen concurrently, and *ACVR1* and *FGFR1* mutations are mutually exclusive with *TP53* alterations and privilege specific locations within the midline of the brain. *ACVR1* mutations do not seem to correlate with differential survival in patients with HGA, although no definite conclusions can be drawn because of our

limited sample size (Supplementary Figure 3.6). The lack of reported central nervous system (CNS) tumor development in humans with FOP or *Acvr1* (*Alk2*) mouse models suggests that aberrant activation of this pathway is not sufficient for tumorigenesis [80] and that it may act in concert with histone H3 p.Lys27Met substitution and other alterations we identified in the PI3K pathway to induce tumorigenesis (Figure 3.1). Interestingly, *ACVR1* is mainly expressed at embryonic day (E) 14 in the cortex of mouse embryos and at very low levels in the brainstem, and aberrantly active ACVR1 leads to increased ventralization of zebrafish embryos [37,79,235]. Aberrant ACVR1 signaling in the brainstem, a midline structure, may specify a patterning defect in DIPG, as this gene is involved in left-right patterning development. FGFR signaling regulates neural progenitor maintenance and the development of the ventral midbrain [154]. Similar to *ACVR1* mutations, the *FGFR1* gain-of-function mutations we identify only lead to grade I astrocytomas if present on their own in a tumor [118] and are commonly found in association with *NF1* and histone H3.3 p.Lys27Met alterations in midline HGA. Mutations affecting histone H3 variants in pediatric HGAs mirror *IDH* gene mutations in their requirement for additional alterations to potentially induce HGA. Mutations encoding p.Gly34Arg and p.Gly34Val have been found in *H3F3A* and not in other histone genes thus far and invariably associate with *TP53* and *ATRX* mutations in the cortex. In mHGA, mutations encoding p.Lys27Met arise in different histone H3 variants depending on age and tumor location. They associate with *TP53* mutations or with activated neurodevelopmental growth factor receptor pathways through distinct hits in *ACVR1*, *FGFR1* or *PDGFRA* to achieve tumorigenesis. These alterations in growth factor receptors and in members of the PI3K pathway offer previously unforeseen therapeutic

possibilities in a deadly cancer, while the observed level of genomic instability calls for caution in the choice of adjuvant therapy whenever possible. Notably, we show that small-needle pretherapy biopsies can reliably identify the mutational landscape in HGA. This technique will allow for the tailoring of available therapies to the results obtained from stereotactic biopsy in children affected by this fatal brain tumor while effort continues to be made to target p.Lys27Met histone alterations.

3.6 Acknowledgments

The authors would like to express their sincere gratitude toward all staff at the McGill University and Génome Québec Innovation Centre for excellent technical expertise, library preparation and sequencing. The authors are very grateful to J.-J. Lebrun (McGill University) for primer sequences and materials for SMAD signaling studies. This work was performed within the context of the I-CHANGE (International Childhood Astrocytoma Integrated Genomics and Epigenomics) Consortium and was supported by funding from Genome Canada, Génome Québec, the Institute for Cancer Research of the Canadian Institutes for Health Research (CIHR), McGill University and the Montreal Children's Hospital Foundation. This work was also supported by Hungarian Scientific Research Fund (OTKA) contract T-04639, National Research and Development Fund (NKFP) contract 1A/002/2004 (P.H. and M.G.) and TÁMOP-4.2.2A-11/1/KONV-2012-0025 (A.K. and L.B.). N.J. is a member of the Penny Cole laboratory and the recipient of a Chercheur Clinicien Senior Award. J. Majewski holds a Canada Research Chair (tier 2). L.G., K.L.L. and M.W.K. are supported by NCI P01CA142536. We acknowledge the support of the Zach Carson DIPG Fund at the Dana-Farber Cancer Institute (DFCI), the

Ellie Kavalieros Fund (DFCI), the Mikey Czech Foundation, the Prayer From Maria Foundation, the Hope for Caroline Fund (DFCI), the Ryan Harvey DIPG Fund (DFCI), the Stop&Shop Pediatric Brain Tumor Program (DFCI) and the Pediatric Brain Tumor Clinical and Research Fund (DFCI). A.M.F. is supported by a studentship from CIHR, as well as by an award from the CIHR Systems Biology Training Program at McGill University. D.B. is supported by a studentship from the T.D. Trust/Montreal Children's Hospital Foundation, and N. Gerges is supported by a studentship from the Cedars Cancer Institute. N.D.J. is supported by an award from the McGill Integrated Cancer Research Training Program.

3.7 Competing financial interests

The authors declare no competing financial interests.

3.8 Figures

Figure 3.1

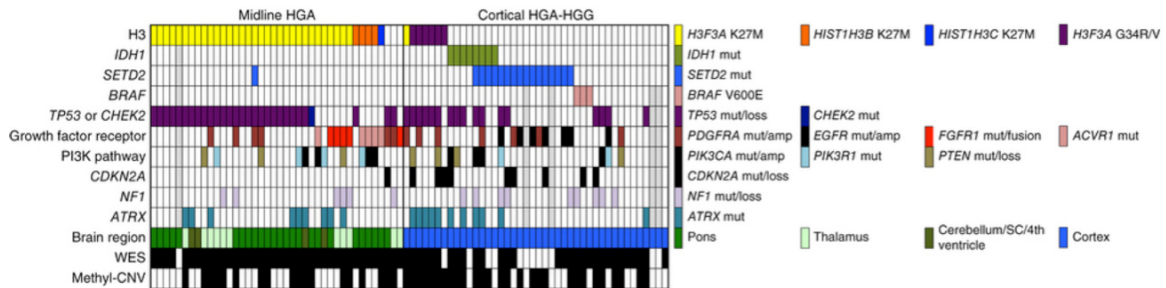


Figure 3.1: Genomic landscape of pediatric midline HGAs.

Distribution of mutations and alterations in 40 pediatric midline high-grade astrocytomas (midline HGA) and 42 cortical high-grade astrocytomas and high-grade gliomas (cortical HGA-HGG) described in the study. Mutations (mut) were identified with whole-exome sequencing (WES) where available and are indicated by colored boxes. Amplifications (amp) and losses were identified using DNA methylation profile–derived copy number variant (methyl-CNV) analysis and are indicated where available by colored boxes. SC, spinal cord. Boxes in light gray indicate samples for which data are not available.

Detailed information on tumor samples included herein can be found in Supplementary Table 3.1, with specific variants and transcript accessions presented in Supplementary Table 3.6.

Figure 3.2

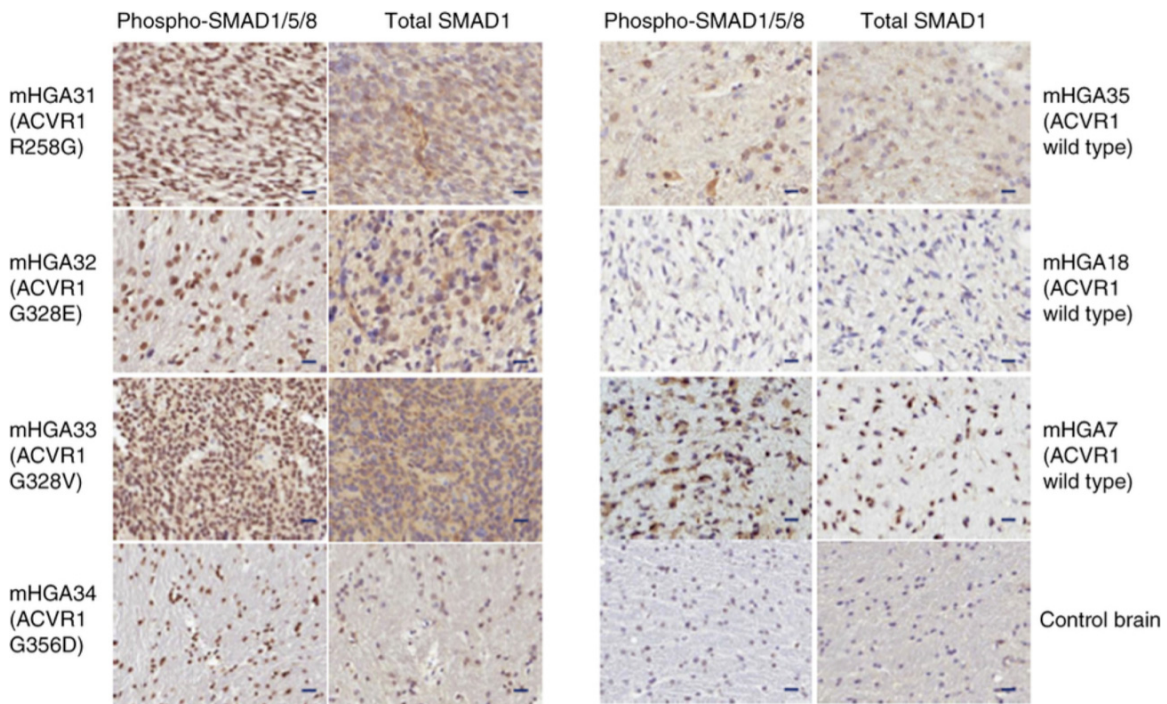


Figure 3.2: Increased levels of phosphorylated SMAD1/5/8 in *ACVRI*-mutant mHGAs.

Immunohistochemical analysis of mHGAs harboring *ACVRI* mutations identified in this study (n = 4; left) demonstrate increased nuclear positivity of phosphorylated SMAD1/5/8 compared to mHGAs with wild-type *ACVRI* (n = 3) and a control brain sample (right), with total-SMAD1 staining shown in each case as a positive control. Scale bars, 20 μ m (20 \times magnification). Clinicopathological and molecular characteristics of tumor samples are presented in Supplementary Table 3.1.

Figure 3.3

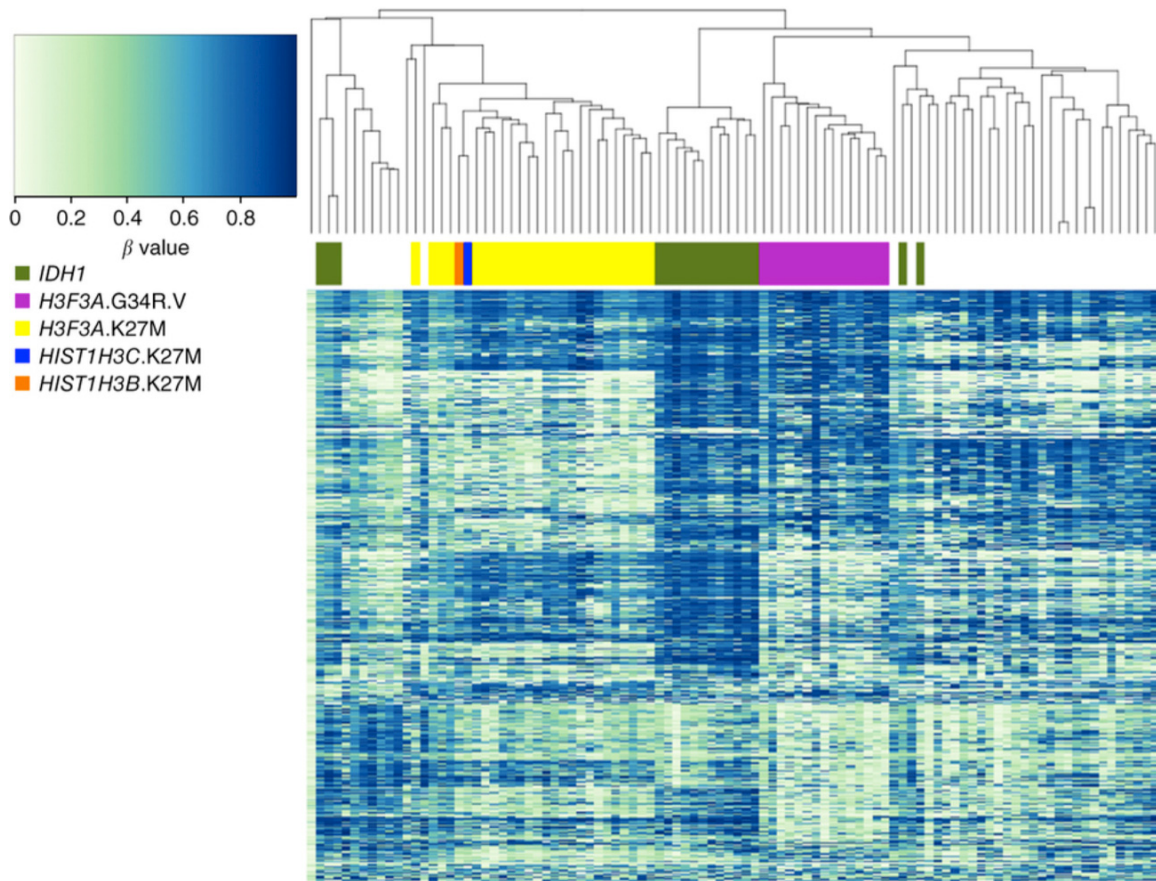


Figure 3.3: Clustering analysis of global DNA methylation profiles for 98 high-grade astrocytomas. Global DNA methylation clustering analysis of high-grade astrocytomas distributed across the brain demonstrates similar impact on epigenomic dysregulation caused by p.Lys27Met alteration regardless of age, brain location, associated mutations or the particular histone H3 variant affected. The top 10,000 most variable normalized methylation β values were used for UPGMA clustering with alterations of interest indicated. Robustness was assessed using multiscale bootstrapping (Supplementary Figure 3.5). Detailed information regarding sample clinicopathological characteristics is included in Supplementary Table 3.1, with methylation-derived CNVs presented in Supplementary Tables 3.4 and 3.5.

Figure 3.4

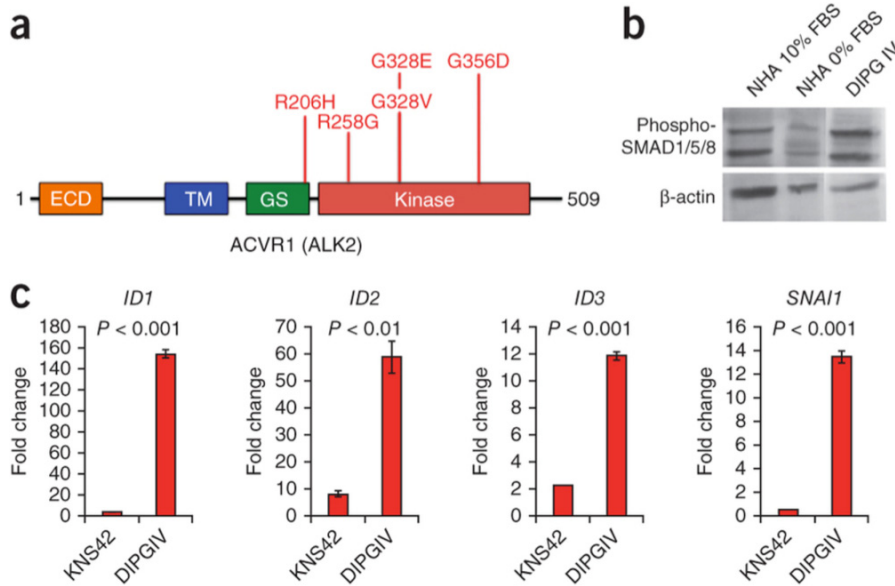
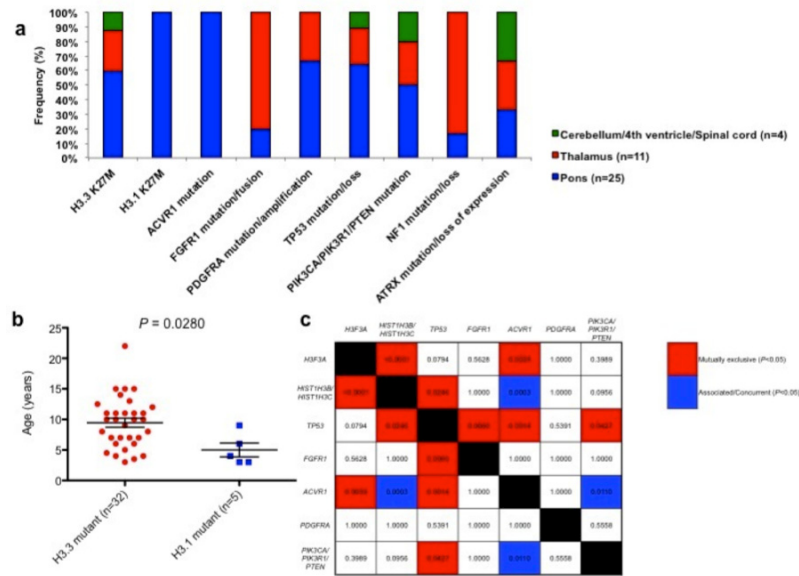


Figure 3.4: Mutations identified in *ACVR1* are associated with activation of downstream SMAD signaling pathways.

(a) Distribution of alterations identified in *ACVR1* ($n = 5$) demonstrating the impact of amino acid substitutions on the kinase domain of the protein. ECD, extracellular domain; TM, transmembrane domain; GS, glycine-serine-rich domain. (b) Immunoblotting analysis of phosphorylated SMAD1/5/8 levels in NHA cells with wild-type *ACVR1* grown in 10% FBS or in NHA and DIPGIV cells (*ACVR1* mutation encoding p.Gly328Val) starved for 1 h in medium free of serum and growth factors (0%). (c) Quantitative PCR (qPCR) analysis of the expression of the downstream BMP effectors *ID1*, *ID2*, *ID3* and *SNAIL* in *ACVR1*-mutant DIPGIV cells and in the glioblastoma (GBM) cell line KNS42 with wild-type *ACVR1*. Values represented are fold changes calculated using the $2^{-\Delta\Delta C_t}$ method, normalized to *ACTB* expression in calibrator NHA cells. P values were calculated using two-tailed t tests for significance, with error bars representing s.d. from two technical replicates.

3.9 Supplementary Material

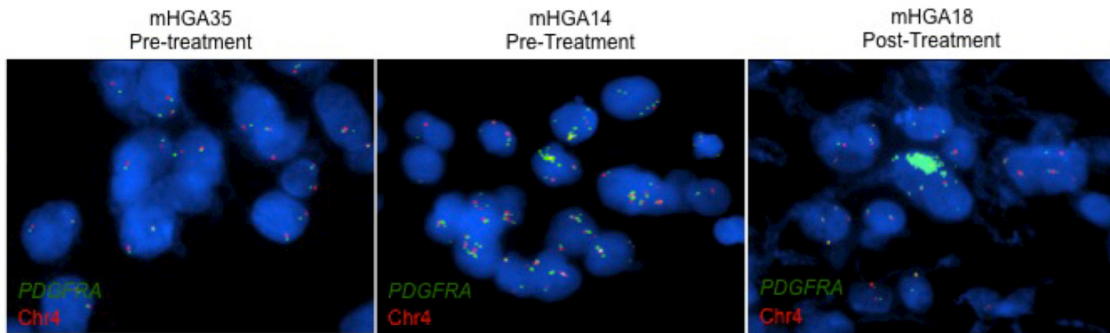
Supplementary Figure 3.1



Supplementary Figure 3.1: Patterns of K27M-associated mutations among midline pediatric high-grade astrocytomas.

A, Neuroanatomical distribution of mutations and alterations of interest in pediatric midline high-grade astrocytomas. **B**, The age of patients harbouring H3.3 and H3.1 mutations is significantly different ($P = 0.0280$; two-tailed t test). **c**, Mutual exclusivity and associative statistical analyses (represented as P values) of mutations in *H3F3A*, *HIST1H3B/HIST1H3C*, *TP53*, *FGFR1*, *ACVR1*, *PDGFRA* and PI3K pathway genes *PIK3CA/PIK3R1/PTEN* demonstrates predilection for co-occurrence of and exclusion of particular mutations as unique mutational groups within 39 midline high-grade astrocytomas profiled by whole-exome sequencing. P values were calculated utilizing Fisher's exact test (two-sided) with highlighted values indicating statistically significant ($P < 0.05$) preferences for co-occurrence or mutual exclusivity.

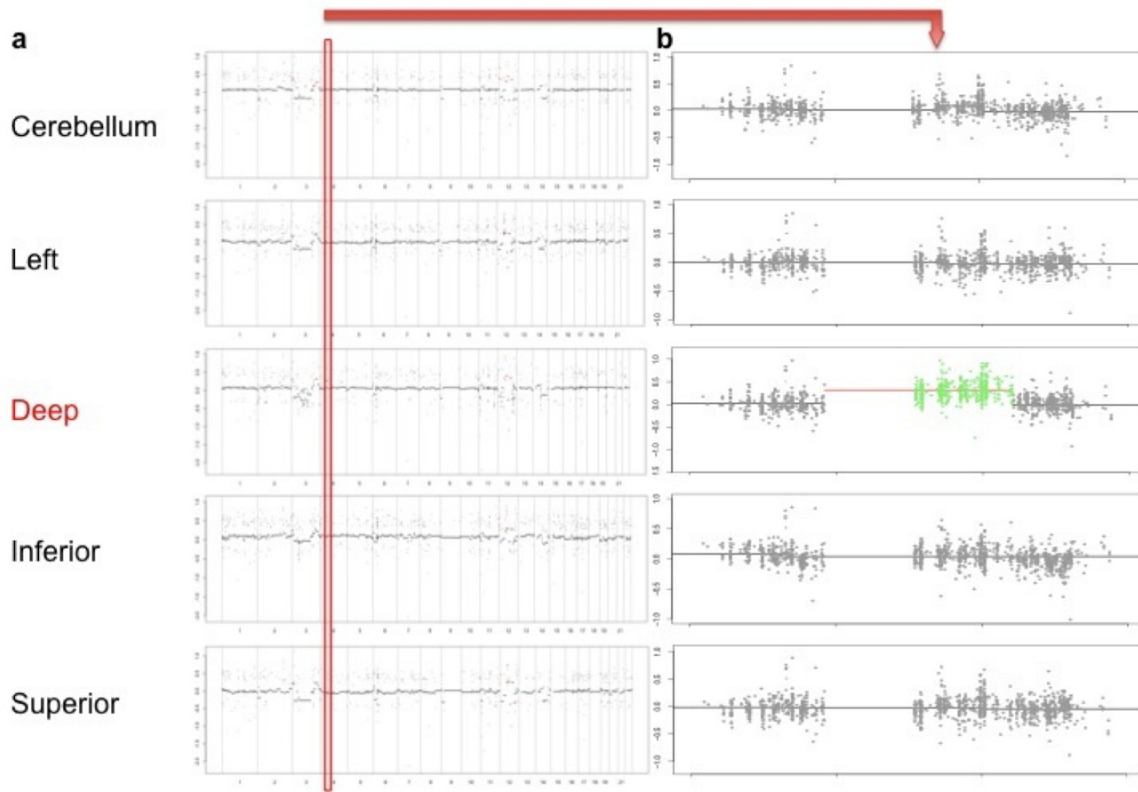
Supplementary Figure 3.2



Supplementary Figure 3.2: *PDGFRA* amplification is present in a minority of cells in DIPG.

Representative images from FISH assay for *PDGFRA* amplification reveal substantial increase in the number of *PDGFRA*-positive nuclei following treatment compared with samples from pretreatment biopsies. Green, *PDGFRA*; red, Chr4/CEN4.

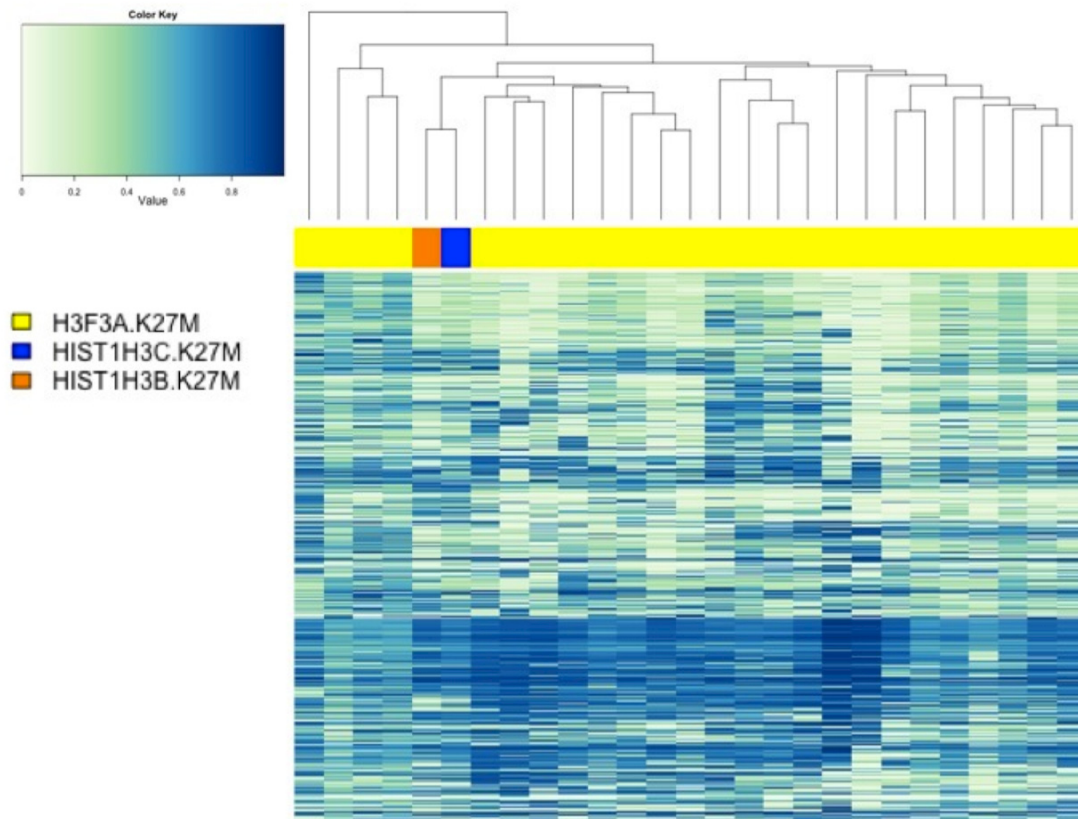
Supplementary Figure 3.3



Supplementary Figure 3.3: Copy number variant analysis using biopsy material from five different anatomical loci in a single tumor.

a, Tumor biopsies (n = 5) show highly similar CNV patterns across the genome. b, Plots depicting 20-Mb zoom-in of chromosome 4, showing significant *PDGFRA*, *KIT* and *KDR* amplification in only the deep tissue biopsy and not others.

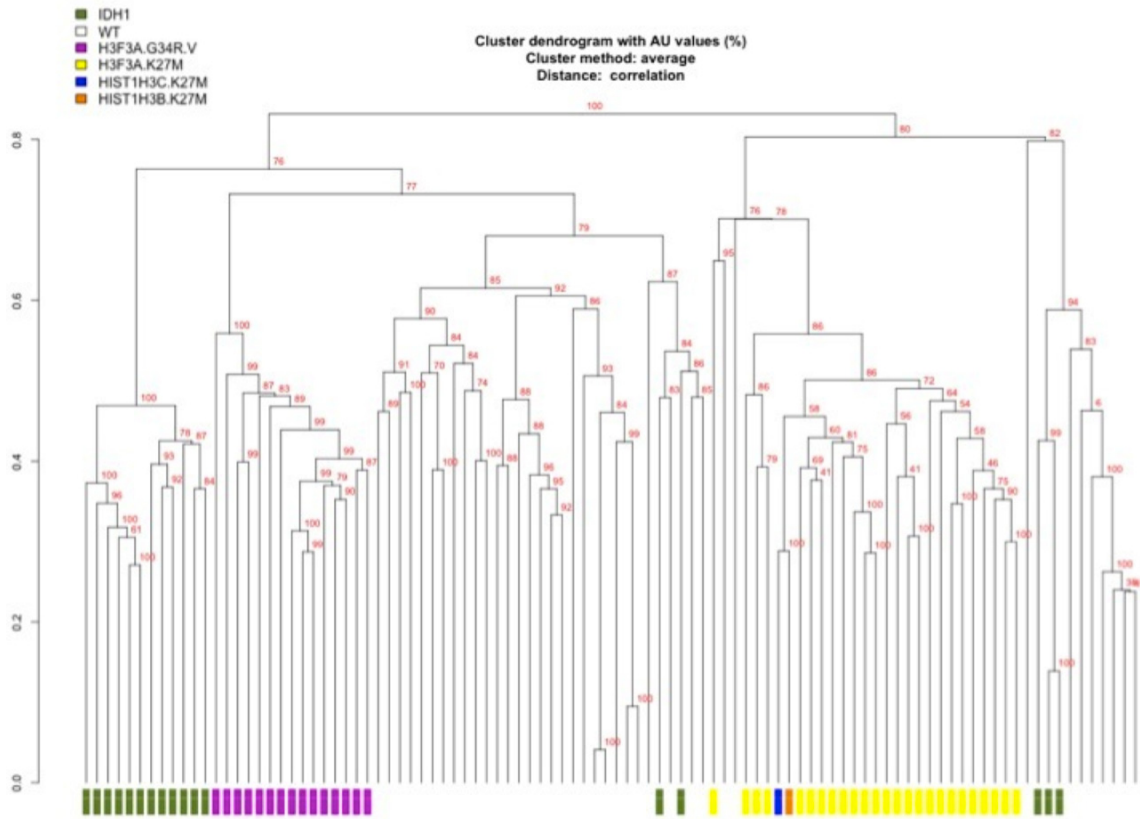
Supplementary Figure 3.4



Supplementary Figure 3.4: H3.1 and H3.3 K27M variants demonstrate similar patterns of global DNA methylation.

Heat map of hierarchical clustering analysis of DNA methylation array data from the top 10,000 most variable β values from 27 K27M-mutant high-grade gliomas demonstrates that H3.3 and H3.1 K27M mutant tumors show similar patterns of global epigenomic dysregulation.

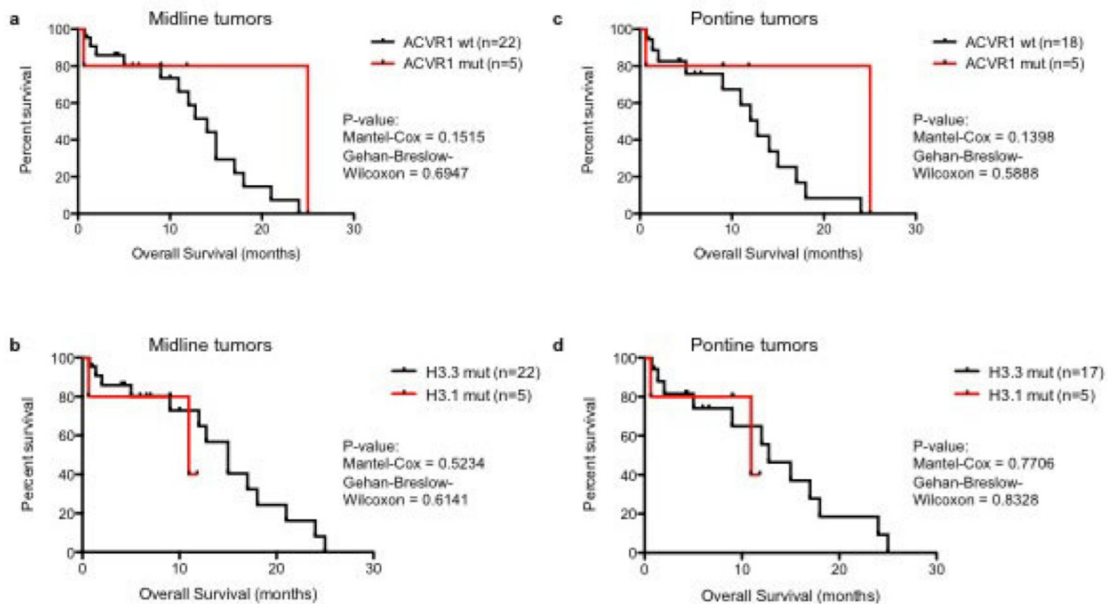
Supplementary Figure 3.5



Supplementary Figure 3.5: Multiscale bootstrapping of the high-grade astrocytoma methylation cluster.

Dendrogram of multiscale bootstrapping of DNA methylation profiles of patient high-grade tumors. *P* values, represented as the red values at the internal nodes, are the approximately unbiased (AU) *P* value computed by the R package pvclust.

Supplementary Figure 3.6



Supplementary Figure 3.6: Mutation subgroup-specific overall survival of midline high-grade astrocytomas (mHGAs) and diffuse intrinsic pontine gliomas (DIPGs).

Kaplan-Meier analysis of overall survival (months) of mHGAs with available outcome data, with indicated *P* values from Mantel-Cox (log-rank) and Gehan-Breslow-Wilcoxon testing for comparison based on **a**, *ACVR1* mutation status (n = 27), **b**, H3.3/H3.1 K27M mutation status (n = 27) and overall survival restricted to tumors of the pontine area based on **c**, *ACVR1* mutation status (n = 23), **d**, H3.3/H3.1 K27M mutation status (n = 22).

Supplementary Table 3.2 Functional assessment of ACVR1 growth factor receptor mutations reported herein

Supplementary Table 2: Functional assessment of ACVR1 growth factor receptor mutations reported herein

ACVR1 Mutation	Reported Effects	Homology modeling and predictions	Reference(s)
p.R206H	Increased ligand dependent (BMP4/6) and independent responses in a BRE luciferase reporter system. Promotion of ventralization of zebrafish embryos.	Critical hydrogen bonds are formed by Arginine 206 mediating stable GS domain interactions with the kinase loop. Shore and colleagues (Nat Genet 2006) predict H206 cannot interact with alpha-helix backbone. Most common mutation seen in FGF.	Shore et al, Nat Genet 2006; Fukuda et al, JBC 2009; Chaikuad et al, JBC 2012; Shen et al, J Clin Invest 2009
p.R258G	Increased phospho-SMAD1/5/8 staining on immunohistochemistry of patient tumors harboring ACVR1 R258G.	Chaikuad and colleagues (JBC 2012) predict that Arginine 258 forms critical hydrogen bonds with the GS loop and lack of these bonds allows the GS domain to separate and no longer regulate the kinase domain. We hypothesize that Glycine 258 identified herein would not recapitulate this critical hydrogen bonding as it is uncharged.	Chaikuad et al, JBC 2012; this study
p.G328V	Increase in endogenous phospho-SMAD1/5/8 signal in DIPG cells harboring ACVR1 G328V. Increased phospho-SMAD1/5/8 staining on immunohistochemistry of patient tumors harboring ACVR1 G328V. Increased endogenous expression of downstream effectors <i>ID1</i> , <i>ID2</i> , <i>ID3</i> and <i>SNAI1</i> in ACVR1 G328V DIPG cultured cells.	Glycine 328 is located inside the E6 loop. Chaikuad et al report that no other side chain can be accommodated here. Homology modeling predicts bulky side chains would produce change in electrostatic potential (in the case of acidic E (Glu) and basic R (Arg) substitutions). Chaikuad et al (JBC 2012) predict that mutations in the mutation cluster at sites L196, R258 and G328 would promote active kinase conformations. We hypothesize that the steric bulk of Valine 328 would produce a change in local protein structure based on the change in physicochemical properties for this residue.	Chaikuad et al, JBC 2012; G328E: Petrie et al, PLoS One 2009; this study
p.G328E	Increased ligand dependent (BMP4/6) and independent responses in a BRE luciferase reporter system. Increased phospho-SMAD1/5/8 staining on immunohistochemistry of patient tumors harboring ACVR1 G328E.	Glycine 328 is located inside the E6 loop. Chaikuad et al report that no other side chain can be accommodated here. Homology modeling predicts bulky side chains would produce change in electrostatic potential (in the case of acidic E (Glu) and basic R (Arg) substitutions). Chaikuad et al (JBC 2012) predict that mutations in the mutation cluster at sites L196, R258 and G328 would promote active kinase conformations.	Chaikuad et al, JBC 2012; G328E: Petrie et al, PLoS One 2009; this study
p.G356D	Increased ligand dependent (BMP4/6) and independent responses in a BRE luciferase reporter system. Increase in phospho-SMAD1/5/8. Increased phospho-SMAD1/5/8 staining on immunohistochemistry of patient tumors harboring ACVR1 G356D.	Destabilizes inhibitory A loop resulting in ALK2 kinase activation.	Chaikuad et al, JBC 2012; Fukuda et al, BBRC 2008; this study

FGFR1 Mutation	Reported Effects	Homology modeling and predictions	Reference(s)
p.N546K	Increased phospho-FGFR and phospho-ERK1/2 positivity on immunohistochemical staining of FGFR1 N546K mutated PA FFPE sections. Increased phospho-ERK1/2 signal in NIH 3T3 cells overexpressing FGFR1 N546K. Liu and colleagues (Development, 2003) report hyperproliferation of midbrain in chick embryos expressing <i>Fgfr1</i> N546K. Autophosphorylation sequence is disrupted FGFR1 N546K.	Rand and colleagues (Proc Natl Acad Sci 2005) predict that adjacent sequence region involving N546K predicted to become more basic with amino acid substitution, in addition to disruption of hydrogen bonding to H541 of the main chain.	Jones et al, Nat Genet 2013; Rand et al, Proc Natl Acad Sci 2005; Liu et al, Development 2003; Lew et al, Sci Signaling 2009
p.655_655del	NA	We hypothesize that this non-frameshift deletion may lead to de-stabilization of the kinase domain and possibly increased autophosphorylation in adjacent critical tyrosine residues (Y654 and Y653).	Jones et al, Nat Genet 2013
p.N546K	Increased phospho-FGFR and phospho-ERK1/2 positivity on immunohistochemical staining of FGFR1 N546K mutated PA FFPE sections. Increased phospho-ERK1/2 signal in NIH 3T3 cells overexpressing FGFR1 N546K. Liu and colleagues (Development, 2003) report hyperproliferation of midbrain in chick embryos expressing <i>Fgfr1</i> N546K. Autophosphorylation sequence is disrupted FGFR1 N546K.	Rand and colleagues (Proc Natl Acad Sci 2005) predict that adjacent sequence region involving N546K predicted to become more basic with amino acid substitution, in addition to disruption of hydrogen bonding to H541 of the main chain.	Jones et al, Nat Genet 2013; Rand et al, Proc Natl Acad Sci 2005; Liu et al, Development 2003; Lew et al, Sci Signaling 2009
p.K656E	Increased phospho-ERK1/2 signal in NIH 3T3 cells overexpressing FGFR1 K656E. Liu and colleagues (Development, 2003) report hyperproliferation of midbrain in chick embryos expressing <i>Fgfr1</i> K656E. Analogous mutation in FGFR3 (K656E) results in partially active kinase in absence of ligand.	Mohammadi and colleagues (Cell 1996) hypothesize that Glutamate 650 (in FGFR3, and homologously E656 in FGFR1) may preferentially stabilize active conformations of the kinase domain.	Jones et al, Nat Genet 2013; Liu et al, Development 2003; Mohammadi et al, Cell 1996
p.K656E	Increased phospho-ERK1/2 signal in NIH 3T3 cells overexpressing FGFR1 K656E. Liu and colleagues (Development, 2003) report hyperproliferation of midbrain in chick embryos expressing <i>Fgfr1</i> K656E. Analogous mutation in FGFR3 (K656E) results in partially active kinase in absence of ligand.	Mohammadi and colleagues (Cell 1996) hypothesize that Glutamate 650 (in FGFR3, and homologously E656 in FGFR1) may preferentially stabilize active conformations of the kinase domain.	Jones et al, Nat Genet 2013; Liu et al, Development 2003; Mohammadi et al, Cell 1996

Supplementary Table 3.3 Deep sequencing statistics for *H3F3A*, *HIST1H3B*, *HIST1H3C* of midline high-grade astrocytomas included in the study (continued on next page)

Sample ID	Chromosome	Position	Reference	number of Reads	R1A	R1G	R1C	R1T	R1J	R2A	R2G	R2C	R2T	R1AS	R1GS	R1CS	R1TS	R1AS	R1GS	R1CS	R1TS	R2AS	R2GS	R2CS	R2TS	AS	GS	CS	TS	Variant %		
miNGA1	c0e1	25022108	T	12566	1	2	53	6488	1	89	20	6919	0	5	81.8734781	0.12750584	0.05559814	0.28782504	0.00787582	0.44100748	0.15915807	0.58178464	0.01918264	0.86518172	0.00194884	0.33533047	0.05526812	0.12738369	0.51133251			
miNGA2	c0e1	25022108	T	9150	1	0	33	4070	1	47	23	4975	0	0	0.01929892	0	0.00052739	0.44889432	0.01029822	0.51186106	0.25138512	0.54172887	0.02195729	0.83981052	0.00912828	0.48991378	0.76340596	0.07746723	0.14489031			
miNGA3	c0e1	25022108	T	8545	4	0	31	2811	4	43	19	4353	0	0	0.04681001	0	0.002182529	0.43782733	0.04411100	0.53121428	0.22323253	0.55147869	0.00826201	0.82318259	0.08172397	0.68102524	0.18137110	0.13717103				
miNGA4	c0e1	25022108	T	1306	0	0	3	646	0	3	0	650	0	0	0.03967749	0.494641226	0	0.22970038	0	0.491720006	0	0.491720006	0	0.22970038	0.330887749	0.2430322	0.76966784	0				
miNGA5	c0e1	25022108	T	21174	7	3	108	9912	7	129	81	12946	0	0.03200266	0.12284541	0.02429169	0.42779213	0.03200266	0.156665324	0.26329029	0.86433072	0.06412531	0.69603369	0.22633196	0.6340297	0.36931502	0	0	0			
miNGA6	c0e1	25022108	T	20372	2	2	88	8071	3	106	46	11148	0	0.00811206	0.00811206	0.00811206	0.00811206	0.00811206	0.00811206	0.00811206	0.00811206	0.00811206	0.00811206	0.00811206	0.00811206	0.00811206	0.00811206	0.00811206	0.00811206	0.00811206		
miNGA7	c0e1	25022108	T	9635	5	2	77	7951	6	78	59	9954	0	0.00951059	0.01202294	0.02829411	0.442509754	0.03008353	0.46889895	0.30957385	0.42742038	0.68912828	0.06912828	0.76340596	0.48991378	0.76340596	0.07746723	0.14489031	0	0		
miNGA8	c0e1	25022108	T	13908	9	1	74	6152	12	75	48	7829	0	0.01161004	0.07199108	0.03269783	0.42335846	0.08281577	0.500633	0.24512518	0.541351119	0.15816241	0.68618467	0.87170292	0.38784504	0.6333973	0	0	0	0		
miNGA9	c0e1	25022108	T	15220	5	0	66	6559	7	101	46	8391	0	0.03821813	0.13514444	0.04592116	0.66360028	0.03223993	0.55149604	0.08543259	0.86300554	0.08543259	0.86300554	0.08543259	0.73587385	0.48883548	0.45883548	0	0	0		
miNGA10	c0e1	25022108	T	5395	0	0	28	2217	1	30	15	3096	0	0.01869073	0.01869073	0.01869073	0.01869073	0.01869073	0.01869073	0.01869073	0.01869073	0.01869073	0.01869073	0.01869073	0.01869073	0.01869073	0.01869073	0.01869073	0.01869073	0.01869073	0.01869073	
miNGA11	c0e1	25022108	T	9086	7	2	48	3968	6	49	30	4963	0	0.07704162	0.02071886	0.02828274	0.431891702	0.00633569	0.53919117	0.33917926	0.54124872	0.14307749	0.86848327	0.86848327	0.86848327	0.86848327	0.86848327	0.86848327	0.86848327	0.86848327	0.86848327	
miNGA12	c0e1	25022108	T	14	0	0	0	0	0	0	0	0	0	0	0	0	0	0	0	0	0	0	0	0	0	0	0	0	0	0	0	
miNGA13	c0e1	25022108	T	8299	1	1	27	2627	5	44	16	4275	0	0.07240445	0.12049445	0.00048223	0.52018436	0.10279413	0.52123275	0.02729769	0.84224004	0.02729769	0.84224004	0.02729769	0.84224004	0.02729769	0.84224004	0.02729769	0.84224004	0.02729769	0.84224004	
miNGA14	c0e1	25022108	T	6484	0	0	39	2895	0	30	27	3903	0	0.05994374	0.00749653	0	0.68465714	0.00749653	0.68465714	0.00749653	0.68465714	0.00749653	0.68465714	0.00749653	0.68465714	0.00749653	0.68465714	0.00749653	0.68465714	0.00749653	0.68465714	0.00749653
miNGA15	c0e1	25022108	T	18248	2	0	70	6198	7	74	47	7945	0	0.07198168	0	0.07198168	0.2100647	0.08174989	0.31182128	0.29161454	0.50179659	0.06272627	0.51822229	0.19358344	0.38917142	0.39419227	0	0	0	0	0	
miNGA16	c0e1	25022108	T	11637	1041	3	74	3966	1324	78	28	4914	0	0.06142006	0.00114863	0.04489334	0.48724038	0.15625382	0.68806634	0.26933448	0.42800911	0.20442002	0.76991359	0.87262838	0.76991359	0.87262838	0.76991359	0.87262838	0.76991359	0.87262838	0.76991359	0.87262838
miNGA17	c0e1	25022108	T	8685	1572	5	89	2241	1694	77	15	2759	0	0.0112721	0.00211838	0.02369125	0.82369125	0.02369125	0.82369125	0.02369125	0.82369125	0.02369125	0.82369125	0.02369125	0.82369125	0.02369125	0.82369125	0.02369125	0.82369125	0.02369125	0.82369125	0.02369125

Supplementary Table 3.6: SNVs and insertion/deletion variants in candidate genes of interest (continued on next 3 pages)

Sample ID	Gene	Transcript accessic	Nucleotide variant	Amino acid change	Mutation type
mHGA1	H3F3A	NM_002107.4	c.83A>T	p.(Lys28Met)	Missense
mHGA2	H3F3A	NM_002107.4	c.83A>T	p.(Lys28Met)	Missense
mHGA3	H3F3A	NM_002107.4	c.83A>T	p.(Lys28Met)	Missense
mHGA4	H3F3A	NM_002107.4	c.83A>T	p.(Lys28Met)	Missense
mHGA5	H3F3A	NM_002107.4	c.83A>T	p.(Lys28Met)	Missense
mHGA6	H3F3A	NM_002107.4	c.83A>T	p.(Lys28Met)	Missense
mHGA7	H3F3A	NM_002107.4	c.83A>T	p.(Lys28Met)	Missense
mHGA8	H3F3A	NM_002107.4	c.83A>T	p.(Lys28Met)	Missense
mHGA9	H3F3A	NM_002107.4	c.83A>T	p.(Lys28Met)	Missense
mHGA10	H3F3A	NM_002107.4	c.83A>T	p.(Lys28Met)	Missense
mHGA11	H3F3A	NM_002107.4	c.83A>T	p.(Lys28Met)	Missense
mHGA12	H3F3A	NM_002107.4	c.83A>T	p.(Lys28Met)	Missense
mHGA13	H3F3A	NM_002107.4	c.83A>T	p.(Lys28Met)	Missense
mHGA14	H3F3A	NM_002107.4	c.83A>T	p.(Lys28Met)	Missense
mHGA15	H3F3A	NM_002107.4	c.83A>T	p.(Lys28Met)	Missense
mHGA16	H3F3A	NM_002107.4	c.83A>T	p.(Lys28Met)	Missense
mHGA17	H3F3A	NM_002107.4	c.83A>T	p.(Lys28Met)	Missense
mHGA18	H3F3A	NM_002107.4	c.83A>T	p.(Lys28Met)	Missense
mHGA19	H3F3A	NM_002107.4	c.83A>T	p.(Lys28Met)	Missense
mHGA20	H3F3A	NM_002107.4	c.83A>T	p.(Lys28Met)	Missense
mHGA21	H3F3A	NM_002107.4	c.83A>T	p.(Lys28Met)	Missense
mHGA22	H3F3A	NM_002107.4	c.83A>T	p.(Lys28Met)	Missense
mHGA23	H3F3A	NM_002107.4	c.83A>T	p.(Lys28Met)	Missense
mHGA24	H3F3A	NM_002107.4	c.83A>T	p.(Lys28Met)	Missense
mHGA25	H3F3A	NM_002107.4	c.83A>T	p.(Lys28Met)	Missense
mHGA26	H3F3A	NM_002107.4	c.83A>T	p.(Lys28Met)	Missense
mHGA27	H3F3A	NM_002107.4	c.83A>T	p.(Lys28Met)	Missense
mHGA28	H3F3A	NM_002107.4	c.83A>T	p.(Lys28Met)	Missense
mHGA29	H3F3A	NM_002107.4	c.83A>T	p.(Lys28Met)	Missense

mHGA38	H3F3A	NM_002107.4	c.83A>T	p.(Lys28Met)	Missense
mHGA39	H3F3A	NM_002107.4	c.83A>T	p.(Lys28Met)	Missense
mHGA40	H3F3A	NM_002107.4	c.83A>T	p.(Lys28Met)	Missense
mHGA33	HIST1H3B	NM_003537.3	c.83A>T	p.(Lys28Met)	Missense
mHGA31	HIST1H3B	NM_003537.3	c.83A>T	p.(Lys28Met)	Missense
mHGA30	HIST1H3B	NM_003537.3	c.83A>T	p.(Lys28Met)	Missense
mHGA32	HIST1H3B	NM_003537.3	c.83A>T	p.(Lys28Met)	Missense
mHGA34	HIST1H3C	NM_003531.2	c.83A>T	p.(Lys28Met)	Missense
mHGA17	SETD2	NM_014159.6	c.3103C>G	p.(His1035Asp)	Missense
mHGA2	ACVR1	NM_001105.4	c.617G>A	p.(Arg206His)	Missense
mHGA31	ACVR1	NM_001105.4	c.772A>G	p.(Arg258Gly)	Missense
mHGA33	ACVR1	NM_001105.4	c.983G>T	p.(Gly328Val)	Missense
mHGA32	ACVR1	NM_001105.4	c.983G>A	p.(Gly328Glu)	Missense
mHGA34	ACVR1	NM_001105.4	c.1067G>A	p.(Gly356Asp)	Missense
mHGA27	FGFR1	NM_001174067.1*	c.1731C>A	p.(Asn577Lys)	Missense
mHGA26	FGFR1	NM_001174067.1*	c.1731C>A	p.(Asn577Lys)	Missense
mHGA26	FGFR1	NM_001174067.1#	c.2058_2060del	p.(Lys687del)	Nonframeshift indel
mHGA29	FGFR1	NM_001174067.1*	c.2059A>G	p.(Lys687Glu)	Missense
mHGA28	FGFR1	NM_001174067.1*	c.2059A>G	p.(Lys687Glu)	Missense
mHGA17	PDGFRA	NM_006206.4	c.983A>G	p.(Asn328Ser)	Missense
mHGA18	PDGFRA	NM_006206.4	c.1021G>A	p.(Ala341Thr)	Missense
mHGA14	PDGFRA	NM_006206.4	c.1630_1631insCAG	p.(Ile543_Val544insA)	Nonframeshift indel
mHGA32	PIK3CA	NM_006218.2	c.1258T>C	p.(Cys420Arg)	Missense
mHGA2	PIK3CA	NM_006218.2	c.1633G>A	p.(Glu545Lys)	Missense
mHGA33	PIK3CA	NM_006218.2	c.3113A>T	p.(Tyr1038Phe)	Missense
mHGA25	PIK3CA	NM_006218.2	c.3140A>G	p.(His1047Arg)	Missense
mHGA9	PTEN	NM_000314.4	c.395G>C	p.(Gly132Ala)	Missense
mHGA28	PTEN	NM_000314.4	c.635-2A>C		Splicing
mHGA11	PIK3R1	NM_181523.2	c.1126G>A	p.(Gly376Arg)	Missense
mHGA24	PIK3R1	NM_181523.2	c.1338_1355del	p.(Lys447_Tyr452de	Nonframeshift indel
mHGA31	PIK3R1	NM_181523.2	c.1346_1348del	p.(Leu449_His450de	Nonframeshift indel

mHGA9	TP53	NM_000546.5	c.390_392del	p.(Asn131del)	Nonframeshift indel
mHGA12	TP53	NM_000546.5	c.404G>A	p.(Cys135Tyr)	Missense
mHGA24	TP53	NM_000546.5	c.452_456del	p.(Pro152Argfs*27)	Frameshift indel
mHGA18	TP53	NM_000546.5	c.469G>T	p.(Val157Phe)	Missense
mHGA17	TP53	NM_000546.5	c.464_465insCCCG	p.(Arg156Profs*17)	Frameshift indel
mHGA19	TP53	NM_000546.5	c.474delC	p.(Ala159Profs*11)	Frameshift indel
mHGA20	TP53	NM_000546.5	c.517G>T	p.(Val173Leu)	Missense
mHGA35	TP53	NM_000546.5	c.517G>T	p.(Val173Leu)	Missense
mHGA21	TP53	NM_000546.5	c.524G>A	p.(Arg175His)	Missense
mHGA22	TP53	NM_000546.5	c.721T>C	p.(Ser241Pro)	Missense
mHGA16	TP53	NM_000546.5	c.742C>T	p.(Arg248Trp)	Missense
mHGA18	TP53	NM_000546.5	c.742C>T	p.(Arg248Trp)	Missense
mHGA8	TP53	NM_000546.5	c.742C>T	p.(Arg248Trp)	Missense
mHGA11	TP53	NM_000546.5	c.742C>T	p.(Arg248Trp)	Missense
mHGA30	TP53	NM_000546.5	c.773A>G	p.(Glu258Gly)	Missense
mHGA10	TP53	NM_000546.5	c.784delG	p.(Gly262Valfs*83)	Frameshift indel
mHGA13	TP53	NM_000546.5	c.817C>T	p.(Arg273Cys)	Missense
mHGA11	TP53	NM_000546.5	c.817C>T	p.(Arg273Cys)	Missense
mHGA3	TP53	NM_000546.5	c.818G>A	p.(Arg273His)	Missense
mHGA15	TP53	NM_000546.5	c.818G>C	p.(Arg273Pro)	Missense
mHGA14	TP53	NM_000546.5	c.844C>T	p.(Arg282Trp)	Missense
mHGA38	TP53	NM_000546.5	c.472C>G	p.(Arg158Gly)	Missense
mHGA39	TP53	NM_000546.5	c.722C>T	p.(Ser241Phe)	Missense
mHGA40	TP53	NM_000546.5	c.659A>G	p.(Tyr220Cys)	Missense
mHGA25	TP53	NM_000546.5	c.916C>T	p.(Arg306*)	Nonsense
mHGA12	NF1	NM_000267.3	c.569T>G	p.(Leu190*)	Nonsense
mHGA28	NF1	NM_000267.3	c.3738_3747del	p.(Phe1247Glyfs*16)	Frameshift indel
mHGA28	NF1	NM_000267.3	c.6687_6689del	p.(Val2230del)	Nonframeshift indel
mHGA27	NF1	NM_000267.3	c.6789_6792del	p.(Tyr2264Thrfs*5)	Frameshift indel
mHGA18	ATRX	NM_000489.4	c.3100delC	p.(Gln1034Lysfs*16)	Frameshift indel
mHGA10	ATRX	NM_000489.4	c.3168delG	p.(Lys1057Argfs*61)	Frameshift indel

mHGA24	ATRX	NM_000489.4	c.3363delT	p.(Cys1122Valfs*8)	Frameshift indel
mHGA25	ATRX	NM_000489.4	c.4552A>T	p.(Arg1518*)	Nonsense
mHGA28	ATRX	NM_000489.4	c.5399T>C	p.(Met1800Thr)	Missense
mHGA26	ATRX	NM_000489.4	c.6719T>G	p.(Leu2240Arg)	Missense
mHGA1	CHEK2	NM_145862.2	c.444+1G>A		Splicing

**FGFR1* mutations have been previously reported in Jones et al, Nat Genet 2013 annotated as:

mHGA27	FGFR1	NM_023110	c.1638C>A	p.Asn546Lys	Missense
mHGA26	FGFR1	NM_023110	c.1638C>A	p.Asn546Lys	Missense
mHGA29	FGFR1	NM_023110	c.1966A>G	p.Lys656Glu	Missense
mHGA28	FGFR1	NM_023110	c.1966A>G	p.Lys656Glu	Missense

#Novel *FGFR1* mutation identified in this study with Jones et al, Nat Genet 2013 annotation:

mHGA26	FGFR1	NM_023110	c.1963_1965del	p.655_655del	Nonframeshift indel
--------	-------	-----------	----------------	--------------	---------------------

Supplementary Table 3.7: Gross structural alterations in high-grade astrocytomas according to *H3F3A* or *IDH1* mutation show increased genomic instability in *H3F3A* G34R/V mutants

	n	average	
H3F3A.G34R.V	15	52.13	
ALL-K27M + IDH1	45	23.33	
pvalue			0.02997
	n	average	
H3F3A.G34R.V	15	52.13	
ALL-K27M	28	24.03	
pvalue			0.042
	n	average	
H3F3A.G34R.V	15	52.13	
IDH1	17	22.18	
pvalue			0.029

Supplementary Table 3.8: Primer sequences utilized for targeted sequencing and quantitative PCR analyses in the study.

Gene	Methodology	Direction	Primer Sequence (5'-3')
<i>TERT</i>	Sanger sequencing	Forward	AGCACCTCGCGGTAGTGG
<i>TERT</i>	Sanger sequencing	Reverse	CACAGCCTAGGCCGATTC
<i>ACTB</i>	qPCR	Forward	CCAGTGGTACGGCCAGA
<i>ACTB</i>	qPCR	Reverse	GCGAGAAGATGACCCAGAT
<i>ID1</i>	qPCR	Forward	AAACGTGCTGCTCTACGACA
<i>ID1</i>	qPCR	Reverse	GAATCTCCACCTTGCTCACC
<i>ID2</i>	qPCR	Forward	GACCACCCTCAACACGGATA
<i>ID2</i>	qPCR	Reverse	CACACAGTGCTTTGCTGTCA
<i>ID3</i>	qPCR	Forward	GCGCGTCATCGACTACATT
<i>ID3</i>	qPCR	Reverse	CTGTCTGGATGGGAAGGTG
<i>SNAI1</i>	qPCR	Forward	GCACTGGTACTTCTTGACATCT
<i>SNAI1</i>	qPCR	Reverse	GGCTGCTACAAGGCCAT

3.10 Connecting text from Chapter 3 to Chapter 4

CHAPTER 3: Recurrent mutations in *ACVR1* in pediatric midline high-grade

astrocytoma

To

CHAPTER 4: Characterization of age-associated aneuploidy in pilocytic

astrocytoma

Thus far in this dissertation, we have explored the mutational landscape of high-grade gliomas originating from distinct areas of the CNS and have shown that indeed these tumors appear to arise harboring diverse epigenomic alterations. We have largely employed the use of next-generation sequencing (NGS) methodology, as well as DNA methylation analysis to investigate this and have validated the functional impact of these mutations. Chapters 2 and 3 implicate H3K36 or H3K27 defects in cortical or midline tumorigenesis respectively. Mutations affecting the epigenome were prominent in both neuroanatomical compartments and associated with distinct partner mutations in specific areas. Neuroanatomical specificity of genetic alterations is also observed in the low-grade astrocytoma, pilocytic astrocytoma (PA). PAs do not naturally progress to higher-grade gliomas and when amenable to gross-total surgical resection, treatment can be curative. Strikingly, very rare cases of PA have demonstrated a similar constellation of mutations as those detailed for GBM in Chapters 2 and 3, harboring mutations in *H3F3A* K27M, *FGFR1* and *NF1* with all tumors with this profile, PA and GBM, being localized to the thalamus [118]. The most common genetic alteration observed overall in PA is *KIAA1549-BRAF* fusion resulting from tandem duplication at chromosome 7q34 that

overwhelmingly characterizes the majority of PA occurring in the cerebellum [117]. Recent reports have demonstrated decreased frequencies of this fusion in adults [101], and an increasing prevalence of numerical whole chromosomal copy number defects, termed aneuploidy, with age in PA [119]. Although its role in cancer is the subject of controversy, aneuploidy has been associated with the vast majority of human cancers to date [88]. In Chapter 4, we examine the whole chromosomal copy number landscapes of a large combined cohort of 222 adult and pediatric PA tumors to better characterize the aneuploid phenotype seen largely in older patients. We describe the association of aneuploidy with clinical and molecular parameters including major alterations such as *BRAF* fusions and mutations in PA. In addition, through an integrative approach, we perform robust differential gene expression and correlation analysis to elucidate novel molecular pathways associated with aneuploid tumors. We identify candidate genes associated with aneuploid PA that may underlie active promotion of or tolerance to numerical chromosome defects seen specifically in these tumors.

CHAPTER 4: Characterization of age-associated aneuploidy in pilocytic astrocytoma

Adam M Fontebasso*, Margret Shirinian*, Dong-Anh Khuong-Quang, Tenzin Gayden, Marcel Kool, Nicolas De Jay, Karine Jacob, Noha Gerges, Huriye Cin, Hendrik Witt, Alexandre Montpetit, Sébastien Brunet, Pierre Lepage, Geneviève Bourret, Almos Klekner, László Bognár, Peter Hauser, Miklós Garami, Jean-Pierre Farmer, Jose-Luis Montes, Jeffrey Atkinson, Adam J Fleming, Sally Lambert, Tony Kwan, Andrey Korshunov, Uri Tabori, V Peter Collins, Steffen Albrecht, Damien Faury, Stefan M Pfister, Werner Paulus, Martin Hasselblatt, David TW Jones[#] & Nada Jabado[#]

*These authors contributed equally to the manuscript.

[#]These authors are co-senior and co-corresponding authors.

4.1 Abstract

Pilocytic astrocytoma (PA) is the most common primary brain tumor in the pediatric years. PAs can also occur in adulthood, however are extremely rare which has contributed to our lack of molecular insight into their pathogenesis in this age group. Recent studies have uncovered an increased propensity toward specific whole chromosomal copy number defects in older patients with PA as well as a decreasing frequency of *KIAA1549-BRAF* fusion transcripts; the most common genetic alteration occurring overall in PA tumors. In this study, we investigated whole chromosomal copy number alterations and global differences in gene expression throughout adult and pediatric populations with a specific focus on elucidating mechanisms associated with increased aneuploidy commonly observed in PA. Herein, we demonstrate across a large dataset of 222 tumors profiled for whole chromosomal copy number gains, that aneuploidy is a common feature of PA tumors, with 22.5% (50/222) of tumors overall showing at least one whole chromosomal gain. In addition, we confirm that the aneuploid phenotype is non-random and significantly favors gains in chromosomes 5, 6, 7 and 11 with statistical under-representation of chromosomes 1, 2, 3, 13, 14 16, 17, 19 and 22 also observed. Adult PA more frequently demonstrated whole-chromosomal copy number gain than pediatric tumors, with the mean age of aneuploid PA tumors being significantly higher, aged approximately 10 years more at diagnosis. Interestingly, across the dataset, aneuploidy and *BRAF* fusion appeared to be largely independent. Moreover, we analyzed genes and pathways aberrantly regulated in aneuploid tumors and identified significance of pathways including CNS development, genes involved in the unfolded protein response as well as the cell cycle. Although no overt differences were seen in

immunohistochemical markers of mutant p53, or senescence marker p16

immunoreactivity between aneuploid and euploid PA tumors that would account for the continued growth of aneuploid cells, we demonstrate that an *MDM2*-correlated 742-gene signature exists robustly in a large dataset of PA tumors, but not other pediatric gliomas.

MDM2-correlated programs were largely enriched in loci located on euploid

chromosomes and included genes involved in the unfolded protein response, cell cycle,

chromosome segregation and others, suggesting a driver and/or reinforcing role in

association with aneuploidy in PA.

4.2 Introduction

Pilocytic astrocytoma (PA) is a World Health Organization (WHO) grade I astrocytoma and is the most common tumor of the childhood years [167,138]. PA tumors, if amenable to gross total surgical resection, generally harbor an excellent prognosis [138,61]. PAs of the pediatric years most commonly occur in the cerebellum, however these tumors can be found throughout supratentorial regions such as the cerebral hemispheres as well as surgically challenging areas such as the thalamus, optic pathway, brainstem and spinal cord in a subset of cases [61]. PA tumors show a dramatic reduction in incidence with age [61], which has contributed to the lack of identification of molecular drivers specific to older patients with PA.

Recent genomic studies have elucidated numerous novel targets in pediatric low-grade gliomas (pLGGs) including PA. To date, the most common genetic alteration occurring in PA tumors is represented by tandem duplication at 7q34 creating an in-frame fusion gene between the MAP kinase *BRAF* and *KIAA1549*, leading to constitutive activation of the MAPK pathway [121,122,117]. MAPK pathway activation has repeatedly established itself as a critical theme in PA biology, as these tumors have mainly been classified as a “single-pathway” disease [118]. With the identification of novel *RAF*-family fusions [122], *BRAF* V600E mutation [228], germline *NF1* mutation or deletion in neurofibromatosis type I associated PAs (reviewed in [117]) and recently identified fibroblast growth factor receptor 1 (*FGFR1*) hotspot mutations, tyrosine kinase domain duplications or fusions [118,291], virtually all PAs can be categorized as harboring an alteration leading to hyper-activation along the MAPK axis. Although in children, *BRAF* fusion frequencies occur in the vast majority of samples, lower

frequencies of fusion transcripts in adult PA tumors have been reported [101]. This suggests that other putative driver alterations or programs may also govern the molecular landscape of adult PA.

Aneuploidy in the form of whole-chromosomal copy number gains has previously been reported in PA tumors [119]. Of note, a non-random pattern of gains favoring chromosomes 5 and 7 most frequently, followed by 6, 11, 15 and 20 has been shown in PA tumors analyzed by array-based comparative genomic hybridization (aCGH) [119]. Interestingly chromosomal gains were identified at greater frequency in older patients with PA [119]. Further characterization of the significance of this phenotype, its relation to *BRAF* and MAPK alterations and the possible mechanisms underlying its development has however, remained largely unknown.

As such, we sought to investigate the genomic landscape of adult PAs utilizing a large combined dataset of 222 adult and pediatric PAs with whole-chromosomal copy number data, including tumors from previously published aCGH and SNP array studies [109,119,121,122,156]. Herein, we focus on the characterization of the aneuploid phenotype present in a large subset of PA tumors and describe its association with major alterations and molecular pathways in PA.

4.3 Materials and Methods

Sample Characteristics and Pathological Review

All samples were obtained with informed consent after approval of the Institutional Review Board of the respective hospitals they were treated in, and independently reviewed by senior pediatric neuropathologists (S.A., A.K., V.P.C., M.H.,

W.P.) according to the WHO guidelines [167,146]. Patients and tumor samples are described in Supplementary Table 4.1. A total of 280 patient tumors were included in our cohort, with copy number data available for 222 tumors, and *KIAA1549-BRAF* fusion/*BRAF* duplication data available for the majority of cases (n=268). *BRAF* mutations were as assessed by sequencing in 174 tumors. A large cohort of PA tumors (n=191) and normal brain samples (n=18) was utilized for gene expression profiling, assembling data from newly processed samples and previously published studies [234,218,118], utilizing the Affymetrix HG-U133 plus 2.0 microarray (Affymetrix), 139 of these tumors had available copy number information. Gene expression data was compared with other published datasets of glioblastoma (n=84) [190], pediatric high-grade glioma (n=53) [199], diffuse-intrinsic pontine glioma (DIPG) (n=37) [198], ependymoma (n=83) [116], normal brain [18], and normal cerebellum [220] as controls. A subset of 201 PA tumors were available for *MDM2* SNP 309 sequencing. The cut-off age used between adult and pediatric age groups was 18 years. Both adult and pediatric tumors were obtained from the London/Ontario Tumor Bank, and from collaborators in Canada, Hungary, the United Kingdom and Germany.

RNA and DNA extraction

RNA and DNA were isolated from tumor samples using the Qiagen RNeasy Lipid Tissue Mini kit, Qiagen QIAmp/DNeasy DNA Mini kits respectively according to instructions of the manufacturer. RNA samples were stored at -80°C and DNA samples were stored at -20°C for further analysis.

KIAA1549-BRAF Fusion Screening

RT-PCR to detect the three most common *KIAA1549-BRAF* fusion transcripts was performed as previously described [121].

DNA hybridization and SNP analysis

For SNP analysis, DNA (250 ng) from PA samples was assayed with the HumanOmni1-Quad & Human Omni2.5 genotyping beadchip platforms according to the recommendations of the manufacturer (Illumina, San Diego, CA, USA). For a subset of formalin-fixed-paraffin-embedded (FFPE) derived DNA samples (n=13, Supplementary Table 4.1), DNA was first rescued utilizing the Illumina FFPE restore assay kit (Illumina, Inc) and subsequently hybridized to the Illumina Omni2.5-8 v1.0 chip. These BeadChip platforms enable whole-genome genotyping of respectively over 1,140,419 (Omni1-Quad) and 2,379,855 (Omni2.5) tagSNP markers derived from the 1,000 Genomes project, all three HapMap phases, and recently published studies. Image intensities were extracted using Illumina's BeadScan software. Data for each BeadChip were self-normalized using information contained within the array. Copy number data was also included from previously published datasets utilizing SNP arrays and array-based comparative genomic hybridization (aCGH) [119,46,109,121,122] with new analyses incorporating whole chromosome copy number profiling from 450K methylation arrays (Illumina) utilizing a previously described method involving a custom algorithm [250] applied to extract copy number information from [46,156]. In total, whole chromosomal copy number data was combined to yield a dataset of 222 tumors with numerical chromosome information to assess aneuploid status.

Gene expression profiling and analysis

Investigation of the role of *MDM2* in a large PA dataset (n=191) [234,218,118] was performed utilizing the online R2: microarray analysis and visualization platform (<http://r2.amc.nl>). Tumors with available aneuploidy status information (n=139) were compared through differential expression analysis using ANOVA at a false discovery rate (FDR) cut-off of <0.001 and these results are displayed in Figure 3. We investigated genes correlating (absolute correlation) with the expression of *MDM2* at a stringent false discovery rate (FDR) corrected criterion of $<1 \times 10^{-15}$, which resulted in 742 robust combinations used for further Gene Ontology (GO) analysis in the full dataset of 191 PA tumors and presented in Supplementary Table 4.2. In control glioma and normal brain datasets detailed above, absolute correlation with less stringent FDR<0.001 was calculated for genes correlating with *MDM2*. Representative heatmaps using transformed z-scores illustrating correlated signatures are displayed in Supplementary Figure 4.2a-c and were generated utilizing the R2 database tool.

MDM2 SNP 309 Sanger sequencing

Sanger sequencing of the *MDM2* promoter SNP 309 was performed on 201 tumors using HotStart FastTaq KIT (Kapa) using forward primer: 5'-TGGTGAGGAGCAGGTACTGG-3' and reverse primer: 5'-CGGAACGTGTCTGAACTTGA-3' with the following PCR cycling conditions: 1 cycle of 1 minute at 96°C, 33 cycles of 10 seconds at 96°C, 5 seconds at 58°C and 1 second at 72°C followed by 1 cycle at 72°C for 30 seconds.

Quantitative RT-PCR determination of MDM2 expression levels

Quantitative determination of *MDM2* expression levels was performed utilizing the Ssofast Evagreen kit (BioRad) with standard conditions indicated by the manufacturer at an annealing temperature of 58°C on the Roche LightCycler 480 (Roche) in a subset of 22 PA samples. Cycle threshold (C_t) values were normalized to β -actin (*ACTB*) and a calibrator normal brain sample with wild-type (TT) *MDM2* SNP 309 genotype using the $2^{-\Delta\Delta C_t}$ method. The following primers were used:

5'-TCTCAAGCTCCGTGTTTGGTCAGT-3', *MDM2* forward

5'-ACCTTGCAACAGCTGCAGATGAAC-3', *MDM2* reverse

5'-GGCACCCAGCACAATGAAGATCAA-3', β -actin forward

5'TAGAAGCATTGCGGTGGACGATGGA-3'. β -actin reverse

Immunohistochemistry

Immunohistochemistry for p53, p16 and Ki67 was performed as previously described on euploid (n=1) and aneuploid PA (n=3) tumor slides [109].

Statistical analyses

Contingency (Fisher's Exact Test), unpaired, two-tailed t-test comparisons and one-way ANOVA were performed utilizing GraphPad Prism to determine *P*-values. ANOVA, absolute correlation and multiple test correction using false discovery rate (FDR) and Gene Ontology (GO) calculations were performed within the R2 online database module for gene expression analysis.

4.4 Results

Aneuploidy is independent of BRAF fusion in pilocytic astrocytoma and is associated with adult disease and a pattern of specific chromosomes

We combined previously published datasets of whole-chromosomal copy number analyses of PA tumors [119,121,122,109] with newly derived copy number analysis of DNA methylation data [46] and assembled copy number data for 222 adult and pediatric PA tumors. In our dataset, whole chromosomal gain in at least one chromosome was common and occurred in 22.5% of PA tumors (50/222 tumors) (Figure 4.1a-d; Supplementary Table 4.1). Aneuploidy was represented in PA tumors occurring throughout the central nervous system, with a notable fraction occurring in surgically challenging areas such as the thalamus, hypothalamus, optic pathway, brainstem, 4th ventricle and spinal cord (Figure 4.1b). Aneuploidy was more common in the adult PA subset (45%; 20/44; $P = 0.0002$; Fisher's Exact Test) and in tumors wild-type for *BRAF* fusion (36%; 23/64; $P = 0.0076$; Fisher's Exact Test) (Figure 4.1c, d). Aneuploid tumors demonstrated an increased frequency (53%, 8/15) of *BRAF* mutations including V600E and insertional mutants (Supplementary Figure 4.1b; $P = 0.0074$; Fisher's exact test). The average age at diagnosis of patients with aneuploid PA tumors was 19.5 +/- 2.1 years, compared to 9.9 +/- 0.8 years for euploid PA tumors, a difference of approximately 10 years ($P < 0.0001$; unpaired, two-tailed t-test) (Supplementary Figure 4.1a). The frequency of individual chromosomes affected demonstrated a specific pattern across the 50 aneuploid PA tumors with the most commonly altered chromosomes in order of frequency being chromosomes 5, 7, 6 and 11 as reported previously [119]. Chromosomes 5, 6, 7 and 11 ($P < 0.0001$ respectively) were statistically over-represented in overall

events among the 50 aneuploid tumors. In addition, chromosomes 1, 2, 3, 13, 14, 16, 17, 19 and 22 ($P < 0.05$) were significantly under-represented across the background of events in the 50 aneuploid tumors (Figure 4.1a).

Aneuploid PA tumors do not show differences in immunohistochemical markers of proliferation or senescence

TP53 mutations have not been recurrently reported as playing a critical role in PA tumorigenesis [43], with recent large-scale genome sequencing studies confirming their absence in these tumors [118,291]. p53 prevents the growth of aneuploid cells [253]. Given that cell cycle arrest and oncogene-induced senescence (OIS) pathways have been shown to be active in PA [110,209], we sought to investigate whether this was also true for a subset (n=3) of highly aneuploid tumors with at least 4 and up to 18 chromosomes affected. Immunohistochemical staining was performed for p53, p16 and Ki67 and was compared to a control euploid PA sample (Figure 4.2). No significant differences were observed for immunopositivity across these markers.

Comparative gene expression analysis identifies specific pathways aberrantly regulated in aneuploid tumors

The continued growth and maintenance of aneuploid cells has been associated with aberrant activity of a subset of molecular pathways. To best assess gene expression programs active or inhibited in aneuploid PA tumors, we utilized a large dataset of 139 tumors with available aneuploidy status (aneuploid PA n=30, euploid PA n=109). We performed supervised analysis within the R2: microarray analysis and visualization

platform (<http://r2.amc.nl>) between these two tumor subgroups and identified differential expression of 503 genes (FDR<0.001, ANOVA). Gene Ontology (GO) analysis of this list of 503 genes revealed significance of molecular pathways including GO terms such as central nervous system development (GO: 7417), cell cycle arrest (GO: 7050), G1/S transition of the mitotic cell cycle (GO: 82) and unfolded protein binding (GO: 51082) (Figure 4.3a). Mapping of these 503 genes to their respective chromosomal locations revealed enrichment of whole chromosomes 5, 6, 7, 8, 10 and 19 and specific chromosome arms (Figure 4.3b). Candidate genes also significantly de-regulated between aneuploidy and euploid PA tumors included *MDM2* (Figure 4.3c) encoding the E3 ubiquitin ligase MDM2, and polo-like kinase 2 (*PLK2*) (Figure 4.3d) which were strongly correlated with each other overall in PA tumors ($P = 1.0 \times 10^{-5}$, Figure 4.3e).

***MDM2* overexpression is associated with aneuploid PA, age and SNP 309 GG-genotypes**

Utilizing the R2 database tool, we wanted to investigate *MDM2* expression comparatively across overall PA, as well as other gliomas including high-grade tumors and control brain samples. Across multiple gene expression datasets including PA tumors, glioblastoma (GBM), pediatric high-grade glioma (pHGG), diffuse intrinsic pontine glioma (DIPG), ependymoma (EP) and normal brain (NB) and cerebellum (CB) samples, aneuploid PA tumors and PA tumors in general, demonstrated the highest overall levels of *MDM2* expression (Figure 4.4a). In a set of 22 PA tumors, along with one control normal brain sample, we examined *MDM2* expression via quantitative PCR (qPCR) between adult and pediatric tumors (Figure 4.4b). *MDM2* expression was

approximately 2-fold higher in adult PA tumors than control normal brain and significantly elevated compared to pediatric PA ($P=0.0296$; unpaired, two-tailed t-test). Although a modest increase, even slight elevations in *MDM2* expression have been reported to accelerate tumorigenesis in association with the *MDM2* promoter SNP 309 [22,207]. We subsequently sequenced SNP 309 in 201 PA tumor samples to determine any association of genotype with expression of *MDM2* and aneuploidy (Figure 4.4c, d and Supplementary Table 4.1). We first correlated *MDM2* expression determined by qPCR in the 22 PA samples described above and confirm that *MDM2* expression in PA tumors indeed correlated strongly with genotype, with tumors homozygous for the SNP 309 G-allele (*MDM2* GG) demonstrating approximately 3-fold elevated expression of *MDM2* compared to a normal brain sample harboring the *MDM2* TT-genotype and significantly increased compared to PA tumors with TG- and TT-genotypes ($P = 0.0069$; one-way ANOVA; Figure 4.4c). *MDM2* SNP 309 genotypes were associated with differential frequencies of aneuploid tumors, with 36.7% of *MDM2* GG tumors demonstrating aneuploidy compared to 27.0% and 17.7% for TT and TG genotypes respectively. Aneuploid PA tumors demonstrated an *MDM2* G-allele frequency of 43%, compared to 40% for euploid tumors (Supplementary Table 4.1).

MDM2-correlated gene signatures are robust in pilocytic astrocytoma

Utilizing the online R2 database tool (<http://r2.amc.nl>) we analyzed genome-wide gene expression correlations with *MDM2* (absolute correlation, $FDR < 0.001$) in PA and other gliomas to determine candidate programs that may lead to aneuploidy in these tumors. Several thousand genes correlated very strongly with the expression of *MDM2*

within the PA dataset (8930 genes at $FDR < 0.001$). Interestingly in other publicly available glioma datasets including pediatric high-grade gliomas [199], DIPGs [198] and ependymomas [116] such correlations with *MDM2* expression do not exist, with very few genes passing FDR criteria ($FDR < 0.001$) (Supplementary Figure 4.2a-c). To best elucidate the molecular pathways most significantly in association with *MDM2* expression in PA, we increased the stringency of our absolute correlation statistics by several orders of magnitude ($FDR < 1 \times 10^{-15}$) and performed Gene Ontology (GO) analysis (Supplementary Table 4.2). Strikingly, this analysis revealed 742 combinations significantly correlated with *MDM2* expression in PA and significant GO terms corresponding to unfolded protein response (GO: 30968), unfolded protein response, activation of signaling protein activity (GO: 6987), cell cycle (GO: 7049), cell cycle arrest (GO: 7050), cell cycle process (GO: 22402) chromosome segregation (GO: 7059) and others (Supplementary Table 4.2). Utilizing the R2 chromosome mapping tool we mapped the 742-gene signature to respective chromosomal positions to determine any specific enrichment across the genome (Figure 4.5a, b). Correlated genes appeared to be over-represented across the q-arm of chromosome 5 ($P = 0.0076$) as well as overall on chromosomes 12 (over-represented) and 20 (under-represented, $P = 0.0068$ and 0.0032 respectively for chromosomes 12 and 20).

4.5 Discussion

Pilocytic astrocytoma (PA) is the most common primary brain tumor of childhood, and if arising in surgically accessible regions, is amenable to gross total resection and excellent patient survival. In adults, the molecular mechanisms leading to

PA tumorigenesis have been largely uncharacterized due to the rarity of the disease in this patient population. Studies over the past few years have placed alterations along the MAPK pathway at the core of PA tumorigenesis through a variety of hits [117]. The most frequent of these, and the most common genetic alteration occurring overall in PA is tandem duplication at chromosomal region 7q34 resulting in formation of a fusion gene involving *KIAA1549-BRAF* that has been shown to occur in lesser frequency with increasing patient age [101]. Phenomena outside of MAPK axis studies have gone largely under-investigated in PA tumors. Aneuploidy was first reported in association with higher patient age in PA tumors in 2006 [119], prior to the first reports of *BRAF* fusion, and has remained an uncharacterized phenotype in PA. Herein, we report the whole chromosomal copy number of 222 adult and pediatric tumors and confirm in a large dataset, that aneuploidy is associated more frequently with adult PA and tumors with patients aged, on average, 10 years older than those with euploid genomes (Figure 4.1a-d and Supplementary Figure 4.1). The association of aneuploidy with increasing age has been identified in cancer, including brain tumors, and other neuropathologies such as Alzheimer's disease but mechanisms leading to its formation and its role in etiology of disease have remained unclear [66]. Aneuploidy can be identified in normal developing and adult mammalian brain, albeit at different frequencies (reviewed in [66]). Work in the developing mouse brain (E11-E15) utilizing Spectral Karyotyping (SKY) has identified a high combined frequency across all chromosomes demonstrating aneuploidy in 33% of embryonic cortical neuroblasts [213]. This frequency (33%) was also identified in a proportion of mitotic cells of the P5-P10 subventricular zone (SVZ) demonstrating that in developing mouse brain, mosaic aneuploidy exists in a variety of brain regions

[134]. Additional work in neuronal progenitor cells (NPCs) derived from P0 and P7 mouse cerebellum revealed 15-20% aneuploid cells [277]. Studies in different adult brain regions including the frontal cortex demonstrate substantially lower aneuploid frequencies overall in mature cells (3-5%), nevertheless illustrating aneuploidy as a common feature of even the developed CNS [214]. Strikingly, further study of aging mouse brain revealed a differential chromosome-specific sensitivity of different brain regions to aneuploidy [67]. Faggioli and colleagues utilized two-color FISH to determine that within a random selection of murine chromosomes 1, 7, 14, 15, 16, 18, 19 and Y, chromosomes 7, 18 and Y were most involved in aneuploidy [67]. Comparing young (4-month) and old (28-month) mice, they identified a 2-fold increase in aneuploidy (2.3% overall per chromosome tested) in older mice [67]. Moreover, individual analysis revealed that neuronal nuclei antigen (NeuN) negative cells (non-neuronal cells i.e. glia) and not neuronal cells demonstrated a significant age-related increase in aneuploidy [67]. The studies described above were performed in cells derived from cerebral cortex, with further comparisons in mouse cerebellum revealing lack of age-related increases in accumulation of aneuploidy [67]. Our study involved a comprehensive dataset of PA tumors located throughout the CNS and identified aneuploidy within tumors originating in diverse brain regions, including surgically problematic and functionally sensitive structures such as the optic pathway, thalamus, hypothalamus, brainstem and spinal cord (Figure 4.1b). In addition, a substantial enrichment of human chromosomes 5, 6, 7 and 11 were seen (Figure 4.1a). Although difficult to assess, murine chromosome 7 seen as preferentially gained by Faggioli and colleagues [67], features elements homologous to human chromosome 11 (amongst many others), gained frequently in PA tumors (NCBI

Homology Maps URL:

<http://www.ncbi.nlm.nih.gov/projects/homology/maps/mouse/chr7/>). Although speculative, it is tempting to hypothesize that the specific chromosomes seen in age-related aneuploidy may feature genes actively promoting, or allowing tolerance to carrying an extra complement of chromosomes. The lack of age-related increases in aneuploidy in cerebellar cells is supportive of our observation in PA tumors. PA tumors overwhelmingly occur in the cerebellum and are often associated with *BRAF* fusion in this region (reviewed in [117]). Although we do identify 42% of aneuploid tumors as occurring in the cerebellum, the proportion of aneuploidy observed in non-cerebellar PA is substantial (>50%) which are otherwise rare locations for PA in general (Figure 4.1b). *BRAF* expression and signaling is required for normal development of the cerebellum and hindbrain structures, and cellular and murine studies of *KIAA1549-BRAF* fusion show preferential growth selectivity of fusion expression in cerebellar neural stem cells [132,133]. Interestingly, an inverse relationship between *BRAF* and aneuploidy has been described, with studies demonstrating inactivation of *BRAF* driving aneuploidy through expression of the related *CRAF* (encoded by *RAF1*) [125]. Within our dataset, aneuploid tumors demonstrated a statistically significant decreased frequency of *BRAF* fusion than euploid tumors (Figure 4.1d). No statistically significant differences are seen in *RAF1* expression between aneuploid and euploid tumors in our dataset however (data not shown), illustrating that future studies are necessary to elucidate the molecular implications of *BRAF* fusion in PA and a relationship with aneuploidy. Strikingly, aneuploid PA tumors were associated with higher frequencies of *BRAF* mutations including V600E and insertional mutants (Supplementary Figure 4.1b; $P=0.0074$;

Fisher's exact test). *BRAF* V600E has been shown to induce aneuploidy through spindle anomalies and supernumerary centrosomes in melanocytic and melanoma cells [52,51,165]. Whether this inverse association of *BRAF* fusion or activating mutation with aneuploidy is driven by subcellular expression patterns of these oncogenic drivers, brain-location specific gene expression programs or MAPK independent functions in PA tumors will necessitate future mechanistic studies.

Faithful chromosomal segregation is critical to avoiding aneuploid defects in cells during cell division. Aneuploidy in the form of chromosomal gain is accompanied by substantial cellular stress of increased gene and protein expression, and is supported by studies that it can act as both oncogenic and tumor suppressor in nature [275].

Aneuploidy can be hypothesized to exist within cells that demonstrate mechanisms that actively promote chromosomal mis-segregation, spindle assembly defects or aberrant cell cycle mechanisms. In addition, cells that harbor up-regulated means of handling the increased gene and protein dosage with the presence of extra chromosomes are in position to tolerate and even drive genetic diversity with aneuploidy. Herein, we utilized microarray gene expression analysis comparing aneuploid and euploid PA tumors and demonstrate 503 genes differentially regulated between these subgroups (Figure 4.3a-e). Significant molecular pathways aberrantly regulated between these groups through Gene Ontology (GO) analysis included CNS developmental pathways, cell cycle and the unfolded protein binding (Figure 4.3a). As discussed above, aneuploid PA tumors were commonly located in non-cerebellar regions that are more rare and difficult to treat surgically (Figure 4.1b). Aberrant regulation of developmental pathways between these tumor subgroups suggests potential involvement of developmental genes in driving or

tolerating aneuploidy. Interestingly, and detailed above, differential sensitivity of different brain regions to chromosome-specific aneuploidy related to aging has been shown [67]. Whether this points to unique cellular origins of aneuploid PA tumor cells, or these developmental genes are programs re-activated from inherent early mammalian developmental stages which demonstrate aneuploidy and proposed to underlie cellular diversity of the CNS (reviewed in [66]), remains to be further studied. Significance of pathways involved in unfolded protein binding illustrates that aneuploid PA tumors harbor mechanisms to tolerate stress accompanying extra chromosomal content. Studies in yeast strains demonstrate that aneuploidy causes proteotoxic stress including accumulation of proteins more challenging to fold [195]. The ability to tolerate this feature through modulation of pathways that may alleviate proteotoxic stress may permit unadulterated growth of aneuploid cells. With studies demonstrating that aneuploidy may represent a large-scale “stress-inducible mutation” [41], significance of unfolded protein binding pathways illustrates that aneuploid PA tumors are in a better position for phenotypic evolution and adaptation. Hyper-active components of the cell cycle can undoubtedly contribute to mitotic checkpoint dysregulation, continued cell growth and ultimately aneuploid defects [88]. Polo-like kinases, including PLK1 and PLK2 are critical regulators of cell division [130,153,24]. PLK2 is required for proper centriole and centrosome duplication [153,24]. *PLK2* was shown to be over-expressed in aneuploid PA tumors (Figure 4.3c) and presents an interesting candidate for promotion and reinforcement of aneuploidy notably based on its chromosomal 5q location. Not surprisingly, many genes differentially regulated between aneuploid and euploid tumors mapped to common trisomic chromosomes 5, 6, and 7, with striking enrichment seen on

the q-arm of chromosome 5 ($P = 7.9 \times 10^{-85}$) (Figure 4.3b), the most frequent chromosome gained across PA tumors. With such striking frequency, it is clear that chromosome 5 gains are not only well-tolerated in PA tumors, but may actively reinforce aneuploidy phenotypes based on candidate mapping of genes including *PLK2*. Although a preliminary hypothesis, this is supported by chromosome 5 gain being found in samples with a single isolated gain as well as in those with multiple gains, showing it as an early aneuploid defect (Figure 4.1a).

Expression of *MDM2* was found to be significantly elevated in aneuploid PA tumors (Figure 4.3c and 4.4a). Furthermore, expression of *PLK2* correlated strongly with *MDM2* (Figure 4.3d). p53 and its regulatory pathways play a critical role in limiting the progression of aneuploidy and preserving the nature of diploid human cells [253]. Three major genes and their gene products comprise the central control of the p53 regulatory pathway these include MDM2, MDM4, USP (also known as HAUSP) [27,128]. MDM2 is upregulated by p53 as an increase in p53 levels leads to increased transcription of *MDM2*, for which the product degrades p53 by ubiquitylation, decreasing its levels resulting in a negative feedback loop [178,208]. Given the lack of reported *TP53* mutations in PA tumors even in large genome-sequencing studies [118,291] and lack of differential immunopositivity seen by IHC in aneuploid tumors (Figure 4.2), increased *MDM2* expression in aneuploid PA tumors may underlie inhibition of p53 function and subsequent continued growth of aneuploid cells. Moreover, *MDM2* expression is highest in PA tumors compared to other gliomas and control brain samples (Figure 4a). Increased *MDM2* expression has been associated with a single nucleotide polymorphism (SNP) in its promoter leading to enhanced Sp1 transcription factor binding and subsequent

expression [22]. We sequenced this promoter SNP, termed SNP 309 and identified a slightly elevated allele frequency within aneuploid PA tumors of approximately 43% compared to the general population (Minor allele frequency (MAF): 36.9% from the 1000 Genomes project, dbSNP, URL: <http://www.ncbi.nlm.nih.gov/snp>), correlating with an increased prevalence of patients with homozygous GG genotypes (26%) within the aneuploid dataset (Figure 4.4d). Expression correlated well with SNP 309 genotype through qRT-PCR, with *MDM2* GG tumors demonstrating the highest expression (Figure 4.4c). Herein we have shown that a statistically robust 742-gene signature (FDR < 1×10^{-15}) of genes correlated with *MDM2* expression exists in a large dataset of 191 PA tumors, but not other gliomas including adult glioblastoma, pediatric high-grade gliomas, diffuse intrinsic pontine gliomas and ependymomas (Figure 4.5a, b, Supplementary Table 4.2 and Supplementary Figure 4.2a-c). These mapped genes point to over-representation of genes on the q-arm of chromosome 5 ($P = 0.0076$), whole chromosome 12 and under-representation on chromosomes 20. *MDM2* correlated genes mapping to chromosome 5q (including *PLK2*) supports a role for *MDM2* in early initiating aneuploid defects, notably given lack of correlated genes on other chromosomes commonly amplified in PA which would otherwise indicate their over-expression secondary to chromosomal gain.

GO analysis of the 742 *MDM2* correlated genes demonstrates significance of GO terms involving unfolded protein response, unfolded protein response activation of signaling protein activity, cell cycle, cell cycle arrest, cell cycle process, chromosome segregation and others (Supplementary Table 4.2). These data, notably based on the distinct specificity of *MDM2* correlations to aneuploid PA tumors and high stringency of gene expression analysis, suggests a central role for *MDM2* mediated programs and

aneuploidy in PA. As above, pathways involved in actively promoting cell cycle aberrations and chromosomal mis-segregation can cause aneuploidy, and those involved in tolerating its detrimental stresses, such as unfolded protein responses and subsequent signalling, can aid in harboring aneuploid phenotypes (reviewed in [88]). In our dataset, *MDM2* expression was higher in adult PA (Figure 4.4b). Mdm2 has been shown to increase age-related aneuploid defects in Mdm2 transgenic mice [171,271]. Interestingly, the effect of Mdm2 over-expression was shown to affect the rate of chromosome gain, but not loss, illustrating its effects in specific forms of aneuploid defects that we observe in our PA dataset. Moreover, earlier work demonstrated that the effect of Mdm2 on genome instability was p53-independent [23]. This supports other *MDM2*-correlated programs and downstream effectors as putative mediators or contributors to age-related aneuploidy in cancer cells and amongst brain tumors, specifically in PA.

In summary, herein we report the integrated genomic analysis of a large dataset of PA and characterize aneuploidy observed in a substantial proportion of tumors. These aneuploid tumors were frequently located in non-traditional PA brain regions and were differentially associated with *BRAF* fusions and activating mutations. Aneuploid tumors demonstrated distinct enrichment of expression of gene pathways mapping to chromosomes commonly amplified in PA and involved in CNS development and the unfolded protein response. This included higher expression of candidates such as *MDM2* and *PLK2* in aneuploid tumors. Aneuploid PA tumors demonstrated higher expression of *MDM2*. PA tumors in general distinctly harbored strong correlations of gene expression programs related to *MDM2* compared to other gliomas. Moreover, these programs mapped to chromosomes largely uninvolved in aneuploid defects illustrating a potential

mode of aneuploidy development. This is supported by their nature as genes involved in the cell cycle, faithful chromosomal segregation and the unfolded protein response potentially supporting proteotoxic stress associated with extra chromosomes. Taken together, our large dataset and integrated analysis has identified potentially intriguing targets for future mechanistic study of aneuploidy and its role in PA tumorigenesis.

4.6 Acknowledgements

The authors are indebted to F. Bacot and D. Vincent and staff at the McGill University and Genome Quebec Innovation Centre for excellent technical assistance. This work was supported by the Cole Foundation and was funded by the Canadian Institute for Health Research (CIHR). A.M.F. is the recipient of a studentship award from the CIHR and an Award from the CIHR-Systems Biology Training Program of McGill University. M.S., K.J. are recipients of fellowships from the Foundation of Stars and the McGill Integrated Cancer Research Training Program. S.L. and V.P.C. are supported by the Samantha Dickson Brain Tumour Trust. S.M.P. is the recipient of the Sybille Assmus Award for Neurooncology in 2009 and N.J. is the recipient of a Chercheur Clinicien Award from Fonds de Recherche en Santé du Québec.

4.7 Conflicts of Interest

The authors declare that they have no conflict of interest.

4.8 Accession Numbers

Gene expression data utilized herein can be access through the Gene Expression Omnibus (GEO) at the following accession numbers:

GSE7696

GSE26576

GSE19578

GSE11882

GSE3526

GSE5675

4.9 Figures

Figure 4.1

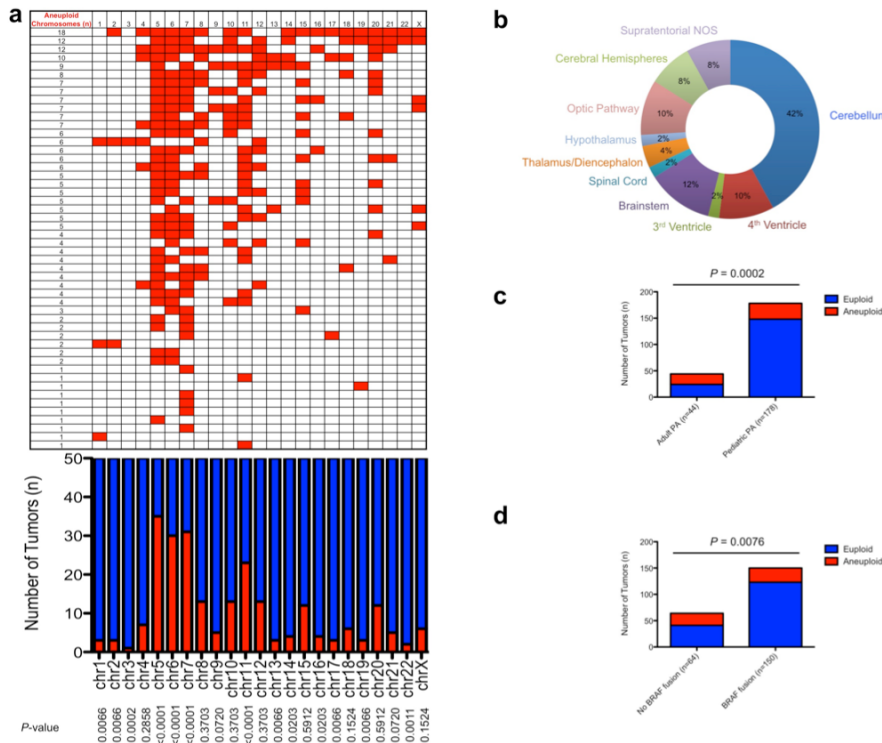


Figure 1

Figure 4.1: Characterization of aneuploidy observed in pilocytic astrocytoma. a, Grid representation of aneuploid defects observed across 22 autosomes and chromosome X in 50 aneuploid PA samples identified in the study (upper panel), with corresponding frequency of specific gains, and their comparative significance represented as P -values (Fisher's Exact Test; lower panel). **b,** Donut representation of neuroanatomical distribution of aneuploid PA tumors demonstrating that a significant proportion occur in surgically inaccessible areas. **c,** Graphical representation of the increased aneuploidy observed amongst adult PA tumors ($P = 0.0002$; Fisher's Exact Test). **d,** Graphical representation of the largely independent occurrence of aneuploidy and *BRAF* fusion in PA tumors ($P = 0.0076$; Fisher's Exact Test).

Figure 4.2

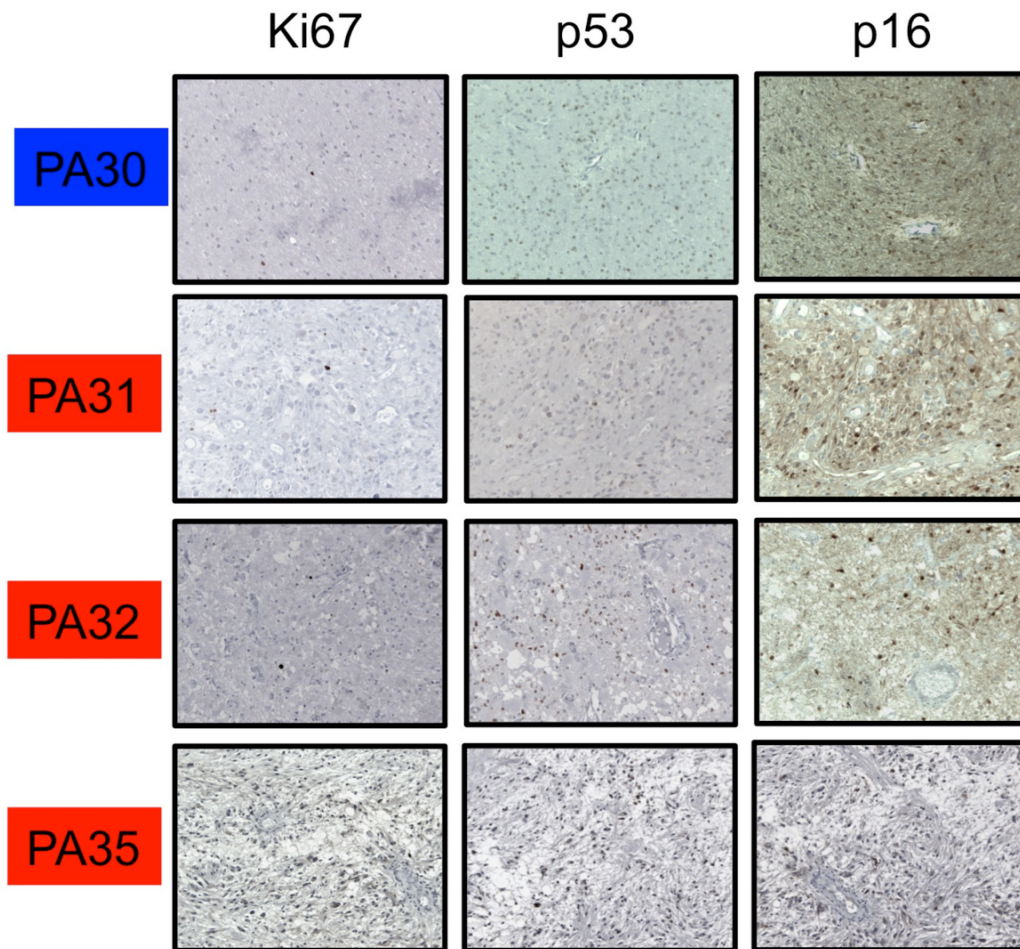


Figure 4.2: Aneuploid PA tumors do not show differential immunohistochemical markers of proliferation or senescence. Representative Ki67, p53 and p16 immunohistochemical stainings for euploid (n=1, indicated in blue) and aneuploid (n=3, indicated in red) PA tumor samples.

Figure 4.3

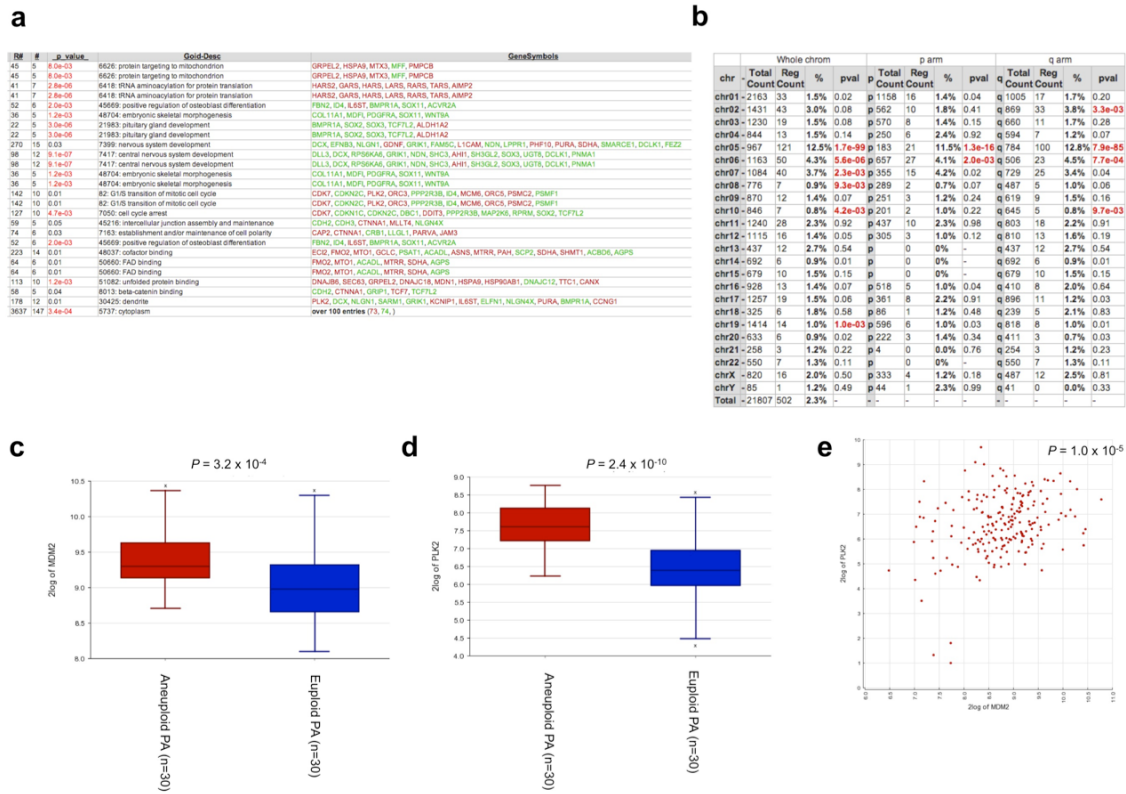


Figure 4.3: Comparative gene expression analysis identifies specific pathways aberrantly regulated in aneuploid tumors. a, Gene Ontology (GO) analysis of 742 gene combinations significantly correlated at $FDR < 1 \times 10^{-15}$ with *MDM2* expression amongst 191 PA tumors. **b**, Chromosomal mapping of the 742 *MDM2* correlated gene combinations. **c, d**, Log2 transformed expression of candidates *MDM2* (**c**) and *PLK2* (**d**) demonstrating significantly increased expression within the aneuploid PA subgroup ($n=30$, $P = 3.2 \times 10^{-4}$ and 2.4×10^{-10} respectively, ANOVA). **e**, Correlation of *MDM2* and *PLK2* expression in 191 PA tumor samples and 18 normal brain samples.

Figure 4.4

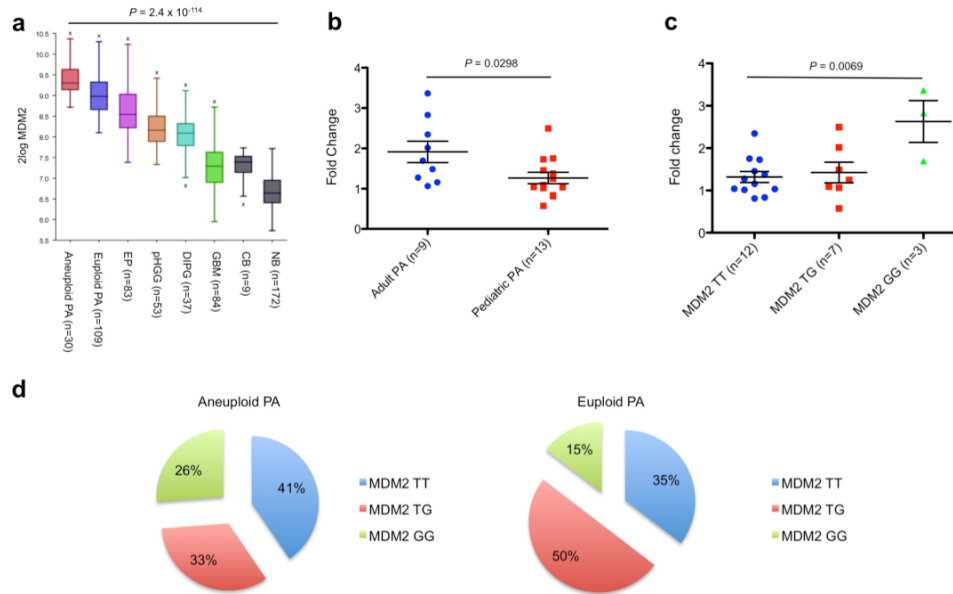


Figure 4.4: Elevated *MDM2* expression is associated with aneuploidy, age and SNP 309 genotypes in pilocytic astrocytoma. **a**, Gene expression analysis of control brain samples and a diverse set of gliomas demonstrates that *MDM2* expression is highest in aneuploid PA tumors ($P = 2.4 \times 10^{-114}$, ANOVA). NB=normal brain, CB=normal cerebellum, GBM=glioblastoma, DIPG=diffuse intrinsic pontine glioma, pHGG=pediatric high-grade glioma, EP=ependymoma, PA=pilocytic astrocytoma. **b**, **c**, qRT-PCR analyses of *MDM2* expression in 22 samples compared by age (**b**) and *MDM2* SNP 309 genotype (**c**). Fold changes values were calculated using the $2^{-\Delta\Delta C_t}$ method and *P*-values calculated using unpaired, two-tailed t-test (**b**) or one-way ANOVA (**c**). **d**, Frequency of *MDM2* SNP 309 genotypes amongst aneuploid and euploid PA tumors shows an increased frequency of the SNP 309 GG-genotype in aneuploid tumors.

Figure 4.5

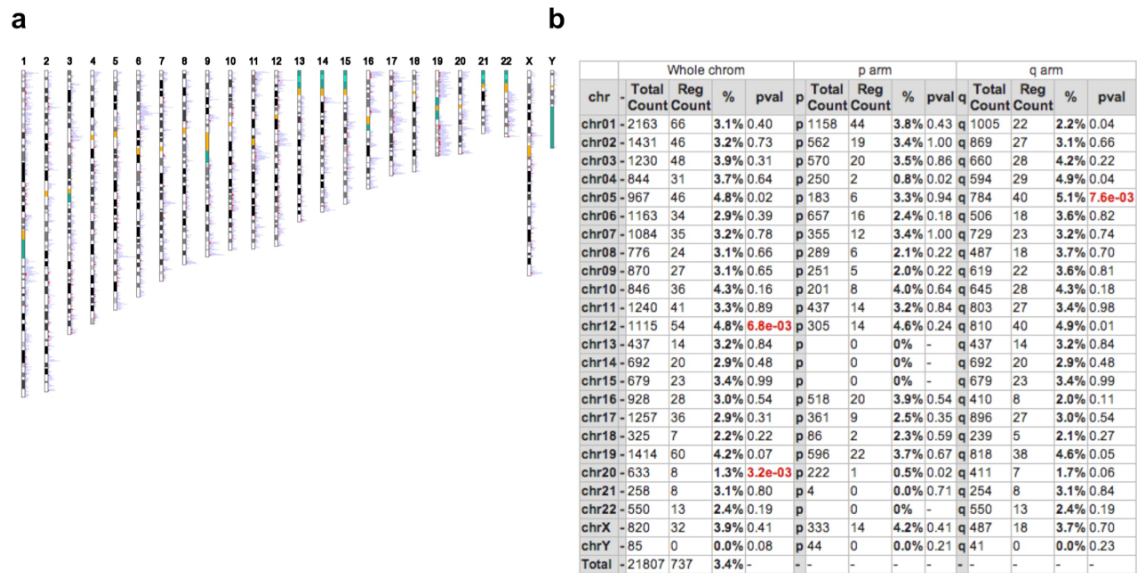
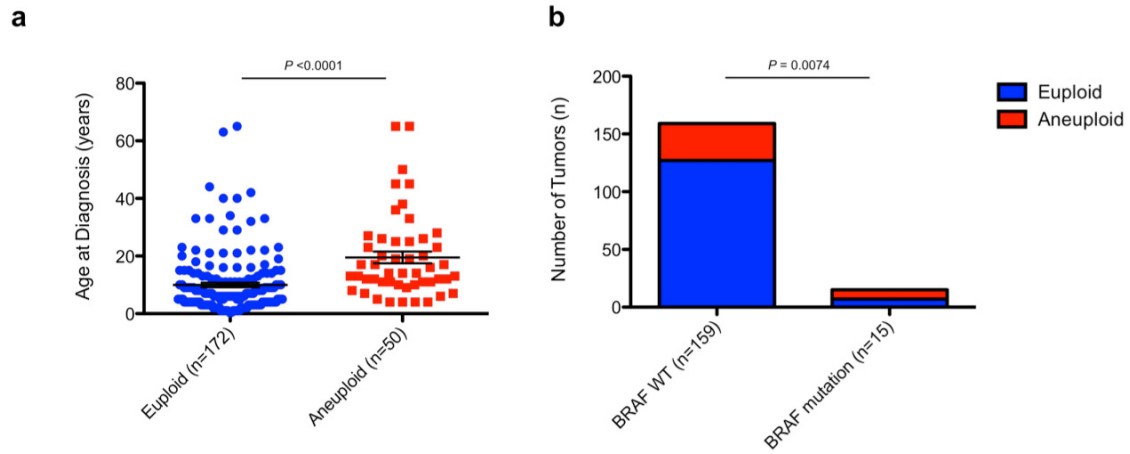


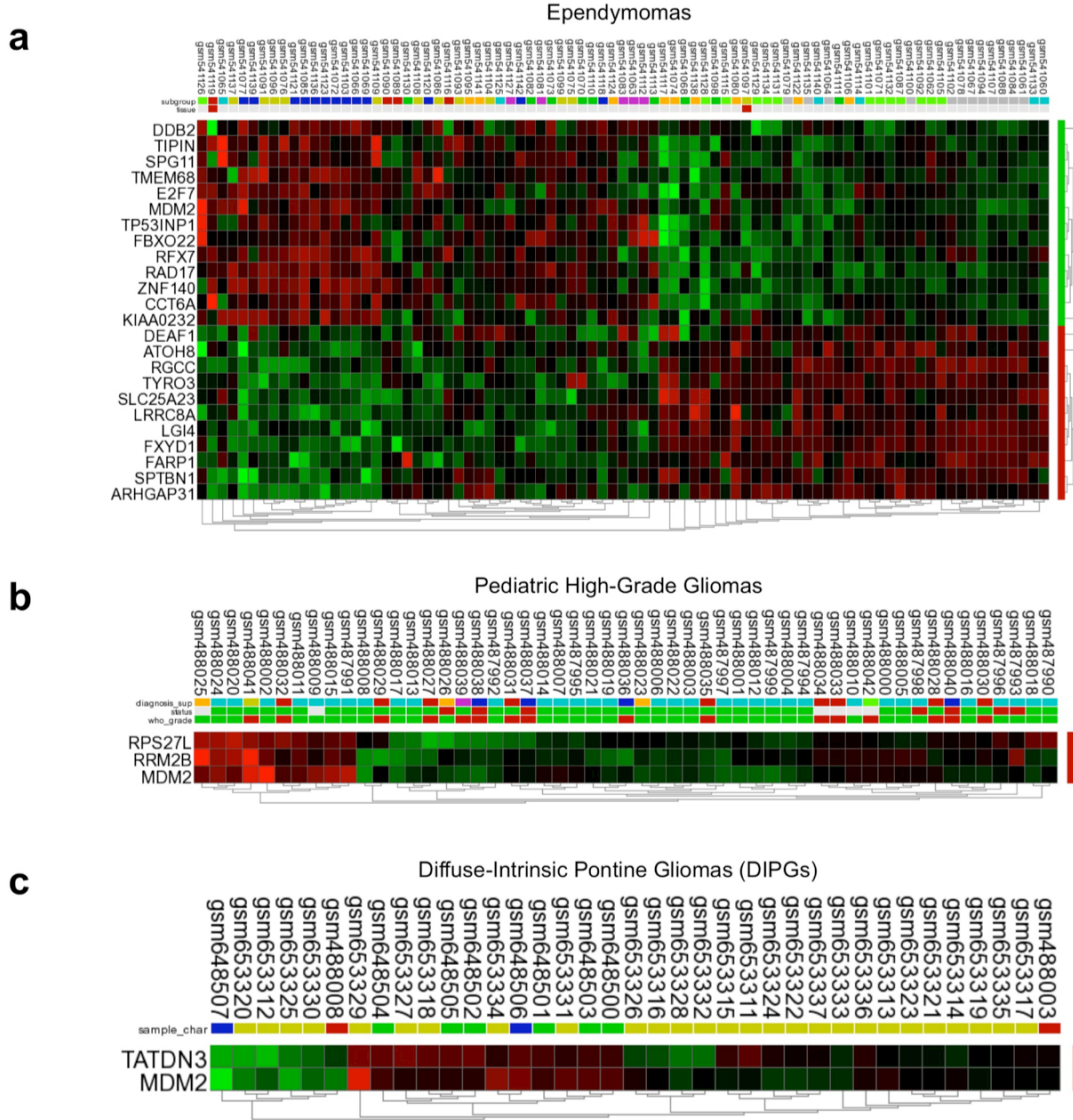
Figure 4.5: Robust *MDM2* correlated signatures exist in pilocytic astrocytoma tumors. **a**, Schematic depicting chromosomal mapping of the *MDM2*-correlated 742 genes (absolute correlation at $FDR < 1 \times 10^{-15}$) in 191 PA tumors. **b**, Statistical representation of chromosomal mapping of *MDM2* correlated genes and respective *P*-values for whole chromosomes and individual p- and q-arms calculated using the R2 online database tool.

Supplementary Figure 4.1



Supplementary Figure 4.1: Aneuploidy is associated with increased age and *BRAF* mutations in PA tumors. **a**, Higher mean age of diagnosis is observed in aneuploid tumors, with a mean age of 19.5 +/-2.1 years and 9.9 +/- 0.8 years seen for aneuploidy and euploid tumors respectively ($P < 0.0001$; unpaired, two-tailed t-test). **b**, Increased frequency of BRAF mutations observed in aneuploid tumors ($P = 0.0074$; Fisher's exact test).

Supplementary Figure 4.2



Supplementary Figure 4.2: *MDM2*-correlated pathways are not observed in non-PA gliomas. Heatmaps of transformed z-scores of genes significantly correlated with *MDM2* expression in ependymomas (a), pediatric high-grade gliomas (b) and DIPGs (c) at FDR<0.001.

PA84	Pediatric	NA	5		Cerebellum	Infratentorial	KMA1548-BRAF	WT	Exhibitor	TT
PA85	Pediatric	NA	14		Cerebral	Supratentorial	KMA1548-BRAF	WT	Exhibitor	TT
PA86	Pediatric	NA	10		Brain stem	Infratentorial	KMA1548-BRAF	WT	NA	NA
PA87	Pediatric	NA	10		Brain stem	Infratentorial	KMA1548-BRAF	WT	NA	NA
PA88	Pediatric	NA	7		Cerebellum	Supratentorial	KMA1548-BRAF	WT	Gain +19	TT
PA89	Pediatric	NA	7		Cerebellum	Infratentorial	KMA1548-BRAF	WT	Exhibitor	TT
PA90	Pediatric	NA	6		Cerebellum	Infratentorial	KMA1548-BRAF	WT	Exhibitor	TG
PA91	Pediatric	NA	6		Cerebellum	Infratentorial	KMA1548-BRAF	WT	Exhibitor	TG
PA92	Pediatric	NA	4		Diaphragm	Supratentorial	Not listed	WT	NA	NA
PA93	Pediatric	NA	4		Cerebellum	Infratentorial	KMA1548-EON-16-BRAF-EON-9	WT	Exhibitor	NA
PA94	Pediatric	M	5		Cerebellum	Infratentorial	KMA1548-EON-16-BRAF-EON-9	WT	Exhibitor	NA
PA95	Pediatric	F	3		Optic nerve	Supratentorial	Not listed	WT	Exhibitor	TT
PA96	Pediatric	F	3		Cerebellum	Supratentorial	Not listed	WT	Exhibitor	TT
PA97	Pediatric	F	9		Cerebellum	Supratentorial	Not listed	WT	Exhibitor	TG
PA98	Pediatric	F	17		Cerebellum	Infratentorial	Not listed	WT	Exhibitor	TG
PA99	Pediatric	F	17		Cerebellum	Infratentorial	Not listed	WT	Exhibitor	NA
PA100	Pediatric	M	14		Cerebellum	Infratentorial	KMA1548-EON-16-BRAF-EON-9	WT	Exhibitor	NA
PA101	Pediatric	M	14		Cerebellum	Infratentorial	KMA1548-EON-16-BRAF-EON-9	WT	Exhibitor	NA
PA102	Pediatric	M	1		Hypothalamus	Supratentorial	Not listed	WT	Exhibitor	NA
PA103	Pediatric	M	13		3rd ventricle	Supratentorial	Not listed	WT	Exhibitor	NA
PA104	Pediatric	M	13		4th ventricle	Supratentorial	Not listed	WT	Exhibitor	NA
PA105	Pediatric	F	5		4th ventricle	Infratentorial	Not listed	WT	Exhibitor	NA
PA106	Pediatric	M	10		Optic nerve	Supratentorial	Not listed	WT	Exhibitor	NA
PA107	Pediatric	M	10		Optic nerve	Supratentorial	Not listed	WT	Exhibitor	NA
PA108	Pediatric	F	13		Cerebellum	Infratentorial	KMA1548-EON-15-BRAF-EON-9	WT	Gain +18 +15	NA
PA109	Pediatric	M	4		Right temporal lobe	Supratentorial	Not listed	WT	Gain +7	NA
PA110	Pediatric	M	4		Optic nerve	Supratentorial	KMA1548-EON-16-BRAF-EON-9	WT	Exhibitor	TT
PA111	Pediatric	M	2		3rd ventricle	Supratentorial	KMA1548-EON-16-BRAF-EON-9	WT	Exhibitor	TT
PA112	Pediatric	M	11		Cerebellum	Infratentorial	KMA1548-EON-16-BRAF-EON-9	WT	Exhibitor	TT
PA113	Pediatric	F	11		Cerebellum	Infratentorial	KMA1548-EON-16-BRAF-EON-9	WT	Gain 5	GG
PA114	Pediatric	M	4		Optic nerve	Supratentorial	KMA1548-EON-15-BRAF-EON-9	WT	Exhibitor	NA
PA115	Pediatric	M	4		Optic nerve	Supratentorial	KMA1548-EON-15-BRAF-EON-9	WT	Gain +7 +12	NA
PA116	Pediatric	M	0.5		Optic nerve	Supratentorial	KMA1548-EON-15-BRAF-EON-9	WT	Exhibitor	NA
PA117	Pediatric	M	1		Optic nerve	Supratentorial	KMA1548-EON-15-BRAF-EON-9	WT	Exhibitor	NA
PA118	Pediatric	M	8		Cerebellum	Infratentorial	KMA1548-EON-16-BRAF-EON-9	WT	Exhibitor	NA
PA119	Pediatric	M	8		Cerebellum	Infratentorial	KMA1548-EON-16-BRAF-EON-9	WT	Exhibitor	NA
PA120	Pediatric	F	5		Cerebellum	Infratentorial	KMA1548-EON-16-BRAF-EON-9	WT	Exhibitor	NA
PA121	Pediatric	M	8		Cerebellum	Infratentorial	KMA1548-EON-16-BRAF-EON-9	WT	Exhibitor	NA
PA122	Pediatric	M	8		Cerebellum	Infratentorial	KMA1548-EON-16-BRAF-EON-9	WT	Exhibitor	NA
PA123	Pediatric	F	6		Cerebellum	Infratentorial	KMA1548-EON-15-BRAF-EON-9	WT	Exhibitor	NA
PA124	Pediatric	F	5		Brain stem	Infratentorial	Not listed	WT	Exhibitor	NA
PA125	Pediatric	F	5		Brain stem	Infratentorial	Not listed	WT	Exhibitor	NA
PA126	Pediatric	F	3		Cerebellum	Infratentorial	KMA1548-EON-16-BRAF-EON-9	WT	Exhibitor	NA
PA127	Pediatric	F	12		Cerebellum	Infratentorial	KMA1548-EON-16-BRAF-EON-9	WT	Gain +8 +7 +11 +18 +18 +X	TT
PA128	Pediatric	M	1		Cerebellum	Infratentorial	Not listed	WT	Exhibitor	TG
PA129	Pediatric	M	1		Cerebellum	Infratentorial	Not listed	WT	Exhibitor	TG
PA130	Pediatric	M	1		Cerebellum	Infratentorial	Not listed	WT	Exhibitor	TT
PA131	Pediatric	NA	4		Cerebellum	Infratentorial	KMA1548-BRAF	WT	Exhibitor	NA
PA132	Pediatric	NA	4		Cerebellum	Infratentorial	KMA1548-BRAF	WT	Exhibitor	TT
PA133	Pediatric	NA	4		Cerebellum	Infratentorial	KMA1548-BRAF	WT	Exhibitor	TT
PA134	Pediatric	NA	4		Cerebellum	Infratentorial	KMA1548-BRAF	WT	Exhibitor	TT
PA135	Pediatric	NA	10		Paranasal lobe	Supratentorial	KMA1548-BRAF	WT	Exhibitor	NA
PA136	Pediatric	NA	4		Cerebellum	Infratentorial	KMA1548-BRAF	WT	Exhibitor	NA
PA137	Pediatric	NA	4		Cerebellum	Infratentorial	KMA1548-BRAF	WT	Exhibitor	NA
PA138	Pediatric	NA	4		Cerebellum	Infratentorial	KMA1548-BRAF	WT	Gain +7 +17	TG
PA139	Pediatric	NA	3		Cerebellum	Infratentorial	Not listed	WT	Exhibitor	GG
PA140	Pediatric	NA	3		Cerebellum	Infratentorial	Not listed	WT	Exhibitor	GG
PA141	Pediatric	NA	6		Cerebellum	Infratentorial	Not listed	WT	Exhibitor	GG
PA142	Pediatric	NA	11		Cerebellum	Infratentorial	Not listed	WT	Exhibitor	GG
PA143	Pediatric	NA	13		Occipital lobe	Supratentorial	Not listed	WT	Exhibitor	GG
PA144	Pediatric	NA	11		Cerebellum	Infratentorial	Not listed	WT	Exhibitor	GG
PA145	Pediatric	NA	4		Brainstem	Infratentorial	Not listed	WT	Exhibitor	GG
PA146	Pediatric	NA	4		Brainstem	Infratentorial	Not listed	WT	Exhibitor	GG
PA147	Pediatric	M	16		Thalamus	Supratentorial	Not listed	WT	Exhibitor	GG
PA148	Pediatric	F	3		3rd ventricle	Supratentorial	KMA1548-EON-16-BRAF-EON-11	WT	NA	TT
PA149	Pediatric	F	1		3rd ventricle	Supratentorial	KMA1548-EON-16-BRAF-EON-11	WT	NA	TT
PA150	Pediatric	M	2		Posterior fossa	Supratentorial	KMA1548-EON-16-BRAF-EON-11	WT	Exhibitor	TT
PA151	Pediatric	F	16.64		Cerebellum	Infratentorial	KMA1548-EON-16-BRAF-EON-9	WT	Exhibitor	TT
PA152	Pediatric	F	4.48		Cerebellum	Infratentorial	Not listed	WT	Exhibitor	GG
PA153	Pediatric	F	11.53		Cerebellum	Infratentorial	Not listed	WT	Exhibitor	GG
PA154	Pediatric	M	11.53		Cerebellum	Infratentorial	Not listed	WT	Exhibitor	GG
PA155	Pediatric	M	12		Suprasellar	Infratentorial	KMA1548-EON-16-BRAF-EON-9	WT	Exhibitor	TT
PA156	Pediatric	M	12		Suprasellar	Infratentorial	KMA1548-EON-16-BRAF-EON-9	WT	Exhibitor	TT
PA157	Pediatric	M	12		Thalamus	Supratentorial	Not listed	WT	Exhibitor	TT
PA158	Pediatric	M	13		Spinal cord	Supratentorial	Not listed	WT	Exhibitor	TT
PA159	Pediatric	M	13		Spinal cord	Supratentorial	Not listed	WT	Exhibitor	TT
PA160	Pediatric	M	13		Spinal cord	Supratentorial	Not listed	WT	Exhibitor	TT
PA161	Pediatric	F	7.83333		Suprasellar/Optic Pathway	Supratentorial	KMA1548-EON-16-BRAF-EON-9	WT	Exhibitor	TT
PA162	Adult	F	36		Supratentorial	Supratentorial	KMA1548-EON-16-BRAF-EON-9	WT	Gain +1.2	TG
PA163	Adult	F	36		Supratentorial	Supratentorial	KMA1548-EON-16-BRAF-EON-9	WT	Exhibitor	TG
PA164	Adult	M	23		Cerebellum	Infratentorial	Not listed	WT	Exhibitor	TG
PA165	Adult	F	65		Cerebellum	Infratentorial	Not listed	WT	Exhibitor	TT
PA166	Adult	F	65		Cerebellum	Infratentorial	Not listed	WT	Exhibitor	TT
PA167	Adult	M	28		Spinal cord	Infratentorial	KMA1548-EON-16-BRAF-EON-9	WT	Gain +1	TG
PA168	Adult	F	21		Supratentorial	Supratentorial	Not listed	WT	Gain +6 +13 +20 +X	TG
PA169	Adult	M	21		Cerebellum	Infratentorial	Not listed	WT	Exhibitor	TG

Supplementary Table 4.2: Gene Ontology (GO) analysis of *MDM2* correlated genes at FDR < 1e-15 (continued on next 3 pages)

R#	#	p-value	GO	Gene Symbols
2745	168	9.40E-05	51234: establishment of localization	GLS, GRM4, SLC39A2, RAB3A, STXB1, VAMP2, SYNI, SYN2, BRSK1
49	9	2.60E-05	7269: neurotransmitter secretion	GLS, MYO6, SLC39A2, RAB3A, STXB1, VAMP2
17	6	6.50E-08	14047: glutamate secretion	STAM2, SLU7, SEC23A, XPO1, STXB1, AP2M1, AP3S1, COPB1, SNX13, ARFGAP3, ARPIP1, HD1, APBA1, MYO6, SARIB, AP5M1, SNX6, ACD, STX5, AP3B2, NAPA, TLK1
161	22	1.60E-07	6868: intracellular protein transport	SEC23A, SARIB, TRAPPC1, SPAST, STX5, TMX1
30	6	0.03	6868: ER to Golgi vesicle-mediated transport	SEC23A, SARIB, TRAPPC1, SPAST, STX5, TMX1
58	7	2.80E-04	6862: post-Golgi vesicle-mediated transport	SEC23A, SARIB, TRAPPC1, SPAST, STX5, TMX1
38	9	2.60E-05	7269: neurotransmitter secretion	GLS, GRM4, SLC39A2, RAB3A, STXB1, VAMP2, SYNI, SYN2, BRSK1
49	7	2.80E-04	6862: post-Golgi vesicle-mediated transport	SEC23A, SARIB, TRAPPC1, SPAST, STX5, TMX1
50	6	0.03	6868: ER to Golgi vesicle-mediated transport	SEC23A, SARIB, TRAPPC1, SPAST, STX5, TMX1
354	33	5.00E-05	15031: protein transport	MYO6, NUP54, ERBB2IP, YWHAE, SYNGR1
161	22	1.60E-07	6868: intracellular protein transport	TRIM3, ARHGAP33, SCAMP5, TMED4, RAB21, MAPK8IP3, RAB26, ARFGAP3, GDI1, SERP1, ARIP1, APBB1, NUP43, IRF3, ARRB2, MDM2, ACD, NMD3, CHMP5, RAB6B, RAB8B, PHAX, SEC61A2, CDDC91, RAB33A, RAB39B, RAB8B, PHAX, VPS13C, SEC61A2, CDDC91, ERBB2IP, RAB3A, RAB31L1, RAB5B, RP2, ZMAT3, STXB1, STXB3, TSNAX, YY1, CEP350, ACTN4, YIPF5, COG8, HOOK3, ADAM9, SNAP23, NAPA, RAB11B, PITPNM1
31	5	9.40E-03	6605: protein targeting	TRIM3, ARHGAP33, SCAMP5, TMED4, RAB21, MAPK8IP3, RAB26, ARFGAP3, GDI1, SERP1, ARIP1, APBB1, NUP43, IRF3, ARRB2, MDM2, ACD, NMD3, CHMP5, RAB6B, RAB8B, PHAX, VPS13C, SEC61A2, CDDC91, ERBB2IP, RAB3A, RAB31L1, RAB5B, RP2, ZMAT3, STXB1, STXB3, TSNAX, YY1, CEP350, ACTN4, YIPF5, COG8, HOOK3, ADAM9, SNAP23, NAPA, RAB11B, PITPNM1
548	45	1.00E-04	33036: macromolecule localization	TRIM3, ARHGAP33, SCAMP5, TMED4, RAB21, MAPK8IP3, RAB26, ARFGAP3, GDI1, SERP1, ARIP1, APBB1, NUP43, IRF3, ARRB2, MDM2, ACD, NMD3, CHMP5, RAB6B, RAB8B, PHAX, VPS13C, SEC61A2, CDDC91, ERBB2IP, RAB3A, RAB31L1, RAB5B, RP2, ZMAT3, STXB1, STXB3, TSNAX, YY1, CEP350, ACTN4, YIPF5, COG8, HOOK3, ADAM9, SNAP23, NAPA, RAB11B, PITPNM1
354	33	5.00E-05	15031: protein transport	TRIM3, ARHGAP33, SCAMP5, TMED4, RAB21, MAPK8IP3, RAB26, ARFGAP3, GDI1, SERP1, ARIP1, APBB1, NUP43, IRF3, ARRB2, MDM2, ACD, NMD3, CHMP5, RAB6B, RAB8B, PHAX, VPS13C, SEC61A2, CDDC91, ERBB2IP, RAB3A, RAB31L1, RAB5B, RP2, ZMAT3, STXB1, STXB3, TSNAX, YY1, CEP350, ACTN4, YIPF5, COG8, HOOK3, ADAM9, SNAP23, NAPA, RAB11B, PITPNM1
317	24	0.02	6468: protein amino acid phosphorylation	TRIM3, ARHGAP33, SCAMP5, TMED4, RAB21, MAPK8IP3, RAB26, ARFGAP3, GDI1, SERP1, ARIP1, APBB1, NUP43, IRF3, ARRB2, MDM2, ACD, NMD3, CHMP5, RAB6B, RAB8B, PHAX, VPS13C, SEC61A2, CDDC91, ERBB2IP, RAB3A, RAB31L1, RAB5B, RP2, ZMAT3, STXB1, STXB3, TSNAX, YY1, CEP350, ACTN4, YIPF5, COG8, HOOK3, ADAM9, SNAP23, NAPA, RAB11B, PITPNM1
55	5	1.60E-03	18105: peptidyl-serine phosphorylation	TRIM3, ARHGAP33, SCAMP5, TMED4, RAB21, MAPK8IP3, RAB26, ARFGAP3, GDI1, SERP1, ARIP1, APBB1, NUP43, IRF3, ARRB2, MDM2, ACD, NMD3, CHMP5, RAB6B, RAB8B, PHAX, VPS13C, SEC61A2, CDDC91, ERBB2IP, RAB3A, RAB31L1, RAB5B, RP2, ZMAT3, STXB1, STXB3, TSNAX, YY1, CEP350, ACTN4, YIPF5, COG8, HOOK3, ADAM9, SNAP23, NAPA, RAB11B, PITPNM1
447	32	0.02	122: negative regulation of transcription from RNA polymerase II promoter	TRIM3, ARHGAP33, SCAMP5, TMED4, RAB21, MAPK8IP3, RAB26, ARFGAP3, GDI1, SERP1, ARIP1, APBB1, NUP43, IRF3, ARRB2, MDM2, ACD, NMD3, CHMP5, RAB6B, RAB8B, PHAX, VPS13C, SEC61A2, CDDC91, ERBB2IP, RAB3A, RAB31L1, RAB5B, RP2, ZMAT3, STXB1, STXB3, TSNAX, YY1, CEP350, ACTN4, YIPF5, COG8, HOOK3, ADAM9, SNAP23, NAPA, RAB11B, PITPNM1
175	16	8.50E-03	6367: transcription initiation from RNA polymerase II promoter	TRIM3, ARHGAP33, SCAMP5, TMED4, RAB21, MAPK8IP3, RAB26, ARFGAP3, GDI1, SERP1, ARIP1, APBB1, NUP43, IRF3, ARRB2, MDM2, ACD, NMD3, CHMP5, RAB6B, RAB8B, PHAX, VPS13C, SEC61A2, CDDC91, ERBB2IP, RAB3A, RAB31L1, RAB5B, RP2, ZMAT3, STXB1, STXB3, TSNAX, YY1, CEP350, ACTN4, YIPF5, COG8, HOOK3, ADAM9, SNAP23, NAPA, RAB11B, PITPNM1
447	32	0.02	122: negative regulation of transcription from RNA polymerase II promoter	TRIM3, ARHGAP33, SCAMP5, TMED4, RAB21, MAPK8IP3, RAB26, ARFGAP3, GDI1, SERP1, ARIP1, APBB1, NUP43, IRF3, ARRB2, MDM2, ACD, NMD3, CHMP5, RAB6B, RAB8B, PHAX, VPS13C, SEC61A2, CDDC91, ERBB2IP, RAB3A, RAB31L1, RAB5B, RP2, ZMAT3, STXB1, STXB3, TSNAX, YY1, CEP350, ACTN4, YIPF5, COG8, HOOK3, ADAM9, SNAP23, NAPA, RAB11B, PITPNM1
175	16	8.50E-03	6367: transcription initiation from RNA polymerase II promoter	TRIM3, ARHGAP33, SCAMP5, TMED4, RAB21, MAPK8IP3, RAB26, ARFGAP3, GDI1, SERP1, ARIP1, APBB1, NUP43, IRF3, ARRB2, MDM2, ACD, NMD3, CHMP5, RAB6B, RAB8B, PHAX, VPS13C, SEC61A2, CDDC91, ERBB2IP, RAB3A, RAB31L1, RAB5B, RP2, ZMAT3, STXB1, STXB3, TSNAX, YY1, CEP350, ACTN4, YIPF5, COG8, HOOK3, ADAM9, SNAP23, NAPA, RAB11B, PITPNM1
98	10	0.02	6006: glucose metabolic process	TRIM3, ARHGAP33, SCAMP5, TMED4, RAB21, MAPK8IP3, RAB26, ARFGAP3, GDI1, SERP1, ARIP1, APBB1, NUP43, IRF3, ARRB2, MDM2, ACD, NMD3, CHMP5, RAB6B, RAB8B, PHAX, VPS13C, SEC61A2, CDDC91, ERBB2IP, RAB3A, RAB31L1, RAB5B, RP2, ZMAT3, STXB1, STXB3, TSNAX, YY1, CEP350, ACTN4, YIPF5, COG8, HOOK3, ADAM9, SNAP23, NAPA, RAB11B, PITPNM1
34	6	1.50E-03	51259: protein oligomerization	TRIM3, ARHGAP33, SCAMP5, TMED4, RAB21, MAPK8IP3, RAB26, ARFGAP3, GDI1, SERP1, ARIP1, APBB1, NUP43, IRF3, ARRB2, MDM2, ACD, NMD3, CHMP5, RAB6B, RAB8B, PHAX, VPS13C, SEC61A2, CDDC91, ERBB2IP, RAB3A, RAB31L1, RAB5B, RP2, ZMAT3, STXB1, STXB3, TSNAX, YY1, CEP350, ACTN4, YIPF5, COG8, HOOK3, ADAM9, SNAP23, NAPA, RAB11B, PITPNM1
39	5	0.04	61231: protein heterooligomerization	TRIM3, ARHGAP33, SCAMP5, TMED4, RAB21, MAPK8IP3, RAB26, ARFGAP3, GDI1, SERP1, ARIP1, APBB1, NUP43, IRF3, ARRB2, MDM2, ACD, NMD3, CHMP5, RAB6B, RAB8B, PHAX, VPS13C, SEC61A2, CDDC91, ERBB2IP, RAB3A, RAB31L1, RAB5B, RP2, ZMAT3, STXB1, STXB3, TSNAX, YY1, CEP350, ACTN4, YIPF5, COG8, HOOK3, ADAM9, SNAP23, NAPA, RAB11B, PITPNM1
94	9	0.04	6112: energy reserve metabolic process	TRIM3, ARHGAP33, SCAMP5, TMED4, RAB21, MAPK8IP3, RAB26, ARFGAP3, GDI1, SERP1, ARIP1, APBB1, NUP43, IRF3, ARRB2, MDM2, ACD, NMD3, CHMP5, RAB6B, RAB8B, PHAX, VPS13C, SEC61A2, CDDC91, ERBB2IP, RAB3A, RAB31L1, RAB5B, RP2, ZMAT3, STXB1, STXB3, TSNAX, YY1, CEP350, ACTN4, YIPF5, COG8, HOOK3, ADAM9, SNAP23, NAPA, RAB11B, PITPNM1
4994	259	0.04	43770: macromolecule metabolic process	TRIM3, ARHGAP33, SCAMP5, TMED4, RAB21, MAPK8IP3, RAB26, ARFGAP3, GDI1, SERP1, ARIP1, APBB1, NUP43, IRF3, ARRB2, MDM2, ACD, NMD3, CHMP5, RAB6B, RAB8B, PHAX, VPS13C, SEC61A2, CDDC91, ERBB2IP, RAB3A, RAB31L1, RAB5B, RP2, ZMAT3, STXB1, STXB3, TSNAX, YY1, CEP350, ACTN4, YIPF5, COG8, HOOK3, ADAM9, SNAP23, NAPA, RAB11B, PITPNM1
132	14	2.40E-03	6511: ubiquitin-dependent protein catabolic process	TRIM3, ARHGAP33, SCAMP5, TMED4, RAB21, MAPK8IP3, RAB26, ARFGAP3, GDI1, SERP1, ARIP1, APBB1, NUP43, IRF3, ARRB2, MDM2, ACD, NMD3, CHMP5, RAB6B, RAB8B, PHAX, VPS13C, SEC61A2, CDDC91, ERBB2IP, RAB3A, RAB31L1, RAB5B, RP2, ZMAT3, STXB1, STXB3, TSNAX, YY1, CEP350, ACTN4, YIPF5, COG8, HOOK3, ADAM9, SNAP23, NAPA, RAB11B, PITPNM1
47	6	0.02	42787: protein ubiquitination during ubiquitin-dependent protein catabolic process	TRIM3, ARHGAP33, SCAMP5, TMED4, RAB21, MAPK8IP3, RAB26, ARFGAP3, GDI1, SERP1, ARIP1, APBB1, NUP43, IRF3, ARRB2, MDM2, ACD, NMD3, CHMP5, RAB6B, RAB8B, PHAX, VPS13C, SEC61A2, CDDC91, ERBB2IP, RAB3A, RAB31L1, RAB5B, RP2, ZMAT3, STXB1, STXB3, TSNAX, YY1, CEP350, ACTN4, YIPF5, COG8, HOOK3, ADAM9, SNAP23, NAPA, RAB11B, PITPNM1
60	8	4.10E-03	6338: chromatin remodeling	TRIM3, ARHGAP33, SCAMP5, TMED4, RAB21, MAPK8IP3, RAB26, ARFGAP3, GDI1, SERP1, ARIP1, APBB1, NUP43, IRF3, ARRB2, MDM2, ACD, NMD3, CHMP5, RAB6B, RAB8B, PHAX, VPS13C, SEC61A2, CDDC91, ERBB2IP, RAB3A, RAB31L1, RAB5B, RP2, ZMAT3, STXB1, STXB3, TSNAX, YY1, CEP350, ACTN4, YIPF5, COG8, HOOK3, ADAM9, SNAP23, NAPA, RAB11B, PITPNM1
264	21	0.02	6281: DNA repair	TRIM3, ARHGAP33, SCAMP5, TMED4, RAB21, MAPK8IP3, RAB26, ARFGAP3, GDI1, SERP1, ARIP1, APBB1, NUP43, IRF3, ARRB2, MDM2, ACD, NMD3, CHMP5, RAB6B, RAB8B, PHAX, VPS13C, SEC61A2, CDDC91, ERBB2IP, RAB3A, RAB31L1, RAB5B, RP2, ZMAT3, STXB1, STXB3, TSNAX, YY1, CEP350, ACTN4, YIPF5, COG8, HOOK3, ADAM9, SNAP23, NAPA, RAB11B, PITPNM1
137	15	1.00E-03	6260: DNA replication	TRIM3, ARHGAP33, SCAMP5, TMED4, RAB21, MAPK8IP3, RAB26, ARFGAP3, GDI1, SERP1, ARIP1, APBB1, NUP43, IRF3, ARRB2, MDM2, ACD, NMD3, CHMP5, RAB6B, RAB8B, PHAX, VPS13C, SEC61A2, CDDC91, ERBB2IP, RAB3A, RAB31L1, RAB5B, RP2, ZMAT3, STXB1, STXB3, TSNAX, YY1, CEP350, ACTN4, YIPF5, COG8, HOOK3, ADAM9, SNAP23, NAPA, RAB11B, PITPNM1
55	8	1.60E-03	18105: peptidyl-serine phosphorylation	TRIM3, ARHGAP33, SCAMP5, TMED4, RAB21, MAPK8IP3, RAB26, ARFGAP3, GDI1, SERP1, ARIP1, APBB1, NUP43, IRF3, ARRB2, MDM2, ACD, NMD3, CHMP5, RAB6B, RAB8B, PHAX, VPS13C, SEC61A2, CDDC91, ERBB2IP, RAB3A, RAB31L1, RAB5B, RP2, ZMAT3, STXB1, STXB3, TSNAX, YY1, CEP350, ACTN4, YIPF5, COG8, HOOK3, ADAM9, SNAP23, NAPA, RAB11B, PITPNM1
317	24	0.02	6468: protein amino acid phosphorylation	TRIM3, ARHGAP33, SCAMP5, TMED4, RAB21, MAPK8IP3, RAB26, ARFGAP3, GDI1, SERP1, ARIP1, APBB1, NUP43, IRF3, ARRB2, MDM2, ACD, NMD3, CHMP5, RAB6B, RAB8B, PHAX, VPS13C, SEC61A2, CDDC91, ERBB2IP, RAB3A, RAB31L1, RAB5B, RP2, ZMAT3, STXB1, STXB3, TSNAX, YY1, CEP350, ACTN4, YIPF5, COG8, HOOK3, ADAM9, SNAP23, NAPA, RAB11B, PITPNM1
371	30	2.50E-03	44419: interspecies interaction between organisms	TRIM3, ARHGAP33, SCAMP5, TMED4, RAB21, MAPK8IP3, RAB26, ARFGAP3, GDI1, SERP1, ARIP1, APBB1, NUP43, IRF3, ARRB2, MDM2, ACD, NMD3, CHMP5, RAB6B, RAB8B, PHAX, VPS13C, SEC61A2, CDDC91, ERBB2IP, RAB3A, RAB31L1, RAB5B, RP2, ZMAT3, STXB1, STXB3, TSNAX, YY1, CEP350, ACTN4, YIPF5, COG8, HOOK3, ADAM9, SNAP23, NAPA, RAB11B, PITPNM1
304	27	7.60E-04	19048: virus-host interaction	TRIM3, ARHGAP33, SCAMP5, TMED4, RAB21, MAPK8IP3, RAB26, ARFGAP3, GDI1, SERP1, ARIP1, APBB1, NUP43, IRF3, ARRB2, MDM2, ACD, NMD3, CHMP5, RAB6B, RAB8B, PHAX, VPS13C, SEC61A2, CDDC91, ERBB2IP, RAB3A, RAB31L1, RAB5B, RP2, ZMAT3, STXB1, STXB3, TSNAX, YY1, CEP350, ACTN4, YIPF5, COG8, HOOK3, ADAM9, SNAP23, NAPA, RAB11B, PITPNM1
49	9	2.60E-05	7269: neurotransmitter secretion	GLS, GRM4, SLC39A2, RAB3A, STXB1, VAMP2, SYNI, SYN2, BRSK1
270	20	0.05	7399: nervous system development	TRIM3, ARHGAP33, SCAMP5, TMED4, RAB21, MAPK8IP3, RAB26, ARFGAP3, GDI1, SERP1, ARIP1, APBB1, NUP43, IRF3, ARRB2, MDM2, ACD, NMD3, CHMP5, RAB6B, RAB8B, PHAX, VPS13C, SEC61A2, CDDC91, ERBB2IP, RAB3A, RAB31L1, RAB5B, RP2, ZMAT3, STXB1, STXB3, TSNAX, YY1, CEP350, ACTN4, YIPF5, COG8, HOOK3, ADAM9, SNAP23, NAPA, RAB11B, PITPNM1
170	14	0.04	1701: in utero embryonic development	TRIM3, ARHGAP33, SCAMP5, TMED4, RAB21, MAPK8IP3, RAB26, ARFGAP3, GDI1, SERP1, ARIP1, APBB1, NUP43, IRF3, ARRB2, MDM2, ACD, NMD3, CHMP5, RAB6B, RAB8B, PHAX, VPS13C, SEC61A2, CDDC91, ERBB2IP, RAB3A, RAB31L1, RAB5B, RP2, ZMAT3, STXB1, STXB3, TSNAX, YY1, CEP350, ACTN4, YIPF5, COG8, HOOK3, ADAM9, SNAP23, NAPA, RAB11B, PITPNM1
584	38	0.04	8719: response to endogenous stimulus	TRIM3, ARHGAP33, SCAMP5, TMED4, RAB21, MAPK8IP3, RAB26, ARFGAP3, GDI1, SERP1, ARIP1, APBB1, NUP43, IRF3, ARRB2, MDM2, ACD, NMD3, CHMP5, RAB6B, RAB8B, PHAX, VPS13C, SEC61A2, CDDC91, ERBB2IP, RAB3A, RAB31L1, RAB5B, RP2, ZMAT3, STXB1, STXB3, TSNAX, YY1, CEP350, ACTN4, YIPF5, COG8, HOOK3, ADAM9, SNAP23, NAPA, RAB11B, PITPNM1
138	18	7.80E-06	18774: response to DNA damage stimulus	TRIM3, ARHGAP33, SCAMP5, TMED4, RAB21, MAPK8IP3, RAB26, ARFGAP3, GDI1, SERP1, ARIP1, APBB1, NUP43, IRF3, ARRB2, MDM2, ACD, NMD3, CHMP5, RAB6B, RAB8B, PHAX, VPS13C, SEC61A2, CDDC91, ERBB2IP, RAB3A, RAB31L1, RAB5B, RP2, ZMAT3, STXB1, STXB3, TSNAX, YY1, CEP350, ACTN4, YIPF5, COG8, HOOK3, ADAM9, SNAP23, NAPA, RAB11B, PITPNM1
80	10	2.30E-03	30868: unfolded protein response	TRIM3, ARHGAP33, SCAMP5, TMED4, RAB21, MAPK8IP3, RAB26, ARFGAP3, GDI1, SERP1, ARIP1, APBB1, NUP43, IRF3, ARRB2, MDM2, ACD, NMD3, CHMP5, RAB6B, RAB8B, PHAX, VPS13C, SEC61A2, CDDC91, ERBB2IP, RAB3A, RAB31L1, RAB5B, RP2, ZMAT3, STXB1, STXB3, TSNAX, YY1, CEP350, ACTN4, YIPF5, COG8, HOOK3, ADAM9, SNAP23, NAPA, RAB11B, PITPNM1
62	9	7.40E-04	6967: unfolded protein response, activation of signaling protein activity	TRIM3, ARHGAP33, SCAMP5, TMED4, RAB21, MAPK8IP3, RAB26, ARFGAP3, GDI1, SERP1, ARIP1, APBB1, NUP43, IRF3, ARRB2, MDM2, ACD, NMD3, CHMP5, RAB6B, RAB8B, PHAX, VPS13C, SEC61A2, CDDC91, ERBB2IP, RAB3A, RAB31L1, RAB5B, RP2, ZMAT3, STXB1, STXB3, TSNAX, YY1, CEP350, ACTN4, YIPF5, COG8, HOOK3, ADAM9, SNAP23, NAPA, RAB11B, PITPNM1
138	18	7.80E-06	6974: response to DNA damage stimulus	TRIM3, ARHGAP33, SCAMP5, TMED4, RAB21, MAPK8IP3, RAB26, ARFGAP3, GDI1, SERP1, ARIP1, APBB1, NUP43, IRF3, ARRB2, MDM2, ACD, NMD3, CHMP5, RAB6B, RAB8B, PHAX, VPS13C, SEC61A2, CDDC91, ERBB2IP, RAB3A, RAB31L1, RAB5B, RP2, ZMAT3, STXB1, STXB3, TSNAX, YY1, CEP350, ACTN4, YIPF5, COG8, HOOK3, ADAM9, SNAP23, NAPA, RAB11B, PITPNM1
264	21	0.02	6281: DNA repair	TRIM3, ARHGAP33, SCAMP5, TMED4, RAB21, MAPK8IP3, RAB26, ARFGAP3, GDI1, SERP1, ARIP1, APBB1, NUP43, IRF3, ARRB2, MDM2, ACD, NMD3, CHMP5, RAB6B, RAB8B, PHAX, VPS13C, SEC61A2, CDDC91, ERBB2IP, RAB3A, RAB31L1, RAB5B, RP2, ZMAT3, STXB1, STXB3, TSNAX, YY1, CEP350, ACTN4, YIPF5, COG8, HOOK3, ADAM9, SNAP23, NAPA, RAB11B, PITPNM1
497	33	0.05	22415: viral reproductive process	TRIM3, ARHGAP33, SCAMP5, TMED4, RAB21, MAPK8IP3, RAB26, ARFGAP3, GDI1, SERP1, ARIP1, APBB1, NUP43, IRF3, ARRB2, MDM2, ACD, NMD3, CHMP5, RAB6B, RAB8B, PHAX, VPS13C, SEC61A2, CDDC91, ERBB2IP, RAB3A, RAB31L1, RAB5B, RP2, ZMAT3, STXB1, STXB3, TSNAX, YY1, CEP350, ACTN4, YIPF5, COG8, HOOK3, ADAM9, SNAP23, NAPA, RAB11B, PITPNM1
304	27	7.60E-04	19048: virus-host interaction	TRIM3, ARHGAP33, SCAMP5, TMED4, RAB21, MAPK8IP3, RAB26, ARFGAP3, GDI1, SERP1, ARIP1, APBB1, NUP43, IRF3, ARRB2, MDM2, ACD, NMD3, CHMP5, RAB6B, RAB8B, PHAX, VPS13C, SEC61A2, CDDC91, ERBB2IP, RAB3A, RAB31L1, RAB5B, RP2, ZMAT3, STXB1, STXB3, TSNAX, YY1, CEP350, ACTN4, YIPF5, COG8, HOOK3, ADAM9, SNAP23, NAPA, RAB11B, PITPNM1

25	5	1.60E-03 30971:	receptor tyrosine kinase binding	SHC4, PONA, PIK3R2, PTPN11, DOK4
38	6	4.20E-03 43130:	ubiquitin binding	DNAJC2, IDE, UBR5, OTUB1, BCL10, USP13
24	5	1.10E-03 19005:	synapsin binding	BLOC1S8, STXBPH1, STXBPH3, SYT3, NHP3
24	5	1.10E-03 1540:	beta-amyloid binding	MAPK8IP2, ARAH1, APBB1, IDE, ACHIE
204	19	2.80E-03 3924:	GTPase activity	TUBB4A, DIRAS1, DNMT1, EEF2A2, RAB21, GNG10, MTF12, SAR1B, RAB6B, RAB8B, RHOT1, RAP2C, RAB3A, RAB5B, RAPTAP, GAP2B, RIT1, TUBA1C, RAB11B
181	18	1.40E-03 4672:	protein kinase activity	HRK3, TRIM28, STK25, CHUK, PLK5, MAP3K1, NEK1, PAK2, CDK17, PDK2, POLR2B, ATR, PRKAA1, RPS3K1, STK3, TGFBR1, FAKTRD3, CDC42BPB
181	18	1.40E-03 4672:	protein kinase activity	HRK3, TRIM28, STK25, CHUK, PLK5, MAP3K1, NEK1, PAK2, CDK17, PDK2, POLR2B, ATR, PRKAA1, RPS3K1, STK3, TGFBR1, FAKTRD3, CDC42BPB
65	9	1.30E-03 19208:	phosphatase regulator activity	DMRK, CABIN1, GTF2F1, PPM1E, TUBA1A, PPP2R4, SFZ2, PPP1R1B, PPP1R9B
395	31	3.70E-03 43229:	intracellular organelle	AASS, STAM2, SLU7, POLI, CHUK, SREK1, DDOST, ELK3, KAZN, RUSC1, RRM2, RAB8B, ATP6V0A1, CROT, SAMD9, CALCOCCO1, ABCD3, SNX
318	24	0.02 43231:	intracellular membrane-bound organelle	6, SC2P, BINP2, SPAST, SPTAN1, ISG20L2, BAP1, TCH, MAP1LC3A, PEK3, CBS, ACBD5, SLC6A3R1
6896	394	2.30E-06 43227:	membrane-bound organelle	AASS, STAM2, SLU7, POLI, CHUK, SREK1, DDOST, ELK3, KAZN, ATP6V0A1, CROT, SAMD9, CALCOCCO1, ABCD3, SNX6, SC2P, BINP2, SPTAN1, ISG20L2
318	24	0.02 43231:	intracellular membrane-bound organelle	over 100 entries (116, 288.)
89	8	0.03 43231:	intracellular membrane-bound organelle	AASS, STAM2, SLU7, POLI, CHUK, SREK1, DDOST, ELK3, KAZN, ATP6V0A1, CROT, SAMD9, CALCOCCO1, ABCD3, SNX6, SC2P, BINP2, SPTAN1, ISG20L2
48	6	0.03 5777:	peroxisome	IDE, NUDT19, PNP1A8, PEK13, CROT, ABCD3, GPP2, NUDT12, PEK3
4320	242	7.80E-04 5854:	nucleus	PNPLA3, RAB8B, PEK13, ABCD3, PEK3, ACBD5
74	8	0.03 31901:	early endosome membrane	over 100 entries (74, 163.)
2625	169	3.30E-04 43228:	non-membrane-bound organelle	STAM2, CLON3, RAB21, SNX13, CLIP3, SNX6, RAB5B, EEA1
112	12	5.00E-03 15630:	microtubule cytoskeleton	over 100 entries (82, 117.)
1433	89	4.80E-03 5730:	nucleolus	TUBB3A, THAP9, TWIST1N, RUSC1, CHUK, PLK5, CPT2, ATF2, SREK1, SPRED1, ELK3, ELK4, SPATA13, TWIST1N, SCFA6, DIS3, WDR43, PI3SA, KAZN, UFL1, MORC3, CABIN1, CD2AP, GABPA, ZNF385A, SENP8, GOLIM4, MED4, DROSHA, APAF1, ZNF260, IMPA1, MDM2, MEN1, NBN, NEK1, RRM2, B, RRP15, NMD3, PONA, SIRT7, PDK2, ZFR, ATP6V0A1, POLR2B, NOL8, PPP2R4, CDDO91, PRPF40A, UTP3, RAD17, RECOL, REST, BDH1, SC2P, LHPH, CCHC7, PHE6, MKI67IP, BRSK1, SMARCA5, PCGF1, PEK3, STXB3, TAF1, TAF13, TBCA, ZEB1, TERF2, TOP1, THTPA, AP3B2, ISG20L2, BAP1, CASP8, Z, NDCCL, ZMAT3, SMARCB1, SP100, SRP19, NEK4, STX5, STXB3, TAF1, TAF13, TBCA, ZEB1, TERF2, TOP1, THTPA, AP3B2, ISG20L2, BAP1, CASP8, Z, CCHC7, PHE6, MKI67IP, BRSK1, SMARCA5, PCGF1, PEK3, TRIM5, CBS, SNAP23, BUB5, DDX21, GORAB
818	58	1.10E-03 31982:	vesicle	ADAM10, SEC23A, FMO2, AP2M1, AP3S1, CLON3, COPB1, CRRH1, SLC30A7, SCAMP5, ABCA2, FASN, RAB21, RUSC1, CLIC4, BLOC1S6, GOLIM4, G, TUBA1C, STX16, STX17, STX18, STX19, STX20, STX21, STX22, STX23, STX24, STX25, STX26, STX27, STX28, STX29, STX30, STX31, STX32, STX33, STX34, STX35, STX36, STX37, STX38, STX39, STX40, STX41, STX42, STX43, STX44, STX45, STX46, STX47, STX48, STX49, STX50, STX51, STX52, STX53, STX54, STX55, STX56, STX57, STX58, STX59, STX60, STX61, STX62, STX63, STX64, STX65, STX66, STX67, STX68, STX69, STX70, STX71, STX72, STX73, STX74, STX75, STX76, STX77, STX78, STX79, STX80, STX81, STX82, STX83, STX84, STX85, STX86, STX87, STX88, STX89, STX90, STX91, STX92, STX93, STX94, STX95, STX96, STX97, STX98, STX99, STX100, STX101, STX102, STX103, STX104, STX105, STX106, STX107, STX108, STX109, STX110, STX111, STX112, STX113, STX114, STX115, STX116, STX117, STX118, STX119, STX120, STX121, STX122, STX123, STX124, STX125, STX126, STX127, STX128, STX129, STX130, STX131, STX132, STX133, STX134, STX135, STX136, STX137, STX138, STX139, STX140, STX141, STX142, STX143, STX144, STX145, STX146, STX147, STX148, STX149, STX150, STX151, STX152, STX153, STX154, STX155, STX156, STX157, STX158, STX159, STX160, STX161, STX162, STX163, STX164, STX165, STX166, STX167, STX168, STX169, STX170, STX171, STX172, STX173, STX174, STX175, STX176, STX177, STX178, STX179, STX180, STX181, STX182, STX183, STX184, STX185, STX186, STX187, STX188, STX189, STX190, STX191, STX192, STX193, STX194, STX195, STX196, STX197, STX198, STX199, STX200, STX201, STX202, STX203, STX204, STX205, STX206, STX207, STX208, STX209, STX210, STX211, STX212, STX213, STX214, STX215, STX216, STX217, STX218, STX219, STX220, STX221, STX222, STX223, STX224, STX225, STX226, STX227, STX228, STX229, STX230, STX231, STX232, STX233, STX234, STX235, STX236, STX237, STX238, STX239, STX240, STX241, STX242, STX243, STX244, STX245, STX246, STX247, STX248, STX249, STX250, STX251, STX252, STX253, STX254, STX255, STX256, STX257, STX258, STX259, STX260, STX261, STX262, STX263, STX264, STX265, STX266, STX267, STX268, STX269, STX270, STX271, STX272, STX273, STX274, STX275, STX276, STX277, STX278, STX279, STX280, STX281, STX282, STX283, STX284, STX285, STX286, STX287, STX288, STX289, STX290, STX291, STX292, STX293, STX294, STX295, STX296, STX297, STX298, STX299, STX300, STX301, STX302, STX303, STX304, STX305, STX306, STX307, STX308, STX309, STX310, STX311, STX312, STX313, STX314, STX315, STX316, STX317, STX318, STX319, STX320, STX321, STX322, STX323, STX324, STX325, STX326, STX327, STX328, STX329, STX330, STX331, STX332, STX333, STX334, STX335, STX336, STX337, STX338, STX339, STX340, STX341, STX342, STX343, STX344, STX345, STX346, STX347, STX348, STX349, STX350, STX351, STX352, STX353, STX354, STX355, STX356, STX357, STX358, STX359, STX360, STX361, STX362, STX363, STX364, STX365, STX366, STX367, STX368, STX369, STX370, STX371, STX372, STX373, STX374, STX375, STX376, STX377, STX378, STX379, STX380, STX381, STX382, STX383, STX384, STX385, STX386, STX387, STX388, STX389, STX390, STX391, STX392, STX393, STX394, STX395, STX396, STX397, STX398, STX399, STX400, STX401, STX402, STX403, STX404, STX405, STX406, STX407, STX408, STX409, STX410, STX411, STX412, STX413, STX414, STX415, STX416, STX417, STX418, STX419, STX420, STX421, STX422, STX423, STX424, STX425, STX426, STX427, STX428, STX429, STX430, STX431, STX432, STX433, STX434, STX435, STX436, STX437, STX438, STX439, STX440, STX441, STX442, STX443, STX444, STX445, STX446, STX447, STX448, STX449, STX450, STX451, STX452, STX453, STX454, STX455, STX456, STX457, STX458, STX459, STX460, STX461, STX462, STX463, STX464, STX465, STX466, STX467, STX468, STX469, STX470, STX471, STX472, STX473, STX474, STX475, STX476, STX477, STX478, STX479, STX480, STX481, STX482, STX483, STX484, STX485, STX486, STX487, STX488, STX489, STX490, STX491, STX492, STX493, STX494, STX495, STX496, STX497, STX498, STX499, STX500, STX501, STX502, STX503, STX504, STX505, STX506, STX507, STX508, STX509, STX510, STX511, STX512, STX513, STX514, STX515, STX516, STX517, STX518, STX519, STX520, STX521, STX522, STX523, STX524, STX525, STX526, STX527, STX528, STX529, STX530, STX531, STX532, STX533, STX534, STX535, STX536, STX537, STX538, STX539, STX540, STX541, STX542, STX543, STX544, STX545, STX546, STX547, STX548, STX549, STX550, STX551, STX552, STX553, STX554, STX555, STX556, STX557, STX558, STX559, STX560, STX561, STX562, STX563, STX564, STX565, STX566, STX567, STX568, STX569, STX570, STX571, STX572, STX573, STX574, STX575, STX576, STX577, STX578, STX579, STX580, STX581, STX582, STX583, STX584, STX585, STX586, STX587, STX588, STX589, STX590, STX591, STX592, STX593, STX594, STX595, STX596, STX597, STX598, STX599, STX600, STX601, STX602, STX603, STX604, STX605, STX606, STX607, STX608, STX609, STX610, STX611, STX612, STX613, STX614, STX615, STX616, STX617, STX618, STX619, STX620, STX621, STX622, STX623, STX624, STX625, STX626, STX627, STX628, STX629, STX630, STX631, STX632, STX633, STX634, STX635, STX636, STX637, STX638, STX639, STX640, STX641, STX642, STX643, STX644, STX645, STX646, STX647, STX648, STX649, STX650, STX651, STX652, STX653, STX654, STX655, STX656, STX657, STX658, STX659, STX660, STX661, STX662, STX663, STX664, STX665, STX666, STX667, STX668, STX669, STX670, STX671, STX672, STX673, STX674, STX675, STX676, STX677, STX678, STX679, STX680, STX681, STX682, STX683, STX684, STX685, STX686, STX687, STX688, STX689, STX690, STX691, STX692, STX693, STX694, STX695, STX696, STX697, STX698, STX699, STX700, STX701, STX702, STX703, STX704, STX705, STX706, STX707, STX708, STX709, STX710, STX711, STX712, STX713, STX714, STX715, STX716, STX717, STX718, STX719, STX720, STX721, STX722, STX723, STX724, STX725, STX726, STX727, STX728, STX729, STX730, STX731, STX732, STX733, STX734, STX735, STX736, STX737, STX738, STX739, STX740, STX741, STX742, STX743, STX744, STX745, STX746, STX747, STX748, STX749, STX750, STX751, STX752, STX753, STX754, STX755, STX756, STX757, STX758, STX759, STX760, STX761, STX762, STX763, STX764, STX765, STX766, STX767, STX768, STX769, STX770, STX771, STX772, STX773, STX774, STX775, STX776, STX777, STX778, STX779, STX780, STX781, STX782, STX783, STX784, STX785, STX786, STX787, STX788, STX789, STX790, STX791, STX792, STX793, STX794, STX795, STX796, STX797, STX798, STX799, STX800, STX801, STX802, STX803, STX804, STX805, STX806, STX807, STX808, STX809, STX810, STX811, STX812, STX813, STX814, STX815, STX816, STX817, STX818, STX819, STX820, STX821, STX822, STX823, STX824, STX825, STX826, STX827, STX828, STX829, STX830, STX831, STX832, STX833, STX834, STX835, STX836, STX837, STX838, STX839, STX840, STX841, STX842, STX843, STX844, STX845, STX846, STX847, STX848, STX849, STX850, STX851, STX852, STX853, STX854, STX855, STX856, STX857, STX858, STX859, STX860, STX861, STX862, STX863, STX864, STX865, STX866, STX867, STX868, STX869, STX870, STX871, STX872, STX873, STX874, STX875, STX876, STX877, STX878, STX879, STX880, STX881, STX882, STX883, STX884, STX885, STX886, STX887, STX888, STX889, STX890, STX891, STX892, STX893, STX894, STX895, STX896, STX897, STX898, STX899, STX900, STX901, STX902, STX903, STX904, STX905, STX906, STX907, STX908, STX909, STX910, STX911, STX912, STX913, STX914, STX915, STX916, STX917, STX918, STX919, STX920, STX921, STX922, STX923, STX924, STX925, STX926, STX927, STX928, STX929, STX930, STX931, STX932, STX933, STX934, STX935, STX936, STX937, STX938, STX939, STX940, STX941, STX942, STX943, STX944, STX945, STX946, STX947, STX948, STX949, STX950, STX951, STX952, STX953, STX954, STX955, STX956, STX957, STX958, STX959, STX960, STX961, STX962, STX963, STX964, STX965, STX966, STX967, STX968, STX969, STX970, STX971, STX972, STX973, STX974, STX975, STX976, STX977, STX978, STX979, STX980, STX981, STX982, STX983, STX984, STX985, STX986, STX987, STX988, STX989, STX990, STX991, STX992, STX993, STX994, STX995, STX996, STX997, STX998, STX999, STX1000, STX1001, STX1002, STX1003, STX1004, STX1005, STX1006, STX1007, STX1008, STX1009, STX1010, STX1011, STX1012, STX1013, STX1014, STX1015, STX1016, STX1017, STX1018, STX1019, STX1020, STX1021, STX1022, STX1023, STX1024, STX1025, STX1026, STX1027, STX1028, STX1029, STX1030, STX1031, STX1032, STX1033, STX1034, STX1035, STX1036, STX1037, STX1038, STX1039, STX1040, STX1041, STX1042, STX1043, STX1044, STX1045, STX1046, STX1047, STX1048, STX1049, STX1050, STX1051, STX1052, STX1053, STX1054, STX1055, STX1056, STX1057, STX1058, STX1059, STX1060, STX1061, STX1062, STX1063, STX1064, STX1065, STX1066, STX1067, STX1068, STX1069, STX1070, STX1071, STX1072, STX1073, STX1074, STX1075, STX1076, STX1077, STX1078, STX1079, STX1080, STX1081, STX1082, STX1083, STX1084, STX1085, STX1086, STX1087, STX1088, STX1089, STX1090, STX1091, STX1092, STX1093, STX1094, STX1095, STX1096, STX1097, STX1098, STX1099, STX1100, STX1101, STX1102, STX1103, STX1104, STX1105, STX1106, STX1107, STX1108, STX1109, STX1110, STX1111, STX1112, STX1113, STX1114, STX1115, STX1116, STX1117, STX1118, STX1119, STX1120, STX1121, STX1122, STX1123, STX1124, STX1125, STX1126, STX1127, STX1128, STX1129, STX1130, STX1131, STX1132, STX1133, STX1134, STX1135, STX1136, STX1137, STX1138, STX1139, STX1140, STX1141, STX1142, STX1143, STX1144, STX1145, STX1146, STX1147, STX1148, STX1149, STX1150, STX1151, STX1152, STX1153, STX1154, STX1155, STX1156, STX1157, STX1158, STX1159, STX1160, STX1161, STX1162, STX1163, STX1164, STX1165, STX1166, STX1167, STX1168, STX1169, STX1170, STX1171, STX1172, STX1173, STX1174, STX1175, STX1176, STX1177, STX1178, STX1179, STX1180, STX1181, STX1182, STX1183, STX1184, STX1185, STX1186, STX1187, STX1188, STX1189, STX1190, STX1191, STX1192, STX1193, STX1194, STX1195, STX1196, STX1197, STX1198, STX1199, STX1200, STX1201, STX1202, STX1203, STX1204, STX1205, STX1206, STX1207, STX1208, STX1209, STX1210, STX1211, STX1212, STX1213, STX1214, STX1215, STX1216, STX1217, STX1218, STX1219, STX1220, STX1221, STX1222, STX1223, STX1224, STX1225, STX1226, STX1227, STX1228, STX1229, STX1230, STX1231, STX1232, STX1233, STX1234, STX1235, STX1236, STX1237, STX1238, STX1239, STX1240, STX1241, STX1242, STX1243, STX1244, STX1245, STX1246, STX1247, STX1248, STX1249, STX1250, STX1251, STX1252, STX1253, STX1254, STX1255, STX1256, STX1257, STX1258, STX1259, STX1260, STX1261, STX1262, STX1263, STX1264, STX1265, STX1266, STX1267, STX1268, STX1269, STX1270, STX1271, STX1272, STX1273, STX1274, STX1275, STX1276, STX1277, STX1278, STX1279, STX1280, STX1281, STX1282, STX1283, STX1284, STX1285, STX1286, STX1287, STX1288, STX1289, STX1290, STX1291, STX1292, STX1293, STX1294, STX1295, STX1296, STX1297, STX1298, STX1299, STX1300, STX1301, STX1302, STX1303, STX1304, STX1305, STX1306, STX1307, STX1308, STX1309, STX1310, STX1311, STX1312, STX1313, STX1314, STX1315, STX1316, STX1317, STX1318, STX1319, STX1320, STX1321, STX1322, STX1323, STX1324, STX1325, STX1326, STX1327, STX1328, STX1329, STX1330, STX1331, STX1332, STX1333, STX1334, STX1335, STX1336, STX1337, STX1338, STX1339, STX1340, STX1341, STX1342, STX1343, STX1344, STX1345, STX1346, STX1347, STX1348, STX1349, STX1350, STX1351, STX1352, STX1353, STX1354, STX1355, STX1356, STX1357, STX1358, STX1359, STX1360, STX1361, STX1362, STX1363, STX1364, STX1365, STX1366, STX1367, STX1368, STX1369, STX1370, STX1371, STX1372, STX1373, STX1374, STX1375, STX1376, STX1377, STX1378, STX1379, STX1380, STX1381, STX1382, STX1383, STX1384, STX1385, STX1386, STX1387, STX1388, STX1389, STX1390, STX1391, STX1392, STX1393, STX1394, STX1395, STX1396, STX1397, STX1398, STX1399, STX1400, STX1401, STX1402, STX1403, STX1404, STX1405, STX1406, STX1407, STX1408, STX1409, STX1410, STX1411, STX1412, STX1413, STX1414, STX1415, STX1416, STX1417, STX1418, STX1419, STX1420, STX1421, STX1422, STX1423, STX1424, STX1425, STX1426, STX1427, STX1428, STX1429, STX1430, STX1431, STX1432, STX1433, STX1434, STX1435, STX1436, STX1437, STX1438, STX1439, STX1440, STX1441, STX1442, STX1443, STX1444, STX1445, STX1446, STX1447, STX1448, STX1449, STX1450, STX1451, STX1452, STX1453, STX1454, STX1455, STX1456, STX1457, STX1458, STX1459, STX1460, STX1461, STX1462, STX1463, STX1464, STX1465, STX1466, STX1467, STX1468, STX1469, STX1470, STX1471, STX1472, STX1473, STX1474, STX1475, STX1476, STX1477, STX1478, STX1479, STX1480, STX1481, STX1482, STX1483, STX1484, STX1485, STX1486, STX1487, STX1488, STX1489, STX1490, STX1491, STX1492, STX1493, STX1494, STX1495, STX1496, STX1497, STX1498, STX1499, STX1500, STX1501, STX1502, STX1503, STX1504, STX1505, STX1506, STX1507, STX1508, STX1509, STX1510, STX1511, STX1512, STX1513, STX1514, STX1515, STX1516, STX1517, STX1518, STX1519, STX1520, STX1521, STX1522, STX1523, STX1524, STX1525, STX1526, STX1527, STX1528, STX1529, STX1530, STX1531, STX1532, STX1533, STX1534, STX1535, STX1536, STX1537, STX1538, STX1539, STX1540, STX1541, STX1542, STX1543, STX1544, STX1545, STX1546, STX1547, STX1548, STX1549, STX1550, STX1551, STX1552, STX1553, STX1554, STX1555, STX1556, STX1557, STX1558, STX1559, STX1560, STX1561, STX1562, STX1563, STX1564, STX1565, STX1566, STX1567, STX1568, STX1569, STX1570, STX1571, STX1572, STX1573, STX1574, STX1575, STX1576, STX1577, STX1578, STX1579, STX1580, STX1581, STX1582, STX1583, STX1584, STX1585, STX1586, STX1587, STX1588, STX15

187	17	6.90E-03 31252 leading edge	APC2, DCTN1, ATN1, SFA1A13, MCF2L, CDZAP, ARPIP2, APBB1, ITGB1, MYO6, PTPN13, RASA1, SAMSIN1, RAP11, PPP1R9B, SLC9A3R1, CDC42BPB
55	8	1.69E-03 42734 presynaptic membrane	ZNRF2, GRIK5, ARBB1, ACHE, SEPT3, NLGN2, SYP, LRRG4B
70	8	0.02 12505 endomembrane system	ADAM10, FAAH, PIP5K1C, BLOC1S6, MAP1LC3A, SLC9A3R1, DOCK2, LAPTM4A
430	32	8.40E-03 139 Golgi membrane	APC2, SEC23A, CLOX, COPB1, SLC30A7, SCAMP5, CHSY1, RAB21, MAPK9IP3, SLC35A3, TMEM69L, ARFGAP3, ARFIP1, GXYLT1, MAN2A1, MGAT2, PNP1A3, SH3GLB1, RAB6B, NDF1P2, CSGALNACT2, RAPIGAP, SREBF2, STX5, BSG, STBS1A4, TNKS2, COG8, GBF1, EBAG9, SLC35A1, HSS211
318	25	9.99E-03 30054 cell junction	ATN1, SCAMP5, ZNRF2, RUSC1, GLRA2, GRIK5, GTF2F1, SHC4, ACHE, OPHNT, SEPT3, NLGN2, RPS6KB1, VAMP2, SYNT1, SYN2, SYP, SY13, BRSK1, TBK1, SHANK3, TANC1, SNAP23, SYNGR1, LRRG4B
430	32	8.40E-03 139 Golgi membrane	APC2, SEC23A, CLOX, COPB1, SLC30A7, SCAMP5, CHSY1, RAB21, MAPK9IP3, SLC35A3, TMEM69L, ARFGAP3, ARFIP1, GXYLT1, MAN2A1, MGAT2, PNP1A3, SH3GLB1, RAB6B, NDF1P2, CSGALNACT2, RAPIGAP, SREBF2, STX5, BSG, STBS1A4, TNKS2, COG8, GBF1, EBAG9, SLC35A1, HSS211
2578	153	1.10E-03 4324 protein complex	over 100 entries (68, 95,)
391	5	0.04152 cytoplasmic mRNA processing body	EIF4E, CNO17, BTBD2, TOP1, TRIMS

CHAPTER 5: Discussion

5.1 General summary and significance of findings

Pediatric brain tumors are devastating diseases that are associated with significant morbidity and mortality due to intrinsically aggressive tumor biology, and sequelae of current standard-of-care treatments. Research into the molecular basis of these tumors is essential to the development of novel therapeutics with limited toxicity and ultimately a better prognosis for these diseases. High-grade gliomas such as glioblastomas (GBMs) and diffuse intrinsic pontine gliomas (DIPGs) are associated with dismal survival rates even with multimodal treatments. These diagnoses are death sentences, and considering the age groups they affect, are particularly tragic for patients and their loved ones. In this dissertation, we have illustrated novel molecular findings in pediatric high-grade and low-grade brain tumors and highlighted the epigenome as a new dimension for further investigation. In pediatric high-grade gliomas (pHGGs) including GBM, we identified recurrent mutations in the H3K36 trimethyltransferase *SETD2* in 15% of cases. We provide evidence that tumors specifically of the cerebral cortex preferentially demonstrate defects involving loss-of-function *SETD2* mutations and others that can affect H3K36me₃ levels, including isocitrate dehydrogenase 1 (*IDH1*) mutations and novel histone H3.3 G34R/V mutations (Chapter 2). In Chapter 3, we describe the mutational landscape of pediatric midline high-grade tumors and demonstrate that H3.3 and H3.1 K27M mutations predominate in these tumors. Moreover, these histone mutations occurred with novel partner mutations distinctly associated with different brain regions, which included for the first time in human cancer, mutations in the activin A receptor type I gene *ACVRI* distinctly located in tumors of the pons. *ACVRI* mutant

tumors and primary cell lines demonstrated hyper-activity of bone morphogenetic protein (BMP)-SMAD family member 1/5/8 (SMAD1/5/8) pathways and may represent a novel target for the treatment of DIPG. In Chapter 4, we describe the whole chromosomal copy number landscapes of 222 PA tumors across the lifespan and characterize the phenotype of aneuploidy in these tumors. We illustrate that aneuploidy is frequent in adult non-cerebellar PA which are more challenging to treat surgically, presents with a non-random pattern of chromosomal gain and is differentially associated with major PA genetic alterations such as *BRAF* fusions and mutations. Expression programs mediated by the E3 ubiquitin ligase MDM2 may underlie the active promotion of or tolerance to aneuploidy in these tumors.

In the next sections we will discuss these molecular findings, their potential roles in gliomagenesis and their implications to the field of pediatric neuro-oncology. Moreover, we will discuss avenues for future investigation needed to best translate these molecular discoveries into better patient care.

5.2 Histone mutations and epigenetic driver mutations as central regulators of tumorigenesis in pediatric brain tumors: possible “epigenetic addiction”?

In 2012, our lab and others discovered recurrent mutations in histone genes for the first time in association with human disease [231,281]. These mutations characterized approximately one-third of pediatric GBM tumors and 78% of DIPGs [231,281]. Mutations in the replication-independent histone variant H3.3 encoded by *H3F3A* were located at or adjacent to critical residues involved in histone post-translational modifications; K27M and G34R/V [231]. Analogous mutations in the replication-

dependent canonical histone variant H3.1, encoded by *HIST1H3B*, were also identified resulting in identical K27M amino acid substitutions [281]. Further work focusing on the characterization of the mechanistic effect of K27M mutation elucidated a profound *trans* mediated inhibitory function on the enzymatic EZH2 component of the Polycomb Repressor Complex 2 (PRC2) [161]. Independent studies have demonstrated decreased global H3K27me2/3 levels and increased total H3K27ac in tissues or overexpressing cell lines without corresponding changes in *EZH2* expression, confirming that the potent effect of K27M mutation is indeed through inhibition of EZH2 H3K27 methyltransferase activity [161,39,261,17]. G34R/V mutations were found to inhibit SET2 mediated trimethylation of heterotypic nucleosomes, with mono- and oligo-nucleosomes containing G34R/V mutations demonstrating decreased levels of H3K36me2/3 [161]. Based on the age groups of H3.3/H3.1 K27M and H3.3 G34R/V mutated patients, they constitute the pediatric counterpart to *IDHI* mutations occurring in young adult disease. *IDHI* mutations have potent effects on histone demethylases and result in changes to histone marks including H3K4, H3K9, H3K27 and H3K36 [168]. Further sequencing studies of CNS tumor heterogeneity has revealed the presence of *IDHI* mutation throughout primary tumors and recurrences in gliomas [115]. This is in contrast to other notable oncogenic drivers such as *BRAF* V600E which appear in only a minority of geographically distinct samples [115]. This is in striking similarity to our report discussed herein in Chapter 3 characterizing *PDGFRA* amplification in only 1 of 5 biopsies from a case of cerebellar GBM, which had virtually identical mutational and epigenetic profiles including K27M mutation [71]. In Chapter 2 we report that about half of hemispheric pHGGs harbor defects leading to aberrant H3K36 methylation, including novel mutations

in *SETD2* [72]. In Chapter 3 we describe an additional histone variant, *HIST1H3C*, with mutation in K27M in midline tumors [71]. Together, this demonstrated that 93% of cases of high-grade tumors, including GBM and DIPG, of the neuroanatomical midline are mutated at residue K27M in H3.3 or H3.1 genes. In addition, we demonstrated that distinct global DNA methylation profiles are associated with K27M mutation, regardless of the individual variant affected, precise brain location or associated mutations [71]. With data demonstrating the prominence of epigenetic driver mutations within large tumor datasets, their presence in geographically distinct regions and longitudinally in disease, CNS high-grade gliomas of the pediatric and young adult years appear to be “addicted” to epigenetic dysregulation (reviewed in [70]). Although further mechanistic studies are necessary to associate “epigenetic addiction” to this tumor type, this provides a specific avenue for further investigation and therapeutic development.

In Chapter 2 we utilize statistical comparisons of WES data to demonstrate genome-wide enrichment of *SETD2* mutations in a dataset of 60 pHGGs compared to 543 non-cancer controls. Within an expanded dataset of 183 gliomas, we identify *SETD2* missense/truncating mutations in 15% of pHGGs and 8% of adult HGGs, and uniquely occurring in tumors arising in the cerebral hemispheres. Functional characterization of *SETD2* mutant tumors demonstrated a loss-of-function phenotype, leading to decreased levels of H3K36me3. DNA methylation analysis revealed that their effect on the global methylation landscape may be independent of G34R/V and more promiscuous. *SETD2* has been reported as the only enzyme in humans to mediate H3K36 trimethylation [64]. H3K36me3 is a mark correlating with transcriptionally active chromatin [259]. Notably, roles for H3K36me3 have been elucidated for critical cellular processes such as

alternative mRNA splicing [170,169], suppression of spurious or cryptic transcription [260], DNA mismatch repair [162] and homologous recombination [10,35,203]. Recent studies of H3.3K36me3 demonstrate the importance of histone “reader” proteins such as ZMYND11, which recognizes this mark specifically on H3.3 variants and co-localizes in gene bodies [276]. As it was also found to link H3.3K36me3 with transcriptional elongation and tumor suppression programs, the authors show a preliminary demonstration that G34R/V mutations abrogate the binding of ZMYND11 to H3.3K36me3 peptides [276]. With such a diversity of critical functions, further exploration into the role of the SETD2-H3K36 pathway in cortical tumorigenesis specifically is warranted and may allow further insight into the potential neurodevelopmental roles of this histone mark.

5.3 ACVR1 mutations: New targets and further evidence for pediatric brain tumors as neurodevelopmental diseases

Mutations in histone genes described throughout this dissertation have changed the way we view pediatric brain tumors. These mutations are novel and had not been identified with any other human disease to date. Due to their frequency, specificity and influence on the epigenome in HGGs, it is clear that modeling and targeting these histone mutations will be the subject of intense effort worldwide as the next critical step in translating their discovery into actionable targets. Mouse modeling and other pre-clinical studies, drug discovery and development will necessitate years of research. How can we target these tumors, which continue to have a dismal survival rate, in the near future? Repurposing existing drugs or compounds to re-orient therapeutic efforts may be a more

rapid solution. The targets of which may be genetic alterations that are distinctly associated with histone mutations.

In Chapter 3 of this thesis and published in [71], we describe the identification of *ACVRI* mutations and other growth factor receptor mutations associated with pediatric mHGAs. These mutations are strongly associated with histone mutations identified in these tumors, shed some needed light on the nature of their origins and offer therapeutic opportunity. *ACVRI* encodes the activin A, receptor type I, ACVR1/ALK2 which is a receptor for BMPs, activator of downstream SMAD signaling and is involved in the development of the nervous system [103]. Germline *ACVRI* mutations have been shown to cause the autosomal dominant debilitating musculoskeletal disease fibrodysplasia ossificans progressiva (FOP), characterized by heterotopic bone formation [238]. As described in Chapter 3, we identify *ACVRI* mutations in 5/39 mHGAs (13%), and 5/24 (21%) DIPGs sequenced by WES. All of these mutant tumors were distinctly located in the pontine region and harbored K27M mutations in H3.1 (the majority, 4/5) or H3.3 (1/5). DIPGs are among the most deadly of tumors occurring in the pediatric years [15]. Survival for children diagnosed with DIPG is 1-2 years with 90% of patients dying of their disease within 2 years [15]. Although our report adds to the recent knowledge-base demonstrating that K27M mutations predominate overwhelmingly in these tumors, lack of current avenues for specific targeted therapy for this mutation hinders progress for translation at the moment. Inhibitors exist for ACVR1/ALK2 that are highly specific for the receptor [288,235,53]. Concurrently with our report, adapted here as Chapter 3, three additional reports were simultaneously published in the same issue of the journal [31,252,282]. All four reports including that of our group, describe the identification of

hotspot *ACVR1* mutations, which strongly associate with histone H3.1 K27M mutations in the pons described above, demonstrating extraordinary reproducibility on large independent cohorts. Moreover, the complementary nature of these studies gives insight into required partner mutations in the specific gliomagenesis of these tumors. Taylor and colleagues utilize the selective ACVR1/ALK2 inhibitor LDN-193189 to treat primary cultures of GBM and DIPG mutant for H3.3 or H3.1 at K27M and associated ACVR1 mutations including novel G328V variants [252]. In these primary cultures they demonstrate significant inhibition of cell viability in all cell lines, which trended towards increased selectivity to ACVR1 mutant cell lines [252]. In their report, they identify the concentrations required to inhibit cell growth by half (defined as GI₅₀) in the range of 0.86-2.1 μM [252]. Parallel to this, and strongly supporting a neurodevelopmental origin of DIPG tumors, Wu and colleagues utilize a previously characterized zebrafish model [235] to functionally characterize ACVR1 mutants [282]. They demonstrate that individual variants harbor the capacity to ventralize zebrafish and lead to aberrant development of zebrafish without head and dorsal structures [282]. In order of increasing severity of the phenotype, ACVR1 R258G, G328E, G328W, R206H, G356D and G328V variants demonstrate differential ventralization ability correlating with levels of activation and downstream SMAD1/5 phosphorylation [282]. Moreover, the selective ACVR1/ALK2 inhibitor LDN-193189 at a concentration of 2.5 μM was capable of partially rescuing dorsal structures and blocked SMAD1/5 phosphorylation [282]. These data demonstrate that selective targeting of ACVR1 through small molecule inhibition may form a novel means of correcting aberrant neurodevelopmental signaling and inhibiting DIPG tumor growth.

The neuroanatomical specificity of *ACVR1* mutations and their strong association with younger patient age suggests a neurodevelopmental origin for DIPG tumorigenesis. Data illustrating increased ventralization of zebrafish in response to *ACVR1* variant expression described above, powerfully implicates such variants in these processes [235]. Gliomas however have not been recurrently reported in patients with germline *ACVR1* mutations and FOP. Heterotopic ossification usually starts to present around age 2-6 years and patients usually die of their disease before the age of 40 due to thoracic muscle ossification and subsequent cardiopulmonary defects [254]. This suggests that additional hits are required for tumorigenesis in the CNS. However, reports of recurrent neurological symptoms such as headache and neuropathic pain amongst other symptoms define the clinical spectrum of FOP patients [145], as well as CNS structural abnormalities such as demyelinated lesions identifiable by MRI [127]. Strikingly, Kan and colleagues report distinct CNS demyelination observed in two mouse models of FOP and four FOP patients. Mouse models, including a transgenic *BMP4* overexpression model, under control of the neuron-specific enolase promoter (*Nse-BMP4*) [126], and a classic FOP *ACVR1* R206H knock-in model [38], demonstrated hyper-intense brain and spinal cord lesions on small animal MRI [127]. Younger FOP patients aged 27 and 33 months respectively, examined by MRI demonstrated pontine and cerebellar type II lesions, more characteristic of developmental demyelination [127]. When mouse hyper-intense regions were examined by IHC for myelin directly (utilizing luxol fast blue) or myelin basic protein (MBP), notable demyelination was observed in these areas, confirming a correlation with MRI hyper-intensities [127]. Interestingly, *ACVR1* R206H knock-in mutant cells that harbor a neomycin resistance marker (*neo+*), did not co-

localize with CNPase, a marker of oligodendrocytes [127]. Further to this, mutant cells were strongly glial fibrillary acidic protein positive (GFAP+) and also expressed neuronal marker β -III tubulin [127]. BMP signaling has been shown to inhibit oligodendroglial lineage commitment and promote astrocyte cell fates [222,87]. Furthermore, BMPs were shown to regulate GBM tumorigenicity in tumor initiating cells (TICs) in a negative manner [205], later shown to occur through epigenetic control of the *BMPRII* promoter by EZH2 which, when activated, was able to restore astroglial differentiation [158]. Interestingly, constitutively active ALK2 mutations, when expressed in endothelial cells, promoted stem-like cell fates through endothelial-to-mesenchymal transition [182]. In the context of DIPG discussed herein, concurrent reports demonstrate *ACVR1* mutations localized exclusively to the pons in H3 K27M mutant tumors (mostly H3.1 K27M), associated with substantial activation of downstream SMAD signaling and transcriptional target expression. Reconciling data illustrating the negative modulation of active BMP signaling on tumorigenicity in GBM TICs, promotion of mesenchymal stem-like cell fates in endothelial cells with the presence of gain-of-function *ACVR1* mutations in DIPG cells and loss of viability with *ACVR1* inhibition is of great interest and necessitates future study. One can surmise that based on its developmental functions notably favoring formation of ventral structures, *ACVR1* hyper-active mutants would favor growth of DIPG cells rather than cells derived from supratentorial regions. *ACVR1* and BMP pathways are critical for embryogenesis and left-right pattern symmetry [144]. In addition, pro-astrocytic differentiation which can be enabled via increased BMP-SMAD signaling in *ACVR1* mutants preferentially in the ventral brainstem, may be aberrantly modulated by concurrent epigenomic dysregulation associated with H3 K27M.

Presence of regionally-specific activating mutations in defined neuroanatomical regions may suggest importance of the microenvironment to tumor growth. Future studies examining the interaction between CNS cellular programming and differentiation and epigenomic dysregulation will be crucial to elucidating specific pathways for gliomagenesis.

5.4 Aneuploidy, aging and pilocytic astrocytoma: Inner workings of a tumor beyond the MAPK pathway

Many independent studies have confirmed a central role for MAPK hyper-activity and PA tumorigenesis. Mouse models created utilizing the avian retroviral RCAS/Tv-a system and mutant *BRAF* have been shown to develop tumors which recapitulated PA histopathology [91]. Recent characterization of PA tumors across the CNS have shed light on the distribution of molecular alterations in these tumors (reviewed in [117]). Seminal work by Jones and colleagues further characterized common 7q34 duplication found to arise in PA tumors as tandem in nature and creating a novel in-frame fusion of *KIAA1549-BRAF* [121]. This fusion was shown to be transforming and allow for constitutive activity of the BRAF kinase domain and characterized the vast majority of PA tumors specifically located in cerebellar areas [121].

PA tumors arising in non-cerebellar areas pose a considerable burden for gross-total surgical resection and are more challenging to treat. PA tumors, much like HGGs, demonstrate neuroanatomical specificity of genetic alterations [117]. Whereas *KIAA1549-BRAF* fusions predominate in cerebellar PA, areas such as the optic pathway, thalamus/diencephalon, cerebral cortex and spinal cord have been shown to harbor lower frequencies [117]. *BRAF* V600E and insertional mutants are more common in non-

cerebellar regions; 16/20 *BRAF* mutant tumors described in Chapter 4 arise outside of the cerebellum. Moreover, PA tumors arising in the context of NF1 syndrome, tend to occur within optic pathways [117]. Novel *FGFR1* mutations in addition have been shown to occur in thalamic regions, notably in association with NF1 and *H3F3A* K27M mutations in thalamic GBM and very rare cases of PA tumors arising here [118]. Taken together, this demonstrates that PA tumors arising in diverse neuroanatomical regions may not only pose considerable burden due to surgical inaccessibility, but are molecularly distinct in their means of activation of the MAPK pathway.

In Chapter 4, we describe the genome-wide whole chromosomal copy number analysis of 222 adult and pediatric PA tumors to better characterize the phenotype of aneuploidy first seen in 2006 in association with age [119]. We demonstrate that aneuploidy is common overall in PA, with 22.5% (50/222) of PA genomes demonstrating at least one chromosomal gain. Whole chromosomal losses were not observed in our dataset, but rather a non-random pattern of chromosomal gains favoring specific chromosomes. Gains of chromosomes 5, 7, 6 and 11 in order of frequency were over-represented across the background level of gains in 50 aneuploid PA tumors, whereas chromosomes 1, 2, 3, 13, 14, 16, 17, 19, 22 were under-represented. Aneuploid tumors occurred across the CNS, and notably more than half of these tumors were localized in non-cerebellar areas. Aneuploid tumors were largely *KIAA1549-BRAF* fusion wild-type. Strikingly, 8/15 tumors harboring *BRAF* V600E or an insertional mutant were aneuploid, illustrating a strong association of gain-of-function *BRAF* point mutants and this phenotype. Aneuploidy was associated strongly with age in PA, and patients with aneuploid tumors were on average approximately 10 years older than those with euploid

tumors. When gene expression profiles of aneuploid tumors were compared to euploid tumors, differential expression revealed correlation with an increased representation of genes on chromosomes involved in gains, including 5, 6 and 7 with a highly significant representation of chromosomes on the q-arm of chromosome 5. These 503 genes included pathways with roles in the cell cycle, CNS development and the unfolded protein response (UPR). Increased expression of the polo-like kinase, *PLK2*, and the E3 ubiquitin ligase *MDM2* was seen in aneuploid tumors. Further analysis revealed that *MDM2* expression was highest amongst aneuploid PA tumors in a comparison with other gliomas and normal brain tissues and correlated with age and *MDM2* SNP 309 genotype in PA. Interestingly, a vast number of genes correlated strongly with *MDM2* expression uniquely in PA tumors and not other gliomas. Application of highly stringent statistical criteria ($FDR < 1 \times 10^{-15}$) and subsequent Gene Ontology (GO) analysis revealed enrichment of pathways involved in cell cycle, chromosomal segregation and the UPR. Notably, mapping of this 742-gene signature revealed representation on chromosome 5q, but not other amplified chromosomes, suggesting a potential driver effect of *MDM2*-correlated programs and aneuploidy in PA.

As described in Chapter 4, *Mdm2* transgenic mice show exacerbated levels of chromosomal gains with age [171]. Importantly, *Mdm2* expression in these mouse models was shown to modulate the frequency of gains, but not loss [171], which is analogous to phenotypes observed in PA tumors. Moreover, we provide strong evidence for robust correlations of genes with *MDM2* expression across PA samples including pathways that could actively promote or provide tolerance to aneuploidy. A variety of mechanisms can lead to aneuploidy in cells, which may include aberrant cell division,

abnormal numbers of centrosomes, dysfunctional mitotic spindle assembly amongst others (reviewed in [88]). Harboring an additional complement of one or more chromosomes is accompanied by a certain degree of genotoxic and proteotoxic stress [88], illustrated by the limited number of germline aneuploid syndromes observed in humans. Accumulation of misfolded proteins as a result necessitates activation of mechanisms which can handle the proteotoxic environment [88]. Ubiquitin-mediated proteosomal degradation may prove an interesting target pathway for investigation in these contexts.

5.5 Future prospects and experimentation

Throughout this thesis we have discussed the literature base and described three studies identifying genetic and epigenetic mechanisms at play within patient gliomas. Investigation utilizing array technology and next-generation sequencing have revolutionized the study of patient samples. In the chapters above, the use of these technologies resulted in the identification of *SETD2* mutations [72], *ACVR1* mutations [71] and characterization of aneuploidy in pediatric brain tumors. Prospective studies will necessitate further characterization of the mechanistic implications of these mutations and the manner in which we can target them to selectively kill tumor cells. As discussed above, recent reports have emerged describing a role for epigenetic modifications, specifically H3K36me3, in mRNA splicing [170,169]. In addition, intricacy of SETD2/H3K36me3 and transcriptional regulation has been well-established [260,10,276]. Future studies focusing on the transcriptomic implications of *SETD2* loss-of-function mutations within cortical gliomas will be of interest for investigation. Given

the recent reports of RNA sequencing analysis within GBM tumors [241,75], and increasing feasibility of RNA sequencing data analysis (reviewed in [272]), focused studies of H3K36-altered tumors will allow for an exploration of transcriptional aberrations. Moreover, integrating epigenomic information enabled by ChIP-seq of histone marks [39,20,17], will enable global characterization of the genomic/epigenomic interface within these tumors.

The identification of distinct growth factor receptor mutations associated with histone H3.3 or H3.1 K27M mutations in different brain regions implicates novel therapeutic avenues [71]. Creating accurate cell culture and mouse models of H3.3 and H3.1 K27M or H3.3 G34R/V mutation will undoubtedly be critical tools for compound screening and the next step for mechanistic investigation. Co-expression of *ACVRI*, *FGFR1*, *PDGFRA* or *TP53* mutations, documented concurrent mutations in association with histone mutations in patient samples, may be a required step prior to accurate recapitulation of tumorigenesis in these models. Indeed, as discussed above, gliomas have not been reported in patients with germline *ACVRI* variants, or mouse models of activated BMP or *ACVRI*. Novel genome engineering strategies enabled by zinc finger nuclease (ZFN) [34], transcription activator-like effector nuclease (TALEN) [257] and notably clustered regularly interspaced short palindromic repeats (CRISPR) [49,174] technologies will undoubtedly be of use for creation of such models. Engineered creation and correction of histone and partner mutations such as *ACVRI* will enable investigation into the sufficiency of these mutation clusters in driving these subgroups of tumors. Patient-derived xenografts in immunocompromised mice through intracranial injections

in corresponding neuroanatomical regions may permit investigation of the microenvironment in contextual growth of tumor cells harboring specific mutations.

In much the same fashion as *ACVR1* mutations form a novel avenue for accelerated therapeutic targeting of DIPGs, the UPR may prove to be a mechanism that has potential for exploitation in aneuploid PA. As we have discussed above aneuploid-specific and *MDM2*-correlated programs include elements related to UPR and mechanisms dealing with dosage compensation in aneuploid PA tumors. Future studies focusing on genetic or pharmacological inhibition of *MDM2* or the UPR in aneuploid PA models will be of interest in assessing this phenotype. Targeting the ubiquitin-proteasome and protein folding pathways as a means to counter mechanisms of dosage compensation has been suggested for selectively killing aneuploid cells [88]. Chromosome transfer strategies coupled with *MDM2*/UPR inhibition may be of interest for future mechanistic studies in this regard. Furthermore, additional studies in PA tumor cells may be of interest to elucidate whether aneuploid defects arise as a result of pre-mitotic DNA replication stress as recently shown by seminal work in colorectal cancer cells [32](reviewed in [33]).

5.6 Conclusion

Brain tumors are among the most feared diagnoses in oncology. Even with modern gold standard treatments, survival for high-grade brain tumors remains dismal. Moreover, the emergence of reports demonstrating distinct molecular mechanisms in pediatric tumors, combined with currently adopted strategies from adult trials, necessitates change for better outcomes. Herein we have explored the genomic

landscapes of pediatric high-grade gliomas including GBM and DIPG, and low-grade PA tumors across the lifespan. We characterize the frequent presence of epigenetic driver mutations, including histone genes and companion chromatin-associated machinery affecting H3K36 methylation, in pediatric tumors of the cerebral hemispheres. We also investigated tumor biopsies of midline regions and determine predominance of H3 K27M mutations and partner growth factor receptor mutations including *ACVRI* in distinct brain regions. Additionally we performed profiling studies and characterized the phenotype of aneuploidy more frequent in adult tumors that may be enabled by specific mechanisms. These data demonstrate that gliomas diagnosed in different age groups and brain locations harbor exquisitely specific molecular profiles, although they appear identical in routine histopathology. As such, moving forward will necessitate the adoption of genomic and epigenomic strategies to complement neuropathology and focus on a molecular re-classification of brain tumors as a critical step to improving the lives of affected patients and their families.

BIBLIOGRAPHY

1. Abecasis GR, Altshuler D, Auton A, Brooks LD, Durbin RM, Gibbs RA, Hurles ME, McVean GA (2010) A map of human genome variation from population-scale sequencing. *Nature* 467:1061-1073. doi:10.1038/nature09534
2. Adzhubei IA, Schmidt S, Peshkin L, Ramensky VE, Gerasimova A, Bork P, Kondrashov AS, Sunyaev SR (2010) A method and server for predicting damaging missense mutations. *Nature methods* 7:248-249. doi:10.1038/nmeth0410-248
3. Aghili M, Zahedi F, Rafiee E (2009) Hydroxyglutaric aciduria and malignant brain tumor: a case report and literature review. *Journal of neuro-oncology* 91:233-236. doi:10.1007/s11060-008-9706-2
4. Aihara K, Mukasa A, Gotoh K, Saito K, Nagae G, Tsuji S, Tatsuno K, Yamamoto S, Takayanagi S, Narita Y, Shibui S, Aburatani H, Saito N (2014) H3F3A K27M

- mutations in thalamic gliomas from young adult patients. *Neuro-oncology* 16:140-146. doi:10.1093/neuonc/not144
5. Akasaka N, Tohyama J, Ogawa A, Takachi T, Watanabe A, Asami K (2013) Refractory infantile spasms associated with mosaic variegated aneuploidy syndrome. *Pediatric neurology* 49:364-367. doi:10.1016/j.pediatrneurol.2013.05.014
 6. Allsopp RC, Vaziri H, Patterson C, Goldstein S, Younglai EV, Futcher AB, Greider CW, Harley CB (1992) Telomere length predicts replicative capacity of human fibroblasts. *Proceedings of the National Academy of Sciences of the United States of America* 89:10114-10118
 7. Armanios M, Blackburn EH (2012) The telomere syndromes. *Nature reviews Genetics* 13:693-704. doi:10.1038/nrg3246
 8. Armanios M, Chen JL, Chang YP, Brodsky RA, Hawkins A, Griffin CA, Eshleman JR, Cohen AR, Chakravarti A, Hamosh A, Greider CW (2005) Haploinsufficiency of telomerase reverse transcriptase leads to anticipation in autosomal dominant dyskeratosis congenita. *Proceedings of the National Academy of Sciences of the United States of America* 102:15960-15964. doi:10.1073/pnas.0508124102
 9. Atak ZK, Gianfelici V, Hulselmans G, De Keersmaecker K, Devasia AG, Geerdens E, Mentens N, Chiaretti S, Durinck K, Uyttebroeck A, Vandenberghe P, Wlodarska I, Cloos J, Foa R, Speleman F, Cools J, Aerts S (2013) Comprehensive analysis of transcriptome variation uncovers known and novel driver events in T-cell acute lymphoblastic leukemia. *PLoS genetics* 9:e1003997. doi:10.1371/journal.pgen.1003997
 10. Aymard F, Bugler B, Schmidt CK, Guillou E, Caron P, Briois S, Iacovoni JS, Daburon V, Miller KM, Jackson SP, Legube G (2014) Transcriptionally active chromatin recruits homologous recombination at DNA double-strand breaks. *Nature structural & molecular biology* 21:366-374. doi:10.1038/nsmb.2796
 11. Ballester R, Marchuk D, Boguski M, Saulino A, Letcher R, Wigler M, Collins F (1990) The NF1 locus encodes a protein functionally related to mammalian GAP and yeast IRA proteins. *Cell* 63:851-859
 12. Bar EE, Lin A, Tihan T, Burger PC, Eberhart CG (2008) Frequent gains at chromosome 7q34 involving BRAF in pilocytic astrocytoma. *Journal of neuropathology and experimental neurology* 67:878-887. doi:10.1097/NEN.0b013e3181845622
 13. Barber LJ, Youds JL, Ward JD, McIlwraith MJ, O'Neil NJ, Petalcorin MI, Martin JS, Collis SJ, Cantor SB, Auclair M, Tissenbaum H, West SC, Rose AM, Boulton SJ (2008) RTEL1 maintains genomic stability by suppressing homologous recombination. *Cell* 135:261-271. doi:10.1016/j.cell.2008.08.016
 14. Barker D, Wright E, Nguyen K, Cannon L, Fain P, Goldgar D, Bishop DT, Carey J, Baty B, Kivlin J, et al. (1987) Gene for von Recklinghausen neurofibromatosis is in the pericentromeric region of chromosome 17. *Science* 236:1100-1102
 15. Bartels U, Hawkins C, Vezina G, Kun L, Souweidane M, Bouffet E (2011) Proceedings of the diffuse intrinsic pontine glioma (DIPG) Toronto Think Tank: advancing basic and translational research and cooperation in DIPG. *Journal of neuro-oncology* 105:119-125. doi:10.1007/s11060-011-0704-4

16. Behjati S, Tarpey PS, Presneau N, Scheipl S, Pillay N, Van Loo P, Wedge DC, Cooke SL, Gundem G, Davies H, Nik-Zainal S, Martin S, McLaren S, Goody V, Robinson B, Butler A, Teague JW, Halai D, Khatri B, Myklebost O, Baumhoer D, Jundt G, Hamoudi R, Tirabosco R, Amary MF, Futreal PA, Stratton MR, Campbell PJ, Flanagan AM (2013) Distinct H3F3A and H3F3B driver mutations define chondroblastoma and giant cell tumor of bone. *Nature genetics* 45:1479-1482. doi:10.1038/ng.2814
17. Bender S, Tang Y, Lindroth AM, Hovestadt V, Jones DT, Kool M, Zapatka M, Northcott PA, Sturm D, Wang W, Radlwimmer B, Hojfeldt JW, Truffaux N, Castel D, Schubert S, Ryzhova M, Seker-Cin H, Gronych J, Johann PD, Stark S, Meyer J, Milde T, Schuhmann M, Ebinger M, Monoranu CM, Ponnuswami A, Chen S, Jones C, Witt O, Collins VP, von Deimling A, Jabado N, Puget S, Grill J, Helin K, Korshunov A, Lichter P, Monje M, Plass C, Cho YJ, Pfister SM (2013) Reduced H3K27me3 and DNA hypomethylation are major drivers of gene expression in K27M mutant pediatric high-grade gliomas. *Cancer cell* 24:660-672. doi:10.1016/j.ccr.2013.10.006
18. Berchtold NC, Cribbs DH, Coleman PD, Rogers J, Head E, Kim R, Beach T, Miller C, Troncoso J, Trojanowski JQ, Zielke HR, Cotman CW (2008) Gene expression changes in the course of normal brain aging are sexually dimorphic. *Proceedings of the National Academy of Sciences of the United States of America* 105:15605-15610. doi:10.1073/pnas.0806883105
19. Bettgowda C, Agrawal N, Jiao Y, Wang Y, Wood LD, Rodriguez FJ, Hruban RH, Gallia GL, Binder ZA, Riggins CJ, Salmasi V, Riggins GJ, Reitman ZJ, Rasheed A, Keir S, Shinjo S, Marie S, McLendon R, Jallo G, Vogelstein B, Bigner D, Yan H, Kinzler KW, Papadopoulos N (2013) Exomic sequencing of four rare central nervous system tumor types. *Oncotarget* 4:572-583
20. Bjerke L, Mackay A, Nandhabalan M, Burford A, Jury A, Popov S, Bax DA, Carvalho D, Taylor KR, Vinci M, Bajrami I, McGonnell IM, Lord CJ, Reis RM, Hargrave D, Ashworth A, Workman P, Jones C (2013) Histone H3.3 Mutations Drive Pediatric Glioblastoma through Upregulation of MYCN. *Cancer discovery*. doi:10.1158/2159-8290.CD-12-0426
21. Boldrini L, Pistolesi S, Gisfredi S, Ursino S, Ali G, Pieracci N, Basolo F, Parenti G, Fontanini G (2006) Telomerase activity and hTERT mRNA expression in glial tumors. *International journal of oncology* 28:1555-1560
22. Bond GL, Hu W, Bond EE, Robins H, Lutzker SG, Arva NC, Bargonetti J, Bartel F, Taubert H, Wuerl P, Onel K, Yip L, Hwang SJ, Strong LC, Lozano G, Levine AJ (2004) A single nucleotide polymorphism in the MDM2 promoter attenuates the p53 tumor suppressor pathway and accelerates tumor formation in humans. *Cell* 119:591-602. doi:10.1016/j.cell.2004.11.022
23. Bouska A, Lushnikova T, Plaza S, Eischen CM (2008) Mdm2 promotes genetic instability and transformation independent of p53. *Molecular and cellular biology* 28:4862-4874. doi:10.1128/MCB.01584-07
24. Brevini TA, Pennarossa G, Maffei S, Tettamanti G, Vanelli A, Isaac S, Eden A, Ledda S, de Eguileor M, Gandolfi F (2012) Centrosome amplification and chromosomal instability in human and animal parthenogenetic cell lines. *Stem cell reviews* 8:1076-1087. doi:10.1007/s12015-012-9379-2

25. Brinkman AB, Gu H, Bartels SJ, Zhang Y, Matarese F, Simmer F, Marks H, Bock C, Gnirke A, Meissner A, Stunnenberg HG (2012) Sequential ChIP-bisulfite sequencing enables direct genome-scale investigation of chromatin and DNA methylation cross-talk. *Genome research* 22:1128-1138. doi:10.1101/gr.133728.111
26. Broderick DK, Di C, Parrett TJ, Samuels YR, Cummins JM, McLendon RE, Fuhs DW, Velculescu VE, Bigner DD, Yan H (2004) Mutations of PIK3CA in anaplastic oligodendrogliomas, high-grade astrocytomas, and medulloblastomas. *Cancer research* 64:5048-5050. doi:10.1158/0008-5472.CAN-04-1170
27. Brooks CL, Li M, Hu M, Shi Y, Gu W (2007) The p53--Mdm2--HAUSP complex is involved in p53 stabilization by HAUSP. *Oncogene* 26:7262-7266. doi:10.1038/sj.onc.1210531
28. Bryan TM, Englezou A, Dalla-Pozza L, Dunham MA, Reddel RR (1997) Evidence for an alternative mechanism for maintaining telomere length in human tumors and tumor-derived cell lines. *Nature medicine* 3:1271-1274
29. Bryan TM, Marusic L, Bacchetti S, Namba M, Reddel RR (1997) The telomere lengthening mechanism in telomerase-negative immortal human cells does not involve the telomerase RNA subunit. *Human molecular genetics* 6:921-926
30. Bryan TM, Reddel RR (1997) Telomere dynamics and telomerase activity in in vitro immortalised human cells. *Eur J Cancer* 33:767-773. doi:10.1016/S0959-8049(97)00065-8
31. Buczkowicz P, Hoeman C, Rakopoulos P, Pajovic S, Letourneau L, Dzamba M, Morrison A, Lewis P, Bouff et E, Bartels U, Zuccaro J, Agnihotri S, Ryall S, Barszczyk M, Chornenkyy Y, Bourgey M, Bourque G, Montpetit A, Cordero F, Castelo-Branco P, Mangerel J, Tabori U, Ho KC, Huang A, Taylor KR, Mackay A, Bendel AE, Nazarian J, Fangusaro JR, Karajannis MA, Zagzag D, Foreman NK, Donson A, Hegert JV, Smith A, Chan J, Lafay-Cousin L, Dunn S, Hukin J, Dunham C, Scheinmann K, Michaud J, Zelcer S, Ramsay D, Cain J, Brennan C, Souweidane MM, Jones C, Allis CD, Brudno M, Becher O, Hawkins C (2014) Genomic analysis of diffuse intrinsic pontine gliomas identifies three molecular subgroups and recurrent activating ACVR1 mutations. *Nature genetics* 46:451-456. doi:10.1038/ng.2936
32. Burrell RA, McClelland SE, Endesfelder D, Groth P, Weller MC, Shaikh N, Domingo E, Kanu N, Dewhurst SM, Gronroos E, Chew SK, Rowan AJ, Schenk A, Sheffer M, Howell M, Kschischo M, Behrens A, Helleday T, Bartek J, Tomlinson IP, Swanton C (2013) Replication stress links structural and numerical cancer chromosomal instability. *Nature* 494:492-496. doi:10.1038/nature11935
33. Burrell RA, McGranahan N, Bartek J, Swanton C (2013) The causes and consequences of genetic heterogeneity in cancer evolution. *Nature* 501:338-345. doi:10.1038/nature12625
34. Carroll D (2011) Genome engineering with zinc-finger nucleases. *Genetics* 188:773-782. doi:10.1534/genetics.111.131433
35. Carvalho S, Vitor AC, Sridhara SC, Martins FB, Raposo AC, Desterro JM, Ferreira J, de Almeida SF (2014) SETD2 is required for DNA double-strand break repair and activation of the p53-mediated checkpoint. *eLife* 3:e02482. doi:10.7554/eLife.02482

36. Cawthon RM, O'Connell P, Buchberg AM, Viskochil D, Weiss RB, Culver M, Stevens J, Jenkins NA, Copeland NG, White R (1990) Identification and characterization of transcripts from the neurofibromatosis 1 region: the sequence and genomic structure of EVI2 and mapping of other transcripts. *Genomics* 7:555-565
37. Chaikuad A, Alfano I, Kerr G, Sanvitale CE, Boergermann JH, Triffitt JT, von Delft F, Knapp S, Knaus P, Bullock AN (2012) Structure of the bone morphogenetic protein receptor ALK2 and implications for fibrodysplasia ossificans progressiva. *The Journal of biological chemistry* 287:36990-36998. doi:10.1074/jbc.M112.365932
38. Chakkalakal SA, Zhang D, Culbert AL, Convente MR, Caron RJ, Wright AC, Maidment AD, Kaplan FS, Shore EM (2012) An Acvr1 R206H knock-in mouse has fibrodysplasia ossificans progressiva. *Journal of bone and mineral research : the official journal of the American Society for Bone and Mineral Research* 27:1746-1756. doi:10.1002/jbmr.1637
39. Chan KM, Fang D, Gan H, Hashizume R, Yu C, Schroeder M, Gupta N, Mueller S, James CD, Jenkins R, Sarkaria J, Zhang Z (2013) The histone H3.3K27M mutation in pediatric glioma reprograms H3K27 methylation and gene expression. *Genes & development* 27:985-990. doi:10.1101/gad.217778.113
40. Chandhok NS, Pellman D (2009) A little CIN may cost a lot: revisiting aneuploidy and cancer. *Current opinion in genetics & development* 19:74-81. doi:10.1016/j.gde.2008.12.004
41. Chen G, Bradford WD, Seidel CW, Li R (2012) Hsp90 stress potentiates rapid cellular adaptation through induction of aneuploidy. *Nature* 482:246-250. doi:10.1038/nature10795
42. Chen YH, Gutmann DH (2014) The molecular and cell biology of pediatric low-grade gliomas. *Oncogene* 33:2019-2026. doi:10.1038/onc.2013.148
43. Cheng Y, Pang JC, Ng HK, Ding M, Zhang SF, Zheng J, Liu DG, Poon WS (2000) Pilocytic astrocytomas do not show most of the genetic changes commonly seen in diffuse astrocytomas. *Histopathology* 37:437-444
44. Chojnacka M, Pedziwiatr K, Skowronska-Gardas A, Perek-Polnik M, Perek D, Olasek P (2014) Second brain tumors following central nervous system radiotherapy in childhood. *The British journal of radiology*:20140211. doi:10.1259/bjr.20140211
45. Chowdhury R, Yeoh KK, Tian YM, Hillringhaus L, Bagg EA, Rose NR, Leung IK, Li XS, Woon EC, Yang M, McDonough MA, King ON, Clifton IJ, Klose RJ, Claridge TD, Ratcliffe PJ, Schofield CJ, Kawamura A (2011) The oncometabolite 2-hydroxyglutarate inhibits histone lysine demethylases. *EMBO reports* 12:463-469. doi:10.1038/embor.2011.43
46. Cin H, Meyer C, Herr R, Janzarik WG, Lambert S, Jones DT, Jacob K, Benner A, Witt H, Remke M, Bender S, Falkenstein F, Van Anh TN, Olbrich H, von Deimling A, Pekrun A, Kulozik AE, Gnekow A, Scheurlen W, Witt O, Omran H, Jabado N, Collins VP, Brummer T, Marschalek R, Lichter P, Korshunov A, Pfister SM (2011) Oncogenic FAM131B-BRAF fusion resulting from 7q34 deletion comprises an alternative mechanism of MAPK pathway activation in

- pilocytic astrocytoma. *Acta neuropathologica* 121:763-774. doi:10.1007/s00401-011-0817-z
47. Cloughesy TF, Mischel PS (2011) New strategies in the molecular targeting of glioblastoma: how do you hit a moving target? *Clinical cancer research : an official journal of the American Association for Cancer Research* 17:6-11. doi:10.1158/1078-0432.CCR-09-2268
 48. Comprehensive genomic characterization defines human glioblastoma genes and core pathways (2008). *Nature* 455:1061-1068. doi:10.1038/nature07385
 49. Cong L, Ran FA, Cox D, Lin S, Barretto R, Habib N, Hsu PD, Wu X, Jiang W, Marraffini LA, Zhang F (2013) Multiplex genome engineering using CRISPR/Cas systems. *Science* 339:819-823. doi:10.1126/science.1231143
 50. Crasta K, Ganem NJ, Dagher R, Lantermann AB, Ivanova EV, Pan Y, Nezi L, Protopopov A, Chowdhury D, Pellman D (2012) DNA breaks and chromosome pulverization from errors in mitosis. *Nature* 482:53-58. doi:10.1038/nature10802
 51. Cui Y, Borysova MK, Johnson JO, Guadagno TM (2010) Oncogenic B-Raf(V600E) induces spindle abnormalities, supernumerary centrosomes, and aneuploidy in human melanocytic cells. *Cancer research* 70:675-684. doi:10.1158/0008-5472.CAN-09-1491
 52. Cui Y, Guadagno TM (2008) B-Raf(V600E) signaling deregulates the mitotic spindle checkpoint through stabilizing Mps1 levels in melanoma cells. *Oncogene* 27:3122-3133. doi:10.1038/sj.onc.1210972
 53. Cuny GD, Yu PB, Laha JK, Xing X, Liu JF, Lai CS, Deng DY, Sachidanandan C, Bloch KD, Peterson RT (2008) Structure-activity relationship study of bone morphogenetic protein (BMP) signaling inhibitors. *Bioorganic & medicinal chemistry letters* 18:4388-4392. doi:10.1016/j.bmcl.2008.06.052
 54. Dahiya S, Yu J, Kaul A, Leonard JR, Gutmann DH (2012) Novel BRAF Alteration in a Sporadic Pilocytic Astrocytoma. *Case reports in medicine* 2012:418672. doi:10.1155/2012/418672
 55. Dalgliesh GL, Furge K, Greenman C, Chen L, Bignell G, Butler A, Davies H, Edkins S, Hardy C, Latimer C, Teague J, Andrews J, Barthorpe S, Beare D, Buck G, Campbell PJ, Forbes S, Jia M, Jones D, Knott H, Kok CY, Lau KW, Leroy C, Lin ML, McBride DJ, Maddison M, Maguire S, McLay K, Menzies A, Mironenko T, Mulderrig L, Mudie L, O'Meara S, Pleasance E, Rajasingham A, Shepherd R, Smith R, Stebbings L, Stephens P, Tang G, Tarpey PS, Turrell K, Dykema KJ, Khoo SK, Petillo D, Wondergem B, Anema J, Kahnoski RJ, Teh BT, Stratton MR, Futreal PA (2010) Systematic sequencing of renal carcinoma reveals inactivation of histone modifying genes. *Nature* 463:360-363. doi:10.1038/nature08672
 56. Dang L, White DW, Gross S, Bennett BD, Bittinger MA, Driggers EM, Fantin VR, Jang HG, Jin S, Keenan MC, Marks KM, Prins RM, Ward PS, Yen KE, Liao LM, Rabinowitz JD, Cantley LC, Thompson CB, Vander Heiden MG, Su SM (2009) Cancer-associated IDH1 mutations produce 2-hydroxyglutarate. *Nature* 462:739-744. doi:10.1038/nature08617
 57. Davies H, Bignell GR, Cox C, Stephens P, Edkins S, Clegg S, Teague J, Woffendin H, Garnett MJ, Bottomley W, Davis N, Dicks E, Ewing R, Floyd Y, Gray K, Hall S, Hawes R, Hughes J, Kosmidou V, Menzies A, Mould C, Parker A, Stevens C,

- Watt S, Hooper S, Wilson R, Jayatilake H, Gusterson BA, Cooper C, Shipley J, Hargrave D, Pritchard-Jones K, Maitland N, Chenevix-Trench G, Riggins GJ, Bigner DD, Palmieri G, Cossu A, Flanagan A, Nicholson A, Ho JW, Leung SY, Yuen ST, Weber BL, Seigler HF, Darrow TL, Paterson H, Marais R, Marshall CJ, Wooster R, Stratton MR, Futreal PA (2002) Mutations of the BRAF gene in human cancer. *Nature* 417:949-954. doi:10.1038/nature00766
58. Dawson MA, Kouzarides T (2012) Cancer epigenetics: from mechanism to therapy. *Cell* 150:12-27. doi:10.1016/j.cell.2012.06.013
59. Dawson MA, Kouzarides T, Huntly BJ (2012) Targeting epigenetic readers in cancer. *The New England journal of medicine* 367:647-657. doi:10.1056/NEJMra1112635
60. Dhayalan A, Tamas R, Bock I, Tattermusch A, Dimitrova E, Kudithipudi S, Ragozin S, Jeltsch A (2011) The ATRX-ADD domain binds to H3 tail peptides and reads the combined methylation state of K4 and K9. *Human molecular genetics* 20:2195-2203. doi:10.1093/hmg/ddr107
61. Dolecek TA, Propp JM, Stroup NE, Kruchko C (2012) CBTRUS statistical report: primary brain and central nervous system tumors diagnosed in the United States in 2005-2009. *Neuro-oncology* 14 Suppl 5:v1-49. doi:10.1093/neuonc/nos218
62. Dunham MA, Neumann AA, Fasching CL, Reddel RR (2000) Telomere maintenance by recombination in human cells. *Nature genetics* 26:447-450. doi:10.1038/82586
63. Eckert A, Kloor M, Giersch A, Ahmadi R, Herold-Mende C, Hampl JA, Heppner FL, Zoubaa S, Holinski-Feder E, Pietsch T, Wiestler OD, von Knebel Doeberitz M, Roth W, Gebert J (2007) Microsatellite instability in pediatric and adult high-grade gliomas. *Brain Pathol* 17:146-150. doi:10.1111/j.1750-3639.2007.00049.x
64. Edmunds JW, Mahadevan LC, Clayton AL (2008) Dynamic histone H3 methylation during gene induction: HYPB/Setd2 mediates all H3K36 trimethylation. *The EMBO journal* 27:406-420. doi:10.1038/sj.emboj.7601967
65. Eisenhardt AE, Olbrich H, Roring M, Janzarik W, Anh TN, Cin H, Remke M, Witt H, Korshunov A, Pfister SM, Omran H, Brummer T (2011) Functional characterization of a BRAF insertion mutant associated with pilocytic astrocytoma. *International journal of cancer Journal international du cancer* 129:2297-2303. doi:10.1002/ijc.25893
66. Faggioli F, Vijg J, Montagna C (2011) Chromosomal aneuploidy in the aging brain. *Mechanisms of ageing and development* 132:429-436. doi:10.1016/j.mad.2011.04.008
67. Faggioli F, Wang T, Vijg J, Montagna C (2012) Chromosome-specific accumulation of aneuploidy in the aging mouse brain. *Human molecular genetics* 21:5246-5253. doi:10.1093/hmg/ddr375
68. Faury D, Nantel A, Dunn SE, Guiot MC, Haque T, Hauser P, Garami M, Bognar L, Hanzely Z, Liberski PP, Lopez-Aguilar E, Valera ET, Tone LG, Carret AS, Del Maestro RF, Gleave M, Montes JL, Pietsch T, Albrecht S, Jabado N (2007) Molecular profiling identifies prognostic subgroups of pediatric glioblastoma and shows increased YB-1 expression in tumors. *Journal of clinical oncology : official journal of the American Society of Clinical Oncology* 25:1196-1208. doi:10.1200/JCO.2006.07.8626

69. Firestein R, Bass AJ, Kim SY, Dunn IF, Silver SJ, Guney I, Freed E, Ligon AH, Vena N, Ogino S, Chheda MG, Tamayo P, Finn S, Shrestha Y, Boehm JS, Jain S, Bojarski E, Mermel C, Barretina J, Chan JA, Baselga J, Tabernero J, Root DE, Fuchs CS, Loda M, Shivdasani RA, Meyerson M, Hahn WC (2008) CDK8 is a colorectal cancer oncogene that regulates beta-catenin activity. *Nature* 455:547-551. doi:10.1038/nature07179
70. Fontebasso AM, Gayden T, Nikbakht H, Neirinck M, Papillon-Cavanagh S, Majewski J, Jabado N (2014) Epigenetic dysregulation: a novel pathway of oncogenesis in pediatric brain tumors. *Acta neuropathologica*. doi:10.1007/s00401-014-1325-8
71. Fontebasso AM, Papillon-Cavanagh S, Schwartzentruber J, Nikbakht H, Gerges N, Fiset PO, Bechet D, Faury D, De Jay N, Ramkissoon LA, Corcoran A, Jones DT, Sturm D, Johann P, Tomita T, Goldman S, Nagib M, Bendel A, Goumnerova L, Bowers DC, Leonard JR, Rubin JB, Alden T, Browd S, Geyer JR, Leary S, Jallo G, Cohen K, Gupta N, Prados MD, Carret AS, Ellezam B, Crevier L, Klekner A, Bogner L, Hauser P, Garami M, Mysers J, Dong Z, Siegel PM, Malkin H, Ligon AH, Albrecht S, Pfister SM, Ligon KL, Majewski J, Jabado N, Kieran MW (2014) Recurrent somatic mutations in ACVR1 in pediatric midline high-grade astrocytoma. *Nature genetics* 46:462-466. doi:10.1038/ng.2950
72. Fontebasso AM, Schwartzentruber J, Khuong-Quang DA, Liu XY, Sturm D, Korshunov A, Jones DT, Witt H, Kool M, Albrecht S, Fleming A, Hadjadj D, Busche S, Lepage P, Montpetit A, Staffa A, Gerges N, Zakrzewska M, Zakrzewski K, Liberski PP, Hauser P, Garami M, Klekner A, Bogner L, Zadeh G, Faury D, Pfister SM, Jabado N, Majewski J (2013) Mutations in SETD2 and genes affecting histone H3K36 methylation target hemispheric high-grade gliomas. *Acta neuropathologica* 125:659-669. doi:10.1007/s00401-013-1095-8
73. Forshew T, Tatevossian RG, Lawson AR, Ma J, Neale G, Ogunkolade BW, Jones TA, Aarum J, Dalton J, Bailey S, Chaplin T, Carter RL, Gajjar A, Broniscer A, Young BD, Ellison DW, Sheer D (2009) Activation of the ERK/MAPK pathway: a signature genetic defect in posterior fossa pilocytic astrocytomas. *The Journal of pathology* 218:172-181. doi:10.1002/path.2558
74. Frange P, Alapetite C, Gaboriaud G, Bours D, Zucker JM, Zerah M, Brisse H, Chevignard M, Mosseri V, Bouffet E, Doz F (2009) From childhood to adulthood: long-term outcome of medulloblastoma patients. The Institut Curie experience (1980-2000). *Journal of neuro-oncology* 95:271-279. doi:10.1007/s11060-009-9927-z
75. Frattini V, Trifonov V, Chan JM, Castano A, Lia M, Abate F, Keir ST, Ji AX, Zoppoli P, Niola F, Danussi C, Dolgalev I, Porrati P, Pellegatta S, Heguy A, Gupta G, Pisapia DJ, Canoll P, Bruce JN, McLendon RE, Yan H, Aldape K, Finocchiaro G, Mikkelsen T, Prive GG, Bigner DD, Lasorella A, Rabadan R, Iavarone A (2013) The integrated landscape of driver genomic alterations in glioblastoma. *Nature genetics* 45:1141-1149. doi:10.1038/ng.2734
76. Freeman CR, Perilongo G (1999) Chemotherapy for brain stem gliomas. *Child's nervous system : ChNS : official journal of the International Society for Pediatric Neurosurgery* 15:545-553

77. Friedman DL, Whitton J, Leisenring W, Mertens AC, Hammond S, Stovall M, Donaldson SS, Meadows AT, Robison LL, Neglia JP (2010) Subsequent neoplasms in 5-year survivors of childhood cancer: the Childhood Cancer Survivor Study. *Journal of the National Cancer Institute* 102:1083-1095. doi:10.1093/jnci/djq238
78. Fryssira H, Leventopoulos G, Psoni S, Kitsiou-Tzeli S, Stavrianeas N, Kanavakis E (2008) Tumor development in three patients with Noonan syndrome. *European journal of pediatrics* 167:1025-1031. doi:10.1007/s00431-007-0636-3
79. Fukuda T, Kanomata K, Nojima J, Kokabu S, Akita M, Ikebuchi K, Jimi E, Komori T, Maruki Y, Matsuoka M, Miyazono K, Nakayama K, Nanba A, Tomoda H, Okazaki Y, Ohtake A, Oda H, Owan I, Yoda T, Haga N, Furuya H, Katagiri T (2008) A unique mutation of ALK2, G356D, found in a patient with fibrodysplasia ossificans progressiva is a moderately activated BMP type I receptor. *Biochemical and biophysical research communications* 377:905-909. doi:10.1016/j.bbrc.2008.10.093
80. Fukuda T, Scott G, Komatsu Y, Araya R, Kawano M, Ray MK, Yamada M, Mishina Y (2006) Generation of a mouse with conditionally activated signaling through the BMP receptor, ALK2. *Genesis* 44:159-167. doi:10.1002/dvg.20201
81. Geisbrecht BV, Gould SJ (1999) The human PICD gene encodes a cytoplasmic and peroxisomal NADP(+)-dependent isocitrate dehydrogenase. *The Journal of biological chemistry* 274:30527-30533
82. Gerges N, Fontebasso AM, Albrecht S, Faury D, Jabado N (2013) Pediatric high-grade astrocytomas: a distinct neuro-oncological paradigm. *Genome medicine* 5:66. doi:10.1186/gm470
83. Gerlinger M, Rowan AJ, Horswell S, Larkin J, Endesfelder D, Gronroos E, Martinez P, Matthews N, Stewart A, Tarpey P, Varela I, Phillimore B, Begum S, McDonald NQ, Butler A, Jones D, Raine K, Latimer C, Santos CR, Nohadani M, Eklund AC, Spencer-Dene B, Clark G, Pickering L, Stamp G, Gore M, Szallasi Z, Downward J, Futreal PA, Swanton C (2012) Intratumor heterogeneity and branched evolution revealed by multiregion sequencing. *The New England journal of medicine* 366:883-892. doi:10.1056/NEJMoa1113205
84. Gessi M, Gielen GH, Hammes J, Dorner E, Muhlen AZ, Waha A, Pietsch T (2013) H3.3 G34R mutations in pediatric primitive neuroectodermal tumors of central nervous system (CNS-PNET) and pediatric glioblastomas: possible diagnostic and therapeutic implications? *Journal of neuro-oncology* 112:67-72. doi:10.1007/s11060-012-1040-z
85. Goldberg AD, Banaszynski LA, Noh KM, Lewis PW, Elsaesser SJ, Stadler S, Dewell S, Law M, Guo X, Li X, Wen D, Chappier A, DeKelver RC, Miller JC, Lee YL, Boydston EA, Holmes MC, Gregory PD, Grelly JM, Rafii S, Yang C, Scambler PJ, Garrick D, Gibbons RJ, Higgs DR, Cristea IM, Urnov FD, Zheng D, Allis CD (2010) Distinct factors control histone variant H3.3 localization at specific genomic regions. *Cell* 140:678-691. doi:10.1016/j.cell.2010.01.003
86. Goldgar DE, Green P, Parry DM, Mulvihill JJ (1989) Multipoint linkage analysis in neurofibromatosis type I: an international collaboration. *American journal of human genetics* 44:6-12

87. Gomes WA, Mehler MF, Kessler JA (2003) Transgenic overexpression of BMP4 increases astroglial and decreases oligodendroglial lineage commitment. *Developmental biology* 255:164-177
88. Gordon DJ, Resio B, Pellman D (2012) Causes and consequences of aneuploidy in cancer. *Nature reviews Genetics* 13:189-203. doi:10.1038/nrg3123
89. Greider CW, Blackburn EH (1989) A telomeric sequence in the RNA of Tetrahymena telomerase required for telomere repeat synthesis. *Nature* 337:331-337. doi:10.1038/337331a0
90. Grondin RT, Scott RM, Smith ER (2009) Pediatric brain tumors. *Advances in pediatrics* 56:249-269. doi:10.1016/j.yapd.2009.08.006
91. Gronych J, Korshunov A, Bageritz J, Milde T, Jugold M, Hambardzumyan D, Remke M, Hartmann C, Witt H, Jones DT, Witt O, Heiland S, Bendszus M, Holland EC, Pfister S, Lichter P (2011) An activated mutant BRAF kinase domain is sufficient to induce pilocytic astrocytoma in mice. *The Journal of clinical investigation* 121:1344-1348. doi:10.1172/JCI44656
92. Gutmann DH, McLellan MD, Hussain I, Wallis JW, Fulton LL, Fulton RS, Magrini V, Demeter R, Wylie T, Kandoth C, Leonard JR, Guha A, Miller CA, Ding L, Mardis ER (2013) Somatic neurofibromatosis type 1 (NF1) inactivation characterizes NF1-associated pilocytic astrocytoma. *Genome research* 23:431-439. doi:10.1101/gr.142604.112
93. Gutmann DH, Wood DL, Collins FS (1991) Identification of the neurofibromatosis type 1 gene product. *Proceedings of the National Academy of Sciences of the United States of America* 88:9658-9662
94. Hakin-Smith V, Jellinek DA, Levy D, Carroll T, Teo M, Timperley WR, McKay MJ, Reddel RR, Royds JA (2003) Alternative lengthening of telomeres and survival in patients with glioblastoma multiforme. *Lancet* 361:836-838
95. Hanahan D, Weinberg RA (2000) The hallmarks of cancer. *Cell* 100:57-70
96. Hanahan D, Weinberg RA (2011) Hallmarks of cancer: the next generation. *Cell* 144:646-674. doi:10.1016/j.cell.2011.02.013
97. Hanks S, Coleman K, Reid S, Plaja A, Firth H, Fitzpatrick D, Kidd A, Mehes K, Nash R, Robin N, Shannon N, Tolmie J, Swansbury J, Irrthum A, Douglas J, Rahman N (2004) Constitutional aneuploidy and cancer predisposition caused by biallelic mutations in BUB1B. *Nature genetics* 36:1159-1161. doi:10.1038/ng1449
98. Haque T, Faury D, Albrecht S, Lopez-Aguilar E, Hauser P, Garami M, Hanzely Z, Bogner L, Del Maestro RF, Atkinson J, Nantel A, Jabado N (2007) Gene expression profiling from formalin-fixed paraffin-embedded tumors of pediatric glioblastoma. *Clinical cancer research : an official journal of the American Association for Cancer Research* 13:6284-6292. doi:10.1158/1078-0432.CCR-07-0525
99. Harley CB, Futcher AB, Greider CW (1990) Telomeres shorten during ageing of human fibroblasts. *Nature* 345:458-460. doi:10.1038/345458a0
100. Hartmann C, Bartels G, Gehlhaar C, Holtkamp N, von Deimling A (2005) PIK3CA mutations in glioblastoma multiforme. *Acta neuropathologica* 109:639-642. doi:10.1007/s00401-005-1000-1
101. Hasselblatt M, Riesmeier B, Lechtape B, Brentrup A, Stummer W, Albert FK, Sepehrnia A, Ebel H, Gerss J, Paulus W (2011) BRAF-KIAA1549 fusion

- transcripts are less frequent in pilocytic astrocytomas diagnosed in adults. *Neuropathology and applied neurobiology* 37:803-806. doi:10.1111/j.1365-2990.2011.01193.x
102. Heaphy CM, de Wilde RF, Jiao Y, Klein AP, Edil BH, Shi C, Bettegowda C, Rodriguez FJ, Eberhart CG, Hebbar S, Offerhaus GJ, McLendon R, Rasheed BA, He Y, Yan H, Bigner DD, Oba-Shinjo SM, Marie SK, Riggins GJ, Kinzler KW, Vogelstein B, Hruban RH, Maitra A, Papadopoulos N, Meeker AK (2011) Altered telomeres in tumors with ATRX and DAXX mutations. *Science* 333:425. doi:10.1126/science.1207313
 103. Hegarty SV, O'Keeffe GW, Sullivan AM (2013) BMP-Smad 1/5/8 signalling in the development of the nervous system. *Progress in neurobiology* 109:28-41. doi:10.1016/j.pneurobio.2013.07.002
 104. Hegi ME, Diserens AC, Gorlia T, Hamou MF, de Tribolet N, Weller M, Kros JM, Hainfellner JA, Mason W, Mariani L, Bromberg JE, Hau P, Mirimanoff RO, Cairncross JG, Janzer RC, Stupp R (2005) MGMT gene silencing and benefit from temozolomide in glioblastoma. *The New England journal of medicine* 352:997-1003. doi:10.1056/NEJMoa043331
 105. Horn S, Figl A, Rachakonda PS, Fischer C, Sucker A, Gast A, Kadel S, Moll I, Nagore E, Hemminki K, Schadendorf D, Kumar R (2013) TERT promoter mutations in familial and sporadic melanoma. *Science* 339:959-961. doi:10.1126/science.1230062
 106. Huang FW, Hodis E, Xu MJ, Kryukov GV, Chin L, Garraway LA (2013) Highly recurrent TERT promoter mutations in human melanoma. *Science* 339:957-959. doi:10.1126/science.1229259
 107. Hudson TJ, Anderson W, Artez A, Barker AD, Bell C, Bernabe RR, Bhan MK, Calvo F, Eerola I, Gerhard DS, Guttmacher A, Guyer M, Hemsley FM, Jennings JL, Kerr D, Klatt P, Kolar P, Kusada J, Lane DP, Laplace F, Youyong L, Nettekoven G, Ozenberger B, Peterson J, Rao TS, Rémacle J, Schafer AJ, Shibata T, Stratton MR, Vockley JG, Watanabe K, Yang H, Yuen MM, Knoppers BM, Bobrow M, Cambon-Thomsen A, Dressler LG, Dyke SO, Joly Y, Kato K, Kennedy KL, Nicolas P, Parker MJ, Rial-Sebbag E, Romeo-Casabona CM, Shaw KM, Wallace S, Wiesner GL, Zeps N, Lichter P, Biankin AV, Chabannon C, Chin L, Clement B, de Alava E, Degos F, Ferguson ML, Geary P, Hayes DN, Hudson TJ, Johns AL, Kasprzyk A, Nakagawa H, Penny R, Piris MA, Sarin R, Scarpa A, Shibata T, van de Vijver M, Futreal PA, Aburatani H, Bayes M, Botwell DD, Campbell PJ, Estivill X, Gerhard DS, Grimmond SM, Gut I, Hirst M, Lopez-Otin C, Majumder P, Marra M, McPherson JD, Nakagawa H, Ning Z, Puente XS, Ruan Y, Shibata T, Stratton MR, Stunnenberg HG, Swerdlow H, Velculescu VE, Wilson RK, Xue HH, Yang L, Spellman PT, Bader GD, Boutros PC, Campbell PJ, Flicek P, Getz G, Guigo R, Guo G, Haussler D, Heath S, Hubbard TJ, Jiang T, Jones SM, Li Q, Lopez-Bigas N, Luo R, Muthuswamy L, Ouellette BF, Pearson JV, Puente XS, Quesada V, Raphael BJ, Sander C, Shibata T, Speed TP, Stein LD, Stuart JM, Teague JW, Totoki Y, Tsunoda T, Valencia A, Wheeler DA, Wu H, Zhao S, Zhou G, Stein LD, Guigo R, Hubbard TJ, Joly Y, Jones SM, Kasprzyk A, Lathrop M, Lopez-Bigas N, Ouellette BF, Spellman PT, Teague JW, Thomas G, Valencia A, Yoshida T, Kennedy KL, Axton M, Dyke SO, Futreal PA,

- Gerhard DS, Gunter C, Guyer M, Hudson TJ, McPherson JD, Miller LJ, Ozenberger B, Shaw KM, Kasprzyk A, Stein LD, Zhang J, Haider SA, Wang J, Yung CK, Cros A, Liang Y, Gnaneshan S, Guberman J, Hsu J, Bobrow M, Chalmers DR, Hasel KW, Joly Y, Kaan TS, Kennedy KL, Knoppers BM, Lowrance WW, Masui T, Nicolas P, Rial-Sebbag E, Rodriguez LL, Vergely C, Yoshida T, Grimmond SM, Biankin AV, Bowtell DD, Cloonan N, deFazio A, Eshleman JR, Etemadmoghadam D, Gardiner BB, Kench JG, Scarpa A, Sutherland RL, Tempero MA, Waddell NJ, Wilson PJ, McPherson JD, Gallinger S, Tsao MS, Shaw PA, Petersen GM, Mukhopadhyay D, Chin L, DePinho RA, Thayer S, Muthuswamy L, Shazand K, Beck T, Sam M, Timms L, Ballin V, Lu Y, Ji J, Zhang X, Chen F, Hu X, Zhou G, Yang Q, Tian G, Zhang L, Xing X, Li X, Zhu Z, Yu Y, Yu J, Yang H, Lathrop M, Tost J, Brennan P, Holcatova I, Zaridze D, Brazma A, Egevard L, Prokhortchouk E, Banks RE, Uhlen M, Cambon-Thomsen A, Viksna J, Ponten F, Skryabin K, Stratton MR, Futreal PA, Birney E, Borg A, Borresen-Dale AL, Caldas C, Foekens JA, Martin S, Reis-Filho JS, Richardson AL, Sotiriou C, Stunnenberg HG, Thoms G, van de Vijver M, van't Veer L, Calvo F, Birnbaum D, Blanche H, Boucher P, Boyault S, Chabannon C, Gut I, Masson-Jacquemier JD, Lathrop M, Pauporte I, Pivot X, Vincent-Salomon A, Tabone E, Theillet C, Thomas G, Tost J, Treilleux I, Calvo F, Bioulac-Sage P, Clement B, Decaens T, Degos F, Franco D, Gut I, Gut M, Heath S, Lathrop M, Samuel D, Thomas G, Zucman-Rossi J, Lichter P, Eils R, Brors B, Korbel JO, Korshunov A, Landgraf P, Lehrach H, Pfister S, Radlwimmer B, Reifemberger G, Taylor MD, von Kalle C, Majumder PP, Sarin R, Rao TS, Bhan MK, Scarpa A, Pederzoli P, Lawlor RA, Delledonne M, Bardelli A, Biankin AV, Grimmond SM, Gress T, Klimstra D, Zamboni G, Shibata T, Nakamura Y, Nakagawa H, Kusada J, Tsunoda T, Miyano S, Aburatani H, Kato K, Fujimoto A, Yoshida T, Campo E, Lopez-Otin C, Estivill X, Guigo R, de Sanjose S, Piris MA, Montserrat E, Gonzalez-Diaz M, Puente XS, Jares P, Valencia A, Himmelbauer H, Quesada V, Bea S, Stratton MR, Futreal PA, Campbell PJ, Vincent-Salomon A, Richardson AL, Reis-Filho JS, van de Vijver M, Thomas G, Masson-Jacquemier JD, Aparicio S, Borg A, Borresen-Dale AL, Caldas C, Foekens JA, Stunnenberg HG, van't Veer L, Easton DF, Spellman PT, Martin S, Barker AD, Chin L, Collins FS, Compton CC, Ferguson ML, Gerhard DS, Getz G, Gunter C, Guttmacher A, Guyer M, Hayes DN, Lander ES, Ozenberger B, Penny R, Peterson J, Sander C, Shaw KM, Speed TP, Spellman PT, Vockley JG, Wheeler DA, Wilson RK, Hudson TJ, Chin L, Knoppers BM, Lander ES, Lichter P, Stein LD, Stratton MR, Anderson W, Barker AD, Bell C, Bobrow M, Burke W, Collins FS, Compton CC, DePinho RA, Easton DF, Futreal PA, Gerhard DS, Green AR, Guyer M, Hamilton SR, Hubbard TJ, Kallioniemi OP, Kennedy KL, Ley TJ, Liu ET, Lu Y, Majumder P, Marra M, Ozenberger B, Peterson J, Schafer AJ, Spellman PT, Stunnenberg HG, Wainwright BJ, Wilson RK, Yang H (2010) International network of cancer genome projects. *Nature* 464:993-998. doi:10.1038/nature08987
108. Iwase S, Xiang B, Ghosh S, Ren T, Lewis PW, Cochrane JC, Allis CD, Picketts DJ, Patel DJ, Li H, Shi Y (2011) ATRX ADD domain links an atypical histone

- methylation recognition mechanism to human mental-retardation syndrome. *Nature structural & molecular biology* 18:769-776. doi:10.1038/nsmb.2062
109. Jacob K, Albrecht S, Sollier C, Faury D, Sader E, Montpetit A, Serre D, Hauser P, Garami M, Bognar L, Hanzely Z, Montes JL, Atkinson J, Farmer JP, Bouffet E, Hawkins C, Tabori U, Jabado N (2009) Duplication of 7q34 is specific to juvenile pilocytic astrocytomas and a hallmark of cerebellar and optic pathway tumours. *British journal of cancer* 101:722-733. doi:10.1038/sj.bjc.6605179
110. Jacob K, Quang-Khuong DA, Jones DT, Witt H, Lambert S, Albrecht S, Witt O, Vezina C, Shirinian M, Faury D, Garami M, Hauser P, Klekner A, Bognar L, Farmer JP, Montes JL, Atkinson J, Hawkins C, Korshunov A, Collins VP, Pfister SM, Tabori U, Jabado N (2011) Genetic aberrations leading to MAPK pathway activation mediate oncogene-induced senescence in sporadic pilocytic astrocytomas. *Clinical cancer research : an official journal of the American Association for Cancer Research* 17:4650-4660. doi:10.1158/1078-0432.CCR-11-0127
111. Jakacki RI, Burger PC, Zhou T, Holmes EJ, Kocak M, Onar A, Goldwein J, Mehta M, Packer RJ, Tarbell N, Fitz C, Vezina G, Hilden J, Pollack IF (2012) Outcome of children with metastatic medulloblastoma treated with carboplatin during craniospinal radiotherapy: a Children's Oncology Group Phase I/II study. *Journal of clinical oncology : official journal of the American Society of Clinical Oncology* 30:2648-2653. doi:10.1200/JCO.2011.40.2792
112. Je EM, Yoo NJ, Kim YJ, Kim MS, Lee SH (2013) Somatic mutation of H3F3A, a chromatin remodeling gene, is rare in acute leukemias and non-Hodgkin lymphoma. *European journal of haematology* 90:169-170. doi:10.1111/ejh.12039
113. Je EM, Yoo NJ, Lee SH (2014) Mutational analysis of H3F3A, a chromatin remodeling gene in common solid tumors. *APMIS : acta pathologica, microbiologica, et immunologica Scandinavica* 122:81-82. doi:10.1111/apm.12124
114. Jiao Y, Killela PJ, Reitman ZJ, Rasheed AB, Heaphy CM, de Wilde RF, Rodriguez FJ, Rosenberg S, Oba-Shinjo SM, Nagahashi Marie SK, Bettegowda C, Agrawal N, Lipp E, Pirozzi C, Lopez G, He Y, Friedman H, Friedman AH, Riggins GJ, Holdhoff M, Burger P, McLendon R, Bigner DD, Vogelstein B, Meeker AK, Kinzler KW, Papadopoulos N, Diaz LA, Yan H (2012) Frequent ATRX, CIC, FUBP1 and IDH1 mutations refine the classification of malignant gliomas. *Oncotarget* 3:709-722
115. Johnson BE, Mazor T, Hong C, Barnes M, Aihara K, McLean CY, Fouse SD, Yamamoto S, Ueda H, Tatsuno K, Asthana S, Jalbert LE, Nelson SJ, Bollen AW, Gustafson WC, Charron E, Weiss WA, Smirnov IV, Song JS, Olshen AB, Cha S, Zhao Y, Moore RA, Mungall AJ, Jones SJ, Hirst M, Marra MA, Saito N, Aburatani H, Mukasa A, Berger MS, Chang SM, Taylor BS, Costello JF (2014) Mutational analysis reveals the origin and therapy-driven evolution of recurrent glioma. *Science* 343:189-193. doi:10.1126/science.1239947
116. Johnson RA, Wright KD, Poppleton H, Mohankumar KM, Finkelstein D, Pounds SB, Rand V, Leary SE, White E, Eden C, Hogg T, Northcott P, Mack S, Neale G, Wang YD, Coyle B, Atkinson J, DeWire M, Kranenburg TA, Gillespie Y, Allen JC, Merchant T, Boop FA, Sanford RA, Gajjar A, Ellison DW, Taylor MD,

- Grundy RG, Gilbertson RJ (2010) Cross-species genomics matches driver mutations and cell compartments to model ependymoma. *Nature* 466:632-636. doi:10.1038/nature09173
117. Jones DT, Gronych J, Lichter P, Witt O, Pfister SM (2012) MAPK pathway activation in pilocytic astrocytoma. *Cellular and molecular life sciences : CMLS* 69:1799-1811. doi:10.1007/s00018-011-0898-9
118. Jones DT, Hutter B, Jager N, Korshunov A, Kool M, Warnatz HJ, Zichner T, Lambert SR, Ryzhova M, Quang DA, Fontebasso AM, Stutz AM, Hutter S, Zuckermann M, Sturm D, Gronych J, Lasitschka B, Schmidt S, Seker-Cin H, Witt H, Sultan M, Ralser M, Northcott PA, Hovestadt V, Bender S, Pfaff E, Stark S, Faury D, Schwartzentruber J, Majewski J, Weber UD, Zapatka M, Raeder B, Schlesner M, Worth CL, Bartholomae CC, von Kalle C, Imbusch CD, Radomski S, Lawrenz C, van Sluis P, Koster J, Volckmann R, Versteeg R, Lehrach H, Monoranu C, Winkler B, Unterberg A, Herold-Mende C, Milde T, Kulozik AE, Ebinger M, Schuhmann MU, Cho YJ, Pomeroy SL, von Deimling A, Witt O, Taylor MD, Wolf S, Karajannis MA, Eberhart CG, Scheurlen W, Hasselblatt M, Ligon KL, Kieran MW, Korbel JO, Yaspo ML, Brors B, Felsberg J, Reifenberger G, Collins VP, Jabado N, Eils R, Lichter P, Pfister SM (2013) Recurrent somatic alterations of FGFR1 and NTRK2 in pilocytic astrocytoma. *Nature genetics* 45:927-932. doi:10.1038/ng.2682
119. Jones DT, Ichimura K, Liu L, Pearson DM, Plant K, Collins VP (2006) Genomic analysis of pilocytic astrocytomas at 0.97 Mb resolution shows an increasing tendency toward chromosomal copy number change with age. *Journal of neuropathology and experimental neurology* 65:1049-1058. doi:10.1097/01.jnen.0000240465.33628.87
120. Jones DT, Jager N, Kool M, Zichner T, Hutter B, Sultan M, Cho YJ, Pugh TJ, Hovestadt V, Stutz AM, Rausch T, Warnatz HJ, Ryzhova M, Bender S, Sturm D, Pleier S, Cin H, Pfaff E, Sieber L, Wittmann A, Remke M, Witt H, Hutter S, Tzaridis T, Weischenfeldt J, Raeder B, Avci M, Amstislavskiy V, Zapatka M, Weber UD, Wang Q, Lasitschka B, Bartholomae CC, Schmidt M, von Kalle C, Ast V, Lawrenz C, Eils J, Kabbe R, Benes V, van Sluis P, Koster J, Volckmann R, Shih D, Betts MJ, Russell RB, Coco S, Tonini GP, Schuller U, Hans V, Graf N, Kim YJ, Monoranu C, Roggendorf W, Unterberg A, Herold-Mende C, Milde T, Kulozik AE, von Deimling A, Witt O, Maass E, Rössler J, Ebinger M, Schuhmann MU, Fruhwald MC, Hasselblatt M, Jabado N, Rutkowski S, von Bueren AO, Williamson D, Clifford SC, McCabe MG, Collins VP, Wolf S, Wiemann S, Lehrach H, Brors B, Scheurlen W, Felsberg J, Reifenberger G, Northcott PA, Taylor MD, Meyerson M, Pomeroy SL, Yaspo ML, Korbel JO, Korshunov A, Eils R, Pfister SM, Lichter P (2012) Dissecting the genomic complexity underlying medulloblastoma. *Nature* 488:100-105. doi:10.1038/nature11284
121. Jones DT, Kocialkowski S, Liu L, Pearson DM, Backlund LM, Ichimura K, Collins VP (2008) Tandem duplication producing a novel oncogenic BRAF fusion gene defines the majority of pilocytic astrocytomas. *Cancer research* 68:8673-8677. doi:10.1158/0008-5472.CAN-08-2097

122. Jones DT, Kocialkowski S, Liu L, Pearson DM, Ichimura K, Collins VP (2009) Oncogenic RAF1 rearrangement and a novel BRAF mutation as alternatives to KIAA1549:BRAF fusion in activating the MAPK pathway in pilocytic astrocytoma. *Oncogene* 28:2119-2123. doi:10.1038/onc.2009.73
123. Joseph CG, Hwang H, Jiao Y, Wood LD, Kinde I, Wu J, Mandahl N, Luo J, Hruban RH, Diaz LA, Jr., He TC, Vogelstein B, Kinzler KW, Mertens F, Papadopoulos N (2014) Exomic analysis of myxoid liposarcomas, synovial sarcomas, and osteosarcomas. *Genes, chromosomes & cancer* 53:15-24. doi:10.1002/gcc.22114
124. Kajii T, Ikeuchi T, Yang ZQ, Nakamura Y, Tsuji Y, Yokomori K, Kawamura M, Fukuda S, Horita S, Asamoto A (2001) Cancer-prone syndrome of mosaic variegated aneuploidy and total premature chromatid separation: report of five infants. *American journal of medical genetics* 104:57-64
125. Kamata T, Hussain J, Giblett S, Hayward R, Marais R, Pritchard C (2010) BRAF inactivation drives aneuploidy by deregulating CRAF. *Cancer research* 70:8475-8486. doi:10.1158/0008-5472.CAN-10-0603
126. Kan L, Hu M, Gomes WA, Kessler JA (2004) Transgenic mice overexpressing BMP4 develop a fibrodysplasia ossificans progressiva (FOP)-like phenotype. *The American journal of pathology* 165:1107-1115. doi:10.1016/S0002-9440(10)63372-X
127. Kan L, Kitterman JA, Procissi D, Chakkalakal S, Peng CY, McGuire TL, Goldsby RE, Pignolo RJ, Shore EM, Kaplan FS, Kessler JA (2012) CNS demyelination in fibrodysplasia ossificans progressiva. *Journal of neurology* 259:2644-2655. doi:10.1007/s00415-012-6563-x
128. Kang HJ, Feng Z, Sun Y, Atwal G, Murphy ME, Rebbeck TR, Rosenwaks Z, Levine AJ, Hu W (2009) Single-nucleotide polymorphisms in the p53 pathway regulate fertility in humans. *Proceedings of the National Academy of Sciences of the United States of America* 106:9761-9766. doi:10.1073/pnas.0904280106
129. Kang HJ, Kawasawa YI, Cheng F, Zhu Y, Xu X, Li M, Sousa AM, Pletikos M, Meyer KA, Sedmak G, Guannel T, Shin Y, Johnson MB, Krsnik Z, Mayer S, Fertuzinhos S, Umlauf S, Lisgo SN, Vortmeyer A, Weinberger DR, Mane S, Hyde TM, Huttner A, Reimers M, Kleinman JE, Sestan N (2011) Spatio-temporal transcriptome of the human brain. *Nature* 478:483-489. doi:10.1038/nature10523
130. Kang YH, Park JE, Yu LR, Soung NK, Yun SM, Bang JK, Seong YS, Yu H, Garfield S, Veenstra TD, Lee KS (2006) Self-regulated Plk1 recruitment to kinetochores by the Plk1-PBIP1 interaction is critical for proper chromosome segregation. *Molecular cell* 24:409-422. doi:10.1016/j.molcel.2006.10.016
131. Kannan K, Inagaki A, Silber J, Gorovets D, Zhang J, Kasthuber ER, Heguy A, Petrini JH, Chan TA, Huse JT (2012) Whole-exome sequencing identifies ATRX mutation as a key molecular determinant in lower-grade glioma. *Oncotarget* 3:1194-1203
132. Kaul A, Chen YH, Emmett RJ, Dahiya S, Gutmann DH (2012) Pediatric glioma-associated KIAA1549:BRAF expression regulates neuroglial cell growth in a cell type-specific and mTOR-dependent manner. *Genes & development* 26:2561-2566. doi:10.1101/gad.200907.112

133. Kaul A, Chen YH, Emmett RJ, Gianino SM, Gutmann DH (2013) Conditional KIAA1549:BRAF mice reveal brain region- and cell type-specific effects. *Genesis* 51:708-716. doi:10.1002/dvg.22415
134. Kaushal D, Contos JJ, Treuner K, Yang AH, Kingsbury MA, Rehen SK, McConnell MJ, Okabe M, Barlow C, Chun J (2003) Alteration of gene expression by chromosome loss in the postnatal mouse brain. *The Journal of neuroscience : the official journal of the Society for Neuroscience* 23:5599-5606
135. Kent WJ, Sugnet CW, Furey TS, Roskin KM, Pringle TH, Zahler AM, Haussler D (2002) The human genome browser at UCSC. *Genome research* 12:996-1006. doi:10.1101/gr.229102. Article published online before print in May 2002
136. Khuong-Quang DA, Buczkowicz P, Rakopoulos P, Liu XY, Fontebasso AM, Bouffet E, Bartels U, Albrecht S, Schwartzenuber J, Letourneau L, Bourgey M, Bourque G, Montpetit A, Bourret G, Lepage P, Fleming A, Lichter P, Kool M, von Deimling A, Sturm D, Korshunov A, Faury D, Jones DT, Majewski J, Pfister SM, Jabado N, Hawkins C (2012) K27M mutation in histone H3.3 defines clinically and biologically distinct subgroups of pediatric diffuse intrinsic pontine gliomas. *Acta neuropathologica* 124:439-447. doi:10.1007/s00401-012-0998-0
137. Khuong-Quang DA, Gerges N, Jabado N (2012) [Mutations in histone H3.3 and chromatin remodeling genes drive pediatric and young adult glioblastomas]. *Medecine sciences : M/S* 28:809-812. doi:10.1051/medsci/20122810004
138. Kieran MW, Walker D, Frappaz D, Prados M (2010) Brain tumors: from childhood through adolescence into adulthood. *Journal of clinical oncology : official journal of the American Society of Clinical Oncology* 28:4783-4789. doi:10.1200/JCO.2010.28.3481
139. Killela PJ, Pirozzi CJ, Healy P, Reitman ZJ, Lipp E, Rasheed BA, Yang R, Diplas BH, Wang Z, Greer PK, Zhu H, Wang CY, Carpenter AB, Friedman H, Friedman AH, Keir ST, He J, He Y, McLendon RE, Herndon JE, 2nd, Yan H, Bigner DD (2014) Mutations in IDH1, IDH2, and in the TERT promoter define clinically distinct subgroups of adult malignant gliomas. *Oncotarget* 5:1515-1525
140. Killela PJ, Reitman ZJ, Jiao Y, Bettegowda C, Agrawal N, Diaz LA, Jr., Friedman AH, Friedman H, Gallia GL, Giovanella BC, Grollman AP, He TC, He Y, Hruban RH, Jallo GI, Mandahl N, Meeker AK, Mertens F, Netto GJ, Rasheed BA, Riggins GJ, Rosenquist TA, Schiffman M, Shih Ie M, Theodorescu D, Torbenson MS, Velculescu VE, Wang TL, Wentzensen N, Wood LD, Zhang M, McLendon RE, Bigner DD, Kinzler KW, Vogelstein B, Papadopoulos N, Yan H (2013) TERT promoter mutations occur frequently in gliomas and a subset of tumors derived from cells with low rates of self-renewal. *Proceedings of the National Academy of Sciences of the United States of America* 110:6021-6026. doi:10.1073/pnas.1303607110
141. Kiltie AE, Lashford LS, Gattamaneni HR (1997) Survival and late effects in medulloblastoma patients treated with craniospinal irradiation under three years old. *Medical and pediatric oncology* 28:348-354
142. Kim NW, Piatyszek MA, Prowse KR, Harley CB, West MD, Ho PL, Coviello GM, Wright WE, Weinrich SL, Shay JW (1994) Specific association of human telomerase activity with immortal cells and cancer. *Science* 266:2011-2015

143. Kingsbury MA, Yung YC, Peterson SE, Westra JW, Chun J (2006) Aneuploidy in the normal and diseased brain. *Cellular and molecular life sciences : CMLS* 63:2626-2641. doi:10.1007/s00018-006-6169-5
144. Kishigami S, Yoshikawa S, Castranio T, Okazaki K, Furuta Y, Mishina Y (2004) BMP signaling through ACVRI is required for left-right patterning in the early mouse embryo. *Developmental biology* 276:185-193. doi:10.1016/j.ydbio.2004.08.042
145. Kitterman JA, Strober JB, Kan L, Roche DM, Cali A, Peeper J, Snow J, Delai PL, Morhart R, Pignolo RJ, Shore EM, Kaplan FS (2012) Neurological symptoms in individuals with fibrodysplasia ossificans progressiva. *Journal of neurology* 259:2636-2643. doi:10.1007/s00415-012-6562-y
146. Kleihues P, Louis DN, Scheithauer BW, Rorke LB, Reifenberger G, Burger PC, Cavenee WK (2002) The WHO classification of tumors of the nervous system. *Journal of neuropathology and experimental neurology* 61:215-225; discussion 226-219
147. Kleinman CL, Gerges N, Papillon-Cavanagh S, Sin-Chan P, Pramatarova A, Quang DA, Adoue V, Busche S, Caron M, Djambazian H, Bemmo A, Fontebasso AM, Spence T, Schwartzenruber J, Albrecht S, Hauser P, Garami M, Klekner A, Bogner L, Montes JL, Staffa A, Montpetit A, Berube P, Zakrzewska M, Zakrzewski K, Liberski PP, Dong Z, Siegel PM, Duchaine T, Perotti C, Fleming A, Faury D, Remke M, Gallo M, Dirks P, Taylor MD, Sladek R, Pastinen T, Chan JA, Huang A, Majewski J, Jabado N (2014) Fusion of TTYH1 with the C19MC microRNA cluster drives expression of a brain-specific DNMT3B isoform in the embryonal brain tumor ETMR. *Nature genetics* 46:39-44. doi:10.1038/ng.2849
148. Koelsche C, Sahm F, Capper D, Reuss D, Sturm D, Jones DT, Kool M, Northcott PA, Wiestler B, Bohmer K, Meyer J, Mawrin C, Hartmann C, Mittelbronn M, Platten M, Brokinkel B, Seiz M, Herold-Mende C, Unterberg A, Schittenhelm J, Weller M, Pfister S, Wick W, Korshunov A, von Deimling A (2013) Distribution of TERT promoter mutations in pediatric and adult tumors of the nervous system. *Acta neuropathologica* 126:907-915. doi:10.1007/s00401-013-1195-5
149. Kolker S, Mayatepek E, Hoffmann GF (2002) White matter disease in cerebral organic acid disorders: clinical implications and suggested pathomechanisms. *Neuropediatrics* 33:225-231. doi:10.1055/s-2002-36741
150. Korbel JO, Campbell PJ (2013) Criteria for inference of chromothripsis in cancer genomes. *Cell* 152:1226-1236. doi:10.1016/j.cell.2013.02.023
151. Korchynskyi O, ten Dijke P (2002) Identification and functional characterization of distinct critically important bone morphogenetic protein-specific response elements in the Id1 promoter. *The Journal of biological chemistry* 277:4883-4891. doi:10.1074/jbc.M111023200
152. Kratz CP, Rapisuwon S, Reed H, Hasle H, Rosenberg PS (2011) Cancer in Noonan, Costello, cardiofaciocutaneous and LEOPARD syndromes. *American journal of medical genetics Part C, Seminars in medical genetics* 157C:83-89. doi:10.1002/ajmg.c.30300
153. Krause A, Hoffmann I (2010) Polo-like kinase 2-dependent phosphorylation of NPM/B23 on serine 4 triggers centriole duplication. *PloS one* 5:e9849. doi:10.1371/journal.pone.0009849

154. Lahti L, Peltopuro P, Piepponen TP, Partanen J (2012) Cell-autonomous FGF signaling regulates anteroposterior patterning and neuronal differentiation in the mesodiencephalic dopaminergic progenitor domain. *Development* 139:894-905. doi:10.1242/dev.071936
155. Lai A, Kharbanda S, Pope WB, Tran A, Solis OE, Peale F, Forrest WF, Pujara K, Carrillo JA, Pandita A, Ellingson BM, Bowers CW, Soriano RH, Schmidt NO, Mohan S, Yong WH, Seshagiri S, Modrusan Z, Jiang Z, Aldape KD, Mischel PS, Liao LM, Escovedo CJ, Chen W, Nghiemphu PL, James CD, Prados MD, Westphal M, Lamszus K, Cloughesy T, Phillips HS (2011) Evidence for sequenced molecular evolution of IDH1 mutant glioblastoma from a distinct cell of origin. *Journal of clinical oncology : official journal of the American Society of Clinical Oncology* 29:4482-4490. doi:10.1200/JCO.2010.33.8715
156. Lambert SR, Witt H, Hovestadt V, Zucknick M, Kool M, Pearson DM, Korshunov A, Ryzhova M, Ichimura K, Jabado N, Fontebasso AM, Lichter P, Pfister SM, Collins VP, Jones DT (2013) Differential expression and methylation of brain developmental genes define location-specific subsets of pilocytic astrocytoma. *Acta neuropathologica* 126:291-301. doi:10.1007/s00401-013-1124-7
157. Lawson AR, Hindley GF, Forshew T, Tatevossian RG, Jamie GA, Kelly GP, Neale GA, Ma J, Jones TA, Ellison DW, Sheer D (2011) RAF gene fusion breakpoints in pediatric brain tumors are characterized by significant enrichment of sequence microhomology. *Genome research* 21:505-514. doi:10.1101/gr.115782.110
158. Lee J, Son MJ, Woolard K, Donin NM, Li A, Cheng CH, Kotliarova S, Kotliarov Y, Walling J, Ahn S, Kim M, Totonchy M, Cusack T, Ene C, Ma H, Su Q, Zenklusen JC, Zhang W, Maric D, Fine HA (2008) Epigenetic-mediated dysfunction of the bone morphogenetic protein pathway inhibits differentiation of glioblastoma-initiating cells. *Cancer cell* 13:69-80. doi:10.1016/j.ccr.2007.12.005
159. Levy MZ, Allsopp RC, Futcher AB, Greider CW, Harley CB (1992) Telomere end-replication problem and cell aging. *Journal of molecular biology* 225:951-960
160. Lewis PW, Elsaesser SJ, Noh KM, Stadler SC, Allis CD (2010) Daxx is an H3.3-specific histone chaperone and cooperates with ATRX in replication-independent chromatin assembly at telomeres. *Proceedings of the National Academy of Sciences of the United States of America* 107:14075-14080. doi:10.1073/pnas.1008850107
161. Lewis PW, Muller MM, Koletsky MS, Cordero F, Lin S, Banaszynski LA, Garcia BA, Muir TW, Becher OJ, Allis CD (2013) Inhibition of PRC2 activity by a gain-of-function H3 mutation found in pediatric glioblastoma. *Science* 340:857-861. doi:10.1126/science.1232245
162. Li F, Mao G, Tong D, Huang J, Gu L, Yang W, Li GM (2013) The histone mark H3K36me3 regulates human DNA mismatch repair through its interaction with MutSalpha. *Cell* 153:590-600. doi:10.1016/j.cell.2013.03.025
163. Li H, Durbin R (2009) Fast and accurate short read alignment with Burrows-Wheeler transform. *Bioinformatics* 25:1754-1760. doi:10.1093/bioinformatics/btp324
164. Li H, Handsaker B, Wysoker A, Fennell T, Ruan J, Homer N, Marth G, Abecasis G, Durbin R (2009) The Sequence Alignment/Map format and SAMtools. *Bioinformatics* 25:2078-2079. doi:10.1093/bioinformatics/btp352

165. Liu J, Cheng X, Zhang Y, Li S, Cui H, Zhang L, Shi R, Zhao Z, He C, Wang C, Zhao H, Zhang C, Fisk HA, Guadagno TM, Cui Y (2013) Phosphorylation of Mps1 by BRAFV600E prevents Mps1 degradation and contributes to chromosome instability in melanoma. *Oncogene* 32:713-723. doi:10.1038/onc.2012.94
166. Liu XY, Gerges N, Korshunov A, Sabha N, Khuong-Quang DA, Fontebasso AM, Fleming A, Hadjadj D, Schwartzentruber J, Majewski J, Dong Z, Siegel P, Albrecht S, Croul S, Jones DT, Kool M, Tonjes M, Reifemberger G, Faury D, Zadeh G, Pfister S, Jabado N (2012) Frequent ATRX mutations and loss of expression in adult diffuse astrocytic tumors carrying IDH1/IDH2 and TP53 mutations. *Acta neuropathologica* 124:615-625. doi:10.1007/s00401-012-1031-3
167. Louis DN, Ohgaki H, Wiestler OD, Cavenee WK, Burger PC, Jouvet A, Scheithauer BW, Kleihues P (2007) The 2007 WHO classification of tumours of the central nervous system. *Acta neuropathologica* 114:97-109. doi:10.1007/s00401-007-0243-4
168. Lu C, Ward PS, Kapoor GS, Rohle D, Turcan S, Abdel-Wahab O, Edwards CR, Khanin R, Figueroa ME, Melnick A, Wellen KE, O'Rourke DM, Berger SL, Chan TA, Levine RL, Mellinghoff IK, Thompson CB (2012) IDH mutation impairs histone demethylation and results in a block to cell differentiation. *Nature* 483:474-478. doi:10.1038/nature10860
169. Luco RF, Allo M, Schor IE, Kornblihtt AR, Misteli T (2011) Epigenetics in alternative pre-mRNA splicing. *Cell* 144:16-26. doi:10.1016/j.cell.2010.11.056
170. Luco RF, Pan Q, Tominaga K, Blencowe BJ, Pereira-Smith OM, Misteli T (2010) Regulation of alternative splicing by histone modifications. *Science* 327:996-1000. doi:10.1126/science.1184208
171. Lushnikova T, Bouska A, Odvody J, Dupont WD, Eischen CM (2011) Aging mice have increased chromosome instability that is exacerbated by elevated Mdm2 expression. *Oncogene* 30:4622-4631. doi:10.1038/onc.2011.172
172. Majewski J, Schwartzentruber J, Lalonde E, Montpetit A, Jabado N (2011) What can exome sequencing do for you? *Journal of medical genetics* 48:580-589. doi:10.1136/jmedgenet-2011-100223
173. Maksimovic J, Gordon L, Oshlack A (2012) SWAN: Subset-quantile within array normalization for illumina infinium HumanMethylation450 BeadChips. *Genome biology* 13:R44. doi:10.1186/gb-2012-13-6-r44
174. Mali P, Yang L, Esvelt KM, Aach J, Guell M, DiCarlo JE, Norville JE, Church GM (2013) RNA-guided human genome engineering via Cas9. *Science* 339:823-826. doi:10.1126/science.1232033
175. Marchuk DA, Saulino AM, Tavakkol R, Swaroop M, Wallace MR, Andersen LB, Mitchell AL, Gutmann DH, Boguski M, Collins FS (1991) cDNA cloning of the type 1 neurofibromatosis gene: complete sequence of the NF1 gene product. *Genomics* 11:931-940
176. Mardis ER, Ding L, Dooling DJ, Larson DE, McLellan MD, Chen K, Koboldt DC, Fulton RS, Delehaunty KD, McGrath SD, Fulton LA, Locke DP, Magrini VJ, Abbott RM, Vickery TL, Reed JS, Robinson JS, Wylie T, Smith SM, Carmichael L, Eldred JM, Harris CC, Walker J, Peck JB, Du F, Dukes AF, Sanderson GE, Brummett AM, Clark E, McMichael JF, Meyer RJ, Schindler JK, Pohl CS, Wallis

- JW, Shi X, Lin L, Schmidt H, Tang Y, Haipok C, Wiechert ME, Ivy JV, Kalicki J, Elliott G, Ries RE, Payton JE, Westervelt P, Tomasson MH, Watson MA, Baty J, Heath S, Shannon WD, Nagarajan R, Link DC, Walter MJ, Graubert TA, DiPersio JF, Wilson RK, Ley TJ (2009) Recurring mutations found by sequencing an acute myeloid leukemia genome. *The New England journal of medicine* 361:1058-1066. doi:10.1056/NEJMoa0903840
177. Maria BL, Rehder K, Eskin TA, Hamed LM, Fennell EB, Quisling RG, Mickle JP, Marcus RB, Jr., Drane WE, Mendenhall NP, et al. (1993) Brainstem glioma: I. Pathology, clinical features, and therapy. *Journal of child neurology* 8:112-128
178. Marine JC, Francoz S, Maetens M, Wahl G, Toledo F, Lozano G (2006) Keeping p53 in check: essential and synergistic functions of Mdm2 and Mdm4. *Cell death and differentiation* 13:927-934. doi:10.1038/sj.cdd.4401912
179. Martin GA, Viskochil D, Bollag G, McCabe PC, Crosier WJ, Haubruck H, Conroy L, Clark R, O'Connell P, Cawthon RM, et al. (1990) The GAP-related domain of the neurofibromatosis type 1 gene product interacts with ras p21. *Cell* 63:843-849
180. McKenna A, Hanna M, Banks E, Sivachenko A, Cibulskis K, Kernytzky A, Garimella K, Altshuler D, Gabriel S, Daly M, DePristo MA (2010) The Genome Analysis Toolkit: a MapReduce framework for analyzing next-generation DNA sequencing data. *Genome research* 20:1297-1303. doi:10.1101/gr.107524.110
181. McPherson A, Hormozdiari F, Zayed A, Giuliany R, Ha G, Sun MG, Griffith M, Heravi Moussavi A, Senz J, Melnyk N, Pacheco M, Marra MA, Hirst M, Nielsen TO, Sahinalp SC, Huntsman D, Shah SP (2011) deFuse: an algorithm for gene fusion discovery in tumor RNA-Seq data. *PLoS computational biology* 7:e1001138. doi:10.1371/journal.pcbi.1001138
182. Medici D, Shore EM, Lounev VY, Kaplan FS, Kalluri R, Olsen BR (2010) Conversion of vascular endothelial cells into multipotent stem-like cells. *Nature medicine* 16:1400-1406. doi:10.1038/nm.2252
183. Mishina Y, Crombie R, Bradley A, Behringer RR (1999) Multiple roles for activin-like kinase-2 signaling during mouse embryogenesis. *Developmental biology* 213:314-326. doi:10.1006/dbio.1999.9378
184. Miyamoto T, Porazinski S, Wang H, Borovina A, Ciruna B, Shimizu A, Kajii T, Kikuchi A, Furutani-Seiki M, Matsuura S (2011) Insufficiency of BUBR1, a mitotic spindle checkpoint regulator, causes impaired ciliogenesis in vertebrates. *Human molecular genetics* 20:2058-2070. doi:10.1093/hmg/ddr090
185. Miyazono K, Maeda S, Imamura T (2005) BMP receptor signaling: transcriptional targets, regulation of signals, and signaling cross-talk. *Cytokine & growth factor reviews* 16:251-263. doi:10.1016/j.cytogfr.2005.01.009
186. Mizoguchi M, Nutt CL, Mohapatra G, Louis DN (2004) Genetic alterations of phosphoinositide 3-kinase subunit genes in human glioblastomas. *Brain Pathol* 14:372-377
187. Monje M, Mitra SS, Freret ME, Raveh TB, Kim J, Masek M, Attema JL, Li G, Haddix T, Edwards MS, Fisher PG, Weissman IL, Rowitch DH, Vogel H, Wong AJ, Beachy PA (2011) Hedgehog-responsive candidate cell of origin for diffuse intrinsic pontine glioma. *Proceedings of the National Academy of Sciences of the United States of America* 108:4453-4458. doi:10.1073/pnas.1101657108

188. Moyzis RK, Buckingham JM, Cram LS, Dani M, Deaven LL, Jones MD, Meyne J, Ratliff RL, Wu JR (1988) A highly conserved repetitive DNA sequence, (TTAGGG)_n, present at the telomeres of human chromosomes. *Proceedings of the National Academy of Sciences of the United States of America* 85:6622-6626
189. Mueller W, Mizoguchi M, Silen E, D'Amore K, Nutt CL, Louis DN (2005) Mutations of the PIK3CA gene are rare in human glioblastoma. *Acta neuropathologica* 109:654-655. doi:10.1007/s00401-005-1001-0
190. Murat A, Migliavacca E, Gorlia T, Lambiv WL, Shay T, Hamou MF, de Tribolet N, Regli L, Wick W, Kouwenhoven MC, Hainfellner JA, Heppner FL, Dietrich PY, Zimmer Y, Cairncross JG, Janzer RC, Domany E, Delorenzi M, Stupp R, Hegi ME (2008) Stem cell-related "self-renewal" signature and high epidermal growth factor receptor expression associated with resistance to concomitant chemoradiotherapy in glioblastoma. *Journal of clinical oncology : official journal of the American Society of Clinical Oncology* 26:3015-3024. doi:10.1200/JCO.2007.15.7164
191. Northcott PA, Shih DJ, Peacock J, Garzia L, Morrissy AS, Zichner T, Stutz AM, Korshunov A, Reimand J, Schumacher SE, Beroukhir R, Ellison DW, Marshall CR, Lionel AC, Mack S, Dubuc A, Yao Y, Ramaswamy V, Luu B, Rolider A, Cavalli FM, Wang X, Remke M, Wu X, Chiu RY, Chu A, Chuah E, Corbett RD, Hoad GR, Jackman SD, Li Y, Lo A, Mungall KL, Nip KM, Qian JQ, Raymond AG, Thiessen NT, Varhol RJ, Birol I, Moore RA, Mungall AJ, Holt R, Kawauchi D, Roussel MF, Kool M, Jones DT, Witt H, Fernandez LA, Kenney AM, Wechsler-Reya RJ, Dirks P, Aviv T, Grajkowska WA, Perek-Polnik M, Haberler CC, Delattre O, Reynaud SS, Doz FF, Pernet-Fattet SS, Cho BK, Kim SK, Wang KC, Scheurlen W, Eberhart CG, Fevre-Montange M, Jouvett A, Pollack IF, Fan X, Muraszko KM, Gillespie GY, Di Rocco C, Massimi L, Michiels EM, Kloosterhof NK, French PJ, Kros JM, Olson JM, Ellenbogen RG, Zitterbart K, Kren L, Thompson RC, Cooper MK, Lach B, McLendon RE, Bigner DD, Fontebasso A, Albrecht S, Jabado N, Lindsey JC, Bailey S, Gupta N, Weiss WA, Bogner L, Klekner A, Van Meter TE, Kumabe T, Tominaga T, Elbabaa SK, Leonard JR, Rubin JB, Liau LM, Van Meir EG, Fouladi M, Nakamura H, Cinalli G, Garami M, Hauser P, Saad AG, Iolascon A, Jung S, Carlotti CG, Vibhakkar R, Ra YS, Robinson S, Zollo M, Faria CC, Chan JA, Levy ML, Sorensen PH, Meyerson M, Pomeroy SL, Cho YJ, Bader GD, Tabori U, Hawkins CE, Bouffett E, Scherer SW, Rutka JT, Malkin D, Clifford SC, Jones SJ, Korbel JO, Pfister SM, Marra MA, Taylor MD (2012) Subgroup-specific structural variation across 1,000 medulloblastoma genomes. *Nature* 488:49-56. doi:10.1038/nature11327
192. Noshmehr H, Weisenberger DJ, Diefes K, Phillips HS, Pujara K, Berman BP, Pan F, Pelloski CE, Sulman EP, Bhat KP, Verhaak RG, Hoadley KA, Hayes DN, Perou CM, Schmidt HK, Ding L, Wilson RK, Van Den Berg D, Shen H, Bengtsson H, Neuvial P, Cope LM, Buckley J, Herman JG, Baylin SB, Laird PW, Aldape K (2010) Identification of a CpG island methylator phenotype that defines a distinct subgroup of glioma. *Cancer cell* 17:510-522. doi:10.1016/j.ccr.2010.03.017
193. Ohgaki H, Kleihues P (2005) Epidemiology and etiology of gliomas. *Acta neuropathologica* 109:93-108. doi:10.1007/s00401-005-0991-y

194. Ohgaki H, Kleihues P (2005) Population-based studies on incidence, survival rates, and genetic alterations in astrocytic and oligodendroglial gliomas. *Journal of neuropathology and experimental neurology* 64:479-489
195. Oromendia AB, Dodgson SE, Amon A (2012) Aneuploidy causes proteotoxic stress in yeast. *Genes & development* 26:2696-2708. doi:10.1101/gad.207407.112
196. Ostrom QT, Gittleman H, Farah P, Ondracek A, Chen Y, Wolinsky Y, Stroup NE, Kruchko C, Barnholtz-Sloan JS (2013) CBTRUS statistical report: Primary brain and central nervous system tumors diagnosed in the United States in 2006-2010. *Neuro-oncology* 15 Suppl 2:ii1-56. doi:10.1093/neuonc/not151
197. Parsons DW, Jones S, Zhang X, Lin JC, Leary RJ, Angenendt P, Mankoo P, Carter H, Siu IM, Gallia GL, Olivi A, McLendon R, Rasheed BA, Keir S, Nikolskaya T, Nikolsky Y, Busam DA, Tekleab H, Diaz LA, Jr., Hartigan J, Smith DR, Strausberg RL, Marie SK, Shinjo SM, Yan H, Riggins GJ, Bigner DD, Karchin R, Papadopoulos N, Parmigiani G, Vogelstein B, Velculescu VE, Kinzler KW (2008) An integrated genomic analysis of human glioblastoma multiforme. *Science* 321:1807-1812. doi:10.1126/science.1164382
198. Paugh BS, Broniscer A, Qu C, Miller CP, Zhang J, Tatevossian RG, Olson JM, Geyer JR, Chi SN, da Silva NS, Onar-Thomas A, Baker JN, Gajjar A, Ellison DW, Baker SJ (2011) Genome-wide analyses identify recurrent amplifications of receptor tyrosine kinases and cell-cycle regulatory genes in diffuse intrinsic pontine glioma. *Journal of clinical oncology : official journal of the American Society of Clinical Oncology* 29:3999-4006. doi:10.1200/JCO.2011.35.5677
199. Paugh BS, Qu C, Jones C, Liu Z, Adamowicz-Brice M, Zhang J, Bax DA, Coyle B, Barrow J, Hargrave D, Lowe J, Gajjar A, Zhao W, Broniscer A, Ellison DW, Grundy RG, Baker SJ (2010) Integrated molecular genetic profiling of pediatric high-grade gliomas reveals key differences with the adult disease. *Journal of clinical oncology : official journal of the American Society of Clinical Oncology* 28:3061-3068. doi:10.1200/JCO.2009.26.7252
200. Pericak-Vance MA, Yamaoka LH, Vance JM, Small K, Rosenwasser GO, Gaskell PC, Jr., Hung WY, Alberts MJ, Haynes CS, Speer MC, et al. (1987) Genetic linkage studies of chromosome 17 RFLPs in von Recklinghausen neurofibromatosis (NF1). *Genomics* 1:349-352
201. Perkins SM, Fei W, Mitra N, Shinohara ET (2013) Late causes of death in children treated for CNS malignancies. *Journal of neuro-oncology* 115:79-85. doi:10.1007/s11060-013-1197-0
202. Pfister S, Janzarik WG, Remke M, Ernst A, Werft W, Becker N, Toedt G, Wittmann A, Kratz C, Olbrich H, Ahmadi R, Thieme B, Joos S, Radlwimmer B, Kulozik A, Pietsch T, Herold-Mende C, Gnekow A, Reifenberger G, Korshunov A, Scheurlen W, Omran H, Lichter P (2008) BRAF gene duplication constitutes a mechanism of MAPK pathway activation in low-grade astrocytomas. *The Journal of clinical investigation* 118:1739-1749. doi:10.1172/JCI33656
203. Pfister SX, Ahrabi S, Zalmas LP, Sarkar S, Aymard F, Bachrati CZ, Helleday T, Legube G, La Thangue NB, Porter AC, Humphrey TC (2014) SETD2-Dependent Histone H3K36 Trimethylation Is Required for Homologous Recombination Repair and Genome Stability. *Cell reports* 7:2006-2018. doi:10.1016/j.celrep.2014.05.026

204. Phillips HS, Kharbanda S, Chen R, Forrest WF, Soriano RH, Wu TD, Misra A, Nigro JM, Colman H, Soroceanu L, Williams PM, Modrusan Z, Feuerstein BG, Aldape K (2006) Molecular subclasses of high-grade glioma predict prognosis, delineate a pattern of disease progression, and resemble stages in neurogenesis. *Cancer cell* 9:157-173. doi:10.1016/j.ccr.2006.02.019
205. Piccirillo SG, Reynolds BA, Zanetti N, Lamorte G, Binda E, Broggi G, Brem H, Olivi A, Dimeco F, Vescovi AL (2006) Bone morphogenetic proteins inhibit the tumorigenic potential of human brain tumour-initiating cells. *Nature* 444:761-765. doi:10.1038/nature05349
206. Pollack IF (1999) Pediatric brain tumors. *Seminars in surgical oncology* 16:73-90
207. Post SM, Quintas-Cardama A, Pant V, Iwakuma T, Hamir A, Jackson JG, Maccio DR, Bond GL, Johnson DG, Levine AJ, Lozano G (2010) A high-frequency regulatory polymorphism in the p53 pathway accelerates tumor development. *Cancer cell* 18:220-230. doi:10.1016/j.ccr.2010.07.010
208. Proctor CJ, Gray DA (2008) Explaining oscillations and variability in the p53-Mdm2 system. *BMC systems biology* 2:75. doi:10.1186/1752-0509-2-75
209. Raabe EH, Lim KS, Kim JM, Meeker A, Mao XG, Nikkhah G, Maciaczyk J, Kahlert U, Jain D, Bar E, Cohen KJ, Eberhart CG (2011) BRAF activation induces transformation and then senescence in human neural stem cells: a pilocytic astrocytoma model. *Clinical cancer research : an official journal of the American Association for Cancer Research* 17:3590-3599. doi:10.1158/1078-0432.CCR-10-3349
210. Rajaraman P, Melin BS, Wang Z, McKean-Cowdin R, Michaud DS, Wang SS, Bondy M, Houlston R, Jenkins RB, Wrensch M, Yeager M, Ahlbom A, Albanes D, Andersson U, Freeman LE, Buring JE, Butler MA, Braganza M, Carreon T, Feychting M, Fleming SJ, Gapstur SM, Gaziano JM, Giles GG, Hallmans G, Henriksson R, Hoffman-Bolton J, Inskip PD, Johansen C, Kitahara CM, Lathrop M, Liu C, Le Marchand L, Linet MS, Lonn S, Peters U, Purdue MP, Rothman N, Ruder AM, Sanson M, Sesso HD, Severi G, Shu XO, Simon M, Stampfer M, Stevens VL, Visvanathan K, White E, Wolk A, Zeleniuch-Jacquotte A, Zheng W, Decker P, Enciso-Mora V, Fridley B, Gao YT, Kosel M, Lachance DH, Lau C, Rice T, Swerdlow A, Wiemels JL, Wiencke JK, Shete S, Xiang YB, Xiao Y, Hoover RN, Fraumeni JF, Jr., Chatterjee N, Hartge P, Chanock SJ (2012) Genome-wide association study of glioma and meta-analysis. *Human genetics* 131:1877-1888. doi:10.1007/s00439-012-1212-0
211. Ramkissoon LA, Horowitz PM, Craig JM, Ramkissoon SH, Rich BE, Schumacher SE, McKenna A, Lawrence MS, Bergthold G, Brastianos PK, Tabak B, Ducar MD, Van Hummelen P, MacConaill LE, Pouissant-Young T, Cho YJ, Taha H, Mahmoud M, Bowers DC, Margraf L, Tabori U, Hawkins C, Packer RJ, Hill DA, Pomeroy SL, Eberhart CG, Dunn IF, Goumnerova L, Getz G, Chan JA, Santagata S, Hahn WC, Stiles CD, Ligon AH, Kieran MW, Beroukhir R, Ligon KL (2013) Genomic analysis of diffuse pediatric low-grade gliomas identifies recurrent oncogenic truncating rearrangements in the transcription factor MYBL1. *Proceedings of the National Academy of Sciences of the United States of America* 110:8188-8193. doi:10.1073/pnas.1300252110

212. Rausch T, Jones DT, Zapatka M, Stutz AM, Zichner T, Weischenfeldt J, Jager N, Remke M, Shih D, Northcott PA, Pfaff E, Tica J, Wang Q, Massimi L, Witt H, Bender S, Pleier S, Cin H, Hawkins C, Beck C, von Deimling A, Hans V, Brors B, Eils R, Scheurlen W, Blake J, Benes V, Kulozik AE, Witt O, Martin D, Zhang C, Porat R, Merino DM, Wasserman J, Jabado N, Fontebasso A, Bullinger L, Rucker FG, Dohner K, Dohner H, Koster J, Molenaar JJ, Versteeg R, Kool M, Tabori U, Malkin D, Korshunov A, Taylor MD, Lichter P, Pfister SM, Korbel JO (2012) Genome sequencing of pediatric medulloblastoma links catastrophic DNA rearrangements with TP53 mutations. *Cell* 148:59-71. doi:10.1016/j.cell.2011.12.013
213. Rehen SK, McConnell MJ, Kaushal D, Kingsbury MA, Yang AH, Chun J (2001) Chromosomal variation in neurons of the developing and adult mammalian nervous system. *Proceedings of the National Academy of Sciences of the United States of America* 98:13361-13366. doi:10.1073/pnas.231487398
214. Rehen SK, Yung YC, McCreight MP, Kaushal D, Yang AH, Almeida BS, Kingsbury MA, Cabral KM, McConnell MJ, Anliker B, Fontanoz M, Chun J (2005) Constitutional aneuploidy in the normal human brain. *The Journal of neuroscience : the official journal of the Society for Neuroscience* 25:2176-2180. doi:10.1523/JNEUROSCI.4560-04.2005
215. Reilly KM, Loisel DA, Bronson RT, McLaughlin ME, Jacks T (2000) Nf1;Trp53 mutant mice develop glioblastoma with evidence of strain-specific effects. *Nature genetics* 26:109-113. doi:10.1038/79075
216. Remke M, Ramaswamy V, Peacock J, Shih DJ, Koelsche C, Northcott PA, Hill N, Cavalli FM, Kool M, Wang X, Mack SC, Barszczyk M, Morrissy AS, Wu X, Agnihotri S, Luu B, Jones DT, Garzia L, Dubuc AM, Zhukova N, Vanner R, Kros JM, French PJ, Van Meir EG, Vibhakkar R, Zitterbart K, Chan JA, Bogner L, Klekner A, Lach B, Jung S, Saad AG, Liau LM, Albrecht S, Zollo M, Cooper MK, Thompson RC, Delattre OO, Bourdeaut F, Doz FF, Garami M, Hauser P, Carlotti CG, Van Meter TE, Massimi L, Fults D, Pomeroy SL, Kumabe T, Ra YS, Leonard JR, Elbabaa SK, Mora J, Rubin JB, Cho YJ, McLendon RE, Bigner DD, Eberhart CG, Fouladi M, Wechsler-Reya RJ, Faria CC, Croul SE, Huang A, Bouffet E, Hawkins CE, Dirks PB, Weiss WA, Schuller U, Pollack IF, Rutkowski S, Meyronet D, Jouvret A, Fevre-Montange M, Jabado N, Perek-Polnik M, Grajkowska WA, Kim SK, Rutka JT, Malkin D, Tabori U, Pfister SM, Korshunov A, von Deimling A, Taylor MD (2013) TERT promoter mutations are highly recurrent in SHH subgroup medulloblastoma. *Acta neuropathologica* 126:917-929. doi:10.1007/s00401-013-1198-2
217. Rihani R, Bazzeh F, Faqih N, Sultan I (2010) Secondary hematopoietic malignancies in survivors of childhood cancer: an analysis of 111 cases from the Surveillance, Epidemiology, and End Result-9 registry. *Cancer* 116:4385-4394. doi:10.1002/cncr.25313
218. Rodriguez FJ, Giannini C, Asmann YW, Sharma MK, Perry A, Tibbetts KM, Jenkins RB, Scheithauer BW, Anant S, Jenkins S, Eberhart CG, Sarkaria JN, Gutmann DH (2008) Gene expression profiling of NF-1-associated and sporadic pilocytic astrocytoma identifies aldehyde dehydrogenase 1 family member L1 (ALDH1L1) as an underexpressed candidate biomarker in aggressive subtypes.

- Journal of neuropathology and experimental neurology 67:1194-1204.
doi:10.1097/NEN.0b013e31818f8be1e
219. Rohle D, Popovici-Muller J, Palaskas N, Turcan S, Grommes C, Campos C, Tsoi J, Clark O, Oldrini B, Komisopoulou E, Kunii K, Pedraza A, Schalm S, Silverman L, Miller A, Wang F, Yang H, Chen Y, Kernytsky A, Rosenblum MK, Liu W, Biller SA, Su SM, Brennan CW, Chan TA, Graeber TG, Yen KE, Mellinghoff IK (2013) An inhibitor of mutant IDH1 delays growth and promotes differentiation of glioma cells. *Science* 340:626-630. doi:10.1126/science.1236062
 220. Roth RB, Hevezi P, Lee J, Willhite D, Lechner SM, Foster AC, Zlotnik A (2006) Gene expression analyses reveal molecular relationships among 20 regions of the human CNS. *Neurogenetics* 7:67-80. doi:10.1007/s10048-006-0032-6
 221. Rozen S, Skaletsky H (2000) Primer3 on the WWW for general users and for biologist programmers. *Methods Mol Biol* 132:365-386
 222. Samanta J, Kessler JA (2004) Interactions between ID and OLIG proteins mediate the inhibitory effects of BMP4 on oligodendroglial differentiation. *Development* 131:4131-4142. doi:10.1242/dev.01273
 223. Samuels Y, Wang Z, Bardelli A, Silliman N, Ptak J, Szabo S, Yan H, Gazdar A, Powell SM, Riggins GJ, Willson JK, Markowitz S, Kinzler KW, Vogelstein B, Velculescu VE (2004) High frequency of mutations of the PIK3CA gene in human cancers. *Science* 304:554. doi:10.1126/science.1096502
 224. Sanford RA, Bowman R, Tomita T, De Leon G, Palka P (1999) A 16-year-old male with Noonan's syndrome develops progressive scoliosis and deteriorating gait. *Pediatric neurosurgery* 30:47-52. doi:28761
 225. Sari N, Akyuz C, Aktas D, Gumruk F, Orhan D, Alikasifoglu M, Aydin B, Alanay Y, Buyukpamukcu M (2009) Wilms tumor, AML and medulloblastoma in a child with cancer prone syndrome of total premature chromatid separation and Fanconi anemia. *Pediatric blood & cancer* 53:208-210. doi:10.1002/pbc.21966
 226. Sasaki M, Knobbe CB, Munger JC, Lind EF, Brenner D, Brustle A, Harris IS, Holmes R, Wakeham A, Haight J, You-Ten A, Li WY, Schalm S, Su SM, Virtanen C, Reifemberger G, Ohashi PS, Barber DL, Figueroa ME, Melnick A, Zuniga-Pflucker JC, Mak TW (2012) IDH1(R132H) mutation increases murine haematopoietic progenitors and alters epigenetics. *Nature* 488:656-659. doi:10.1038/nature11323
 227. Schiffman JD, Hodgson JG, VandenBerg SR, Flaherty P, Polley MY, Yu M, Fisher PG, Rowitch DH, Ford JM, Berger MS, Ji H, Gutmann DH, James CD (2010) Oncogenic BRAF mutation with CDKN2A inactivation is characteristic of a subset of pediatric malignant astrocytomas. *Cancer research* 70:512-519. doi:10.1158/0008-5472.CAN-09-1851
 228. Schindler G, Capper D, Meyer J, Janzarik W, Omran H, Herold-Mende C, Schmieider K, Wesseling P, Mawrin C, Hasselblatt M, Louis DN, Korshunov A, Pfister S, Hartmann C, Paulus W, Reifemberger G, von Deimling A (2011) Analysis of BRAF V600E mutation in 1,320 nervous system tumors reveals high mutation frequencies in pleomorphic xanthoastrocytoma, ganglioglioma and extra-cerebellar pilocytic astrocytoma. *Acta neuropathologica* 121:397-405. doi:10.1007/s00401-011-0802-6

229. Schmierer B, Hill CS (2007) TGFbeta-SMAD signal transduction: molecular specificity and functional flexibility. *Nature reviews Molecular cell biology* 8:970-982. doi:10.1038/nrm2297
230. Schuettpelz LG, McDonald S, Whitesell K, Desruisseau DM, Grange DK, Gurnett CA, Wilson DB (2009) Pilocytic astrocytoma in a child with Noonan syndrome. *Pediatric blood & cancer* 53:1147-1149. doi:10.1002/pbc.22193
231. Schwartzentruber J, Korshunov A, Liu XY, Jones DT, Pfaff E, Jacob K, Sturm D, Fontebasso AM, Quang DA, Tonjes M, Hovestadt V, Albrecht S, Kool M, Nantel A, Konermann C, Lindroth A, Jager N, Rausch T, Ryzhova M, Korbel JO, Hielscher T, Hauser P, Garami M, Klekner A, Bogner L, Ebinger M, Schuhmann MU, Scheurlen W, Pekrun A, Fruhwald MC, Roggendorf W, Kramm C, Durken M, Atkinson J, Lepage P, Montpetit A, Zakrzewska M, Zakrzewski K, Liberski PP, Dong Z, Siegel P, Kulozik AE, Zapatka M, Guha A, Malkin D, Felsberg J, Reifenberger G, von Deimling A, Ichimura K, Collins VP, Witt H, Milde T, Witt O, Zhang C, Castelo-Branco P, Lichter P, Faury D, Tabori U, Plass C, Majewski J, Pfister SM, Jabado N (2012) Driver mutations in histone H3.3 and chromatin remodelling genes in paediatric glioblastoma. *Nature* 482:226-231. doi:10.1038/nature10833
232. Seizinger BR, Rouleau G, Lane AH, Ozelius LJ, Faryniarz AG, Iannazzi J, Hobbs W, Roy JC, Falcone B, Huson S, et al. (1987) DNA linkage analysis in Von Recklinghausen neurofibromatosis. *Journal of medical genetics* 24:529-530
233. Seizinger BR, Rouleau GA, Ozelius LJ, Lane AH, Faryniarz AG, Chao MV, Huson S, Korf BR, Parry DM, Pericak-Vance MA, et al. (1987) Genetic linkage of von Recklinghausen neurofibromatosis to the nerve growth factor receptor gene. *Cell* 49:589-594
234. Sharma MK, Mansur DB, Reifenberger G, Perry A, Leonard JR, Aldape KD, Albin MG, Emmett RJ, Loeser S, Watson MA, Nagarajan R, Gutmann DH (2007) Distinct genetic signatures among pilocytic astrocytomas relate to their brain region origin. *Cancer research* 67:890-900. doi:10.1158/0008-5472.CAN-06-0973
235. Shen Q, Little SC, Xu M, Haupt J, Ast C, Katagiri T, Mundlos S, Seemann P, Kaplan FS, Mullins MC, Shore EM (2009) The fibrodysplasia ossificans progressiva R206H ACVR1 mutation activates BMP-independent chondrogenesis and zebrafish embryo ventralization. *The Journal of clinical investigation* 119:3462-3472. doi:10.1172/JCI37412
236. Shete S, Hosking FJ, Robertson LB, Dobbins SE, Sanson M, Malmer B, Simon M, Marie Y, Boisselier B, Delattre JY, Hoang-Xuan K, El Hallani S, Idbaih A, Zelenika D, Andersson U, Henriksson R, Bergenheim AT, Feychting M, Lonn S, Ahlbom A, Schramm J, Linnebank M, Hemminki K, Kumar R, Hepworth SJ, Price A, Armstrong G, Liu Y, Gu X, Yu R, Lau C, Schoemaker M, Muir K, Swerdlow A, Lathrop M, Bondy M, Houlston RS (2009) Genome-wide association study identifies five susceptibility loci for glioma. *Nature genetics* 41:899-904. doi:10.1038/ng.407
237. Shimizu A, Asakawa S, Sasaki T, Yamazaki S, Yamagata H, Kudoh J, Minoshima S, Kondo I, Shimizu N (2003) A novel giant gene CSMD3 encoding a protein with CUB and sushi multiple domains: a candidate gene for benign adult familial

- myoclonic epilepsy on human chromosome 8q23.3-q24.1. *Biochemical and biophysical research communications* 309:143-154
238. Shore EM, Xu M, Feldman GJ, Fenstermacher DA, Cho TJ, Choi IH, Connor JM, Delai P, Glaser DL, LeMerrer M, Morhart R, Rogers JG, Smith R, Triffitt JT, Urtizberea JA, Zasloff M, Brown MA, Kaplan FS (2006) A recurrent mutation in the BMP type I receptor ACVR1 causes inherited and sporadic fibrodysplasia ossificans progressiva. *Nature genetics* 38:525-527. doi:10.1038/ng1783
239. Siegel PM, Ryan ED, Cardiff RD, Muller WJ (1999) Elevated expression of activated forms of Neu/ErbB-2 and ErbB-3 are involved in the induction of mammary tumors in transgenic mice: implications for human breast cancer. *The EMBO journal* 18:2149-2164. doi:10.1093/emboj/18.8.2149
240. Sievert AJ, Jackson EM, Gai X, Hakonarson H, Judkins AR, Resnick AC, Sutton LN, Storm PB, Shaikh TH, Biegel JA (2009) Duplication of 7q34 in pediatric low-grade astrocytomas detected by high-density single-nucleotide polymorphism-based genotype arrays results in a novel BRAF fusion gene. *Brain Pathol* 19:449-458. doi:10.1111/j.1750-3639.2008.00225.x
241. Singh D, Chan JM, Zoppoli P, Niola F, Sullivan R, Castano A, Liu EM, Reichel J, Porrati P, Pellegatta S, Qiu K, Gao Z, Ceccarelli M, Riccardi R, Brat DJ, Guha A, Aldape K, Golfinos JG, Zagzag D, Mikkelsen T, Finocchiaro G, Lasorella A, Rabadan R, Iavarone A (2012) Transforming fusions of FGFR and TACC genes in human glioblastoma. *Science* 337:1231-1235. doi:10.1126/science.1220834
242. Smith MA, Altekruze SF, Adamson PC, Reaman GH, Seibel NL (2014) Declining childhood and adolescent cancer mortality. *Cancer*. doi:10.1002/cncr.28748
243. Solomon DA, Kim T, Diaz-Martinez LA, Fair J, Elkahloun AG, Harris BT, Toretsky JA, Rosenberg SA, Shukla N, Ladanyi M, Samuels Y, James CD, Yu H, Kim JS, Waldman T (2011) Mutational inactivation of STAG2 causes aneuploidy in human cancer. *Science* 333:1039-1043. doi:10.1126/science.1203619
244. Statham AL, Robinson MD, Song JZ, Coolen MW, Stirzaker C, Clark SJ (2012) Bisulfite sequencing of chromatin immunoprecipitated DNA (BisChIP-seq) directly informs methylation status of histone-modified DNA. *Genome research* 22:1120-1127. doi:10.1101/gr.132076.111
245. Stephens K, Riccardi VM, Rising M, Ng S, Green P, Collins FS, Rediker KS, Powers JA, Parker C, Donis-Keller H (1987) Linkage studies with chromosome 17 DNA markers in 45 neurofibromatosis 1 families. *Genomics* 1:353-357
246. Stephens PJ, Greenman CD, Fu B, Yang F, Bignell GR, Mudie LJ, Pleasance ED, Lau KW, Beare D, Stebbings LA, McLaren S, Lin ML, McBride DJ, Varela I, Nik-Zainal S, Leroy C, Jia M, Menzies A, Butler AP, Teague JW, Quail MA, Burton J, Swerdlow H, Carter NP, Morsberger LA, Iacobuzio-Donahue C, Follows GA, Green AR, Flanagan AM, Stratton MR, Futreal PA, Campbell PJ (2011) Massive genomic rearrangement acquired in a single catastrophic event during cancer development. *Cell* 144:27-40. doi:10.1016/j.cell.2010.11.055
247. Struys EA, Salomons GS, Achouri Y, Van Schaftingen E, Grosso S, Craigen WJ, Verhoeven NM, Jakobs C (2005) Mutations in the D-2-hydroxyglutarate dehydrogenase gene cause D-2-hydroxyglutaric aciduria. *American journal of human genetics* 76:358-360. doi:10.1086/427890

248. Stupp R, Mason WP, van den Bent MJ, Weller M, Fisher B, Taphoorn MJ, Belanger K, Brandes AA, Marosi C, Bogdahn U, Curschmann J, Janzer RC, Ludwin SK, Gorlia T, Allgeier A, Lacombe D, Cairncross JG, Eisenhauer E, Mirimanoff RO (2005) Radiotherapy plus concomitant and adjuvant temozolomide for glioblastoma. *The New England journal of medicine* 352:987-996. doi:10.1056/NEJMoa043330
249. Sturm D, Bender S, Jones DT, Lichter P, Grill J, Becher O, Hawkins C, Majewski J, Jones C, Costello JF, Iavarone A, Aldape K, Brennan CW, Jabado N, Pfister SM (2014) Paediatric and adult glioblastoma: multiform (epi)genomic culprits emerge. *Nature reviews Cancer* 14:92-107. doi:10.1038/nrc3655
250. Sturm D, Witt H, Hovestadt V, Khuong-Quang DA, Jones DT, Konermann C, Pfaff E, Tonjes M, Sill M, Bender S, Kool M, Zapatka M, Becker N, Zucknick M, Hielscher T, Liu XY, Fontebasso AM, Ryzhova M, Albrecht S, Jacob K, Wolter M, Ebinger M, Schuhmann MU, van Meter T, Fruhwald MC, Hauch H, Pekrun A, Radlwimmer B, Niehues T, von Komorowski G, Durken M, Kulozik AE, Madden J, Donson A, Foreman NK, Drissi R, Fouladi M, Scheurlen W, von Deimling A, Monoranu C, Roggendorf W, Herold-Mende C, Unterberg A, Kramm CM, Felsberg J, Hartmann C, Wiestler B, Wick W, Milde T, Witt O, Lindroth AM, Schwartzentruber J, Faury D, Fleming A, Zakrzewska M, Liberski PP, Zakrzewski K, Hauser P, Garami M, Klekner A, Bogner L, Morrissy S, Cavalli F, Taylor MD, van Sluis P, Koster J, Versteeg R, Volckmann R, Mikkelsen T, Aldape K, Reifenberger G, Collins VP, Majewski J, Korshunov A, Lichter P, Plass C, Jabado N, Pfister SM (2012) Hotspot mutations in H3F3A and IDH1 define distinct epigenetic and biological subgroups of glioblastoma. *Cancer cell* 22:425-437. doi:10.1016/j.ccr.2012.08.024
251. Suzuki R, Shimodaira H (2006) Pvcust: an R package for assessing the uncertainty in hierarchical clustering. *Bioinformatics* 22:1540-1542. doi:10.1093/bioinformatics/btl117
252. Taylor KR, Mackay A, Truffaux N, Butterfield YS, Morozova O, Philippe C, Castel D, Grasso CS, Vinci M, Carvalho D, Carcaboso AM, de Torres C, Cruz O, Mora J, Entz-Werle N, Ingram WJ, Monje M, Hargrave D, Bullock AN, Puget S, Yip S, Jones C, Grill J (2014) Recurrent activating ACVR1 mutations in diffuse intrinsic pontine glioma. *Nature genetics* 46:457-461. doi:10.1038/ng.2925
253. Thompson SL, Compton DA (2010) Proliferation of aneuploid human cells is limited by a p53-dependent mechanism. *The Journal of cell biology* 188:369-381. doi:10.1083/jcb.200905057
254. Tumolo M, Moscatelli A, Silvestri G (2006) Anaesthetic management of a child with fibrodysplasia ossificans progressiva. *British journal of anaesthesia* 97:701-703. doi:10.1093/bja/ael251
255. Turcan S, Rohle D, Goenka A, Walsh LA, Fang F, Yilmaz E, Campos C, Fabius AW, Lu C, Ward PS, Thompson CB, Kaufman A, Guryanova O, Levine R, Heguy A, Viale A, Morris LG, Huse JT, Mellinghoff IK, Chan TA (2012) IDH1 mutation is sufficient to establish the glioma hypermethylator phenotype. *Nature* 483:479-483. doi:10.1038/nature10866

256. Upadhyaya M, Sarfarazi M, Huson SM, Harper PS (1987) Further exclusion data for the Von Recklinghausen neurofibromatosis gene: a genetic linkage study of 19 polymorphic markers. *Journal of medical genetics* 24:534-536
257. Valton J, Cabaniols JP, Galetto R, Delacote F, Duhamel M, Paris S, Blanchard DA, Lebuhotel C, Thomas S, Moriceau S, Demirdjian R, Letort G, Jacquet A, Gariboldi A, Rolland S, Daboussi F, Juillerat A, Bertonati C, Duclert A, Duchateau P (2014) Efficient strategies for TALEN-mediated genome editing in mammalian cell lines. *Methods*. doi:10.1016/j.ymeth.2014.06.013
258. Varela I, Tarpey P, Raine K, Huang D, Ong CK, Stephens P, Davies H, Jones D, Lin ML, Teague J, Bignell G, Butler A, Cho J, Dalgliesh GL, Galappaththige D, Greenman C, Hardy C, Jia M, Latimer C, Lau KW, Marshall J, McLaren S, Menzies A, Mudie L, Stebbings L, Largaespada DA, Wessels LF, Richard S, Kahnoski RJ, Anema J, Tuveson DA, Perez-Mancera PA, Mustonen V, Fischer A, Adams DJ, Rust A, Chan-on W, Subimerb C, Dykema K, Furge K, Campbell PJ, Teh BT, Stratton MR, Futreal PA (2011) Exome sequencing identifies frequent mutation of the SWI/SNF complex gene PBRM1 in renal carcinoma. *Nature* 469:539-542. doi:10.1038/nature09639
259. Varier RA, Timmers HT (2011) Histone lysine methylation and demethylation pathways in cancer. *Biochimica et biophysica acta* 1815:75-89. doi:10.1016/j.bbcan.2010.10.002
260. Venkatesh S, Smolle M, Li H, Gogol MM, Saint M, Kumar S, Natarajan K, Workman JL (2012) Set2 methylation of histone H3 lysine 36 suppresses histone exchange on transcribed genes. *Nature* 489:452-455. doi:10.1038/nature11326
261. Venneti S, Garimella MT, Sullivan LM, Martinez D, Huse JT, Heguy A, Santi M, Thompson CB, Judkins AR (2013) Evaluation of histone 3 lysine 27 trimethylation (H3K27me3) and enhancer of Zest 2 (EZH2) in pediatric glial and glioneuronal tumors shows decreased H3K27me3 in H3F3A K27M mutant glioblastomas. *Brain Pathol* 23:558-564. doi:10.1111/bpa.12042
262. Verhaak RG, Hoadley KA, Purdom E, Wang V, Qi Y, Wilkerson MD, Miller CR, Ding L, Golub T, Mesirov JP, Alexe G, Lawrence M, O'Kelly M, Tamayo P, Weir BA, Gabriel S, Winckler W, Gupta S, Jakkula L, Feiler HS, Hodgson JG, James CD, Sarkaria JN, Brennan C, Kahn A, Spellman PT, Wilson RK, Speed TP, Gray JW, Meyerson M, Getz G, Perou CM, Hayes DN (2010) Integrated genomic analysis identifies clinically relevant subtypes of glioblastoma characterized by abnormalities in PDGFRA, IDH1, EGFR, and NF1. *Cancer cell* 17:98-110. doi:10.1016/j.ccr.2009.12.020
263. Villard L, Gecz J, Mattei JF, Fontes M, Saugier-veber P, Munnich A, Lyonnet S (1996) XNP mutation in a large family with Juberg-Marsidi syndrome. *Nature genetics* 12:359-360. doi:10.1038/ng0496-359
264. Vinagre J, Almeida A, Populo H, Batista R, Lyra J, Pinto V, Coelho R, Celestino R, Prazeres H, Lima L, Melo M, da Rocha AG, Preto A, Castro P, Castro L, Pardal F, Lopes JM, Santos LL, Reis RM, Cameselle-Teijeiro J, Sobrinho-Simoes M, Lima J, Maximo V, Soares P (2013) Frequency of TERT promoter mutations in human cancers. *Nature communications* 4:2185. doi:10.1038/ncomms3185

265. Viskochil D, Buchberg AM, Xu G, Cawthon RM, Stevens J, Wolff RK, Culver M, Carey JC, Copeland NG, Jenkins NA, et al. (1990) Deletions and a translocation interrupt a cloned gene at the neurofibromatosis type 1 locus. *Cell* 62:187-192
266. Vulliamy T, Marrone A, Szydlo R, Walne A, Mason PJ, Dokal I (2004) Disease anticipation is associated with progressive telomere shortening in families with dyskeratosis congenita due to mutations in TERC. *Nature genetics* 36:447-449. doi:10.1038/ng1346
267. Wagner EJ, Carpenter PB (2012) Understanding the language of Lys36 methylation at histone H3. *Nature reviews Molecular cell biology* 13:115-126. doi:10.1038/nrm3274
268. Wallace MR, Marchuk DA, Andersen LB, Letcher R, Odeh HM, Saulino AM, Fountain JW, Brereton A, Nicholson J, Mitchell AL, et al. (1990) Type 1 neurofibromatosis gene: identification of a large transcript disrupted in three NF1 patients. *Science* 249:181-186
269. Walsh KM, Codd V, Smirnov IV, Rice T, Decker PA, Hansen HM, Kollmeyer T, Kosel ML, Molinaro AM, McCoy LS, Bracci PM, Cabriga BS, Pekmezci M, Zheng S, Wiemels JL, Pico AR, Tihan T, Berger MS, Chang SM, Prados MD, Lachance DH, O'Neill BP, Sicotte H, Eckel-Passow JE, van der Harst P, Wiencke JK, Samani NJ, Jenkins RB, Wrensch MR (2014) Variants near TERT and TERC influencing telomere length are associated with high-grade glioma risk. *Nature genetics*. doi:10.1038/ng.3004
270. Wang K, Li M, Hakonarson H (2010) ANNOVAR: functional annotation of genetic variants from high-throughput sequencing data. *Nucleic acids research* 38:e164. doi:10.1093/nar/gkq603
271. Wang P, Lushnikova T, Odvody J, Greiner TC, Jones SN, Eischen CM (2008) Elevated Mdm2 expression induces chromosomal instability and confers a survival and growth advantage to B cells. *Oncogene* 27:1590-1598. doi:10.1038/sj.onc.1210788
272. Wang Z, Gerstein M, Snyder M (2009) RNA-Seq: a revolutionary tool for transcriptomics. *Nature reviews Genetics* 10:57-63. doi:10.1038/nrg2484
273. Ward E, DeSantis C, Robbins A, Kohler B, Jemal A (2014) Childhood and adolescent cancer statistics, 2014. *CA: a cancer journal for clinicians* 64:83-103. doi:10.3322/caac.21219
274. Ward PS, Patel J, Wise DR, Abdel-Wahab O, Bennett BD, Collier HA, Cross JR, Fantin VR, Hedvat CV, Perl AE, Rabinowitz JD, Carroll M, Su SM, Sharp KA, Levine RL, Thompson CB (2010) The common feature of leukemia-associated IDH1 and IDH2 mutations is a neomorphic enzyme activity converting alpha-ketoglutarate to 2-hydroxyglutarate. *Cancer cell* 17:225-234. doi:10.1016/j.ccr.2010.01.020
275. Weaver BA, Silk AD, Montagna C, Verdier-Pinard P, Cleveland DW (2007) Aneuploidy acts both oncogenically and as a tumor suppressor. *Cancer cell* 11:25-36. doi:10.1016/j.ccr.2006.12.003
276. Wen H, Li Y, Xi Y, Jiang S, Stratton S, Peng D, Tanaka K, Ren Y, Xia Z, Wu J, Li B, Barton MC, Li W, Li H, Shi X (2014) ZMYND11 links histone H3.3K36me3 to transcription elongation and tumour suppression. *Nature* 508:263-268. doi:10.1038/nature13045

277. Westra JW, Peterson SE, Yung YC, Mutoh T, Barral S, Chun J (2008) Aneuploid mosaicism in the developing and adult cerebellar cortex. *The Journal of comparative neurology* 507:1944-1951. doi:10.1002/cne.21648
278. White R, Nakamura Y, O'Connell P, Leppert M, Lalouel JM, Barker D, Goldgar D, Skolnick M, Carey J, Wallis CE, et al. (1987) Tightly linked markers for the neurofibromatosis type 1 gene. *Genomics* 1:364-367
279. Willard HF, Greig GM, Powers VE, Waye JS (1987) Molecular organization and haplotype analysis of centromeric DNA from human chromosome 17: implications for linkage in neurofibromatosis. *Genomics* 1:368-373
280. Wrensch M, Jenkins RB, Chang JS, Yeh RF, Xiao Y, Decker PA, Ballman KV, Berger M, Buckner JC, Chang S, Giannini C, Halder C, Kollmeyer TM, Kosel ML, LaChance DH, McCoy L, O'Neill BP, Patoka J, Pico AR, Prados M, Quesenberry C, Rice T, Rynearson AL, Smirnov I, Tihan T, Wiemels J, Yang P, Wiencke JK (2009) Variants in the CDKN2B and RTEL1 regions are associated with high-grade glioma susceptibility. *Nature genetics* 41:905-908. doi:10.1038/ng.408
281. Wu G, Broniscer A, McEachron TA, Lu C, Paugh BS, Becksfort J, Qu C, Ding L, Huether R, Parker M, Zhang J, Gajjar A, Dyer MA, Mullighan CG, Gilbertson RJ, Mardis ER, Wilson RK, Downing JR, Ellison DW, Zhang J, Baker SJ (2012) Somatic histone H3 alterations in pediatric diffuse intrinsic pontine gliomas and non-brainstem glioblastomas. *Nature genetics* 44:251-253. doi:10.1038/ng.1102
282. Wu G, Diaz AK, Paugh BS, Rankin SL, Ju B, Li Y, Zhu X, Qu C, Chen X, Zhang J, Easton J, Edmonson M, Ma X, Lu C, Nagahawatte P, Hedlund E, Rusch M, Pounds S, Lin T, Onar-Thomas A, Huether R, Kriwacki R, Parker M, Gupta P, Becksfort J, Wei L, Mulder HL, Boggs K, Vadodaria B, Yergeau D, Russell JC, Ochoa K, Fulton RS, Fulton LL, Jones C, Boop FA, Broniscer A, Wetmore C, Gajjar A, Ding L, Mardis ER, Wilson RK, Taylor MR, Downing JR, Ellison DW, Zhang J, Baker SJ (2014) The genomic landscape of diffuse intrinsic pontine glioma and pediatric non-brainstem high-grade glioma. *Nature genetics* 46:444-450. doi:10.1038/ng.2938
283. Wu YM, Su F, Kalyana-Sundaram S, Khazanov N, Ateeq B, Cao X, Lonigro RJ, Vats P, Wang R, Lin SF, Cheng AJ, Kunju LP, Siddiqui J, Tomlins SA, Wyngaard P, Sadis S, Roychowdhury S, Hussain MH, Feng FY, Zalupski MM, Talpaz M, Pienta KJ, Rhodes DR, Robinson DR, Chinnaiyan AM (2013) Identification of targetable FGFR gene fusions in diverse cancers. *Cancer discovery* 3:636-647. doi:10.1158/2159-8290.CD-13-0050
284. Xu GF, Lin B, Tanaka K, Dunn D, Wood D, Gesteland R, White R, Weiss R, Tamanai F (1990) The catalytic domain of the neurofibromatosis type 1 gene product stimulates ras GTPase and complements ira mutants of *S. cerevisiae*. *Cell* 63:835-841
285. Xu GF, O'Connell P, Viskochil D, Cawthon R, Robertson M, Culver M, Dunn D, Stevens J, Gesteland R, White R, et al. (1990) The neurofibromatosis type 1 gene encodes a protein related to GAP. *Cell* 62:599-608
286. Xu W, Yang H, Liu Y, Yang Y, Wang P, Kim SH, Ito S, Yang C, Wang P, Xiao MT, Liu LX, Jiang WQ, Liu J, Zhang JY, Wang B, Frye S, Zhang Y, Xu YH, Lei QY, Guan KL, Zhao SM, Xiong Y (2011) Oncometabolite 2-hydroxyglutarate is a

- competitive inhibitor of alpha-ketoglutarate-dependent dioxygenases. *Cancer cell* 19:17-30. doi:10.1016/j.ccr.2010.12.014
287. Yan H, Parsons DW, Jin G, McLendon R, Rasheed BA, Yuan W, Kos I, Batinic-Haberle I, Jones S, Riggins GJ, Friedman H, Friedman A, Reardon D, Herndon J, Kinzler KW, Velculescu VE, Vogelstein B, Bigner DD (2009) IDH1 and IDH2 mutations in gliomas. *The New England journal of medicine* 360:765-773. doi:10.1056/NEJMoa0808710
288. Yu PB, Deng DY, Lai CS, Hong CC, Cuny GD, Bouxsein ML, Hong DW, McManus PM, Katagiri T, Sachidanandan C, Kamiya N, Fukuda T, Mishina Y, Peterson RT, Bloch KD (2008) BMP type I receptor inhibition reduces heterotopic [corrected] ossification. *Nature medicine* 14:1363-1369. doi:10.1038/nm.1888
289. Zarghooni M, Bartels U, Lee E, Buczkowicz P, Morrison A, Huang A, Bouffet E, Hawkins C (2010) Whole-genome profiling of pediatric diffuse intrinsic pontine gliomas highlights platelet-derived growth factor receptor alpha and poly (ADP-ribose) polymerase as potential therapeutic targets. *Journal of clinical oncology : official journal of the American Society of Clinical Oncology* 28:1337-1344. doi:10.1200/JCO.2009.25.5463
290. Zhang J, Ding L, Holmfeldt L, Wu G, Heatley SL, Payne-Turner D, Easton J, Chen X, Wang J, Rusch M, Lu C, Chen SC, Wei L, Collins-Underwood JR, Ma J, Roberts KG, Pounds SB, Ulyanov A, Becksfort J, Gupta P, Huether R, Kriwacki RW, Parker M, McGoldrick DJ, Zhao D, Alford D, Espy S, Bobba KC, Song G, Pei D, Cheng C, Roberts S, Barbato MI, Campana D, Coustan-Smith E, Shurtleff SA, Raimondi SC, Kleppe M, Cools J, Shimano KA, Hermiston ML, Doulatov S, Eppert K, Laurenti E, Notta F, Dick JE, Basso G, Hunger SP, Loh ML, Devidas M, Wood B, Winter S, Dunsmore KP, Fulton RS, Fulton LL, Hong X, Harris CC, Dooling DJ, Ochoa K, Johnson KJ, Obenauer JC, Evans WE, Pui CH, Naeve CW, Ley TJ, Mardis ER, Wilson RK, Downing JR, Mullighan CG (2012) The genetic basis of early T-cell precursor acute lymphoblastic leukaemia. *Nature* 481:157-163. doi:10.1038/nature10725
291. Zhang J, Wu G, Miller CP, Tatevossian RG, Dalton JD, Tang B, Orisme W, Punchihewa C, Parker M, Qaddoumi I, Boop FA, Lu C, Kandoth C, Ding L, Lee R, Huether R, Chen X, Hedlund E, Nagahawatte P, Rusch M, Boggs K, Cheng J, Becksfort J, Ma J, Song G, Li Y, Wei L, Wang J, Shurtleff S, Easton J, Zhao D, Fulton RS, Fulton LL, Dooling DJ, Vadodaria B, Mulder HL, Tang C, Ochoa K, Mullighan CG, Gajjar A, Kriwacki R, Sheer D, Gilbertson RJ, Mardis ER, Wilson RK, Downing JR, Baker SJ, Ellison DW (2013) Whole-genome sequencing identifies genetic alterations in pediatric low-grade gliomas. *Nature genetics* 45:602-612. doi:10.1038/ng.2611
292. Zhu Y, Guignard F, Zhao D, Liu L, Burns DK, Mason RP, Messing A, Parada LF (2005) Early inactivation of p53 tumor suppressor gene cooperating with NF1 loss induces malignant astrocytoma. *Cancer cell* 8:119-130. doi:10.1016/j.ccr.2005.07.004
293. Zhu Y, Parada LF (2002) The molecular and genetic basis of neurological tumours. *Nature reviews Cancer* 2:616-626. doi:10.1038/nrc866